frontiers | Research Topics

Diffuse large B cell lymphoma: Updates on diagnosis and treatments

Edited by
Robert Ohgami and Shimin Hu

Published in
Frontiers in Oncology

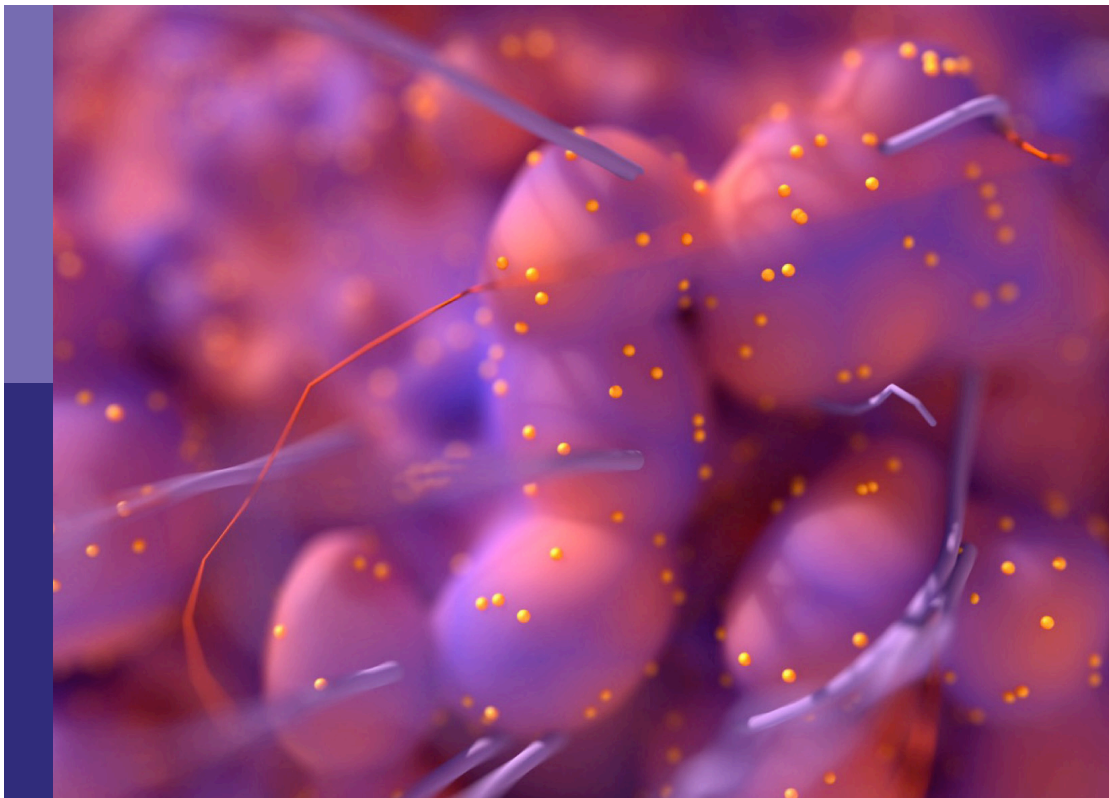

ISSN 1664-8714
ISBN 978-2-8325-5422-7
DOI 10.3389/978-2-8325-5422-7

About Frontiers

Frontiers is more than just an open access publisher of scholarly articles: it is a pioneering approach to the world of academia, radically improving the way scholarly research is managed. The grand vision of Frontiers is a world where all people have an equal opportunity to seek, share and generate knowledge. Frontiers provides immediate and permanent online open access to all its publications, but this alone is not enough to realize our grand goals.

Frontiers journal series

The Frontiers journal series is a multi-tier and interdisciplinary set of open-access, online journals, promising a paradigm shift from the current review, selection and dissemination processes in academic publishing. All Frontiers journals are driven by researchers for researchers; therefore, they constitute a service to the scholarly community. At the same time, the *Frontiers journal series* operates on a revolutionary invention, the tiered publishing system, initially addressing specific communities of scholars, and gradually climbing up to broader public understanding, thus serving the interests of the lay society, too.

Dedication to quality

Each Frontiers article is a landmark of the highest quality, thanks to genuinely collaborative interactions between authors and review editors, who include some of the world's best academicians. Research must be certified by peers before entering a stream of knowledge that may eventually reach the public - and shape society; therefore, Frontiers only applies the most rigorous and unbiased reviews. Frontiers revolutionizes research publishing by freely delivering the most outstanding research, evaluated with no bias from both the academic and social point of view. By applying the most advanced information technologies, Frontiers is catapulting scholarly publishing into a new generation.

What are Frontiers Research Topics?

Frontiers Research Topics are very popular trademarks of the *Frontiers journals series*: they are collections of at least ten articles, all centered on a particular subject. With their unique mix of varied contributions from Original Research to Review Articles, Frontiers Research Topics unify the most influential researchers, the latest key findings and historical advances in a hot research area.

Find out more on how to host your own Frontiers Research Topic or contribute to one as an author by contacting the Frontiers editorial office: frontiersin.org/about/contact

Diffuse large B cell lymphoma: Updates on diagnosis and treatments

Topic editors

Robert Ohgami — The University of Utah, United States

Shimin Hu — University of Texas MD Anderson Cancer Center, United States

Citation

Ohgami, R., Hu, S., eds. (2024). *Diffuse large B cell lymphoma: Updates on diagnosis and treatments*. Lausanne: Frontiers Media SA. doi: 10.3389/978-2-8325-5422-7

Table of contents

frontiers | Frontiers in Oncology

TYPE Original Research
PUBLISHED 31 October 2022
DOI 10.3389/fonc.2022.1048741

OPEN ACCESS

EDITED BY
Giuseppe Maurizio Campo,
University of Messina, Italy

REVIEWED BY
Dan Ma,
Affiliated Hospital of Guizhou Medical University, China
Aaron Domina,
Husson University, United States

*CORRESPONDENCE
Przemysław Juszczyński
pjuszczynski@ihit.waw.pl

SPECIALTY SECTION
This article was submitted to Hematologic Malignancies, a section of the journal Frontiers in Oncology

RECEIVED 19 September 2022
ACCEPTED 13 October 2022
PUBLISHED 31 October 2022

CITATION
Piechna K, Żołyniak A, Jabłońska E, Noyszewska-Kania M, Szydłowski M, Żerek B, Kulecka M, Rumieńczyk I, Mikula M and Juszczyński P (2022) Activity and rational combinations of a novel, engineered chimeric, TRAIL-based ligand in diffuse large B-cell lymphoma.
Front. Oncol. 12:1048741.
doi: 10.3389/fonc.2022.1048741

Activity and rational combinations of a novel, engineered chimeric, TRAIL-based ligand in diffuse large B-cell lymphoma

Karolina Piechna[1], Aleksandra Żołyniak[1], Ewa Jabłońska[1], Monika Noyszewska-Kania[1], Maciej Szydłowski[1], Bartłomiej Żerek[2], Maria Kulecka[3,4], Izabela Rumieńczyk[3], Michał Mikula[3] and Przemysław Juszczyński[1]*

[1]Department of Experimental Hematology, Institute of Hematology and Transfusion Medicine, Warsaw, Poland, [2]Department of Drug Discovery, Adamed Pharma S.A. Pienkow, Czosnow, Poland, [3]Department of Genetics, Maria Sklodowska-Curie National Institute of Oncology, Warsaw, Poland, [4]Department of Gastroenterology, Hepatology and Clinical Oncology, Centre for Postgraduate Medical Education, Warsaw, Poland

Background: TRAIL (TNF-related apoptosis inducing ligand) exhibits selective proapoptotic activity in multiple tumor types, while sparing normal cells. This selectivity makes TRAIL an attractive therapeutic candidate. However, despite encouraging activity in preclinical models, clinical trials with TRAIL mimetics/death receptor agonists demonstrated insufficient activity, largely due to emerging resistance to these agents. Herein, we investigated the cytotoxic activity of a novel, TRAIL-based chimeric protein AD-O51.4 combining TRAIL and VEGFA-derived peptide sequences, in hematological malignancies. We characterize key molecular mechanisms leading to resistance and propose rational pharmacological combinations sensitizing cells to AD-O51.4.

Methods: Sensitivity of DLBCL, classical Hodgkin lymphoma, (cHL), Burkitt lymphoma (BL) and acute myeloid leukemia (AML) to AD-O51.4 was assessed *in vitro* with MTS assay and apoptosis tests (Annexin V/PI staining). Markers of apoptosis were assessed using immunoblotting, flow cytometry or fluorogenic caspase cleavage assays. Resistant cell lines were obtained by incubation with increasing doses of AD-O51.4. Transcriptomic analyses were performed by RNA sequencing. Sensitizing effects of selected pathway modulators (BCL2, dynamin and HDAC inhibitors) were assessed using MTS/apoptosis assays.

Results: AD-O51.4 exhibited low-nanomolar cytotoxic activity in DLBCL cells, but not in other lymphoid or AML cell lines. AD-O51.4 induced death-receptor (DR) mediated, caspase-dependent apoptosis in sensitive DLBCL cells, but not in primary resistant cells. The presence of DRs and caspase 8 in cancer cells was crucial for AD-O51.4-induced apoptosis. To understand the potential mechanisms of resistance in an unbiased way, we engineered AD-O51.4-

resistant cells and evaluated resistance-associated transcriptomic changes. Resistant cells exhibited changes in the expression of multiple genes and pathways associated with apoptosis, endocytosis and HDAC-dependent epigenetic reprogramming, suggesting potential therapeutic strategies of sensitization to AD-O51.4. In subsequent analyses, we demonstrated that HDAC inhibitors, BCL2 inhibitors and endocytosis/dynamin inhibitors sensitized primary resistant DLBCL cells to AD-O51.4.

Conclusions: Taken together, we identified rational pharmacologic strategies sensitizing cells to AD-O51.4, including BCL2, histone deacetylase inhibitors and dynamin modulators. Since AD-O51.4 exhibits favorable pharmacokinetics and an acceptable safety profile, its further clinical development is warranted. Identification of resistance mechanisms in a clinical setting might indicate a personalized pharmacological approach to override the resistance.

KEYWORDS

TRAIL, apoptosis, DLBCL, venetoclax, drug resistance, endocytosis

Introduction

Programmed cell death - apoptosis - is a conserved, highly controlled process, essential for the development and maintenance of homeostasis in multicellular organisms (1). Apoptosis can be triggered by extrinsic (receptor) or intrinsic (mitochondrial) pathways, both culminating in the activation of caspases, a family of enzymes cleaving a large variety of different substrates and leading eventually to cell death (2). Resistance to apoptosis allows unrestricted cell growth, and is considered a hallmark of cancer (3). Accordingly, most of the current cancer therapeutic strategies act through the induction of programmed cell death in target tumor cells. However, primary or acquired resistance to drug-induced apoptosis is a major cause of therapy failure. Thus, therapeutic reactivation/facilitation of apoptotic pathways represents a promising approach to elicit cell death in cancer cells.

TRAIL (*TNF-related apoptosis inducing ligand)*, a pro-apoptotic Tumor Necrosis Factor family member, represents an attractive strategy in this aspect owing to its several unique characteristics. Most importantly, TRAIL exhibits marked selectivity towards tumor cells, while sparing normal cells. This selectivity is related to higher expression of TRAIL receptors DR4 and DR5 (*death receptor 4 and 5*) on tumor than on normal cells, but involves multiple additional mechanisms, such as cFLIP- and XIAP-dependent inhibition of apoptosis or overexpression of TRAIL decoy receptors in normal cells (4, 5). Secondly, unlike TNF, TRAIL does not elicit shock-like symptoms after systemic administration. However, the clinical use of native TRAIL is severely limited by its short half-life (6, 7). To circumvent these limitations, a variety of TRAIL recombinant analogs or TRAIL mimetics/death receptor agonists have been developed. Their activity has been studied in clinical trials. However, these studies have demonstrated only modest clinical effects of the TRAIL-based strategies due to insufficient activity and the development of resistance (8–10).

Diffuse large B-cell lymphoma (DLBCL) is the most common type of aggressive B-cell lymphoma in adults. DLBCL exhibits highly heterogeneous clinical behavior and a complex molecular background (11–15). Depending on their transcriptomic profiles, DLBCLs can be classified into distinct categories: germinal center-like (GCB) and activated B-cell-like (ABC) subtypes, which differ also in clinical behavior (13, 16). Despite molecular heterogeneity, R-CHOP immunochemotherapy remains a standard of care in the first-line DLBCL treatment. However, this approach is ineffective in about 1/3 of patients who are either refractory to frontline therapy or relapse after the initial response, underscoring the need for better treatment modalities.

In this study, we investigated cytotoxic activity, potential resistance mechanisms and synergies of a novel, chimeric protein AD-O51.4 in DLBCL models. AD-O51.4 comprises a TRAIL-derived sequence fused to tandemly arranged VEGFA-derived peptides. The positively-charged, N-terminal VEGFA-derived peptides increase the cell surface binding of the fusion protein and thus facilitate the TRAIL portion interactions with its cognate receptors (17). Consistent with its hybrid structure, AD-O51.4 in previous studies was demonstrated to elicit dual activity: cytotoxic effects in tumor cells and antiangiogenic effects on the vascular endothelium (17). Herein, we studied AD-O51.4 activity in a broad panel of lymphoid and myeloid

tumor cells lines. We show that AD-O51.4 induces apoptosis at sub-nanomolar concentrations in the sensitive DLBCL cell lines. We characterize potential targetable AD-O51.4 resistance mechanisms and propose HDAC, dynamin and BCL2 inhibitors as pharmacological modulators with a potential to restore the sensitivity to TRAIL-induced apoptosis.

Materials and methods

Cell culture and chemicals

Human DLBCL cell lines were maintained in RPMI-1640 (Lonza; DHL-4, DHL-6, TOLEDO, U2932, K422, RIVA, PFEIFFER) or Iscove's Modified Dulbecco's Medium (Lonza; Ly-1, Ly-3, Ly-4, Ly-7, Ly-18, Ly-19, HBL-1), each supplemented with 100 U/mL penicillin, 100 U/mL streptomycin (Lonza), 10% or 20% heat-inactivated fetal bovine serum (Biowest), L-glutamine (2mM, Lonza) and HEPES (10Mm, Lonza). Cell GCB- and ABC designations were determined previously (18). Cells were grown in a humidified atmosphere at 37°C with 5% CO2. AD-O51.4 was synthesized and provided by Adamed S.A. TRAIL was purchased from R&D. Dynasore, venetoclax, SAHA and panobinostat were purchased from Selleckchem. Methyl-β-cyclodextrin (MβCD) and filipin were purchased from Sigma Aldrich. Caspase 3 inhibitor (Z-DEVD-FMK), caspase 8 inhibitor (Z-IETD-FMK), caspase 9 inhibitor (Ac-LEHD-CMK) and pan-caspase inhibitor (Z-VAD-FMK) were purchased from Merck-Millipore and used at 20 μM (caspase 8 and 9 inhibitors and pan-caspase inhibitor) or 50 μM (caspase 3 inhibitor) final concentration.

Cell viability, apoptosis and caspase activity assays

DLBCL cells were incubated on a 96-well plate with either full medium or medium with indicated inhibitors used at concentrations specified in figures and figure legends. After incubation, cell viability was assessed with the 3-(4, 5 dimethylthiazol-2-yl)-5-(3-carboxymethoxyphenyl-2-(4-sulfophenyl)-2H-tetrazolium (MTS) assay (Promega). IC_{50} values were calculated using GraphPad Prism v6.0 software. Detection of apoptosis was performed with Annexin V-FITC Apoptosis Detection Kit BD Biosciences and analyzed using FACS Canto flow cytometer (BD Biosciences). Caspase activity was measured using Caspase 3/7 Glo assay (Promega). Briefly, 0.15 $\times 10^6$/mL cells were incubated overnight with either AD-O51.4 or TRAIL (0.1 nM). Thereafter, Caspase Glo reagent was automatically injected to wells and the luminescence was measured using TriStar LB 941 plate reader (Berthold Technologies).

Flow cytometry

Cells were washed with PBS and incubated with fluorochrome-conjugated mouse anti-DR4-PE, anti-DR5-PE, DcR1-PE (eBioscience) or anti-VEGFR1/2 (R&D Systems), or with control isotype-matched antibodies for 30 minutes, then washed again and analyzed using FACS Canto flow cytometer (BD Biosciences). To determine receptor changes after incubation with endocytosis modulator dynasore, cells were fixed with 4% paraformaldehyde (Polysciences) for 15 min at 37°C, chilled on ice, washed 3 times with PBS and stained with anti-DR4 and anti-DR5 antibodies as above.

Measurement of the membrane cholesterol content

Cells were incubated for 1 hour with 10, 20 or 40 mM MβCD to elute membrane cholesterol and disrupt lipid raft integrity. Depletion of cholesterol was confirmed with filipin staining (50 ng/mL) and flow cytometry as previously described (19).

Immunoblotting

Immunoblotting was performed as previously described (20, 21). Briefly, protein lysates were resolved by SDS-PAGE, transferred to PVDF membranes (Millipore) and immunoblotted with primary and appropriate HRP-labelled secondary antibodies (listed in Supplemental Table 1). Signals were developed by enhanced luminescence using ECL reagent (Perkin Elmer) and a digital image acquisition system (G:Box, Syngene). To re-probe with another antibody, blots were incubated in the stripping buffer (2%SDS, 62,5mM Tris/HCl, pH 6.8, 0,8% β-mercaptoethanol) at 50°C for 30 minutes, washed extensively in Tris-buffered saline and analyzed as described above.

RNA sequencing

RNA was extracted using Gene MATRIX Universal RNA/miRNA Purification Kit (EURx), according to manufacturer instructions. High-quality samples (RIN≥8, determined with Bioanalyzer instrument) were enriched in poly(A)-containing mRNA using Dynabeads mRNA DIRECT Micro Kit (Thermo). The libraries were prepared with Ion Total RNA-Seq Kit v2 (Thermo) and sequenced on Ion Porton sequencer as described before (22). The raw reads were processed with Ion Torrent RNASEQ Analysis pipeline (Torrent Suite version 5.0.4) which maps reads to hg19 genome with STAR2 and bowtie2 aligners.

Gene counts were generated with htseq-count version 0.6. Gene expression analysis was performed in R environment (v 4.0.4) using DESeq2, ClusterProfiler, fgsea and enrichplot packages (23, 24). Sequencing results are available *via* Gen Expression omnibus under accession number GSE208543.

Statistical analysis

All experiments were performed in biological duplicates or triplicates as indicated in figure legends. The results show average values including standard deviations. To evaluate the differences between groups, Mann-Whitney test or Student's *t*-test (for variables with normal distribution) were used, with $p<0.05$ as a significance level. Densitometric quantifications of band intensities were performed using ImageJ software (www.imagej.net) as described (25). Drug interactions were evaluated using CompuSyn software using Chou-Talalay method (26).

Results

Cytotoxic activity of AD-O51.4 and its mechanisms in lymphoma and leukemia cell lines

We first evaluated the activity of the novel chimeric molecule AD-O51.4 in a panel of lymphoma and leukemia cell lines (DLBCL, Burkitt lymphoma (BL), Hodgkin lymphoma (HL) and acute myeloid leukemia (AML)). We found that AML, cHL and BL cells were resistant to AD-O51.4 and TRAIL (Supplemental Figure 1). In contrast, most DLBCL cell lines were sensitive to AD-O51.4 (Figure 1A and Supplemental Figure 2). Of note, TRAIL exhibited similar activity in these models. On the basis of established AD-O51.4 IC_{50} in viability assays, DLBCL cell lines were termed sensitive (IC_{50} from 0.01 nM to 0.1 nM: DHL4, LY7, RIVA), moderately sensitive (IC_{50} from 0.1 nM to 1 nM: DHL6, U2932), or resistant (IC_{50} >1 nM: LY4, TOLEDO; Table 1 and Supplemental Figure 2). Twenty-four hour incubation of DLBCL cell lines with 0.1 nM AD-O51.4 markedly increased the fraction of apoptotic cells in sensitive lines, but had only moderate or no effect in moderately sensitive lines and resistant lines (Figure 1A, Supplemental Figure 3). We did not observe differences in response between GCB- and ABC-DLBCL subtypes (Supplemental Figure 4). To further determine the mechanism of cell death in DLBCL cells, we evaluated the expression of proteins activated in extrinsic (caspase 8), intrinsic (caspase 9, tBID), and in common apoptosis pathway (caspase 3, PARP). In sensitive lines, AD-O51.4 markedly induced caspase 3, 8 and 9 activation and tBID and PARP cleavage, indicating that extrinsic, intrinsic and effector pathways are activated in response to the drug. In contrast, resistant cell lines showed no cleavage of these proteins (Figure 1B). Since death receptors can trigger cell death in caspase-independent mechanisms [e.g *via* necroptosis (27)], we next assessed whether AD-O51.4 cytotoxicity requires caspase activation. In these experiments, caspase 8 or pan-caspase inhibition blocked cell death induced by AD-O51.4 entirely, even with extended incubation times (up to 120h; Figures 1C, D). These studies demonstrate that the extrinsic apoptotic pathway is the principal cell death mechanism triggered by AD-O51.4.

These findings prompted us to determine whether the sensitivity of DLBCL cells to AD-O51.4 depends on the DR4/DR5 or caspase 8 expression. Sensitive cell lines showed significantly higher surface expression of DR4 ($p=0.081$) and markedly higher expression of caspase 8 ($p=0.028$, Figure 2). Of note, other TRAIL surface receptors (decoy receptors 1 and 2) were expressed at very low levels. Since AD-O51.4 includes VEFG-derived peptide domains, we also determined the VEGFR1 and VEGFR2 expression on the surface of DLBCL cell lines. Expression of these receptors was low or undetectable, indicating that their role in the AD-O51.4 cytotoxicity in DLBCL cells is unlikely.

Previous reports demonstrated that in certain B-cell malignancies, the membrane microarchitecture and constitutive localization of death receptors in lipid rafts are required for TRAIL-induced apoptosis (28). To determine whether the same spatial arrangement is required for AD-O51.4 activity in DLBCL cell lines, we used a cholesterol-eluting and lipid rafts disrupting agent, methyl-β-cyclodextrin (MβCD). In sensitive DLBCL cells LY1 and LY7, MβCD effectively depleted cholesterol from the cell membrane, but did not affect AD-O51.4 activity (Supplemental Figure 5).

Mechanisms of acquired AD-O51.4 resistance

To define the molecular mechanisms associated with AD-O51.4 resistance, we first developed drug-resistant isogenic cell lines by incubating sensitive RIVA and LY7 lines with increasing concentrations of AD-O51.4 until they reached complete resistance to 0.1 nM of AD-O51.4 (Figure 3A). Similar to cells with primary resistance (Figure 2), cells with acquired resistance exhibited decreased caspase 8 and DR4 expression (Figures 3B, C). DR5 expression decreased in RIVA, but not in resistant LY7 cells (Figure 3C). Thereafter, to understand the mechanisms of resistance in DLBCL cell lines in an unbiased manner and without *a priori* hypotheses, we compared gene expression profiles of parental and resistant cell lines using RNA sequencing and analyzed the gene ontology term enrichment in the genes differentially expressed (adjusted p value <0.05) between isogenic sensitive and resistant lines (Figure 4). In these analyses, we noted the enrichment of genes associated with cell membrane dynamics (membrane ruffle and lamellipodia formation, clathrin-mediated endocytosis, endocytic vesicle transport, cytoskeleton reorganization, protein membrane

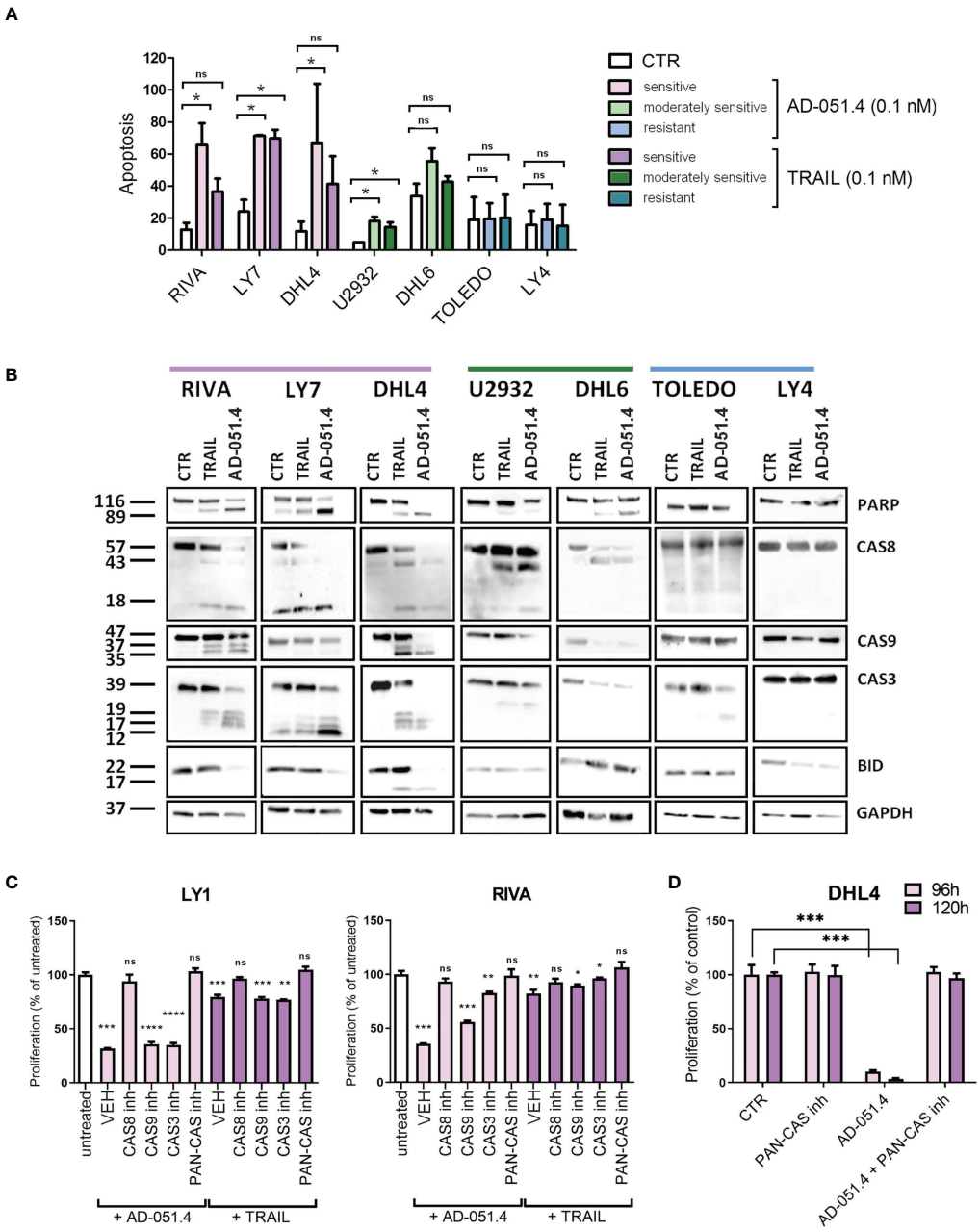

FIGURE 1
AD-O51.4 induces apoptosis in DLBCL cells. **(A)** Fraction of apoptotic cells in DLBCL cell lines incubated with 0.1 nM AD-O51.4, 0.1 nM TRAIL or PBS (control, CTR) for 24h. Early- and late–apoptotic cells are pooled together (Annexin V+/PI- and AnnexinV+/PI+, respectively). Corresponding dot-plots of a representative experiment are shown in Supplemental Figure 3. Experiments were performed in 2 replicates. Error bars indicate standard deviations (SD). Differences between number in apoptotic cells are indicated (Student *t*-test, *p-value<0.05, **p-value<0.005, ***p-value<0.001, ****p-value<0.0005, ns – not significant. **(B)** Processing of PARP, Caspase 8, 9, 3 and BID in DLBCL cell lines incubated with AD-O51.4 or TRAIL. Cells were incubated with the AD-O51.4 or TRAIL for 6h, lysed and processing/cleavage of indicated proteins was evaluated using immunoblotting. GAPDH served as a loading control. Cleavage of the protein is manifested either by appearance of its cleaved (lighter) form (e.g. PARP, CASP3, CASP8), or by disappearance of a full-length protein (e.g BID). **(C)** Caspase inhibition blocks induction of apoptosis in AD-O51.4-sensitive DLBCL cells. LY1 or RIVA cells were pre-incubated with caspase 3, 8 9, pan-caspase inhibitor or DMSO (vehicle, VEH) for 1 h, then with 0.1 nM AD-O51.4, 0.1 nM TRAIL for subsequent 48 h. Viability was assessed with an MTS assay. Bars represent the average of three independent experiments, error bars represent standard deviations, statistical differences are indicated as in panel A.**(D)** Prolonged incubation with AD-O51.4 does not induce caspase-independent cell death in DLBCL cells. DHL4 cells were pretreated with Z-VAD-FMK pan-caspase inhibitor (20 μM, 1 h), and then incubated with AD-O51.4 for 96-120h. Cell viability was evaluated with an MTS assay. Bars represent the average of three independent experiments, error bars represent standard deviations, statistical differences are indicated as in panel **(A)** Results were normalized to untreated cells (viability =100%).

10.3389/fonc.2022.1048741

TABLE 1 AD-O51.4 and TRAIL half maximal inhibitory concentrations (IC_{50}) in DLBCL cell lines.

DLBCL cell line	AD-O51.4 IC_{50} [nM]	TRAIL IC_{50} [nM]
DHL4	0.012	0.014
K422	0.011	0.066
LY1	0.047	0.04
LY7	0.04	0.039
RIVA	0.05	0.013
LY18	0.042	0.17
LY19	0.028	0.564
HBL1	0.07	0.13
DHL6	0.14	0.17
U2932	0.25	>1
LY4	>1	>1
TOLEDO	>1	>1
PFEIFFER	>1	>1
LY3	>1	>1

Cells with IC_{50} less than 0.1 nM were considered highly sensitive, cells with IC_{50} between 0.1 and 1 nM were considered moderately sensitive, and cells with IC_{50} greater than 0.1 nM were considered resistant.

trafficking, GTP-ase activity), and regulation of apoptosis. To further understand the mechanisms of acquired resistance to AD-O51.4, we performed Gene Set Enrichment Analysis (GSEA; Figure 5). Consistent with the results of GO term enrichment, these analyses confirmed that AD-O51.4-resistant cells are characterized by overexpression of gene sets associated with clathrin-mediated endocytosis, dynamin pathway and cytoskeleton reorganization, suggesting that AD-O51.4 resistance might be acquired through increased receptor endocytosis. Resistant cells also showed differential expression of genes associated with apoptosis, indicating that modulation of apoptosis executing proteins might be another mechanism leading to resistance. Third, resistant cells demonstrated differential expression of HDAC-dependent genes. Since epigenetic mechanisms facilitate adaptive reprogramming of gene expression in response to various stress stimuli, including cytotoxic drugs, and are responsible for cell phenotypic plasticity (29), we hypothesized that epigenetic changes might be also involved in acquisition of AD-O51.4 resistance. Importantly, since increased endocytosis of death receptors, modulation of the apoptosis-controlling genes and/or epigenetic reprogramming can be pharmacologically targeted, we hypothesized that modulation of these pathways would restore the AD-O51.4 sensitivity.

Pharmacological modulation of AD-O51.4 resistance in DLBCL models

To verify these hypotheses, we first tested the synergy between AD-O51.4 and a proapoptotic BCL2 inhibitor, venetoclax. In these experiments, we used a resistant cell line TOLEDO and a moderately sensitive line U2932. As predicted, venetoclax synergized with AD-O51.4 (Combination Index [CI]<0.5, for all dose combinations, Figures 6A-D). To confirm these observations, we assessed the biochemical markers of AD-O51.4-induced apoptosis in these cells. While venetoclax or AD-O51.4 induced weak or no PARP and caspase cleavage, the combination of these drugs induced a markedly increased abundance of cleaved forms of these markers (Figures 6E-F). Next, we asked whether HDAC inhibitors would sensitize resistant cells to AD-O51.4-mediated apoptosis. For these experiments, we used pan-HDAC inhibitors - SAHA and panobinostat. While each of the HDAC inhibitors showed little activity when used as a single agent, they markedly sensitized resistant/moderately sensitive DLBCL cell lines to AD-O51.4 (CI<0.54 and CI<0.52 for SAHA + AD-O51.4 combinations in Toledo and U2932, respectively; CI<0.44 and CI<0.77 for panobinostat + AD-O51.4 combinations in Toledo and U2932, respectively; Figure 7).

Finally, we determined whether modulation of clathrin-mediated endocytosis increases AD-O51.4 activity. To test this hypothesis, we used dynasore, a cell-permeable, non-competitive inhibitor of GTPase activity of dynamin 1 and 2 (DNM1/2), essential for clathrin- coated vesicle formation and subsequent scission of nascent endosome (30). As expected, dynasore increased surface expression of DR4 and DR5 in resistant/moderately sensitive cell lines TOLEDO and U2932 in a dose-dependent manner (Figures 8A, B). Importantly, dynasore used as a single agent in these experiments showed no cytotoxic activity over short incubation periods. Consistent with the increased death receptor expression, dynasore-pretreated TOLEDO and U2932 cells exhibited dramatically increased levels of apoptosis (Figures 8C, D).

Discussion

TRAIL exhibits unique proapoptotic activity against a variety of tumor cells while sparing non-transformed cells. These characteristics placed the TRAIL ligand-receptor system in the spotlight as a potential cancer therapy and multiple TRAIL mimetics were evaluated in clinical trials. Results of these studies generally demonstrated acceptable toxicity, but the limited activity of TRAIL-based approaches due to the rapid development of resistance. The resistance to TRAIL mimetics/analogs can emerge in several mechanisms. First, since TRAIL requires death receptors 4 and 5 (DR4/5) for activity, loss of the surface receptors, their post-translational modifications, changes in lipid rafts or induction of decoy receptors expression confers resistance to TRAIL-based therapies. Second, blockades in TRAIL-initiated apoptotic signal transduction or induction of anti-apoptotic proteins attenuate TRAIL therapeutic activity. Third, multiple transcriptional and epigenetic mechanisms, triggered in response to TRAIL signaling, can program tumor cells for TRAIL or TRAIL mimetics resistance.

10.3389/fonc.2022.1048741

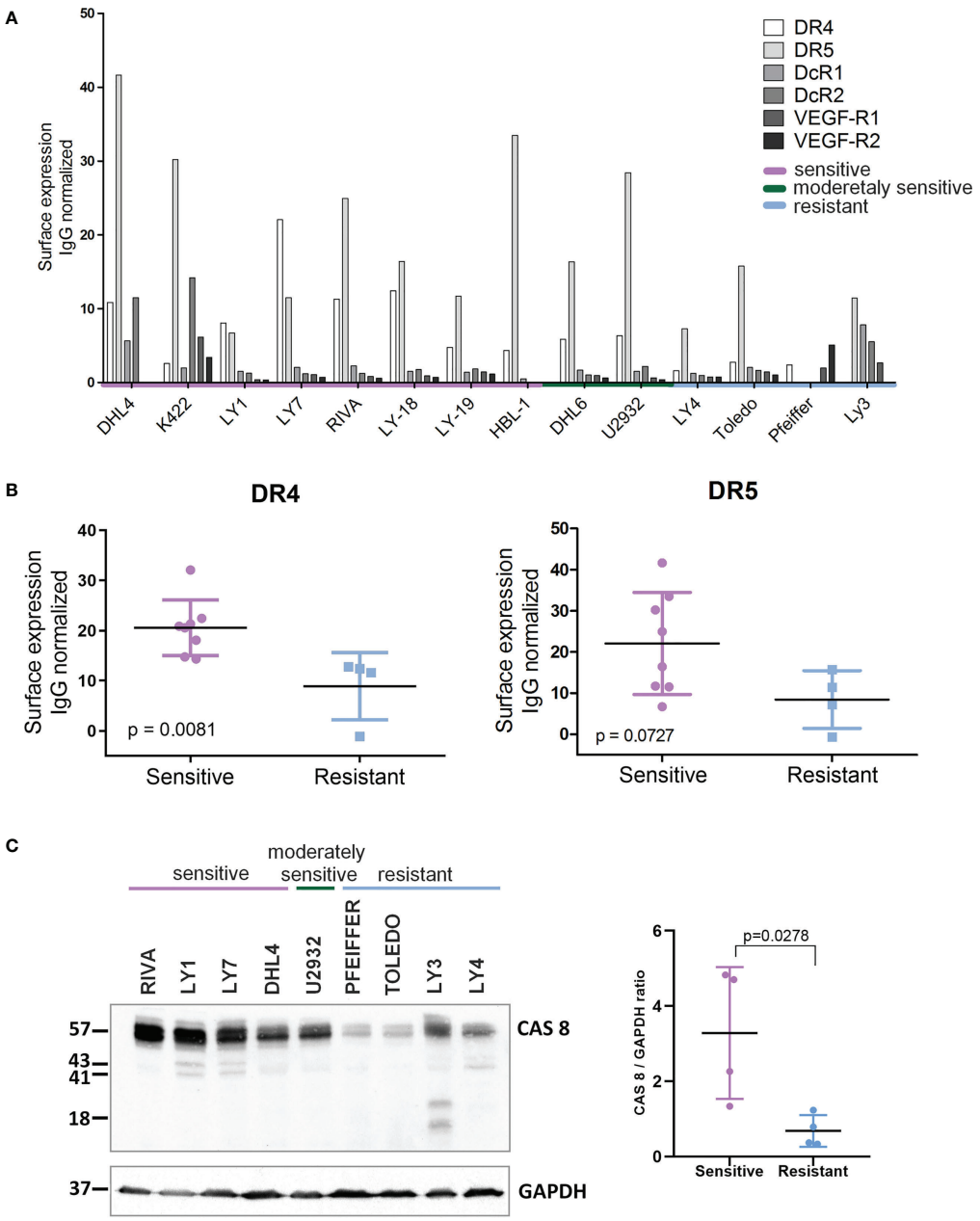

FIGURE 2
Expression of death receptors and caspase 8 is higher in AD-O51.4 –sensitive DLBCL cell lines. **(A)** Expression of death receptors 4 and 5 (DR4, DR5) decoy receptors 1 and 2 (DcR1, DcR2) and VEGF receptors 1 and 2 (VEGF-R1, VEGF-R2) was assessed in DLBCL cell lines using FACS and appropriate fluorochrome – conjugated antibodies. Bars indicate isotype control-normalized mean fluorescence values for each receptor. The bar plot represents the representative of three independent experiments. **(B)** Comparison of isotype-control normalized MFI values of DR4 and DR5 for AD-O51.4 -sensitive and –resistant DLBCL cell lines. **(C)** Left panel: expression of caspase 8 in AD-O51.4 -sensitive and –resistant DLBCL cell lines was assessed by immunoblotting. GAPDH served as a loading control. Right panel: CASP8 band intensities were quantified using pixel densitometry and normalized to GAPDH levels. Differences between sensitive and resistant cell lines were calculated using Student *t*-test.

Since TRAIL/TRAIL mimetics exhibit a very attractive safety profile, despite the limited efficacy and development of resistance, TRAIL-based therapeutic strategies remain still in the focus of researchers and clinicians as a potential therapeutic strategy. The reversible nature of at least some of TRAIL resistance mechanisms leaves a relatively broad space for sensitization to TRAIL or TRAIL mimetics. Detailed characterization of these mechanisms and identification of

10.3389/fonc.2022.1048741

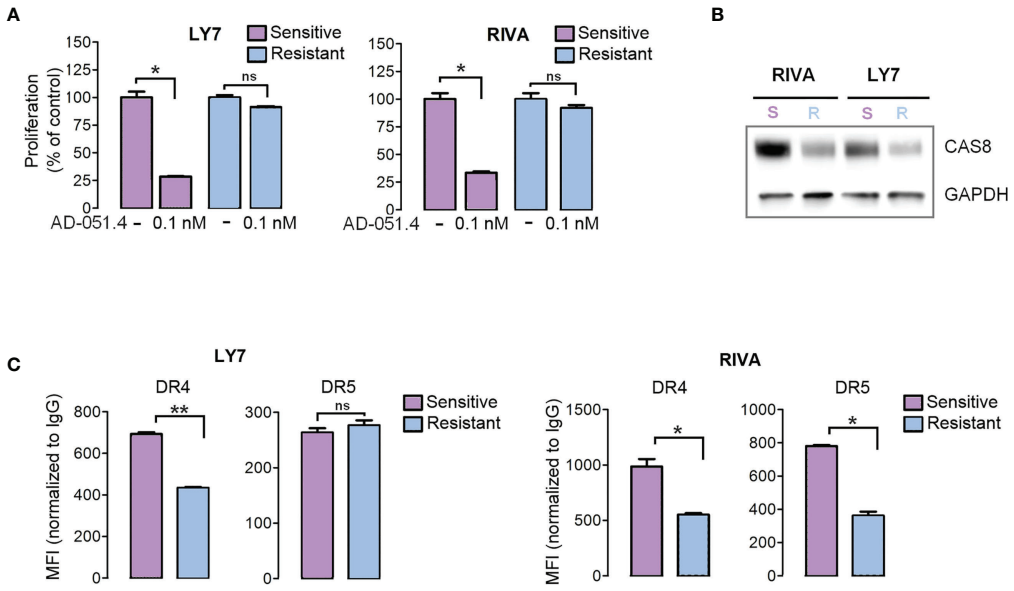

FIGURE 3
Engineered AD-O51.4 - resistant DLBCL cell lines have decreased caspase 8 and death receptor expression. **(A)** LY7 and RIVA cell lines were incubated with increasing doses of AD-O51.4 until reached complete resistance to 0.1 nM AD-O51.4. The viability of parental (purple bars) and engineered resistant (blue bars) cells is shown. Bars indicate the average of three experiments and error bars represent standard deviations. Results were normalized to untreated (control) cells. **(B)** Expression of caspase 8 in parental *vs* resistant LY7 and RIVA cells was assessed by immunoblotting. **(C)** Surface expression of DR4 and DR5 in parental *vs* resistant LY7 and RIVA cells was assessed by flow cytometry. Boxes represent average MFI from 3 replicates normalized to isotype-matched antibody, error bars represent standard deviations. *p-value<0.05, **p-value<0.005, ns – not significant.

potential targetable vulnerabilities in preclinical models is crucial for future precise pharmacological interventions restoring sensitivity.

In this study, we evaluated a newly developed TRAIL mimetic, AD-O51.4. AD-O51.4 is a hybrid protein, composed of TRAIL-derived DR ligand fused to N-terminal VEGF derived, positively charged peptide. This molecule exhibits several unique characteristics making it a promising clinical candidate. First, AD-O51.4 exhibits favorable pharmacokinetics, including extended plasma half-life, large volume of distribution and preferential accumulation in tumors (17). In preclinical models, AD-O51.4 demonstrated a very good safety profile – neither mice nor monkeys treated with AD-O51.4 demonstrated symptoms of drug toxicity (17). AD-O51.4 exhibited promising toxicity in solid tumor models (cell lines and patient derived xenografts - lung adenocarcinoma, colorectal, large-cell lung, esophageal, pancreatic, bladder, and kidney cancers, hepatoblastoma and osteosarcoma) (17). Recently, the efficacy of AD-O51.4 has been also demonstrated in a broad panel of colorectal cancer cell lines and patient derived xenografts (31). These studies also highlighted the unique mechanism of action of AD-O51.4, combining death receptor signaling with DR-unrelated mechanism, driven by VEGF-derived portion of AD-O51.4, which induced FAK (focal adhesion kinase) signaling and remodeling of the actin cytoskeleton (17). The VEGF-derived AD-O51.4 portion also suppressed angiogenesis *in vitro* and *in vivo* (17).

Herein, we demonstrate that AD-O51.4 exhibits high activity in several DLBCL cell lines. We demonstrated that DR4/5 expression was higher in sensitive cells and the caspase activation is crucial for AD-O51.4 activity, while caspase-independent cell death pathways are not involved. In solid tumors, binding of the VEGF-derived, positively charged N-terminal portion of AD-O51.4 to the cell surface led to FAK activation and abnormalities in the actin cytoskeleton, characteristic of integrin mediated death. Similarly to DR-induced apoptosis, integrin-mediated death involves activation of caspase 8, although in complexes with actin and integrins, not with FADD and DRs (32). Consistent with this, neutralization of the positive charge of AD-O51.4 attenuated its proapoptotic activity in solid tumor models (17). However, given the low expression of VEGFR in DLBCL cells, VEGFR-mediated activity in these tumors is unlikely. Regardless of the upstream mechanism triggered by AD-O51.4 in DLBCL, apoptosis initiated by this ligand requires high expression of caspase 8. This is consistent with previous studies, which demonstrated resistance of cell lines with low caspase 8 expression to TRAIL (33, 34).

Consistent with previous clinical experience with TRAIL analogues, several DLBLC cell line models exhibited primary

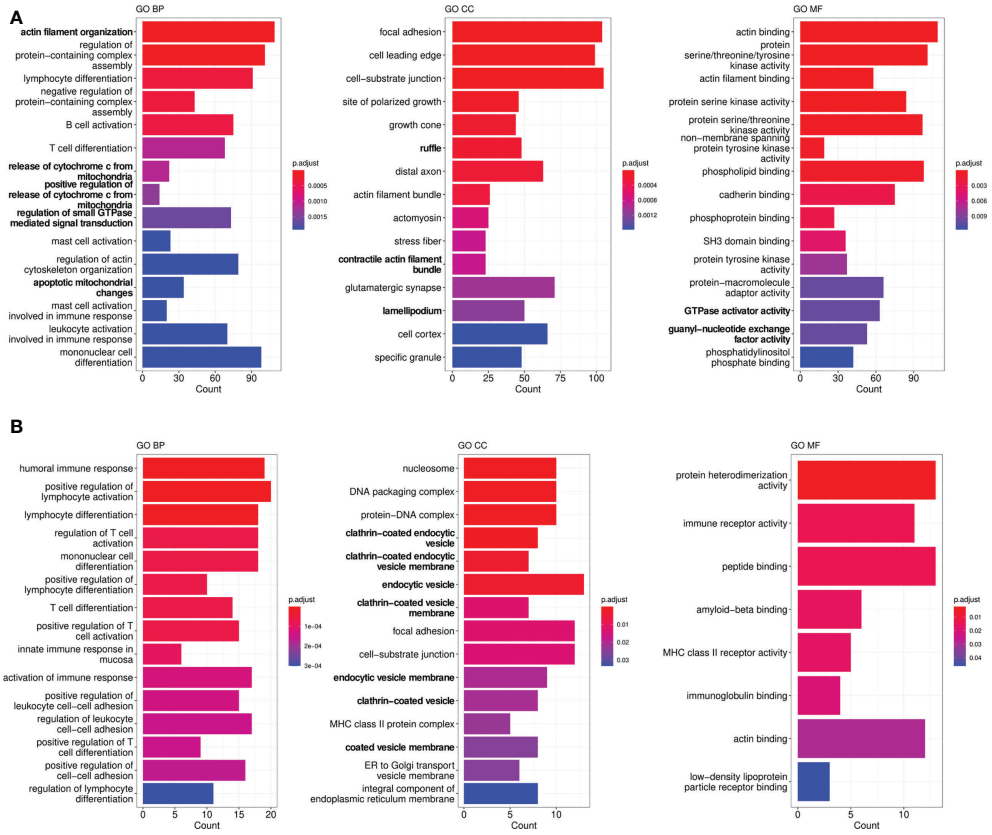

FIGURE 4
Gene ontology (GO) enrichment analysis in genes differentiating sensitive (parental) and engineered resistant LY7 **(A)** and RIVA cells **(B)**. Graphs demonstrate top significantly enriched GO CC (*cellular component*), GO BP (*biological process*) and GO MF (*molecular function*) terms.

resistance to AD-O51.4. We also demonstrated that the resistance can be acquired through repeated/extended exposure to the drug, mimicking acquired resistance during therapy. To identify potential strategies sensitizing to AD-O51.4, we characterized the key biological mechanisms driving primary and acquired resistance in these cells. We demonstrated that AD-O51.4 sensitivity can be increased by blocking DR internalization (dynasore), blocking BCL2 antiapoptotic activity (venetoclax) or by modulating epigenetic mechanisms, such as histone acetylation (SAHA, panobinostat). Although endocytosis inhibitors used in these studies are "tool" compounds, unlikely to enter clinical trials, there are clinically available modulators of clathrin-dependent endocytosis. For example, certain phenothiazine derivatives, such as chloropromazine, inhibit dynamin 1 and 2 GTP-ase activity at clinically achievable concentrations. Given the critical role of dynamins in the scission of nascent vesicles and endocytosis, such an approach appears to be a rational strategy to increase DR density on target cells.

Since the identified resistance mechanisms are likely operating redundantly in the same cells, and are likely susceptible to clonal selection, triple- and higher-order drug combinations might exhibit synergistic AD-O51.4 (re)sensitizing effect. Importantly, numerous studies of combinations of TRAIL analogues with empirical chemotherapeutics/targeted agents indicated that these strategies are generally well tolerated. However, these studies were not driven by biomarkers and involved all-comers. Given the empirical nature of these combinations, ignorant to individual and sometimes redundant molecular mechanisms driving resistance, it is not surprising that they also exhibited limited activity. Thus, future strategies involving TRAIL analogues including AD-O51.4, should be more personalized, biomarker and knowledge-driven. For example, based on the preclinical data presented herein - low caspase 8 expression might represent the biomarker of resistance and exclusion criterion. Second, given the mechanism of action and cellular plasticity leading to resistance, the therapeutic strategies should be designed upfront to maximize the response and eliminate tumor cells before resistance occurs. This goal can

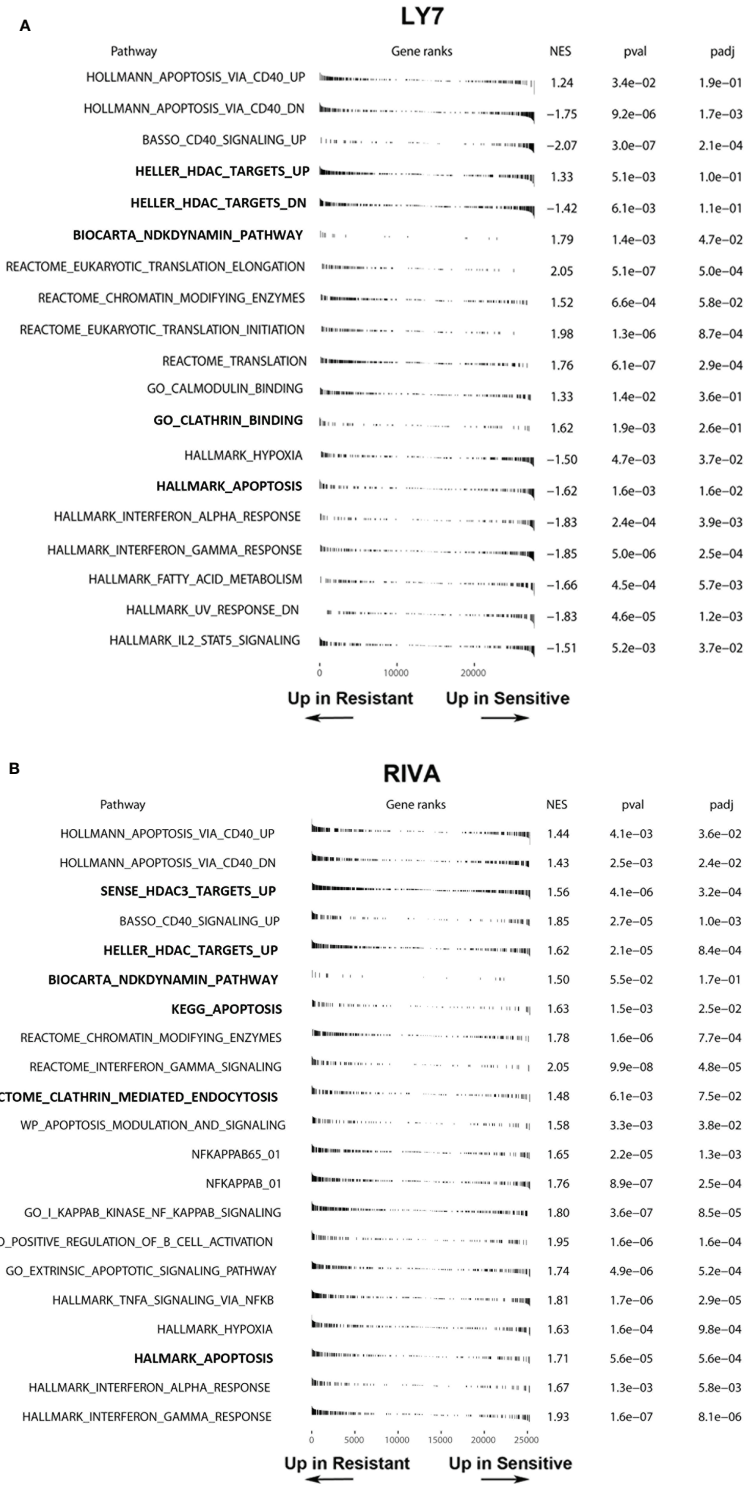

FIGURE 5
Gene set enrichment analysis showing differentially expressed gene sets in parental (sensitive) and engineered resistant LY7 **(A)** and RIVA **(B)** cells. Normalized enrichment scores, raw and adjusted p-values of apoptosis, endocytosis and HDAC-related gene-sets are shown. Plots indicate the positions of genes from a given gene set in a list of differentially expressed genes ranked by the value of Wald statistics. NES, Normalized Enrichment Score; padj, adjusted p-value.

10.3389/fonc.2022.1048741

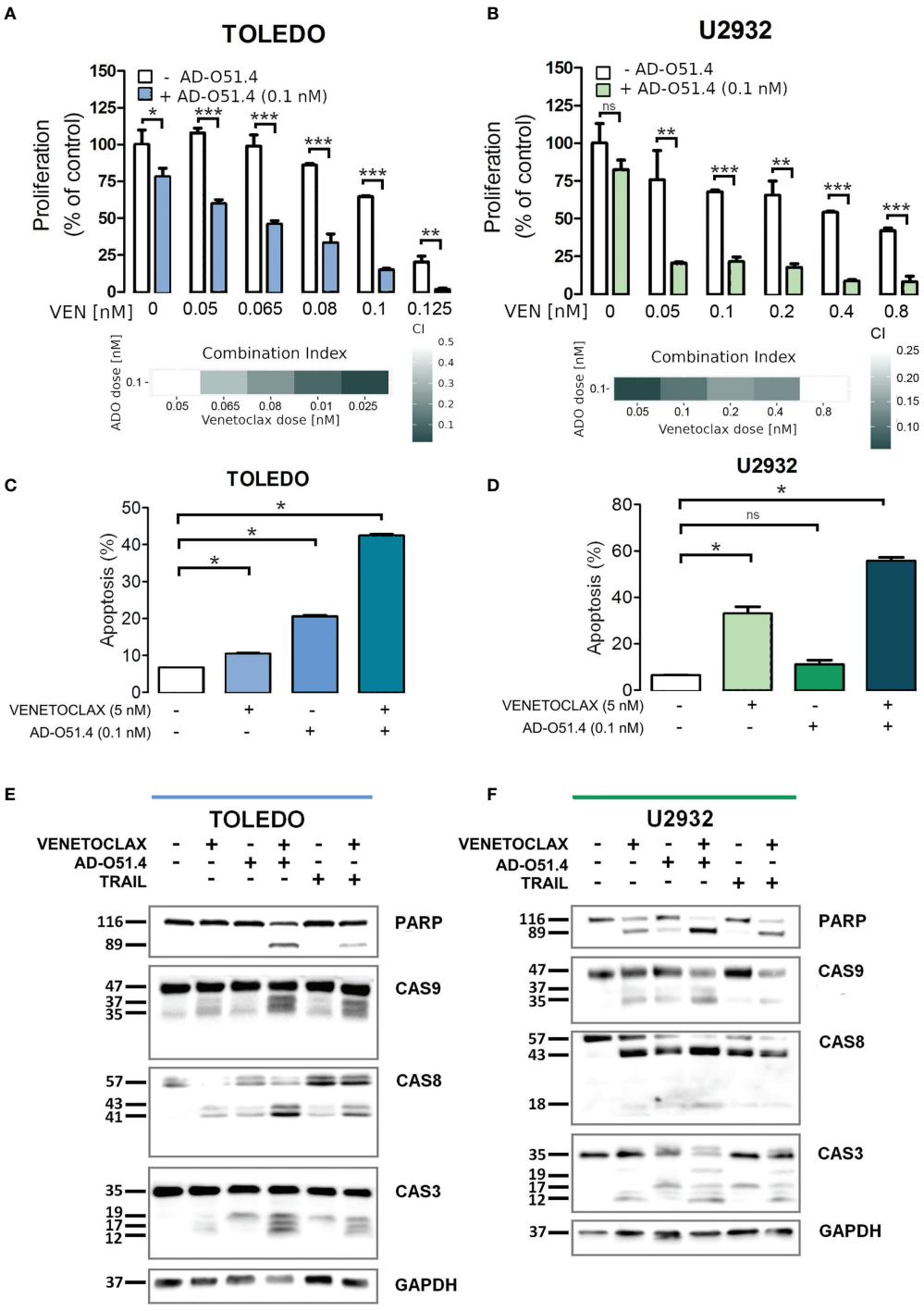

FIGURE 6
Venetoclax sensitizes resistant DLBCL cells to AD-O51.4 **A, B**. Primary resistant TOLEDO and U2932 cells were preincubated (5h) with indicated doses of venetoclax and then treated with AD-O51.4 for 72 h. Cell viability was assessed using an MTS assay in triplicates. Results were normalized to control (untreated) cells. Combination indexes (CI) for all dose combinations are indicated below the plots. **C, D.** Increased apoptosis in primary resistant TOLEDO and U2932 cells incubated with a combination of venetoclax and AD-O51.4. Cells were preincubated (5h) with 5 nM venetoclax and subsequently treated with z 0.1 nM AD-O51.4 for 24 h. Apoptosis was assessed using Annexin V/PI staining. Bars indicate the average of the combined fraction of early and late apoptotic cells (PI-/AnnexinV+ and PI+/AnnexinV+, respectively) from three replicates. Error bars indicate standard deviations. **E, F.** Expression and cleavage of caspase 3, 8, 9 and PARP in TOLEDO and U2932 cells after 1 h of preincubation with venetoclax (5 nM) and subsequent 5 h treatment with 0.1 nM AD-O51.4. In panels A-D, statistical differences were evaluated by *t*-test; *p-value<0.05, **p-value<0.005, ***p-value<0.001, ns – not significant.

10.3389/fonc.2022.1048741

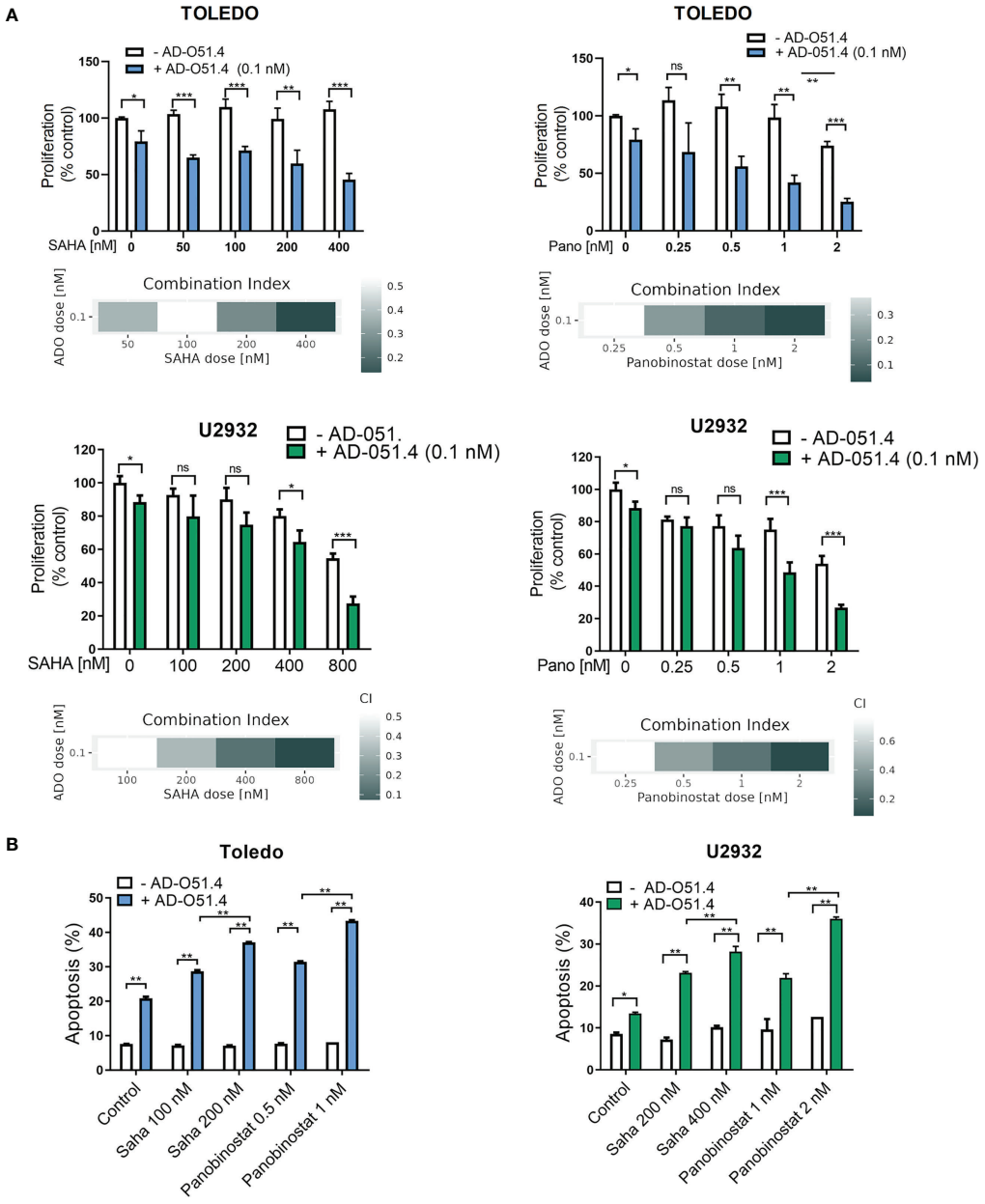

FIGURE 7
HDAC inhibitors sensitize resistant DLBCL cells to AD-O51.4. **(A)** Primary resistant TOLEDO and U2932 were preincubated with HDAC inhibitors SAHA (100 to 800 nM) or panobinostat (0.25 to 2 nM) or DMSO (control) for 24 h. Thereafter, cells were treated with 0.1 nM AD-O51.4 or PBS for additional 48 h. Cell viability was assessed using an MTS assay in triplicates. Bars and error bars indicate averages and standard deviations, respectively. Results were normalized to untreated cells (control). Combination indexes (CI) for all dose combinations are indicated below the plots. **(B)** Cells were treated as in A for 24h, and apoptosis was determined using Annexin V/PI staining. Bars indicate the average of the combined fraction of early and late apoptotic cells (PI-/AnnexinV+ and PI+/AnnexinV+, respectively) from two replicates. Error bars indicate standard deviations. In panels A-B, statistical differences were evaluated by *t*-test; *p-value<0.05, **p-value<0.005, ***p-value<0.001, ns – not significant.

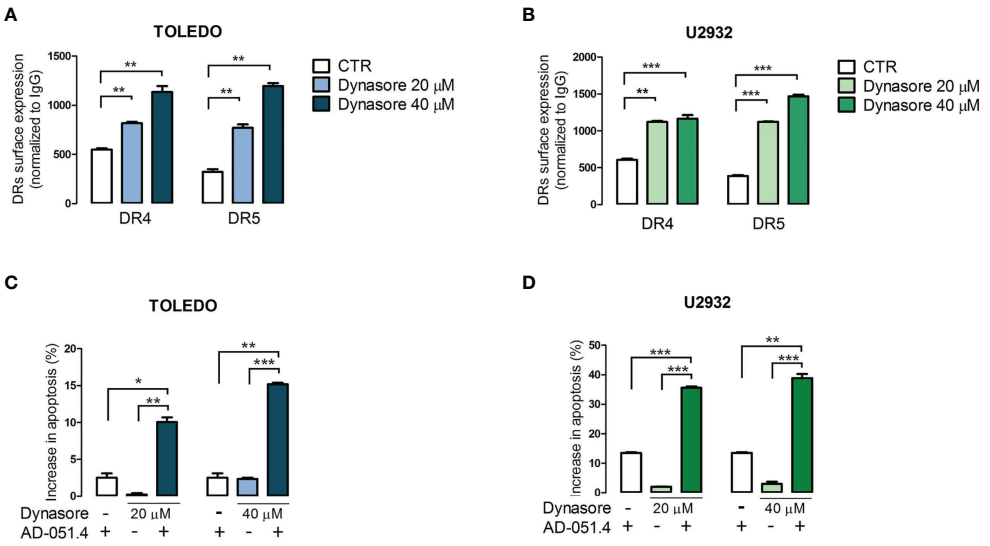

FIGURE 8
Dynamin inhibition increases the surface expression of death receptors and increases sensitivity to AD-O51.4. **A, B.** Dynamin inhibitor dynasore increases surface DR4 and DR5 expression in TOLEDO and U2932 in a dose-dependent manner. Cells were incubated with DMSO (control) or 20 - 40 μM dynasore for 30 minutes and fixed to prevent further endocytosis/recycling of DR4 and DR5. The expression of death receptors was assessed by flow cytometry. Bars indicate mean fluorescence intensity (MFI) normalized to isotype-matched antibody. Data represents an average of 3 experiments, error bars represent standard deviations. **C, D.** Inhibition of endocytosis sensitizes primary resistant TOLEDO and U2932 cells to AD-O51.4 -induced apoptosis. Cells were pretreated with dynasore (20 - 40 μM) for 1 h and treated with 0.1 nM AD-O51.4 for 24 h. Apoptosis was determined using Annexin V/PI staining. Bars indicate the average of the combined fraction of early and late apoptotic cells (PI-/AnnexinV+ and PI+/AnnexinV+, respectively) from two replicates. Error bars indicate standard deviations. In panels A-D, statistical differences were evaluated by *t*-test; *p-value<0.05, **p-value<0.005, ***p-value<0.001, ns – non significant.

be achieved by rational combinations, such as presented herein. Individualized therapeutic approaches based on such principles are most likely to increase the success rate of TRAIL-based clinical trials.

Data availability statement

The datasets presented in this study can be found in online repositories. The names of the repository/repositories and accession number(s) can be found below: https://www.ncbi.nlm.nih.gov/geo, accession number GSE208543.

Author contributions

KP designed experiments, performed research and wrote the manuscript. AŻ interpreted results and wrote the manuscript. EJ designed experiments and performed research. MN-K designed experiments and performed research. MS designed experiments, performed research and interpreted data. BŻ designed experiments, acquired funding and interpreted data. MK analyzed data. IR performed RNA-Seq. MM analyzed data. PJ acquired funding, designed experiments, performed research, analyzed data, wrote the manuscript. All authors contributed to the article and approved the submitted version.

Funding

The study was funded by the National Center for Research and Development grant STRATEGMED2/265566/6/NCBR/2015.

Acknowledgments

The authors would like to thank ADAMED S.A. for providing AD-O51.4.

Conflict of interest

BŻ is an ADAMED S.A. employee.

The remaining authors declare that the research was conducted in the absence of any commercial or financial relationships that could be construed as a potential conflict of interest.

Publisher's note

All claims expressed in this article are solely those of the authors and do not necessarily represent those of their affiliated organizations, or those of the publisher, the editors and the reviewers. Any product that may be evaluated in this article, or claim that may be made by its manufacturer, is not guaranteed or endorsed by the publisher.

Supplementary material

The Supplementary Material for this article can be found online at: https://www.frontiersin.org/articles/10.3389/fonc.2022.1048741/full#supplementary-material

References

1. Nicholson DW. From bench to clinic with apoptosis-based therapeutic agents. *Nature* (2000) 407(6805):810–6. doi: 10.1038/35037747

2. Carneiro BA, El-Deiry WS. Targeting apoptosis in cancer therapy. *Nat Rev Clin Oncol* (2020) 17(7):395–417. doi: 10.1038/s41571-020-0341-y

3. Hanahan D, Weinberg RA. Hallmarks of cancer: The next generation. *Cell* (2011) 144(5):646–74. doi: 10.1016/j.cell.2011.02.013

4. van Dijk M, Halpin-McCormick A, Sessler T, Samali A, Szegezdi E. Resistance to TRAIL in non-transformed cells is due to multiple redundant pathways. *Cell Death Dis* (2013) 4:e702. doi: 10.1038/cddis.2013.214

5. Sheridan JP, Marsters SA, Pitti RM, Gurney A, Skubatch M, Baldwin D, et al. Control of TRAIL-induced apoptosis by a family of signaling and decoy receptors. *Science* (1997) 277(5327):818–21. doi: 10.1126/science.277.5327.818

6. Walczak H, Miller RE, Ariail K, Gliniak B, Griffith TS, Kubin M, et al. Tumoricidal activity of tumor necrosis factor-related apoptosis-inducing ligand in vivo. *Nat Med* (1999) 5(2):157–63. doi: 10.1038/5517

7. Ashkenazi A, Pai RC, Fong S, Leung S, Lawrence DA, Marsters SA, et al. Safety and antitumor activity of recombinant soluble Apo2 ligand. *J Clin Invest* (1999) 104(2):155–62. doi: 10.1172/JCI6926

8. Forero A, Bendell JC, Kumar P, Janisch L, Rosen M, Wang Q, et al. First-in-human study of the antibody DR5 agonist DS-8273a in patients with advanced solid tumors. *Invest New Drugs* (2017) 35(3):298–306. doi: 10.1007/s10637-016-0420-1

9. Trarbach T, Moehler M, Heinemann V, Köhne CH, Przyborek M, Schulz C, et al. Phase II trial of mapatumumab, a fully human agonistic monoclonal antibody that targets and activates the tumour necrosis factor apoptosis-inducing ligand receptor-1 (TRAIL-R1), in patients with refractory colorectal cancer. *Br J Cancer* (2010) 102(3):506–12. doi: 10.1038/sj.bjc.6605507

10. Greco FA, Bonomi P, Crawford J, Kelly K, Oh Y, Halpern W, et al. Phase 2 study of mapatumumab, a fully human agonistic monoclonal antibody which targets and activates the TRAIL receptor-1, in patients with advanced non-small cell lung cancer. *Lung Cancer* (2008) 61(1):82–90. doi: 10.1016/j.lungcan.2007.12.011

11. Chapuy B, Stewart C, Dunford AJ, Kim J, Kamburov A, Redd RA, et al. Molecular subtypes of diffuse large b cell lymphoma are associated with distinct pathogenic mechanisms and outcomes. *Nat Med* (2018) 24(5):679–90. doi: 10.1038/s41591-018-0016-8

12. Wright GW, Huang DW, Phelan JD, Coulibaly ZA, Roulland S, Young RM, et al. A probabilistic classification tool for genetic subtypes of diffuse Large b cell lymphoma with therapeutic implications. *Cancer Cell* (2020) 37(4):551–568.e14. doi: 10.1016/j.ccell.2020.03.015

13. Alizadeh AA, Eisen MB, Davis RE, Ma C, Lossos IS, Rosenwald A, et al. Distinct types of diffuse large b-cell lymphoma identified by gene expression profiling. *Nature* (2000) 403(6769):503–11. doi: 10.1038/35000501

14. Monti S, Savage KJ, Kutok JL, Feuerhake F, Kurtin P, Mihm M, et al. Molecular profiling of diffuse large b-cell lymphoma identifies robust subtypes including one characterized by host inflammatory response. *Blood* (2011), 105 (5):1851–61. doi: 10.1182/blood-2004-07-2947

15. Schmitz R, Wright GW, Huang DW, Johnson CA, Phelan JD, Wang JQ, et al. Genetics and pathogenesis of diffuse Large b-cell lymphoma. *New Engl J Med* (2018) 378(15):1396–407. doi: 10.1056/NEJMoa1801445

16. Rosenwald A, Wright G, Chan WC, Connors JM, Campo E, Fisher RI, et al. The use of molecular profiling to predict survival after chemotherapy for diffuse large-b-cell lymphoma. *N Engl J Med* (2002) 346(25):1937–47. doi: 10.1056/NEJMoa012914

17. Rozga P, Kloska D, Pawlak S, Teska-Kaminska M, Galazka M, Bukato K, et al. Novel engineered TRAIL-based chimeric protein strongly inhibits tumor growth and bypasses TRAIL resistance. *Int J Cancer* (2020) 147(4):1117–30. doi: 10.1002/ijc.32845

18. Polo JM, Juszczynski P, Monti S, Cerchietti L, Ye K, Greally JM, et al. Transcriptional signature with differential expression of BCL6 target genes accurately identifies BCL6-dependent diffuse large b cell lymphomas. *Proc Natl Acad Sci U S A.* (2007) 104(9):3207–12. doi: 10.1073/pnas.0611399104

19. Chen L, Monti S, Juszczynski P, Ouyang J, Chapuy B, Neuberg D, et al. SYK inhibition modulates distinct PI3K/AKT- dependent survival pathways and cholesterol biosynthesis in diffuse Large b cell lymphomas. *Cancer Cell* (2013) 23 (6):826–38. doi: 10.1016/j.ccr.2013.05.002

20. Szydłowski M, Garbicz F, Jabłońska E, Górniak P, Komar D, Pyrzyńska B, et al. Inhibition of PIM kinases in DLBCL targets MYC transcriptional program and augments the efficacy of anti-CD20 antibodies. *Cancer Res* (2021) 81 (23):6029–43. doi: 10.1158/0008-5472.CAN-21-1023

21. Białopiotrowicz E, Noyszewska-Kania M, Kachamakova-Trojanowska N, Łoboda A, Cybulska M, Grochowska A, et al. Serine biosynthesis pathway supports MYC–miR-494–EZH2 feed-forward circuit necessary to maintain metabolic and epigenetic reprogramming of Burkitt lymphoma cells. *Cancers* (2020) 12(3):580. doi: 10.1038/s41419-020-03156-8

22. Rumienczyk I, Kulecka M, Ostrowski J, Mar D, Bomsztyk K, Standage SW, et al. Multi-organ transcriptome dynamics in a mouse model of cecal ligation and puncture-induced polymicrobial sepsis. *J Inflammation Res* (2021) 14:2377–88. doi: 10.2147/JIR.S307305

23. Kim D, Paggi JM, Park C, Bennett C, Salzberg SL. Graph-based genome alignment and genotyping with HISAT2 and HISAT-genotype. *Nat Biotechnol* (2019) 37(8):907–15. doi: 10.1038/s41587-019-0201-4

24. Yu G, Wang LG, Han Y, He QY. clusterProfiler: an r package for comparing biological themes among gene clusters. *OMICS: A J Integr Biol* (2012) 16(5):284–7. doi: 10.1089/omi.2011.0118

25. Polak A, Bialopiotrowicz E, Krzymieniewska B, Wozniak J, Stojak M, Cybulska M, et al. SYK inhibition targets acute myeloid leukemia stem cells by blocking their oxidative metabolism. *Cell Death Dis* (2020) 11(11):956. doi: 10.1038/s41419-020-03156-8

26. Chou TC, Talalay P. Quantitative analysis of dose-effect relationships: the combined effects of multiple drugs or enzyme inhibitors. *Adv Enzyme Regul* (1984) 22:27–55. doi: 10.1016/0065-2571(84)90007-4

27. Jouan-Lanhouet S, Arshad MI, Piquet-Pellorce C, Martin-Chouly C, Le Moigne-Muller G, Van Herreweghe F, et al. TRAIL induces necroptosis involving RIPK1/RIPK3-dependent PARP-1 activation. *Cell Death Differ* (2012) 19 (12):2003–14. doi: 10.1038/cdd.2012.90

28. Marconi M, Ascione B, Ciarlo L, Vona R, Garofalo T, Sorice M, et al. Constitutive localization of DR4 in lipid rafts is mandatory for TRAIL-induced apoptosis in b-cell hematologic malignancies. *Cell Death Dis* (2013) 4:e863. doi: 10.1038/cddis.2013.389

29. Hajji N, García-Domínguez DJ, Hontecillas-Prieto L, O'Neill K, de Álava E, Syed N. The bitter side of epigenetics: variability and resistance to chemotherapy. *Epigenomics* (2021) 13(5):397–403. doi: 10.2217/epi-2017-0112

30. Mettlen M, Chen PH, Srinivasan S, Danuser G, Schmid SL. Regulation of clathrin-mediated endocytosis. *Annu Rev Biochem* (2018) 87:871–96. doi: 10.1146/annurev-biochem-062917-012644

31. Kopczynski M, Statkiewicz M, Cybulska M, Kuklinska U, Unrug-Bielawska K, Sandowska-Markiewicz Z, et al. Cytotoxic efficacy and resistance mechanism of a TRAIL and VEGFA-peptide fusion protein in colorectal cancer models. *Int J Mol Sci* (2021) 22(6):3160. doi: 10.3390/ijms22063160

32. Stupack DG, Cheresh DA. Get a ligand, get a life: Integrins, signaling and cell survival. *J Cell Sci* (2002) 115(19):3729–38. doi: 10.1242/jcs.00071

33. Polanski R, Vincent J, Polanska UM, Petreus T, Tang EKY. Caspase-8 activation by TRAIL monotherapy predicts responses to IAPi and TRAIL combination treatment in breast cancer cell lines. *Cell Death Disease* (2015) 6 (10):e1893–3. doi: 10.1038/cddis.2015.234

34. Zhang L, Zhu H, Teraishi F, Davis JJ, Guo W, Fan Z, et al. Accelerated degradation of caspase-8 protein correlates with TRAIL resistance in a DLD1 human colon cancer cell line. *Neoplasia* (2005) 7(6):594–602. doi: 10.1593/neo.04688

frontiers | Frontiers in Oncology

TYPE Original Research
PUBLISHED 17 November 2022
DOI 10.3389/fonc.2022.1003957

OPEN ACCESS

EDITED BY
Aliyah Sohani,
Department of Pathology,
Massachusetts General Hospital and
Harvard Medical School, United States

REVIEWED BY
Youngwoo Jeon,
Catholic University of Korea,
South Korea
Mir Basharath Alikhan,
NorthShore University HealthSystem,
United States

*CORRESPONDENCE
Liping Su
sulp2005@163.com
Wenbin Qian
qianwb@zju.edu.cn
Jun Du
dujun@mail.sysu.edu.cn

†These authors have contributed equally to this work and share first authorship

SPECIALTY SECTION
This article was submitted to Hematologic Malignancies, a section of the journal Frontiers in Oncology

RECEIVED 26 July 2022
ACCEPTED 17 October 2022
PUBLISHED 17 November 2022

CITATION
Guan T, Zhang M, Liu X, Li J, Xin B, Ren Y, Yang Y, Wang H, Zhao M, Huang Y, Guo X, Du J, Qian W and Su L (2022) Circulating tumor DNA mutation profile is associated with the prognosis and treatment response of Chinese patients with newly diagnosed diffuse large B-cell lymphoma. *Front. Oncol.* 12:1003957. doi: 10.3389/fonc.2022.1003957

Circulating tumor DNA mutation profile is associated with the prognosis and treatment response of Chinese patients with newly diagnosed diffuse large B-cell lymphoma

Tao Guan[1†], Min Zhang[1†], Xiaolan Liu[1†], Jing Li[2], Beibei Xin[3], Yanxin Ren[4], Yuchao Yang[1], Hui Wang[1], Mengjing Zhao[5], Yunpeng Huang[1], Xiaojing Guo[1], Jun Du[6*], Wenbin Qian[7*] and Liping Su[1*]

[1]Shanxi Province Cancer Hospital/Shanxi Hospital Affiliated to Cancer Hospital, Chinese Academy of Medical Sciences/Cancer Hospital Affiliated to Shanxi Medical University, Taiyuan, China, [2]Department of Pathology, Shanxi Cancer Hospital, Affiliated Cancer Hospital of Shanxi Medical University, Taiyuan, China, [3]Department of Medicine, Shanghai Yuanqi Biomedical Technology Co., Ltd., Shanghai, China, [4]Department of Technology, Shanghai Yuanqi Biomedical Technology Co., Ltd., Shanghai, China, [5]Department of Biochemistry and Molecular Biology, School of Basic Medical Sciences, Shanxi Medical University, Taiyuan, China, [6]Department of Microbial and Biochemical Pharmacy, School of Pharmaceutical Sciences, Sun Yat-sen University, Guangzhou, China, [7]Department of Hematology, The Second Affiliated Hospital, College of Medicine, Zhejiang University, Hangzhou, China

Background: Characterization of gene mutation profiles can provide new treatment options for patients with diffuse large B-cell lymphoma (DLBCL). However, this method is challenged by the limited source of tissue specimens, especially those of DLBCL patients at advanced stages. Therefore, in the current study, we aimed to describe the gene mutation landscape of DLBCL using circulating tumor DNA (ctDNA) samples obtained from patients' blood samples, as well as to explore the relationship between ctDNA mutations and the prognosis and treatment response of patients with newly diagnosed DLBCL.

Methods: A total of 169 newly diagnosed Chinese DLBCL patients were included in this study, among which 85 patients were divided into a training set and 84 were assigned into a validation set. The mutation profile of a 59-gene panel was analyzed by targeted next generation sequencing (NGS) of the patients' ctDNA samples. Differences in clinical factors between patients with and without ctDNA mutations were analyzed. In addition, we also explored gene mutation frequencies between GCB and non-GCB subtypes, and the relationship between gene mutation status, clinical factors, mean VAF (variant allele frequencies) and the patients' overall survival (OS) and progression-free survival (PFS).

Results: ctDNA mutations were detected in 64 (75.3%) patients of the training set and 67 (79.8%) patients of the validation set. The most commonly mutated genes in both sets were *PCLO*, *PIM1*, *MYD88*, *TP53*, *KMT2D*, *CD79B*, *HIST1H1E* and *LRP1B*, with mutation frequencies of >10%. Patients with detectable ctDNA mutations trended to present advanced Ann Arbor stages (III-IV), elevated LDH (lactate dehydrogenase) levels, shorter OS and PFS, and a lower complete response (CR) rate to the R-CHOP regimen compared with DLBCL patients without ctDNA mutations. In addition, mean VAF (≥4.94%) and *PCLO* mutations were associated with poor OS and PFS.

Conclusion: We investigated the ctDNA mutation landscape in Chinese patients with newly diagnosed DLBCL and found that ctDNA could reflect tumor burden and patients with detectable ctDNA mutations trended to have shorter OS and PFS and a lower CR rate.

KEYWORDS

diffuse large B cell lymphoma, circulating tumor DNA, targeted next-generation sequencing, mutation, prognosis

Background

Diffuse large B-cell lymphoma (DLBCL) is the most common type of non-Hodgkin's lymphoma (NHL) worldwide with high clinical and genetic heterogeneity and worse outcomes (1). Gene expression profiling (GEP) divides DLBCL into two main subtypes, namely the germinal center B-cell (GCB) and activated B-cell (ABC) subtypes, with different responses to chemotherapy and targeted agents (2, 3). Recently, Schmitz et al. (4) and Wright et al. (5) classified DLBCL into five and seven genetic subtypes based on gene mutation and translocation profiles. Although these current genotyping techniques are widely accepted, they are challenged by the limited source of tissue specimens, especially for the detection of minimal residual disease (MRD). Thus, it is vital to develop alternative genotyping methods based on patients' body fluids.

Liquid biopsy is a non-invasive method reflecting intra-tumor heterogeneity with no need for fresh tissues (6) and has potential values in diagnosis, MRD monitoring and treatment choice of lymphomas (7, 8). Circulating tumor DNA (ctDNA) is the DNA fragment derived from tumor cells, which accounts for about 0.1% of cell-free DNA (cfDNA) and emerges as one of the most powerful tools for the early diagnosis of cancers (9). Evidence has demonstrated that the allele frequencies (AFs) of individual mutations detected in tumor samples are highly correlated with those observed in paired plasma cfDNA samples (8, 10). Thus, an analysis of ctDNA in cancer patients can reveal both genetic alterations, including single nucleotide variants (SNVs), insertions/deletions (Indels), chromosomal rearrangements, and copy number variations (CNVs), which can be used for genotyping, and ctDNA content, which can reflect tumor burden (11). Kurtz et al. (11) explored the prognostic value of ctDNA level before and during immunochemotherapy for patients with DLBCL from North America and Europe; they found that pretreatment ctDNA level was an independent prognostic factor in DLBCL. Liu et al. (10) explored the mutation profiles in Chinese patients with newly diagnosed and relapsed/refractory (R/R) DLBCL and observed highly consistent ctDNA and tissue mutation profiles in these patients (sensitivity: 87.50%).

Considering that different races can have varied gene mutation profiles and that the clinical value of ctDNA in Chinese patients remains largely unknown, in this study, we explored the clinical significance of ctDNA in 169 newly diagnosed Chinese DLBCL patients. These patients were first divided into a training set and a validation set. Then we assessed the relationship between ctDNA mutations and clinicopathological features, as well as the roles of ctDNA mutations, including the detected mutation site/gene number, the mean VAF (variant allele frequency) and the mutation status of genes, in the overall survival (OS) and progression-free survival (PFS) in these patients.

Patients and methods

Patients

A total of 169 newly diagnosed Chinese DLBCL patients were enrolled at Shanxi Cancer Hospital from June 2018 to December 2019. Patients were considered eligible for inclusion if they aged ≥ 18 years and had histologically confirmed DLBCL according to the 2016 World Health Organization (WHO) Classification of Tumors

of Haematopoietic and Lymphoid Tissues (12). The patients were classified into GCB and non-GCB subgroups according to the Hans algorithm (13). The disease was staged based on the 2014 Lugano Classification and the international prognositic index (IPI) was applied for risk stratification. Bone marrow involvement was assessed by flow cytometry, combined with immunoglobulin (Ig) gene rearrangement and positron emission tomography-computed tomography (PET-CT). A tumor lesion was judged as a bulky disease if the product of length and width of the tumor was ≥ 7.5 cm. All the patients were treated with the R-CHOP regimen (rituximab, cyclophosphamide, doxorubicin, vindesine, prednisone) and followed up until March, 2022. The treatment response, including CR (complete response), PR (partial response), SD (stable disease) and PD (progression disease), was assessed by CT/magnetic resonance imaging (MRI) and PET/CT according to the 2022 Guidelines of Chinese Society of Clinical Oncology (CSCO) after two to four cycles of the R-CHOP regimen. The data described in this manuscript were approved by the Ethics Committee of Shanxi Cancer Hospital (Ethical approval No.2021013) and conducted in accordance with the Helsinki declaration.

All study activities were approved by the Ethics Committee of Shanxi Cancer Hospital (Ethical approval No.2021013), and informed consent was obtained in accordance with the Declaration of Helsinki.

DNA extraction and targeted sequencing

Ten milimeter of peripheral blood samples were collected using EDTA-containing tubes within 1 week of receiving anticancer treatment and centrifuged at 820 g for 10 min to obtain plasma samples, which were centrifuged at 20,000 g for 10 min. Next, cfDNA was extracted using the QIAamp Circulating Nucleic Acid Kit (QIAGEN, Gemany) according to the manufacturer's instructions. Subsequently, the mutation profile of a 59-gene panel based on literatures (8, 14) was analyzed by targeted next generation sequencing (NGS) of the cfDNA samples (Shanghai Rightongene Bio-tech Co. Ltd, Shanghai, China; Supplementary Table 1) with Illumina NovaSeq 5000 (2×150-bp paired-end sequencing). In this study, VAF was defined as the ratio of the number of mutated alleles to the total number of alleles detected by NGS at a specific genome locus. Mutations with a VAF value ranging from 45% to 55% and ≥ 95% were identified and considered as heterozygous and homozygous germline mutations, respectively. Mean VAF was calculated as follows: Mean VAF = The sum of VAF values of all mutations/the total number of mutations.

Statistical analysis

The maftools ("clinical Enrichment") package of R was used to analyze the differences in clinical factors and gene mutation frequencies between the GCB and non-GCB subgroups using Chi-square test or Fisher's exact test. The tableone package of R was applied to analyze the differences in mean VAF between the two groups. Survival probabilities were estimated using the Kaplan-Meier method. We considered two survival endpoints: PFS, the time intervals from diagnosis to progression, relapse, or death from any cause; and OS, the time intervals from diagnosis to death resulting from any cause. Factors with a P value <0.1 were included in the multivariate Cox regression models. P values < 0.05 were considered as statistically significant.

Results

Relationship between clinicopathological features and ctDNA mutation status in patients with newly diagnosed DLBCL

A total of 169 newly diagnosed DLBCL cases with valid targeted NGS data were included in this study, with 85 patients in the training set and 84 in the validation set. Detailed clinical information of the 169 patients is provided in Supplementary Table 2. Sixty-four (75.3%) patients of the training set carried ctDNA mutations. These patients were significantly enriched in Ann Arbor stages III-IV (69.8% vs. 38.1% in Ann Arbor stages I-II, P=0.002) and tended to have elevated LDH (lactic dehydrogenase) levels (53.1% vs. 14.3%, P=0.004) as compared with the patients without detectable ctDNA mutations (Table 1). Similar results were observed in the validation set, in which 67 (79.8%) patients having detectable ctDNA mutations were significantly enriched in advanced Ann Arbor stages (76.1% vs. 47.1%, P=0.041) and exhibited elevated LDH levels (56.7% vs. 18.8%, P=0.014) as compared with those without detectable ctDNA mutations (Table 2). In addition, the presence of ctDNA mutations was also associated with a higher incidence of bulky disease (41.8% vs. 0.0%, P=0.003) only in the validation group (Table 2). These results indicated that ctDNA mutation status was closely associated with the staging and LDH level of newly diagnosed DLBCL patients.

ctDNA mutation profiles of patients with newly diagnosed DLBCL

Next, we explored the ctDNA mutation profiles of DLBCL patients of the training and validation sets. Detailed information on mutation sites is provided in Supplementary Table 3 and Supplementary Table 4. On average, we detected 6.1 ± 7.1 genetic mutations in patients with confirmed ctDNA mutation. Mutations in *PCLO* (26%), *PIM1* (25%), *MYD88* (21%), *TP53* (20%), *KMT2D* (16%), *CD79B* (12%), *HIST1H1E* (12%) and *LRP1B* (11%) genes were the most frequently detected variations, with mutations in each of the genes being found in no less than 9 patients (10%) of the training set (Figure 1A).

TABLE 1 The clinicopathologic features of DLBCL patients with mutation or without in training group.

Clinicopathologic features	Non-mutation group	Mutation group	*P*
Age, n (%)			0.663
≤60	10 (47.6)	25 (39.1)	
>60	11 (52.4)	39 (60.9)	
Gender			1.000
Female	8 (38.1)	24 (37.5)	
Male	13 (61.9)	40 (62.5)	
Bone marrow involvement, n (%)			0.192
No	21 (100.0)	54 (87.1)	
Yes	0 (0.0)	8 (12.9)	
Bulky disease, n (%)			0.131
No	19 (90.5)	44 (71.0)	
Yes	2 (9.5)	18 (29.0)	
Ann Arbor stage, n (%)			0.002
I-II	13 (61.9)	19 (30.2)	
II-IV	8 (38.1)	44 (69.8)	
Han's classification, n (%)			0.319
GCB	9 (45.0)	19 (29.7)	
Non-GCB	11 (55.0)	45 (70.3)	
IPI score, n (%)			0.103
0-3	20 (95.2)	47 (75.8)	
4-5	1 (4.8)	15 (24.2)	
LDH, n (%)			0.004
Normal	18 (85.7)	30 (46.9)	
Elevated	3 (14.3)	34 (53.1)	
Response to therapy, n (%)			0.048
CR	14 (20.3)	26 (37.7)	
PR+SD+PD	4 (5.8)	25 (36.2)	

LDH, lactic dehydrogenase; CR, complete response; PR, partial response; SD, stable disease; PD, progression disease.

Consistently, *PCLO* (26%), *PIM1* (24%), *MYD88* (20%), *TP53* (24%), *KMT2D* (17%), *CD79B* (17%), *HIST1H1E* (17%) and *LRP1B* (20%) genes also showed high mutation frequencies in the validation set (Figure 1B). In addition, we assessed the difference in ctDNA mutation profile between the GCB and non-GCB subtypes in the 169 DLBCL patients. The results demonstrated that the mutation frequencies of *PIM1* (30.4% vs. 12.7%) and *CD79B* (18.8% vs. 5.5%) were significantly higher in patients of the non-GCB subtype than in those of the GCB subtype (Figure 1C). These results depicted the ctDNA mutation landscape of patients with newly diagnosed DLBCL.

ctDNA mutation status was associated with the response to R-CHOP and clinical manifestation in newly diagnosed DLBCL patients

Next, we assessed the relationship between ctDNA mutation status and the response to R-CHOP regimen in newly diagnosed DLBCL patients. The CR rate in DLBCL patients without ctDNA mutations was obviously higher than that in those carrying ctDNA mutations in both the training (P=0.048) and validation sets (P=0.050) (Tables 1, 2). However, there were no valid differences in the rates of PR, SD and PD between DLBCL patients with different mutation numbers, which is mean VAF values and mutation profiles because the training and validation sets exhibited inconsistent findings. In addition, we compared the mean VAF value in patients with different ages (≤60 vs. >60 years), genders (male vs. female), bone marrow involvement statuses (positive vs. negative), Hans classifications (GCB vs. non-GCB), bulky disease statuses (positive vs. negative), IPIs (1-3 vs. 4-5), Ann Arbor stages (I-II vs. III-IV) and LDH levels (high vs. low). The results showed that the mean VAF value was significantly increased in patients with bone marrow involvement, higher IPI scores (4, 5) and elevated LDH levels in both of the training (Figures 2A–C) and validation sets (Figures 2D–F). Collectively, these results demonstrated that ctDNA mutations were associated with a lower CR rate and

TABLE 2 The clinicopathologic features of DLBCL patients with mutation or without in validation group.

Clinicopathologic features	Non-mutation group	Mutation group	*P*
Age, n (%)			0.029
≤60	14 (82.4)	33 (49.3)	
>60	3 (17.6)	34 (50.7)	
Gender, n (%)			1.000
Female	7 (41.2)	29 (43.3)	
Male	10 (58.8)	38 (56.7)	
Bone marrow involvement, n (%)			0.525
No	17 (100.0)	58 (92.1)	
Yes	0 (0.0)	5 (7.9)	
Bulky disease			0.003
No	17 (100.0)	39 (58.2)	
Yes	0 (0.0)	28 (41.8)	
Ann Arbor stage, n (%)			0.041
I-II	9 (52.9)	16 (23.9)	
III-IV	8 (47.1)	51 (76.1)	
Han's classification, n (%)			0.085
GCB	9 (52.9)	18 (27.3)	
Non-GCB	8 (47.1)	48 (72.7)	
IPI score, n (%)			0.058
0-3	17 (100.0)	51 (76.1)	
4-5	0 (0.0)	16 (23.9)	
LDH, n (%)			0.014
Normal	13 (81.2)	29 (43.3)	
Elevated	3 (18.8)	38 (56.7)	
Response to therapy, n (%)			
CR	12 (16.9)	26 (36.6)	
PR+SD+PD	4 (5.6)	29 (40.8)	

LDH, lactic dehydrogenase; CR, complete response; PR, partial response; SD, stable disease; PD, progression disease.

aggressive clinical manifestation in patients with newly diagnosed DLBCL.

DLBCL patients carrying ctDNA mutations demonstrated poor prognosis

We also compared survival outcomes between patients with and without ctDNA mutations. In the training set, the 64 patients with ctDNA mutations exhibited significantly shorter OS than the 19 patients without ctDNA mutations (P=0.03) (Figure 3A). PFS was also shorter in patients with ctDNA mutations, albeit the difference was not statistically significant (P=0.095) (Figure 3B). Next, we validated these results in the validation set, in which 67 patients had detectable ctDNA mutations and 17 patients did not. Compared with patients without ctDNA mutations, both OS (P=0.011) (Figure 3C) and PFS (P=0.0032) (Figure 3D) were significantly shorter in patients with ctDNA mutations. These results indicated that ctDNA mutations were associated with poor prognosis in patients with newly diagnosed DLBCL.

Mean VAF and *PCLO* mutations were associated with poor prognosis in patients with newly diagnosed DLBCL

To further explore the relationship between ctDNA mutation status and the prognosis of patients with newly diagnosed DLBCL, we assessed the effects of mutation number, mutated gene number and mean VAF on OS and PFS using Kaplan-Meier curves generated based the parameters' average/median values. The results demonstrated that only mean VAF (the median value of which was 4.94%) was closely associated with patients' prognosis in the training set. Specifically, the OS (P=0.024) and PFS (P=0.043) of patients with a mean VAF ≥ 4.94% were significantly shorter than those of patients with a mean VAF < 4.94% in the training set (Figures 4A, B). We next verified these findings in the

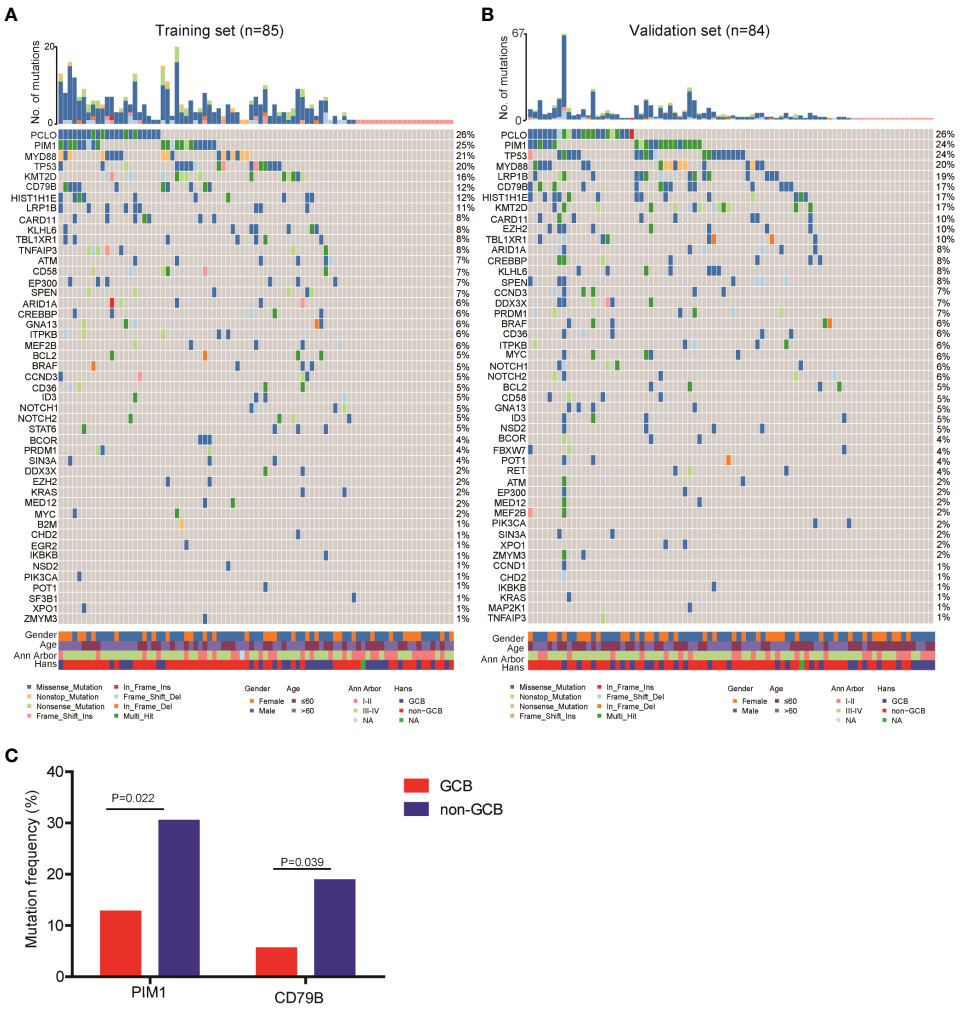

FIGURE 1
Mutation landscape of ctDNA samples from newly diagnosed DLBCL patients. ctDNA mutation profiles of newly diagnosed DLBCL patients in the **(A)** training and **(B)** validation sets. **(C)** The mutation frequencies of *PIM1* and *CD79B* were significantly increased in the ctDNA samples of non-GCB DLBCL patients as compared with GCB DLBCL patients.

validation set. Compared with those in patients with a mean VAF < 4.94%, the OS (P=0.093) and PFS (P=0.014) were shorter in patients with a mean VAF ≥ 4.94%, albeit the difference in OS was not statistically significant (Figures 4C, D).

In addition, we assessed the effects of gene mutation status on the OS and PFS of patients with newly diagnosed DLBCL. Due to the relatively small sample size, we only assessed genes with a mutation frequency ≥ 10%. In the training set, *LRP1B* (Supplementary Figures 1A, B) and *PCLO* mutations (Figures 5A, B) were significantly associated with shorter OS and PFS; whereas in the validation set, only *PCLO* mutations were significantly associated with shorter OS and PFS (Figures 5C, D). These results demonstrated that a high mean VAF value and *PCLO* mutations predicted poor prognosis in patients with newly diagnosed DLBCL.

Multivariate analysis of prognostic factors in patients with newly diagnosed DLBCL

Finally, multivariate Cox analysis was performed to further explore prognostic factors in patients with newly diagnosed DLBCL. The univariate Cox analysis showed that age > 60 years was an influencing factor on both OS (P=0.038) and PFS (P=0.083) in the training set; meanwhile, bulky disease status (P=0.099) was an influencing factor on PFS in the training set (Table 3). Afterwards, factors with a P value < 0.1, namely the clinical factors (age and/or bulky disease status), mean VAF, and *PCLO* mutation status, were included in the multivariate analysis. The results showed that age (> 60 years) and mean VAF (≥ 4.94%) were independent influencing factors on both OS

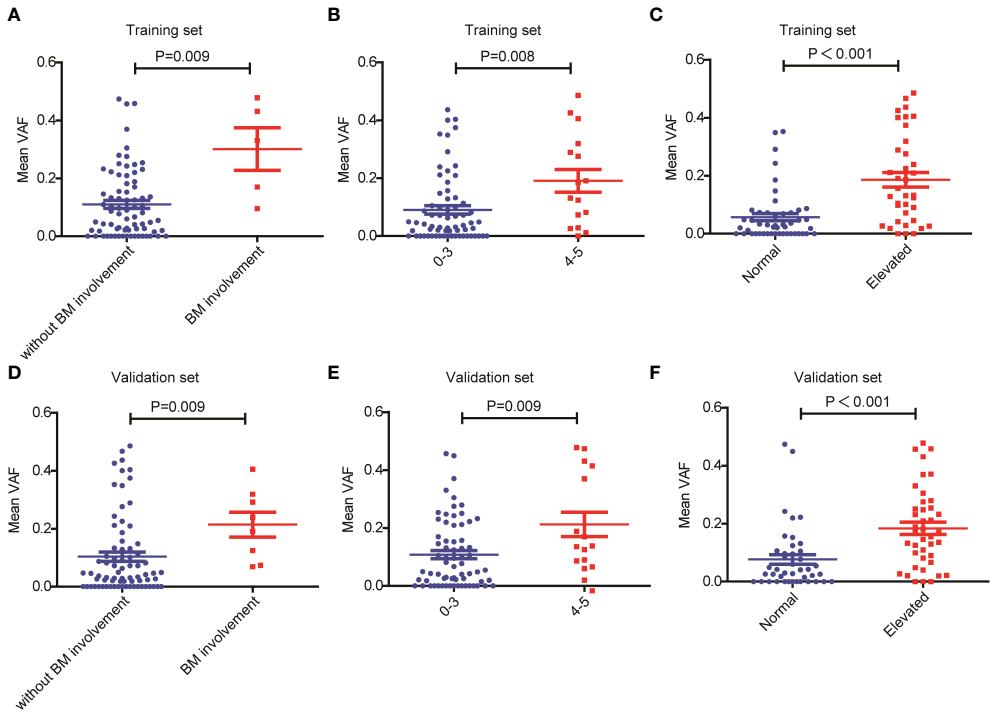

FIGURE 2
Relationship between mean VAF and clinical features in patients with newly diagnosed DLBCL. Mean VAF was increased in patients with **(A, D)** bone marrow involvement, **(B, E)** higher IPI scores and **(C, F)** elevated LDH levels in the training and validation sets.

and PFS in the training set (Table 4). In the validation set, age (> 60 years) and *PCLO* mutation status were influencing factors on OS, while age (> 60 years) and bulky disease status were influencing factors on PFS (Table 4) . These results further verified the close relationship between ctDNA mutation and the prognosis of patients with newly diagnosed DLBCL.

Discussion

Genetic heterogeneity is a major cause of increased risk and treatment failure in DLBCL. Several studies (8, 10, 14–16) have proved that the mutations detected in blood samples were similar to those identified in tumor tissue, with a concordance rate over 80%.In the present study, we performed targeted sequencing of 59 lymphoma-related genes, the same panel as Liu et al. (10) to analyze the clinical value of ctDNA mutation in 169 Chinese patients with newly diagnosed DLBCL. To increase the reliability of our findings, the 169 patients were randomly divided into a training set (n=85) and a validation set (n=84). Our results demonstrated that detectable ctDNA mutations, a mean VAF value ≥ 4.94%, and *PCLO* mutations were strongly associated with shorter OS and PFS in the newly diagnosed DLBCL patients.

We found that *PCLO* (piccolo presynaptic cytomatrix protein), *PIM1, CD79B* and *MYD88* (genes involved in the NF-κB signaling pathway), *LRP1B* and *TP53* (tumor suppressive genes), as well as *KMT2D* and *HIST1H1E* (histone modifying genes) were the most commonly mutated genes in the 169 newly diagnosed DLBCL patients. According to the genetic landscape of DLBCL in western countries, the most frequently mutated genes are sequentially *KMT2D*, *MYD88*, *CREBBP*, *TP53* and *PIM1* (17, 18). In contract, the most frequently mutated genes in Chinese DLBCL patients are sequentially *PIM1*, *BTG2*, *TP53*, *HIST1H1E* and *KMT2D* (19). The higher proportion of non-GCB DLBCL cases in Chinese patients may be a reason for this difference. According to literature, genes related to histone methylation or acetylation (*EZH2*, *EP300*, *CREBBP* and *KMT2D*) and the PI3K/AKT and JAK/STAT pathways are commonly mutated in the GCB subtype of DLBCL patients, while genes related to the B-cell receptor and NF-κB signaling pathways, such as *MYD88*, *CD79A/B*, *CARD11*, *PIM1* and *TNFAIP3*, are commonly mutated in the ABC subtype (20). Consistently, we found that the mutation frequencies of *PIM1* and *CD79B* were significantly higher in DLBCL patients with the non-GCB subtype than in those with the GCB subtype.

In addition, we were able to detect ctDNA mutations in 64 (75.3%) out of 85 patients in the training set and 67 (79.8%) out of 84 patients in the validation set. Rivas-Delgado et al. (21) were able to detect at least one ctDNA mutation in 69 of 79 patients (87%) with DLBCL. This slight difference in ctDNA mutation

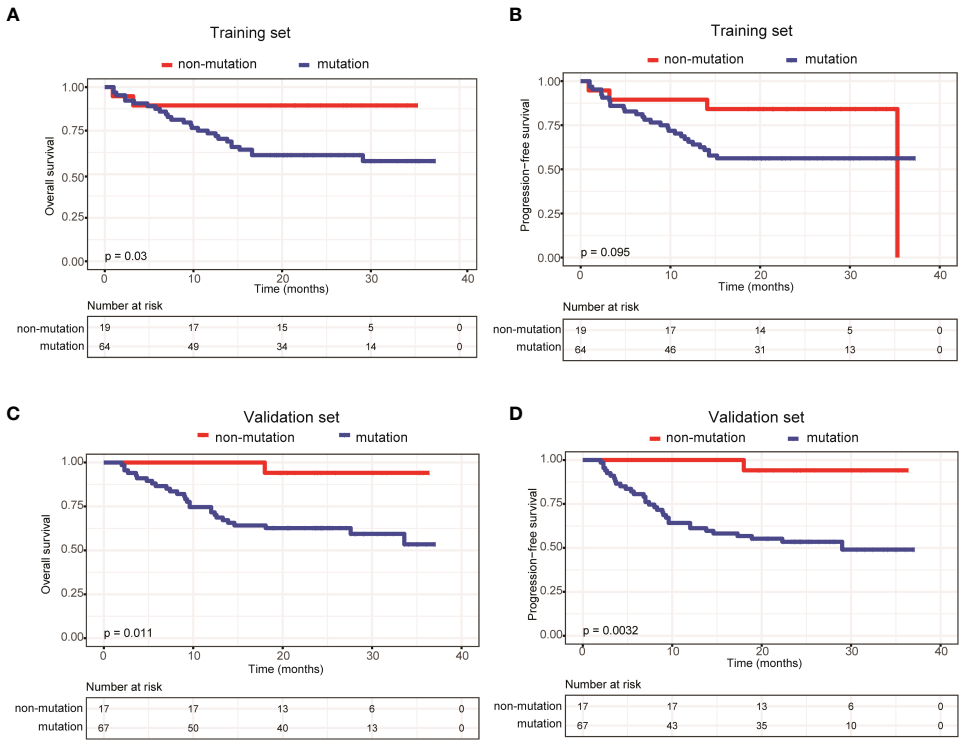

FIGURE 3
Patients carrying ctDNA mutations trended to have poor prognosis. Kaplan-Meier curves were applied to compare the **(A)** OS and **(B)** PFS between patients with and without ctDNA mutations in the training set. Kaplan-Meier curves were applied to compare the **(C)** OS and **(D)** PFS between patients with and without ctDNA mutations in the validation set.

detection rate may be caused by different panels of genes sequenced: Rivas-Delgado et al. (21) performed targeted sequencing on 112 genes, while we analyzed 59 genes. In addition, we found that patients with detectable ctDNA mutations had shorter OS and PFS in both the training and validation sets. Furthermore, patients carrying ctDNA mutations were significantly enriched in more advanced Ann Arbor stages (stages III-IV) and generally exhibited elevated LDH levels. These findings establish a link between ctDNA mutation status and the prognosis of patients with DLBCL. Recently, Kurtz et al. (22) indicated that 25% of ctDNA-negative patients demonstrated by cancer personalized profiling by deep sequencing (CAPP-Seq) were found to be ctDNA-positive, as revealed by phased variant enrichment and detection sequencing (PhasED-Seq), after two cycles of therapy and presented with poor outcomes.

ctDNA VAF has been closely associated with the clinical features and prognosis of various cancers, and is considered as a new biomarker for tumor burden (23, 24). For example, Fu et al. (25) found that the VAF values of *TP53* p.Y88C and *LATS2* p.F972L were decreased in B-cell lymphoma patients with CR. Desch et al. (26) reported that ctDNA VAF values were strongly associated with total metabolic tumor volume (TMTV) and the incidence of bulky disease in pediatric Hodgkin's lymphoma. In addition. the median VAF of non-DNMT3A clones increased from 1% at the time of autologous stem cell transplantation (ASCT) to 37% at the diagnosis of therapy-related myeloid neoplasms (tMNs) (27). In the present study, we found that the mean VAF values were significantly increased in patients with bone marrow involvement, higher IPI scores and elevated LDH levels in both the training and validation sets. Additionally, we observed that in the training set, patients with a mean VAF ≥ 4.94% showed inferior OS and PFS as compared with patients with a mean VAF < 4.94%. This finding was verified in the validation set.

Moreover, we assessed the relationship between ctDNA mutation status and the prognosis of patients with newly diagnosed DLBCL. Notably, we found that patients with *PCLO* mutations had shorter OS and PFS. *PCLO* encodes a protein that functions as a part of the presynaptic cytoskeletal matrix, which is thought to be involved in neurotransmitter release regulation. It has been suggested that *PCLO* might play a role in calcium sensing. *PCLO* mutations have been detected by whole-exom sequencing in a variety of tumors, including DLBCL (28–31). In the mesenchymal subtype of glioblastomas, *PCLO* mutations have been shown to be associated with poor prognosis (31), but

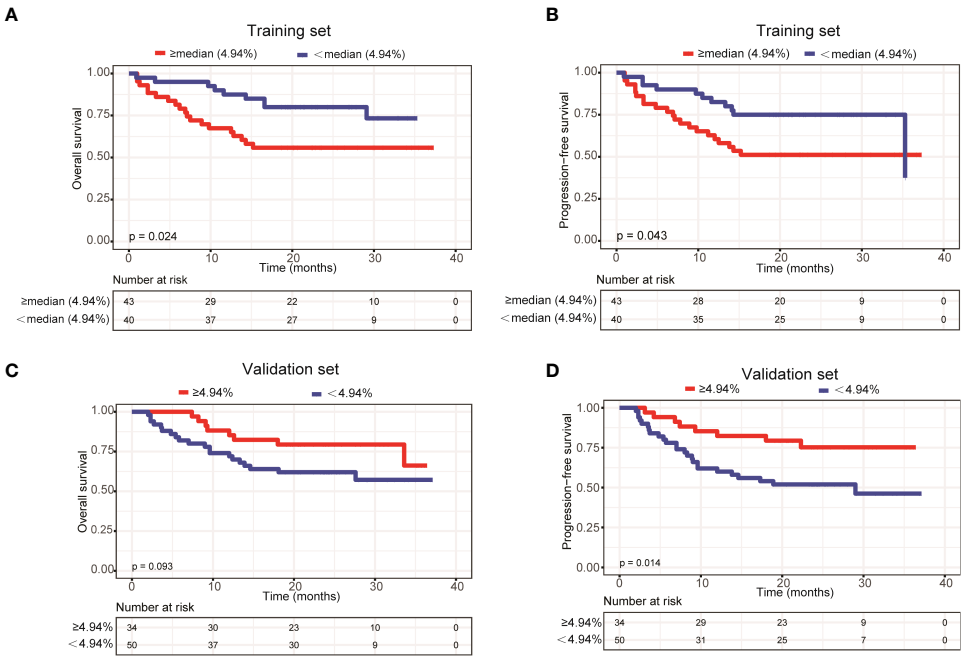

FIGURE 4
Patients with a mean VAF value ≥ 4.94% trended to have poor prognosis. Kaplan-Meier curves were applied to compare the **(A)** OS and **(B)** PFS between patients with mean VAF values ≥ 4.94% and < 4.94% in the training set. Kaplan-Meier curves were applied to compare the **(C)** OS and **(D)** PFS between patients with mean VAF values ≥ 4.94% and < 4.94% in the validation set.

its association with the prognosis of DLBCL has not been reported. Mutations in *PCLO* are usually considered as passenger mutations with no functional consequences in DLBCL (28). In this study, *PIM1* (34.1%), *MYD88* (31.8%) and *TP53* (20.5%) were the most common co-mutated genes with *PCLO* mutations detected in the ctDNA samples of DLBCL patients. Furthermore, we found that the mutation frequency of *TNFAIP3* in *PCLO* mutated DLBCL patients was significantly higher than that of DLBCL patients without *PCLO* mutations [1.6% (2/125) vs. 13.6% (6/44)]. These four genes (*PIM1*, *MYD88*, *TP53*, *TNFAIP3*) has been identified to be the mutational drivers in DLBCL, which might partly explain the poor prognosis of patients carrying *PCLO* mutations (32–35). Additional work is needed to resolve the mechanism of action and role of *PCLO* mutations in DLBCL.

Evidence has demonstrated that ctDNA mutations are correlated with treatment response in DLBCL patients (36). According to the current gold standard for evaluating treatment response in lymphoma, the sensitivity and specificity of ctDNA profiling were 94.7% and 83.3% in refractory or relapse (r/r) DLBCL patients after CAR-T treatment; the median numbers of baseline ctDNA mutations in patients who remained long-term CR and in patients who relapsed or became refractory to CAR-T therapy were 3.0 and 14.3, respectively (36). Herein, we explored the relationship between ctDNA mutation status, the number of ctDNA mutations and mean VAF and the curative effect of R-CHOP regimen in DLBCL patients. Our results showed that patients without detectable ctDNA mutations had a higher CR rate to R-CHOP treatment as compared with patients with detectable ctDNA mutations, while the ctDNA mutation number and mean VAF showed no significant impacts on the CR rate.

Our study showed that age (> 60 years) and mean VAF (≥ 4.94%) were independent influencing factors on prognosis in the training set, while age (> 60 years), *PCLO* mutations and bulky disease status were independent influencing factors on prognosis in the validation set. The high heterogeneity of DLBCL may have caused these differences between the training and validation sets. Of course, the small sample size of our study may be another reason for the differences. In fact, the relatively small sample size is the main limitation of the present study, although we have recruited the largest cohort of Chinese DLBCL patients to date. To this end, we intend to include more Chinese DLBCL patients for analysis in the future.

Taken together, we herein have described the ctDNA mutation landscape of a largest cohort of Chinese patients with newly diagnosed DLBCL to date. Our results suggested that patients with detectable ctDNA mutations, a higher mean VAF value or *PCLO* mutations trended to have shorter OS and PFS and a lower CR rate. Our study provides evidence to support the feasibility of using ctDNA samples obtained from patients' blood in prognosis prediction of newly diagnosed DLBCL.

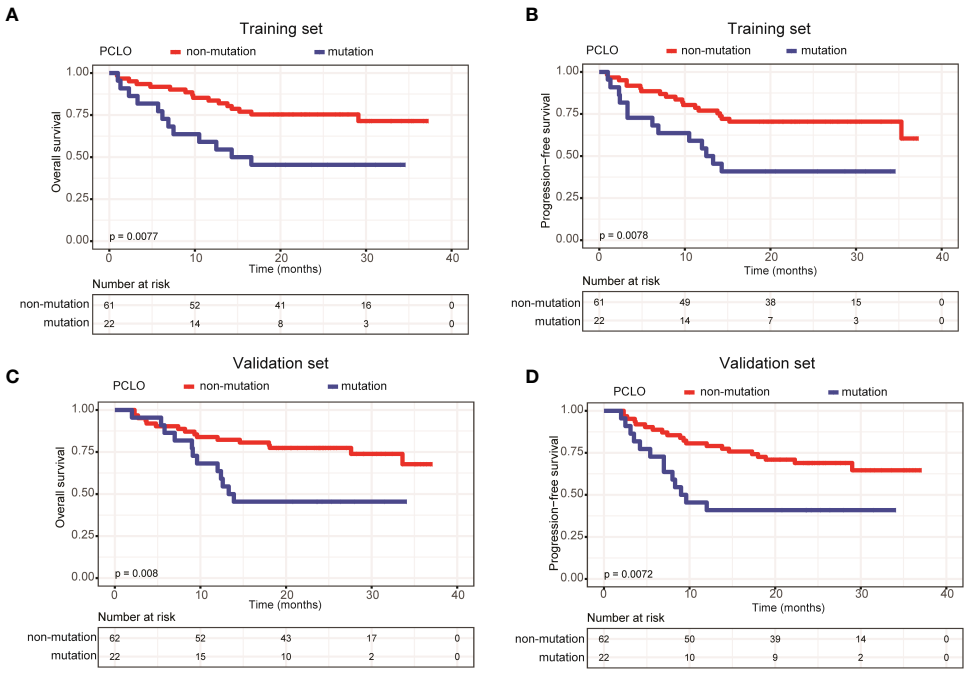

FIGURE 5
Patients carrying *PCLO* mutations trended to have poor prognosis. Kaplan-Meier curves were applied to compare the **(A)** OS and **(B)** PFS between patients with and without *PCLO* mutations in the training set. Kaplan-Meier curves were applied to compare the **(C)** OS and **(D)** PFS between patients with and without *PCLO* mutations in the validation set.

TABLE 3 Univariate Cox analysis of the influencing factors of PFS and OS in the training set.

Clinical factors	OS		PFS	
	HR (95% CI)	P	HR (95% CI)	P
Age (>60)	2.651 (1.053-6.671)	0.038	2.066 (0.909-4.694)	0.083
Ann Arbor stage (III-IV)	1.673 (0.697-4.013)	0.249	1.583 (0.697, 3.594)	0.273
Han's classification (non-GCB)	0.710 (0.314-1.607)	0.411	0.870 (0.394-1.924)	0.731
Bulky disease	1.920 (0.846-4.360)	1.920	1.918 (0.885-4.159)	0.099
LDH level (elevated)	1.760 (0.799-3.881)	0.161	1.699 (0.808-3.572)	0.162

HR, Hazard ratio; CI, confidence interval.

TABLE 4 Multivariate Cox analysis of the influencing factors of PFS and OS in the training set and validation set.

Clinical factors	Training set				Validation set			
	OS		PFS		OS		PFS	
	HR (95% CI)	P	HR (95% CI)	P	HR (95% CI)	P	HR (95% CI)	P
Age (>60)	3.6 (1.4-9.2)	0.01	2.6 (1.1-6.4)	0.03	2.2 (1.0-4.9)	0.05	2.1 (1.0-4.4)	0.04
Bulky disease	—	—	1.2 (0.5-2.7)	0.69	—	—	2.4 (1.1-5.0)	0.03
VAF (4.94%)	2.6 (1.1-6.4)	0.04	2.5 (1.1-5.8)	0.04	1.4 (0.6-3.5)	0.51	1.4 (0.6-3.6)	0.48
PCLO mutation	1.9 (0.8-4.3)	0.15	1.8 (0.8-4.0)	0.17	2.7 (1.2-4.3)	0.02	2.0 (1.0-4.3)	0.06

HR, Hazard ratio; CI, confidence interval.

Data availability statement

The data presented in the study are deposited in the National Genomics Data Center repository (https://ngdc.cncb.ac.cn), accession number PRJCA012539.

Ethics statement

The studies involving human participants were reviewed and approved by The Ethics Committee of Shanxi Cancer Hospital. Written informed consent for participation was not required for this study in accordance with the national legislation and the institutional requirements.

Author contributions

Concept and design: LS, WQ, JD. Acquisition, analysis, or interpretation of data: TG, MeZ, JL, XL, YR, YY, HW, XG, YH. Patients' follow-up: MiZ, YY, MeZ. Statistical analysis: BX, TG, MJZ. Drafting of the manuscript: TG, MiZ, BX. Supervision: LS. All authors contributed to the article and approved the submitted version.

Funding

This study was supported by the foundation of Key Laboratory Construction Project Supported by Health Commission of Shanxi Province (Grant No. 2020SYS11), Shanxi Province Health Research Project Supported by Health Commission of Shanxi Province (Grant No. 2022121), and Research Project Supported by Shanxi Scholarship Council of China (Grant No. 2020-194).

Acknowledgments

We thank Shanghai Rightongene Biotechnology Co. Ltd. (Shanghai, China) for the assistance in targeted sequencing and mutation analysis. In the meanwhile, we sincerely thank Hongsheng Wang, Department of Tumor Pharmacology, SUN YAT-SEN UNIVERSITY, for his linguistic and logic advise.

Conflict of interest

Author BX and YR are employed by Shanghai Yuanqi Biomedical Technology Co., Ltd.

The remaining authors declare that the research was conducted in the absence of any commercial or financial relationships that could be construed as a potential conflict of interest.

Publisher's note

Supplementary material

The Supplementary Material for this article can be found online at: https://www.frontiersin.org/articles/10.3389/fonc.2022.1003957/full#supplementary-material

References

1. Coiffier B, Thieblemont C, Van Den Neste E, Lepeu G, Plantier I, Castaigne S, et al. Long-term outcome of patients in the lnh-98.5 trial, the first randomized study comparing rituximab-chop to standard chop chemotherapy in dlbcl patients: A study by the groupe d'etudes des lymphomes de l'adulte. *Blood* (2018) 2010(12):2040–5.

2. Alizadeh AA, Eisen MB, Davis RE, Ma C, Lossos IS, Rosenwald A, et al. Distinct types of diffuse Large b-cell lymphoma identified by gene expression profiling. *Nature* (2000) 403(6769):503–11. doi: 10.1038/35000501

3. Rosenwald A, Wright G, Chan WC, Connors JM, Campo E, Fisher RI, et al. The use of molecular profiling to predict survival after chemotherapy for diffuse Large-B-Cell lymphoma. *N Engl J Med* (2002) 346(25):1937–47. doi: 10.1056/NEJMoa012914

4. Schmitz R, Wright GW, Huang DW, Johnson CA, Phelan JD, Wang JQ, et al. Genetics and pathogenesis of diffuse Large b-cell lymphoma. *N Engl J Med* (2018) 378(15):1396–407. doi: 10.1056/NEJMoa1801445

5. Wright GW, Huang DW, Phelan JD, Coulibaly ZA, Roulland S, Young RM, et al. A probabilistic classification tool for genetic subtypes of diffuse Large b cell lymphoma with therapeutic implications. *Cancer Cell* (2020) 37(4):551–68.e14. doi: 10.1016/j.ccell.2020.03.015

6. Decruyenaere P, Offner F, Vandesompele J. Circulating rna biomarkers in diffuse Large b-cell lymphoma: A systematic review. *Exp Hematol Oncol* (2021) 10 (1):13. doi: 10.1186/s40164-021-00208-3

7. Cirillo M, Craig AFM, Borchmann S, Kurtz DM. Liquid biopsy in lymphoma: Molecular methods and clinical applications. *Cancer Treat Rev* (2020) 91:102106. doi: 10.1016/j.ctrv.2020.102106

8. Rossi D, Diop F, Spaccarotella E, Monti S, Zanni M, Rasi S, et al. Diffuse Large b-cell lymphoma genotyping on the liquid biopsy. *Blood* (2017) 129(14):1947–57. doi: 10.1182/blood-2016-05-719641

9. Cescon DW, Bratman SV, Chan SM, Siu LL. Circulating tumor DNA and liquid biopsy in oncology. *Nat Cancer* (2020) 1(3):276–90. doi: 10.1038/s43018-020-0043-5

10. Liu H, Yang C, Zhao X, Le J, Wu G, Wei J, et al. Genotyping on ctdna identifies shifts in mutation spectrum between newly diagnosed and Relapse/Refractory dlbcl. *Onco Targets Ther* (2020) 13:10797–806. doi: 10.2147/OTT.S275334

11. Kurtz DM, Scherer F, Jin MC, Soo J, Craig AFM, Esfahani MS, et al. Circulating tumor DNA measurements as early outcome predictors in diffuse Large

b-cell lymphoma. *J Clin Oncol* (2018) 36(28):2845–53. doi: 10.1200/JCO.2018.78.5246

12. Swerdlow SH, Campo E, Pileri SA, Harris NL, Stein H, Siebert R, et al. The 2016 revision of the world health organization classification of lymphoid neoplasms. *Blood* (2016) 127(20):2375–90. doi: 10.1182/blood-2016-01-643569

13. Hans CP, Weisenburger DD, Greiner TC, Gascoyne RD, Delabie J, Ott G, et al. Confirmation of the molecular classification of diffuse Large b-cell lymphoma by immunohistochemistry using a tissue microarray. *Blood* (2004) 103(1):275–82. doi: 10.1182/blood-2003-05-1545

14. Scherer F, Kurtz DM, Newman AM, Stehr H, Craig AF, Esfahani MS, et al. Distinct biological subtypes and patterns of genome evolution in lymphoma revealed by circulating tumor DNA. *Sci Transl Med* (2016) 8(364):364ra155. doi: 10.1126/scitranslmed.aai8545

15. Bohers E, Viailly PJ, Dubois S, Bertrand P, Maingonnat C, Mareschal S, et al. Somatic mutations of cell-free circulating DNA detected by next-generation sequencing reflect the genetic changes in both germinal center b-Cell-Like and activated b-Cell-Like diffuse Large b-cell lymphomas at the time of diagnosis. *Haematologica* (2015) 100(7):e280–4. doi: 10.3324/haematol.2015.123612

16. Camus V, Sarafan-Vasseur N, Bohers E, Dubois S, Mareschal S, Bertrand P, et al. Digital pcr for quantification of recurrent and potentially actionable somatic mutations in circulating free DNA from patients with diffuse Large b-cell lymphoma. *Leuk Lymphoma* (2016) 57(9):2171–9. doi: 10.3109/10428194.2016.1139703

17. Karube K, Enjuanes A, Dlouhy I, Jares P, Martin-Garcia D, Nadeu F, et al. Integrating genomic alterations in diffuse Large b-cell lymphoma identifies new relevant pathways and potential therapeutic targets. *Leukemia* (2018) 32(3):675–84. doi: 10.1038/leu.2017.251

18. Reddy A, Zhang J, Davis NS, Moffitt AB, Love CL, Waldrop A, et al. Genetic and functional drivers of diffuse Large b cell lymphoma. *Cell* (2017) 171(2):481–94.e15. doi: 10.1016/j.cell.2017.09.027

19. Ren W, Ye X, Su H, Li W, Liu D, Pirmoradian M, et al. Genetic landscape of hepatitis b virus-associated diffuse Large b-cell lymphoma. *Blood* (2018) 131(24):2670–81. doi: 10.1182/blood-2017-11-817601

20. Pasqualucci L, Dalla-Favera R. Genetics of diffuse Large b-cell lymphoma. *Blood* (2018) 131(21):2307–19. doi: 10.1182/blood-2017-11-764332

21. Rivas-Delgado A, Nadeu F, Enjuanes A, Casanueva-Eliceiry S, Mozas P, Magnano L, et al. Mutational landscape and tumor burden assessed by cell-free DNA in diffuse Large b-cell lymphoma in a population-based study. *Clin Cancer Res* (2021) 27(2):513–21. doi: 10.1158/1078-0432.CCR-20-2558

22. Kurtz DM, Soo J, Co Ting Keh L, Alig S, Chabon JJ, Sworder BJ, et al. Enhanced detection of minimal residual disease by targeted sequencing of phased variants in circulating tumor DNA. *Nat Biotechnol* (2021) 39(12):1537–47. doi: 10.1038/s41587-021-00981-w

23. van Velzen MJM, Creemers A, van den Ende T, Schokker S, Krausz S, Reinten RJ, et al. Circulating tumor DNA predicts outcome in metastatic gastroesophageal cancer. *Gastric Cancer* (2022) 25(5):906–15. doi: 10.1007/s10120-022-01313-w

24. Arisi MF, Dotan E, Fernandez SV. Circulating tumor DNA in precision oncology and its applications in colorectal cancer. *Int J Mol Sci* (2022) 23(8):4441. doi: 10.3390/ijms23084441

25. Fu H, Zhou H, Qiu Y, Wang J, Ma Z, Li H, et al. Sept6_Trim33 gene fusion and mutated Tp53 pathway associate with unfavorable prognosis in patients with b-cell lymphomas. *Front Oncol* (2021) 11:765544. doi: 10.3389/fonc.2021.765544

26. Desch AK, Hartung K, Botzen A, Brobeil A, Rummel M, Kurch L, et al. Genotyping circulating tumor DNA of pediatric Hodgkin lymphoma. *Leukemia* (2020) 34(1):151–66. doi: 10.1038/s41375-019-0541-6

27. Soerensen JF, Aggerholm A, Rosenberg CA, Bill M, Kerndrup GB, Ebbesen LH, et al. Clonal evolution in patients developing therapy-related myeloid neoplasms following autologous stem cell transplantation. *Bone marrow Transplant* (2022) 57(3):460–5. doi: 10.1038/s41409-022-01567-z

28. Lohr JG, Stojanov P, Lawrence MS, Auclair D, Chapuy B, Sougnez C, et al. Discovery and prioritization of somatic mutations in diffuse Large b-cell lymphoma (Dlbcl) by whole-exome sequencing. *Proc Natl Acad Sci U S A* (2012) 109(10):3879–84. doi: 10.1073/pnas.1121343109

29. Wang H, Shen L, Li Y, Lv J. Integrated characterisation of cancer genes identifies key molecular biomarkers in stomach adenocarcinoma. *J Clin Pathol* (2020) 73(9):579–86. doi: 10.1136/jclinpath-2019-206400

30. Qiu Z, Lin A, Li K, Lin W, Wang Q, Wei T, et al. A novel mutation panel for predicting etoposide resistance in small-cell lung cancer. *Drug Des Devel Ther* (2019) 13:2021–41. doi: 10.2147/DDDT.S205633

31. Park AK, Kim P, Ballester LY, Esquenazi Y, Zhao Z. Subtype-specific signaling pathways and genomic aberrations associated with prognosis of glioblastoma. *Neuro Oncol* (2019) 21(1):59–70. doi: 10.1093/neuonc/noy120

32. Juskevicius D, Lorber T, Gsponer J, Perrina V, Ruiz C, Stenner-Liewen F, et al. Distinct genetic evolution patterns of relapsing diffuse Large b-cell lymphoma revealed by genome-wide copy number aberration and targeted sequencing analysis. *Leukemia* (2016) 30(12):2385–95. doi: 10.1038/leu.2016.135

33. Ngo VN, Young RM, Schmitz R, Jhavar S, Xiao W, Lim KH, et al. Oncogenically active Myd88 mutations in human lymphoma. *Nature* (2011) 470(7332):115–9. doi: 10.1038/nature09671

34. Lu TX, Young KH, Xu W, Li JY. Tp53 dysfunction in diffuse Large b-cell lymphoma. *Crit Rev Oncol Hematol* (2016) 97:47–55. doi: 10.1016/j.critrevonc.2015.08.006

35. Chapuy B, Stewart C, Dunford AJ, Kim J, Kamburov A, Redd RA, et al. Molecular subtypes of diffuse Large b cell lymphoma are associated with distinct pathogenic mechanisms and outcomes. *Nat Med* (2018) 24(5):679–90. doi: 10.1038/s41591-018-0016-8

36. Zhou L, Zhao H, Shao Y, Chen X, Hong R, Wang L, et al. Serial surveillance by circulating tumor DNA profiling after chimeric antigen receptor T therapy for the guidance of R/R diffuse Large b cell lymphoma precise treatment. *J Cancer* (2021) 12(18):5423–31. doi: 10.7150/jca.60390

frontiers | Frontiers in Oncology

TYPE Systematic Review
PUBLISHED 20 January 2023
DOI 10.3389/fonc.2022.1094400

OPEN ACCESS

EDITED BY
Alberto Fabbri,
Siena University Hospital, Italy

REVIEWED BY
Emanuele Cencini,
Siena University Hospital, Italy
Sabino Ciavarella,
National Cancer Institute Foundation (IRCCS), Italy

*CORRESPONDENCE
Mei Lin
linmei70@hotmail.com

SPECIALTY SECTION
This article was submitted to Hematologic Malignancies, a section of the journal Frontiers in Oncology

RECEIVED 10 November 2022
ACCEPTED 29 December 2022
PUBLISHED 20 January 2023

CITATION
Lin M, Ma S, Sun L and Qin Z (2023) The prognostic value of tumor-associated macrophages detected by immunostaining in diffuse large B cell lymphoma: A meta-analysis.
Front. Oncol. 12:1094400.
doi: 10.3389/fonc.2022.1094400

The prognostic value of tumor-associated macrophages detected by immunostaining in diffuse large B cell lymphoma: A meta-analysis

Mei Lin[1]*, Shupei Ma[2], Lingling Sun[3] and Zhiqiang Qin[4]

[1]Department of Pathology, School of Basic Medicine, Qingdao University, Qingdao, Shandong, China,
[2]Department of Hematology, Qingdao Municipal Hospital, Qingdao, Shandong, China,
[3]Department of Pathology, The Affiliated Hospital of Qingdao University, Qingdao, Shandong, China,
[4]Department of Pathology, People Hospital of Changzhi, Changzhi, Shanxi, China

Background: The prognostic implication of tumor-associated macrophages (TAMs) in the microenvironment of diffuse large B cell lymphoma (DLBCL) remains controversial.

Methods: A systematic and comprehensive search of relevant studies was performed in PubMed, Embase and Web of Science databases. The quality of the included studies was estimated using Newcastle-Ottawa Scale (NOS).

Results: Twenty-three studies containing a total of 2992 DLBCL patients were involved in this study. They were all high-quality studies scoring ≥ 6 points. High density of M2 TAMs in tumor microenvironment significantly associated with both advanced disease stage (OR= 1.937, 95% CI: 1.256-2.988, P = 0.003) and unfavorable overall survival (OS) (HR = 1.750, 95% CI: 1.188-2.579, P = 0.005) but not associated with poor progression free survival (PFS) (HR = 1.672, 95% CI: 0.864-3.237, P = 0.127) and international prognostic index (IPI) (OR= 1.705, 95% CI: 0.843-3.449, P = 0.138) in DLBCL patients. No significant correlation was observed between the density of $CD68^+$ TAMs and disease stage (OR= 1.433, 95% CI: 0.656-3.130, P = 0.366), IPI (OR= 1.391, 95% CI: 0.573-3.379, P = 0.466), OS (HR=0.929, 95% CI: 0.607-1.422, P = 0.734) or PFS (HR= 0.756, 95% CI: 0.415-1.379, P = 0.362) in DLBCL patients.

Conclusion: This meta-analysis demonstrated that high density of M2 TAMs in the tumor microenvironment was a robust predictor of adverse outcome for DLBCL patients.

Systematic review registration: https://www.crd.york.ac.uk/PROSPERO, identifier CRD42022343045.

KEYWORDS

diffuse large B cell lymphoma (DLBCL), prognosis, meta-analysis, tumor-associated macrophages (TAMs), M2 TAMs

Background

Diffuse large B-cell lymphoma (DLBCL), the most common subtype of non-Hodgkin lymphoma (NHL), occupying 30-40% of newly diagnosed NHL (1, 2). DLBCL was heterogenous and patients with DLBCL showed various clinical outcomes (3). Approximately 60-70% DLBCL patients can be cured by anti-CD20 based immunochemotherapy. However, relapsed and refractory patients still die from DLBCL and its complications (4–6). Further improvement of DLBCL patients' therapeutic outcome relies on identifying high-risk patients and individualizing treatment regimens.

Recent studies by molecular profiling showed that tumor microenvironment (TME) was associated with clinical behavior of DLBCL. Lenz and colleagues demonstrated that the prognosis of DLBCL patients was influenced by differences of TME. They also demonstrated that high stromal-2 signature predicted poor outcome (7). Using gene expression and sequencing, several other studies also obtained promising results in identifying high-risk DLBCL patients (8–12). However, molecular profiling has the disadvantage of low applicability in daily practice.

Tumor-associated macrophages (TAMs) are the most abundant component of TME (13). Recent studies have demonstrated that TAMs were critical for the survival, growth, metastasis, and drug resistance of tumors (14, 15). In response to different environmental stimuli, TAMs differentiated into M1 type (classically activated phenotype) and M2 type (alternatively activated phenotype) (16). The two types of TAMs were distinguished in functions and surface markers. M1 TAMs prevented tumor growth (17, 18). whereas M2 TAMs promoted angiogenesis and was involved in the progression of tumor (17–19). CD68 is a general marker for all TAMs and CD163 is a specific marker for M2 TAMs (3).

In DLBCL, the role of TAMs in the progression of DLBCL and the prognostic value of TAMs remains inconclusive due to the contradictory results obtained by previous studies. Several studies showed that a high density of $CD68^+$ TAMs was associated with favorable prognosis (3, 20, 21). A few other studies failed to demonstrate such association (4, 18, 22–27). By contrast, Cai et al. (28) and Carreras et al. (17) showed that high density of $CD68^+$ TAMs correlated with inferior outcome. The correlation between M2 TAMs and survival of DLBCL patients was also unsettled. Some researchers showed that a high density of M2 TAMs was correlated with shortened survival in DLBCL (1, 3, 17, 23). However, several other studies did not demonstrate such association (20, 24, 25, 27, 29–32). Therefore, we performed this meta-analysis to explore the role of TAMs in DLBCL progression and the prognostic value of TAMs in DLBCL patients.

Methods

Literature search

Relevant articles were systemically searched in PubMed, Embase and Web of Science databases with an end date of August 5th, 2022. The searching terms were "macrophage" or "macrophages" or "TAM" or "TAMs" or "tumor-infiltrating macrophage" or "tumor-associated macrophage" or "intratumoral macrophage" and "diffuse large B-cell lymphoma" or "DLBCL". In addition, we also searched the references of relevant studies for eligibility. The literature search was performed by two independent reviewers (Mei Lin and Shupei Ma) and disagreement was resolved by consensus.

Inclusion criteria

Our inclusion criteria were as follows (1): proven diagnosis of DLBCL; (2) $CD68^+$ TAMs, $CD163^+$ TAMs or $CD163^+/CD68^+$ TAMs were detected by immunohistochemical or immunofluorescence staining; (3) patients were categorized into high and low density TAMs groups; (4) Odds ratio (OR) or hazard ratio (HR) and 95% confidence interval (CI) on the density of $CD68^+$, $CD163^+$ or $CD163^+/CD68^+$ TAMs and disease stage, international prognostic index (IPI), overall survival (OS) or progression free survival (PFS) could be obtained.

Data extraction and quality assessment

The data extraction was performed by two reviewers (Shupei Ma and Mei Lin) independently. For each eligible study, we extracted the following data: surname of the first author, year of publication, number of patients, country, treatment, median/mean/average follow-up, method, antibody (clone), analysis. For studies that HR and its 95% CI were not reported, the data was extracted using the Tierney's calculation method (33). The Newcastle-Ottawa Scale (NOS) was used to assess the quality of the involved studies and any study scores ≥ 6 was considered as a high-quality literature.

Statistical analysis

Pooled OR and 95% CI were used to estimate the correlation between the density of TAMs and disease stage or IPI. Pooled HR and 95% CI were used to investigate the effect of TAMs on prognosis. To evaluate the interstudy heterogeneity, chi-squared test (Q test) and I^2 test were used. $P > 0.10$ and $I^2 < 50\%$ indicated no significant heterogeneity existed. In this case, fixed-effect model was used. Otherwise, random-effect model was applied. Sensitivity analysis and subgroup analysis were applied to explore the source of heterogeneity. Publication bias was evaluated by funnel plot and Egger test. All statistical analysis was performed using Stata 12.0 software. $P < 0.05$ was considered statistically significant.

Results

Identification of eligible studies

A total of 1152 literatures were retrieved according to the abovementioned searching strategy, including 240 from PubMed, 587 from Embase and 325 from Web of Science. A total of 446 duplication was excluded. By carefully reviewing the title and abstract,

we excluded 651 articles which are non-original, irrelevant or laboratory studies on animals or cell lines. The remaining 55 studies were further investigated by reading the full text carefully. Thirty-two studies were then excluded due to not fulfilling the inclusion criteria. Finally, 23 studies were eligible for this meta-analysis (Figure 1).

Characteristics of included studies and quality assessment

The basic characteristics of the 23 eligible studies was shown in Table 1. The included studies were published between 2011-2022 and the number of participants ranged from 36 to 430. Of the 23 included studies, 5 were from Japan (17, 26, 27, 31, 32) and China (1, 23, 28, 34, 35) respectively; 4 from Korea (3, 20, 29, 36), 3 from USA (4, 22, 30) and Italy (21, 24, 37) respectively; 1 from Finland (18), India (25) and Egypt (38) respectively. Immunohistochemistry or immunofluorescence was performed by the included studies. Antibodies against CD68 was used to detect total TAMs and anti-CD163 antibody or double staining with antibodies against CD68 and CD163 was applied to estimate M2 TAMs by the eligible studies.

The quality of the 23 included studies was estimated by NOS. The scores were all ≥ 6 points (Supplementary Table 1). This suggested that all the eligible studies were high-quality studies.

Total TAMs and IPI, disease stage or prognosis

In this study, the density of total TAMs was not correlated with IPI (≥3/0-2: OR= 1.391, 95% CI: 0.573-3.379, P= 0.466) with significant heterogeneity (P= 0.000, I^2 =78.4%) (Figure 2A). No correlation was observed between the density of total TAMs and disease stage (Ann Arbor stage, III+IV/I+II: OR= 1.433, 95% CI: 0.656-3.130, P = 0.366) with evident heterogeneity (P = 0.052, I^2 = 61.2%) (Figure 2B).

Of the 23 eligible studies, 13 or 9 studies reported the association between the density of $CD68^+$ TAMs and OS or PFS respectively. In our meta-analysis, no significant correlation was observed between the density of total TAMs and OS (HR=0.929, 95% CI: 0.607-1.422, P = 0.734), with significant heterogeneity (P = 0.002, I^2 = 61.1%) (Figure 2C). No significant association was identified between the density of total TAMs and PFS (HR= 0.756, 95% CI: 0.415-1.379, P = 0.362) and the heterogeneity was significant (P = 0.000, I^2 = 72.9%) (Figure 2D).

M2 TAMs and IPI, disease stage or prognosis

In this study, no correlation was observed between the density of M2 TAMs and IPI (OR= 1.705, 95% CI: 0.843-3.449, P = 0.138) with evident heterogeneity (P = 0.061, I^2 = 59.3%) (Figure 3A). High density of M2 TAMs associated with disease stage (OR= 1.937, 95% CI: 1.256-2.988, P = 0.003) with no heterogeneity (P = 0.639, I^2 = 0.0%) (Figure 3B).

In this study, the pooled results of 14 studies showed that high density of M2 TAMs in the microenvironment of DLBCL patients correlated with unfavorable OS (HR = 1.750, 95% CI: 1.188-2.579, P = 0.005), with significant heterogeneity (P = 0.000, I^2 = 64.8%) (Figure 3C). Pooled HR for PFS in 9 studies showed that high density of M2 TAMs was not significantly associated with poor PFS (HR = 1.672, 95% CI: 0.864-3.237, P = 0.127), with evident heterogeneity (P = 0.000, I^2 = 80.1%) (Figure 3D).

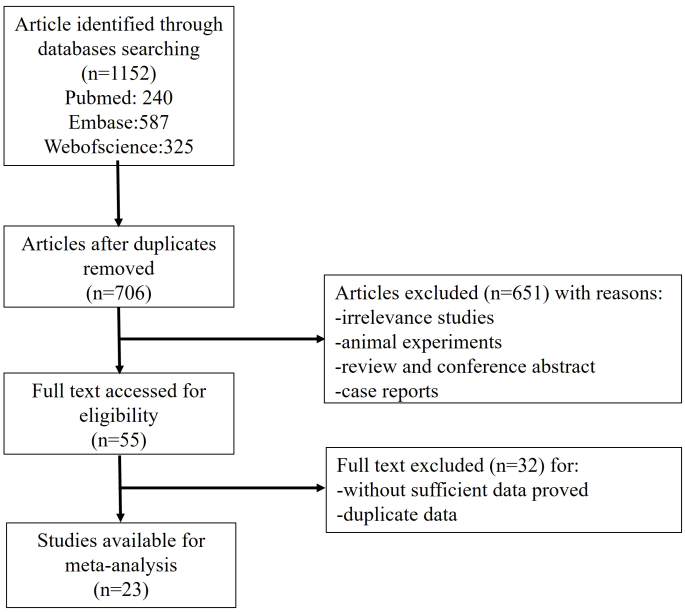

FIGURE 1
Flow chart of study selection.

TABLE 1 Characteristics of the eligible studies.

Author	Year	N	Country	Treatment	Follow-up median/mean/ average (months)	Method	Antibody (clone)	Analysis
Asano	2022	82	Japan	RT/RT+HD-MTX/R-MPV+RT/HD-MTX/R-MPV/others	ND	IHC	CD163(MRQ26)	OS, PFS
Cai	2012	112	China	CHOP/CHOP+RT	72 (2–135)	IHC	CD68(KP1)	OS, PFS
Carreras	2022	132	Japan	R-CHOP/R-CHOP- like/others	ND	IHC	CD68(514H12), CD163(10D6)	OS, PFS
Cencini	2020	37	Italy	CHOP-like/R-CHOP	60	IHC	CD68(PG-M1), CD163(ND)	OS,PFS, IPI,stage
Croci	2021	430	Italy	R-CHOP like	ND	IHC	CD68(PG-M1)	OS, PFS
Gomez-Gelvez	2016	70	USA	R-CHOP	49.2(7.2-144)	IHC	CD68(KP1)	OS, PFS
Jeong	2017	185	Korea	ND	38.7(mean)	IHC	CD163(MRQ26)	OS
Li	2019	221	China	CHOP/R-CHOP	42(3-118)	IHC	CD68(KP1), CD163 (10D6)	OS,PFS, IPI,stage
Marchesi	2015	61	Italy	R-chop/R-chop like	24.7	IFA	CD163(ND)/CD68 (ND)	OS
Matsuki	2019	94	USA	CT/R+CT	64.8	IHC	CD163(10D6)	OS, PFS
Meyer	2011	242	USA	R-CHOP/CHOP like	ND	IHC	CD68(KP1)	OS
Nam	2014	109	Korea	R-CHOP	43(16-178)	IHC	CD68(PG-M1), CD163(10D6)	OS, PFS
Nam	2018	144	Korea	MVP/HD-MTX/RT/R-MVP/others	31.35*(0.2-178)	IHC	CD68(PG-M1), CD163(10D6)	OS, PFS
Parkhi	2021	44	India	CT ± R/RT+CT ± R/RT/not received	ND	IHC	CD68(PG-M1), CD163(MRQ26)	OS
Riihijarvi	2015	181	Finland	CT/R+CT	65,65,85	IHC	CD68(KP1)	OS, PFS, IPI
Wada	2012	101	Japan	R+CT (most)	28^{+}(9.5-38.5)	IHC	CD68 (PG-M1) CD163(ND)/CD68 (PG-M1)	OS, IPI, stage
Wang	2017	355	China	R-CHOP	53.71	IHC	CD163(ND)	OS, PFS
Xu	2013	92	China	ND	ND	IHC	CD163(10D6)	OS, IPI
Yamamoto	2014	36	Japan	R-CHOP	37.2	IHC	CD163(10D6)	PFS
Yoshida	2013	47	Japan	R-chop/R+THP-COP	ND	IHC	CD68(KP1), CD163 (10D6)	OS
Ghorab	2022	65	Egypt	ND	ND	IHC	CD68(KP1)	IPI
Wang	2015	81	China	R-CHOP	ND	IHC	CD68(514H12)	IPI, stage
Lee	2011	71	Korea	CT+R/CT/CT+RT/operation	45.6(6-132)	IHC	CD68(KP1)	IPI, stage

N: number of patients; RT, radiotherapy; HD, high-dose; MTX, methotrexate; R, rituximab; MPVA, MTX, procarbazine, vincristine, and Ara-C; MPV, MTX, procarbazine, vincristine; ND, not described; IHC, immunohistochemistry; IFA, immunofluorescence assay; OS, overall survival; PFS, progression free survival; MVP, methotrexate, vincristine, procarbazine; CHOP, cyclophosphamide, doxorubicin, vincristine, prednisone; CT, chemotherapy; THP-COP, pirarubicin, cyclophosphamide, vincristine, prednisolone; * median follow-up for the group of patients who did not receive rituximab; + average follow-up.

Sensitivity analysis

Sensitivity analysis was conducted by removing one study each time and recalculating the remaining studies (39). In the analysis of M2 TAMs and OS or PFS, the heterogeneity become insignificant (M2 TAMs and OS: P = 0.108, I^2 = 34.3%; M2 TAMs and PFS: P = 0.115, I^2= 39.6%) after removing Wang et al.'s study (1). In the study of total TAMs and IPI or disease stage, there was no heterogeneity after removing Li et al.'s study (23). In the analysis of M2 TAMs and IPI, the heterogeneity become insignificant after removing Li et al.'s study (P = 0.306, I^2= 15.7%) (23) or Xu et al.'s study (P = 0.179, I^2= 41.9%) (34).

After removing Xu et al.'s study (34), high density of M2 TAMs was related to high and high-intermediate IPI (OR= 2.239, 95% CI: 1.140-4.396, P = 0.019). After removing Li et al.'s study (23), the density of M2 TAMs was not correlated with disease stage (OR=1.552,

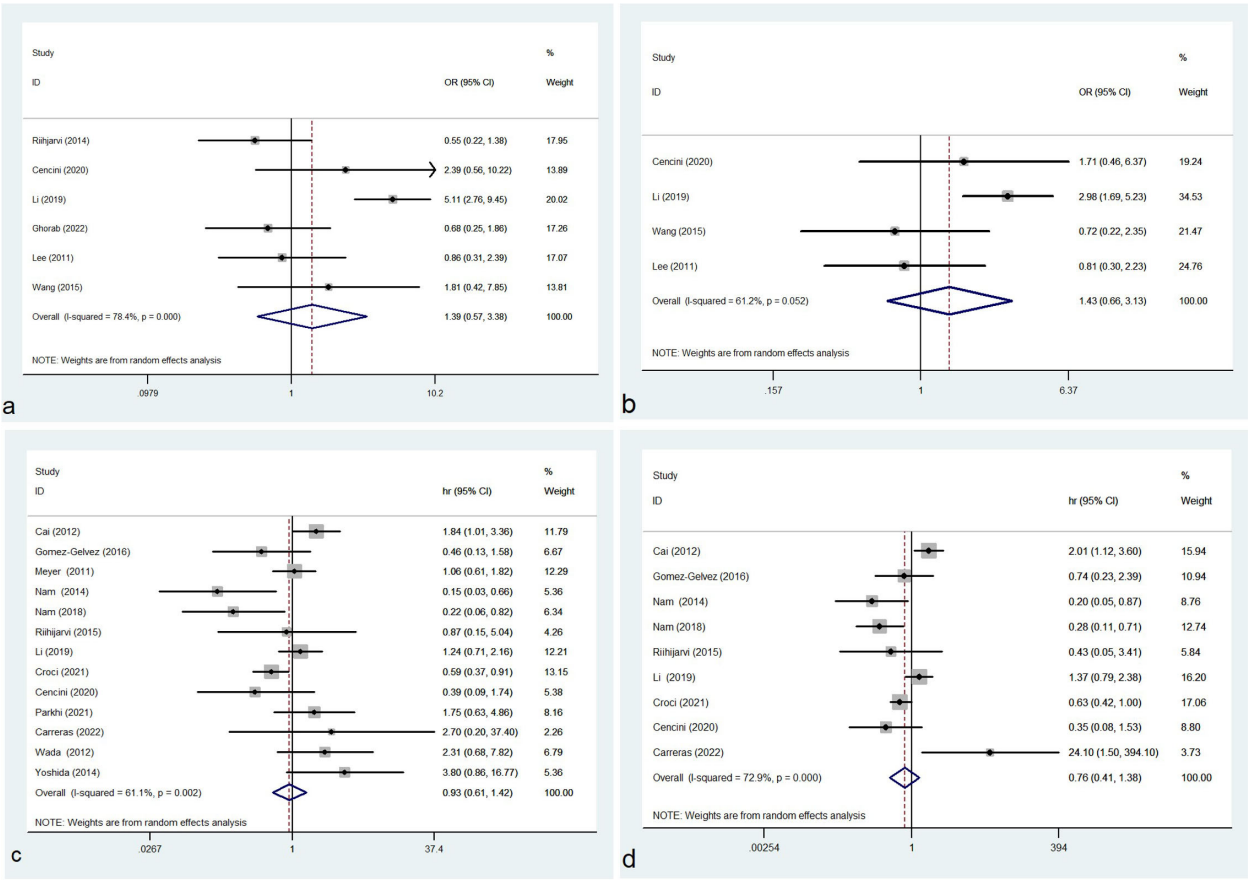

FIGURE 2
Forest plot of total TAMs and IPI **(A)**, disease stage **(B)**, OS **(C)** and PFS **(D)**; OR, odds ratio; hr, hazard ratio; CI, confidence interval.

95% CI: 0.758-3.180, P = 0.229). Except the abovementioned 2 studies, no other study significantly influenced the pooled results in this meta-analysis.

Subgroup analysis

Subgroup analysis was performed in the studies of total TAMs or M2 TAMs and survival of DLBCL patients. The eligible studies were divided into two subgroups according to whether the study focused on central nervous system DLBCL (CNS DLBCL). Our results showed that high density of total TAMs was not correlated with OS in both CNS (HR=0.652, 95% CI: 0.087-4.881, P = 0.677) and non-CNS DLBCL patients (HR=0.974, 95% CI: 0.626-1.515, P = 0.906) (Table 2). A high density of total TAMs was associated with favorable PFS in CNS DLBCL patients (HR=0.275, 95% CI: 0.106-0.714, P = 0.008) but not in non-CNS patients (HR=0.881, 95% CI: 0.478-1.624, P = 0.684) (Table 2). High density of M2 TAMs correlated with poor OS (HR=2.038, 95% CI: 1.345-3.087, P = 0.001) and PFS (HR=2.195, 95% CI: 1.090-4.420, P = 0.028) in non-CNS DLBCL patients. The density of M2 TAMs was not correlated with both OS and PFS in CNS DLBCL patients (Table 3).

Based on geographic region, the included patients were classified into Asian group and non-Asian group. High density of total TAMs correlated with favorable OS (HR=0.704, 95% CI: 0.511-0.971, P = 0.032) and PFS (HR=0.604, 95% CI: 0.410-0.890, P = 0.011) in non-Asian patients with no heterogeneity (total TAMs and OS: P = 0.421, I^2 = 0.00%; total TAMs and PFS: P = 0.858, I^2 = 0.00%). However, the density of total TAMs was not correlated with both OS and PFS in Asian patients (Table 2). High density of M2 TAMs associated with poor OS (HR=1.751, 95% CI: 1.158-2.646, P = 0.008) and showed a trend of association with poor PFS (HR=1.915, 95% CI: 0.897-4.089, P = 0.093) in Asian patients. The density of M2 TAMs was not correlated with both OS and PFS in non-Asian patients (Table 3).

In the subgroup analysis according to whether rituximab was included in the treatment regimen, a high density of total TAMs was significantly correlated with favorable PFS (HR=0.410, 95%CI: 0.219-0.769, P=0.005) but not significantly correlated with OS (HR=0.546, 95% CI: 0.256-1.164, P = 0.117) in patients treated with rituximab-containing regimen (Table 2). In contrast, no correlation was observed between the density of total TAMs and OS or PFS in patients treated without rituximab (Table 2). High density of M2 TAMs significantly correlated with unfavorable OS (HR=2.620, 95% CI: 1.232-5.572, P = 0.012) and PFS (HR=3.475, 95% CI: 1.210-9.985, P = 0.021) in patients treated with rituximab-containing regimen. However, no correlation was found between the density of M2 TAMs and prognosis of patients treated without rituximab (Table 3).

Subgroup analysis according to different clones of anti-CD68 antibody was also performed. In the subgroup detected CD68 with clone PG-M1, total TAMs correlated with PFS (HR=0.421, 95% CI:

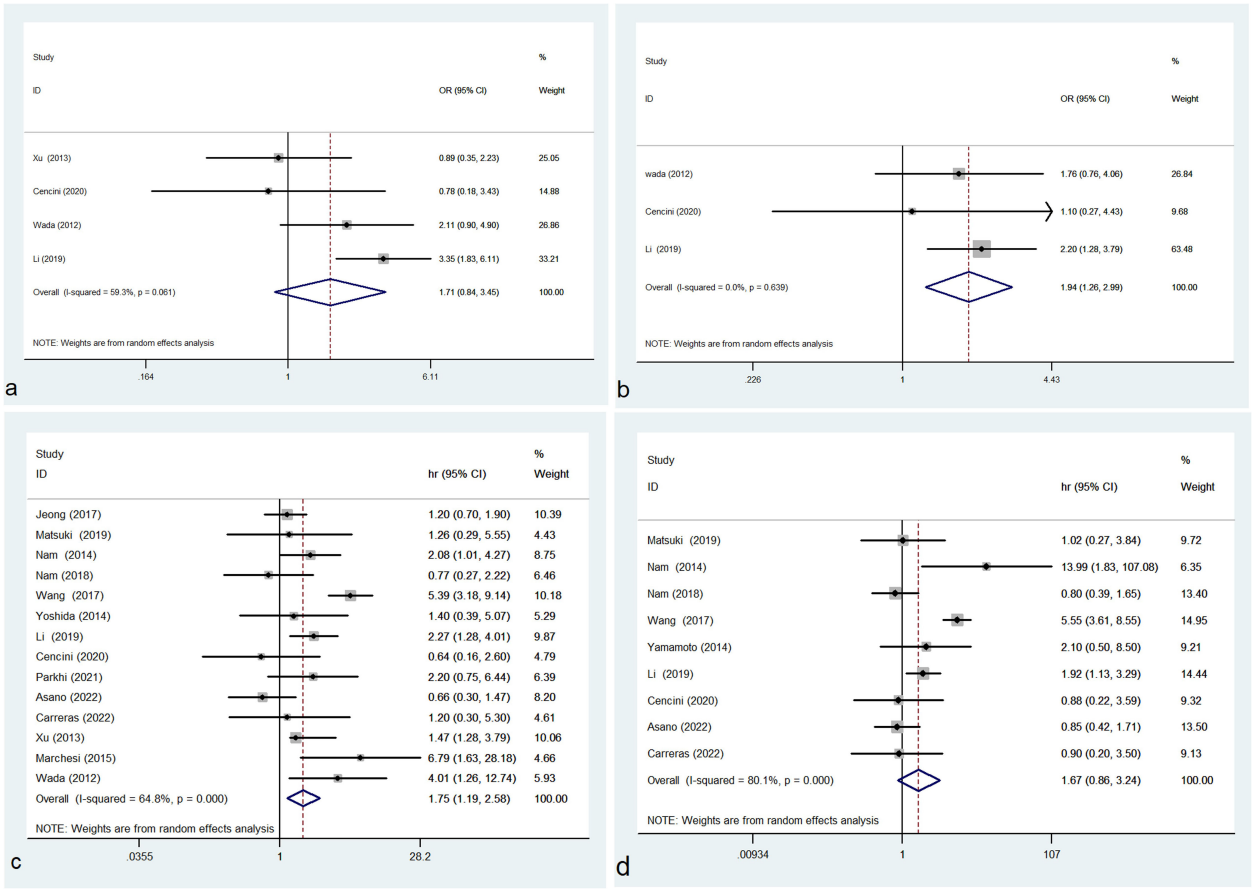

FIGURE 3
Forest plot of M2 TAMs and IPI **(A)**, disease stage **(B)**, OS **(C)** and PFS **(D)**; OR, odds ratio; hr, hazard ratio; CI, confidence interval.

0.244-0.729, P = 0.002) but not correlated with OS (HR=0.609, 95% CI: 0.289-1.283, P = 0.192) (Table 2). In KP1 subgroup, no correlation was observed between total TAMs and OS (HR=1.269, 95% CI: 0.866-1.862, P = 0.222) or PFS (HR=1.391, 95% CI: 0.881-2.195, P = 0.157) (Table 2).

Among the 14 studies reported the correlation between M2 TAMs and OS, 12 studies used anti-CD163 antibody and 2 studies applied double staining with antibodies against CD163 and CD68 to estimate M2 TAMs. The density of $CD163^+$ TAMs and $CD163^+/CD68^+$ TAMs was both correlated with OS ($CD163^+$ TAMs: HR=1.549, 95% CI: 1.038-2.313, P = 0.032; $CD163^+/CD68^+$ TAMs: HR=4.941, 95% CI: 2.012-12.129, P = 0.000) (Table 3).

Publication bias

Funnel plots and Egger tests were used to assess the publication bias. The funnel plots of this meta-analysis were shown in Supplementary Figure 1 and Supplementary Figure 2. The yielded P values of Egger test were: 0.180 for total TAMs and disease stage, 0.302 for total TAMs and IPI, 0.860 for total TAMs and OS, 0.707 for total TAMs and PFS, 0.018 for M2 TAMs and disease stage, 0.150 for M2 TAMs and IPI, 0.598 for M2 TAMs and OS, 0.321for M2 TAMs and PFS. The results of Egger test showed that there was publication bias in the analysis of M2 TAM and disease stage. Except this, no publication bias existed in the other analysis of this meta-analysis.

Discussion

Previous studies showed that TME is critical for the progression of tumors (14). TAMs are important component of TME (28). The prognostic significance of total TAMs and M2 TAMs have been investigated in a variety of cancers by meta-analysis (40–44). In lymphoma, meta-analysis investigated the association of total TAMs or M2 TAMs and outcome of patients have been reported in non-Hodgkin's lymphoma (NHL) (45) and Hodgkin's lymphoma (HL) (46). DLBCL is the most common type of NHL. However, meta-analysis investigating the prognostic value of TAMs in DLBCL is still unavailable.

Consistent with the results obtained by meta-analysis in HL (46), gastric cancer (40) and NHL (45), we demonstrated that high density of M2 TAMs correlated with unfavorable prognosis in DLBCL. This suggested that high density of M2 TAMs can be used as an indicator of poor prognosis in DLBCL patients. Xu et al.'s study reported that high density of $CD68^+$ TAMs correlated with poor OS and PFS in NHL (45) and several previous studies suggested that TAMs' infiltration was significantly correlated with favorable (3, 20, 21) or

TABLE 2 Subgroup analysis of total TAMs and survival.

survival	Subgroups	Number of studies	Pooled results (95%CI)	P-value	Heterogeneity	
					P	I^2
OS	**Site**					
	CNS DLBCL	2	0.652 (0.087-4.881)	0.677	0.015	83.2%
	Non-CNS DLBCL	11	0.974 (0.626-1.515)	0.906	0.006	59.5%
	Region					
	Asian	8	1.162 (0.615-2.198)	0.643	0.006	65.0%
	Non-Asian	5	0.704 (0.511-0.971)	0.032	0.421	0.0%
	Treatment					
	With Rituximab	6	0.546(0.256-1.164)	0.117	0.072	50.5%
	Without Rituximab	3	1.194 (0.404-3.523)	0.748	0.023	73.5%
	Clone of antibody					
	KP1	6	1.269 (0.866-1.862)	0.222	0.239	26.1%
	PG-M1	6	0.609 (0.289-1.283)	0.192	0.012	66.1%
PFS	**Site**					
	CNS DLBCL	1	0.275 (0.106-0.714)	0.008	–	–
	Non-CNS DLBCL	8	0.881 (0.478-1.624)	0.684	0.001	70.2%
	Region					
	Asian	5	0.972 (0.360-2.625)	0.955	0.000	82.2%
	Non-Asian	4	0.604 (0.410-0.890)	0.011	0.858	0.0%
	Treatment					
	With Rituximab	5	0.410 (0.219-0.769)	0.005	0.145	41.4%
	Without Rituximab	3	1.145 (0.336-3.904)	0.828	0.002	84.5%
	Clone of antibody					
	KP1	4	1.391(0.881-2.195)	0.157	0.281	21.6%
	PG-M1	4	0.421(0.244-0.729)	0.002	0.239	28.8%

OS, overall survival; PFS, progression free survival; CI, confidence interval; CNS-DLBCL, primary diffuse large B cell lymphoma of the central nervous system

poor outcome (17, 28) in DLBCL. However, no correlation between the density of $CD68^+$ TAMs and prognosis in DLBCL patients was found in this meta-analysis. This was in accordance with previous studies in bladder (41) and ovarian cancers (42). Taken together, these results suggested that M2 TAMs rather than total TAMs might contribute to the progression of DLBCL and lead to unfavorable outcome in DLBCL patients.

In this study, high density of M2 TAMs was correlated with unfavorable prognosis in Asian subgroup but not in non-Asian subgroup. These suggested that M2 TAMs may play an important role in the disease progression and acted as an indicator of poor prognosis in Asian patients. In this meta-analysis, high density of $CD68^+$ TAMs associated with favorable outcome in non-Asian DLBCL patients but not in Asian patients. This suggested that high density of $CD68^+$ TAMs predicted favorable survival in non-Asian patients but not in Asian patients.

Rituximab, a human/murine chimeric antibody, shows high affinity and specificity for CD20 which is a transmembrane protein of B-lymphocyte. Rituximab has become a standard component of treatment modality for a number of B-cell malignancies including DLBCL (47). Taskinen and colleagues reported that addition of rituximab to the same group of patients at relapse reversed the negative prognostic effect of high density $CD68^+$ TAMs in tumor environment to favorite (48). In this meta-analysis, high density of $CD68^+$ TAMs correlated with favorable outcome in the subgroup of patients treated with rituximab-containing regimen. In contrast, no correlation was found between high density of $CD68^+$ TAMs and prognosis in patients treated without rituximab. These results were in accordance with previous study and suggested that TAMs might obtain tumor-inhibiting function in response to rituximab or TAMs modulated the therapeutic efficiency of rituximab.

The results of our meta-analysis showed that the association of M2 TAMs and outcome of DLBCL patients was also influenced by whether rituximab was included in the treatment regimen. Pooled results of this meta-analysis showed that high density of M2 TAMs in tumor microenvironment associated with unfavorable outcome in

TABLE 3 Subgroup analysis of M2 TAMs and survival.

survival	Subgroups	Number of studies	Pooled results (95%CI)	P-value	Heterogeneity	
					P	I^2
OS	**Site**					
	CNS DLBCL	3	0.982 (0.480-2.008)	0.961	0.194	39.0%
	Non-CNS DLBCL	11	2.038 (1.345- 3.087)	0.001	0.003	62.7%
	Region					
	Asian	11	1.751 (1.158-2.646)	0.008	0.001	68.0%
	Non-Asian	3	1.760 (0.437- 7.083)	0.426	0.059	64.7%
	Treatment					
	With R	5	2.620 (1.232-5.572)	0.012	0.021	65.5%
	Without R	2	1.197 (0.363-3.952)	0.768	0.221	33.3%
	Antibody					
	CD163	12	1.549 (1.038-2.313)	0.032	0.001	65.3%
	CD163+CD68 double staining	2	4.941 (2.012-12.129)	0.000	0.573	0.0%
PFS	**Site**					
	CNS DLBCL	2	0.822 (0.496-1.362)	0.447	0.912	0.0%
	Non-CNS DLBCL	7	2.195 (1.090- 4.420)	0.028	0.002	71.6%
	Region					
	Asian	7	1.915 (0.897-4.089)	0.093	0.000	83.8%
	Non-Asian	2	0.951 (0.364 – 2.487)	0.919	0.881	0.0%
	Treatment					
	With R	4	3.475 (1.210-9.985)	0.021	0.068	58.0%
	Without R	2	0.891 (0.459-1.731)	0.734	0.453	0.0%

OS, overall survival; PFS, progression free survival; CI, confidence interval; CNS DLBCL: primary diffuse large B cell lymphoma of the central nervous system; R, rituximab.

patients treated with rituximab. In contrast, no correlation was observed between the density of M2 TAMs and prognosis in patients treated without rituximab. This emphasized the importance of targeting M2 macrophage in rituximab era.

TAMs centered therapeutic strategies includes suppressing the recruitment of TAMs, depletion of TAMs and reprogramming M2 TAMs to M1 type (49). Administration of antibody against chemokine (C-C motif) ligand-2 (CCL2) led to decreased infiltration of TAMs and impacted tumor growth in animal models of human cancers (50, 51). Colony stimulating factor 1 (CSF-1) is a major factor for the survival of TAMs. Targeting CSF-1 receptor with a humanized antibody RG7155 led to obvious reduction of TAMs in various tumor tissues (52). Maeda et al. showed that toll-like receptor 3 (TLR3) agonist Poly (I:C) was effective in reprogramming macrophage to anti-tumor type by an *in vitro* study (53). Repolarization of TAMs can also be achieved through manipulation of CD40 (54) and CD47 pathways (55). Currently, a variety of antibodies against CD40 (56) or CD47 (57) are being evaluated in clinical trials. A phase IIb clinical trial was performed to investigate the therapeutic efficacy of anti-CD40 antibody dacetuzumab plus rituximab, ifosfamide, carboplatin, and etoposide in 151 patients with relapsed and refractory DLBCL. The complete remission (CR) rate of the dacetuzumab group was not superior compared to the group using placebo in place of dacetuzumab (58). A phase Ib/II clinical trials of anti-CD47 antibody Hu5F9-G4 combined with rituximab in 75 patients with relapsed and refractory lymphoma showed promising results (57). In DLBCL patients treated with rituximab-containing regimen, the pooled results of this meta-analysis showed that high density of total TAMs significantly correlated with favorable outcome while high density of M2 TAMs significantly associated with poor prognosis. This suggested that repolarization of TAMs from M2 to M1 might have more clinical benefit than the methods of merely reducing the number of M2 TAMs in the treatment of DLBCL patients who received rituximab-containing regimen.

In the subgroup analysis according to different clones of anti-CD68 antibody, high density of total TAMs correlated with favorable PFS in the subgroup using clone PG-M1. While no association was identified between total TAMs and OS or PFS in KP1 subgroup. These suggested that high density of total TAMs detected by PG-M1 rather than KP1 was an indicator of favorable prognosis in DLBCL patients.

The current study is the first systemic meta-analysis investigating the association between the density of total TAMs or M2 TAMs and prognosis in DLBCL patients. However, several limitations in this study need to be addressed. First, some of the involved studies did not report HR. We extracted data from the Kaplan-Meier curves of these studies. In this case, deviation from the real value of HR may be caused. Second, the

treatment of DLBCL patients in the included studies are variable. This may influence the survival of patients and contribute to heterogeneity. Third, significant heterogeneity exists in this meta-analysis. The interstudy heterogeneity might be derived from the differences in origin of patients, sample size, location of locus, tumor stages, inconsistency of cut-off value and the antibody used to estimate TAMs. Forth, significant publication bias was observed in the study of M2 TAMs and disease stage in this meta-analysis. This may be due to that studies with positive results are more likely to be published than those reporting negative results. In addition, only three studies were eligible for this analysis. Therefore, more studies are needed to verify our results.

Conclusion

This meta-analysis demonstrated that a high density of M2 TAMs was a robust predictor of unfavorable outcome for DLBCL patients.

Data availability statement

The original contributions presented in the study are included in the article/Supplementary Material. Further inquiries can be directed to the corresponding author.

Author contributions

ML designed the study and revised the manuscript, ML, SM, LS, and ZQ selected the study, extracted and analyzed the data and wrote the manuscript. All authors contributed to the article and approved the submitted version.

Conflict of interest

The authors declare that the research was conducted in the absence of any commercial or financial relationships that could be construed as a potential conflict of interest.

Publisher's note

Supplementary material

The Supplementary Material for this article can be found online at: https://www.frontiersin.org/articles/10.3389/fonc.2022.1094400/full#supplementary-material

SUPPLEMENTARY FIGURE 1
Funnel plot for publication bias of total TAMs and IPI **(A)**, disease stage **(B)**, OS **(C)** and PFS **(D)**.

SUPPLEMENTARY FIGURE 2
Funnel plot for publication bias of M2 TAMs and IPI **(A)**, disease stage **(B)**, OS **(C)** and PFS **(D)**.

SUPPLEMENTARY TABLE 1
Newcastle-Ottawa Quality Assessment Scale. * A study can be awarded a maximum of one star for each numbered item within the Selection and Outcome categories. A maximum of two stars can be given for Comparability. http://www.ohri.ca/programs/clinical_epidemiology/oxford.asp

References

1. Wang J, Gao K, Lei W, Dong L, Xuan Q, Feng M, et al. Lymphocyte-to-monocyte ratio is associated with prognosis of diffuse large B-cell lymphoma: Correlation with CD163 positive M2 type tumor-associated macrophages, not PD-1 positive tumor-infiltrating lymphocytes. *Oncotarget* (2017) 8(3):5414–25. doi: 10.18632/oncotarget.14289

2. Swerdlow SH, Campo E, Pileri SA, Harris NL, Stein H, Siebert R, et al. The 2016 revision of the world health organization classification of lymphoid neoplasms. *Blood* (2016) 127(20):2375–90. doi: 10.1182/blood-2016-01-643569

3. Nam SJ, Go H, Paik JH, Kim TM, Heo DS, Kim CW, et al. An increase of M2 macrophages predicts poor prognosis in patients with diffuse large b-cell lymphoma treated with rituximab, cyclophosphamide, doxorubicin, vincristine and prednisone. *Leuk Lymphoma.* (2014) 55(11):2466–76. doi: 10.3109/10428194.2013.879713

4. Gomez-Gelvez JC, Salama ME, Perkins SL, Leavitt M, Inamdar KV. Prognostic impact of tumor microenvironment in diffuse large B-cell lymphoma uniformly treated with r-CHOP chemotherapy. *Am J Clin Pathol* (2016) 145(4):514–23. doi: 10.1093/ajcp/aqw034

5. Tilly H, Gomes da Silva M, Vitolo U, Jack A, Meignan M, Lopez-Guillermo A, et al. Diffuse large B-cell lymphoma (DLBCL): ESMO clinical practice guidelines for diagnosis, treatment and follow-up. *Ann Oncol* (2015) 26 Suppl 5:v116–25. doi: 10.1093/annonc/mdv304

6. Coiffier B, Thieblemont C, Van Den Neste E, Lepeu G, Plantier I, Castaigne S, et al. Long-term outcome of patients in the LNH-98.5 trial, the first randomized study comparing rituximab-CHOP to standard CHOP chemotherapy in DLBCL patients: A study by the groupe d'Etudes des lymphomes de l'Adulte. *Blood* (2010) 116(12):2040–5. doi: 10.1182/blood-2010-03-276246

7. Lenz G, Wright G, Dave SS, Xiao W, Powell J, Zhao H, et al. Stromal gene signatures in large-B-cell lymphomas. *N Engl J Med* (2008) 359(22):2313–23. doi: 10.1056/NEJMoa0802885

8. Staiger AM, Altenbuchinger M, Ziepert M, Kohler C, Horn H, Huttner M, et al. A novel lymphoma-associated macrophage interaction signature (LAMIS) provides robust risk prognostication in diffuse large B-cell lymphoma clinical trial cohorts of the DSHNHL. *Leukemia* (2020) 34(2):543–52. doi: 10.1158/2159-8290.CD-20-0839

9. Vegliante MC, Mazzara S, Zaccaria GM, De Summa S, Esposito F, Melle F, et al. NR1H3 (LXRα) is associated with pro-inflammatory macrophages, predicts survival and suggests potential therapeutic rationales in diffuse large B-cell lymphoma. *Hematol Oncol* (2022) 40(5):864–75. doi: 10.1038/nrclinonc.2016.217

10. Autio M, Leivonen SK, Brück O, Mustjoki S, Mészáros Jørgensen J, Karjalainen-Lindsberg ML, et al. Immune cell constitution in the tumor microenvironment predicts the outcome in diffuse large B-cell lymphoma. *Haematologica* (2021) 106(3):718–29. doi: 10.1016/j.cub.2020.06.081

11. Wright GW, Huang DW, Phelan JD, Coulibaly ZA, Roulland S, Young RM, et al. A probabilistic classification tool for genetic subtypes of diffuse large B cell lymphoma with therapeutic implications. *Cancer Cell* (2020) 37(4):551–568.e14. doi: 10.3390/cancers14061469

12. Kotlov N, Bagaev A, Revuelta MV, Phillip JM, Cacciapuoti MT, Antysheva Z, et al. Clinical and biological subtypes of B-cell lymphoma revealed by microenvironmental signatures. *Cancer Discovery* (2021) 11(6):1468–89. doi: 10.1155/2016/9720912

13. Mantovani A, Marchesi F, Malesci A, Laghi L, Allavena P. Tumour-associated macrophages as treatment targets in oncology. *Nat Rev Clin Oncol* (2017) 14(7):399–416. doi: 10.1111/cas.15179

14. Anderson NM, Simon MC. The tumor microenvironment. *Curr Biol* (2020) 30 (16):R921–5. doi: 10.3324/haematol.2014.113472

15. García-Domínguez DJ, Hontecillas-Prieto L, Palazón-Carrión N, Jiménez-Cortegana C, Sánchez-Margalet V, de la Cruz-Merino L. Tumor immune microenvironment in lymphoma: Focus on epigenetics. *Cancers (Basel)* (2022) 14 (6):1469. doi: 10.3390/jcm9082418

16. Guo Q, Jin Z, Yuan Y, Liu R, Xu T, Wei H, et al. New mechanisms of tumor-associated macrophages on promoting tumor progression: Recent research advances and

potential targets for tumor immunotherapy. *J Immunol Res* (2016) 2016:9720912. doi: 10.1080/2162402X.2018.1442164

17. Carreras J, Kikuti YY, Hiraiwa S, Miyaoka M, Tomita S, Ikoma H, et al. High PTX3 expression is associated with a poor prognosis in diffuse large B-cell lymphoma. *Cancer Sci* (2022) 113(1):334–48. doi: 10.1016/j.annonc.2021.08.1991

18. Riihijärvi S, Fiskvik I, Taskinen M, Vajavaara H, Tikkala M, Yri O, et al. Prognostic influence of macrophages in patients with diffuse large B-cell lymphoma: A correlative study from a Nordic phase II trial. *Haematologica* (2015) 100(2):238–45. doi: 10.1309/AJCPJX4BJV9NLQHY

19. Tamma R, Ranieri G, Ingravallo G, Annese T, Oranger A, Gaudio F, et al. Inflammatory cells in diffuse large B cell lymphoma. *J Clin Med* (2020) 9(8):2418. doi: 10.1186/s12885-019-6208-x

20. Nam SJ, Kim S, Kwon D, Kim H, Kim S, Lee E, et al. Prognostic implications of tumor-infiltrating macrophages, M2 macrophages, regulatory T-cells, and indoleamine 2,3-dioxygenase-positive cells in primary diffuse large B-cell lymphoma of the central nervous system. *Oncoimmunology* (2018) 7(7):e1442164. doi: 10.1080/2162402X.2018.1442164

21. Croci GA, Au-Yeung RKH, Reinke S, Staiger AM, Koch K, Oschlies IR, et al. SPARC-Positive macrophages are the superior prognostic factor in the microenvironment of diffuse large B-cell lymphoma and independent of MYC rearrangement and double-/triple-hit status. *Ann Oncol* (2021) 32(11):1400–9. doi: 10.1111/apm.13195

22. Meyer PN, Fu K, Greiner T, Smith L, Delabie J, Gascoyne R. The stromal cell marker SPARC predicts for survival in patients with diffuse large B-cell lymphoma treated with rituximab. *Am J Clin Pathol* (2011) 135(1):54–61. doi: 10.1309/AJCPJX4BJV9NLQHY

23. Li YL, Shi ZH, Wang X, Gu KS, Zhai ZM. Tumor-associated macrophages predict prognosis in diffuse large B-cell lymphoma and correlation with peripheral absolute monocyte count. *BMC Cancer.* (2019) 19(1):1049. doi: 10.1371/journal.pone.0078730

24. Cencini E, Fabbri A, Schiattone L, Sicuranza A, Mecacci B, Granai M. Prognostic impact of tumor-associated macrophages, lymphocyte-to-monocyte and neutrophil-to-lymphocyte ratio in diffuse large B-cell lymphoma. *Am J Blood Res* (2020) 10(4):97–108. doi: 10.1007/s12032-011-0123-6

25. Parkhi M, Chatterjee D, Bal A, Vias P, Yadav BS, Prakash G. Prognostic implications of the tumor immune microenvironment and immune checkpoint pathway in primary central nervous system diffuse large B-cell lymphoma in the north Indian population. *APMIS* (2022) 130(2):82–94. doi: 10.1016/j.humpath.2017.04.012

26. Wada N, Zaki MA, Hori Y, Hashimoto K, Tsukaguchi M, Tatsumi Y, et al. Osaka Lymphoma study group. *Tumour-associated macrophages diffuse large B-cell lymphoma: Study Osaka Lymphoma Study Group Histopathology.* (2012) 60(2):313–9. doi: 10.1097/PAI.0000000000000645

27. Yoshida N, Oda M, Kuroda Y, Katayama Y, Okikawa Y, Masunari T, et al. Clinical significance of sIL-2R levels in B-cell lymphomas. *PloS One* (2013) 8(11):e78730. doi: 10.1007/s10014-022-00427-4

28. Cai QC, Liao H, Lin SX, Xia Y, Wang XX, Gao Y, et al. High expression of tumor-infiltrating macrophages correlates with poor prognosis in patients with diffuse large B-cell lymphoma. *Med Oncol* (2012) 29(4):2317–22. doi: 10.3109/10428194.2014.893311

29. Jeong J, Oh EJ, Yang WI, Kim SJ, Yoon SO. Implications of infiltrating immune cells within bone marrow of patients with diffuse large B-cell lymphoma. *Hum Pathol* (2017) 64:222–31. doi: 10.1186/1745-6215-8-16

30. Matsuki E, Bohn OL, El Jamal S, Pichardo JD, Zelenetz AD, Younes A, et al. Lymphocyte-to-monocyte ratio may serve as a better prognostic indicator than tumor-associated macrophages in DLBCL treated with rituximab. *Appl Immunohistochem Mol Morphol.* (2019) 27(8):572–80. doi: 10.1097/PAI.0000000000000645

31. Asano K, Yamashita Y, Ono T, Natsumeda M, Beppu T, Matsuda K, et al. Clinicopathological risk factors for a poor prognosis of primary central nervous system lymphoma in elderly patients in the tohoku and niigata area: A multicenter, retrospective, cohort study of the tohoku brain tumor study group. *Brain Tumor Pathol* (2022) 39 (3):139–50. doi: 10.1016/j.anndiagpath.2015.04.008

32. Yamamoto W, Nakamura N, Tomita N, Takeuchi K, Ishii Y, Takahashi H, et al. Human leukocyte antigen-DR expression on flow cytometry and tumor-associated macrophages in diffuse large B-cell lymphoma treated by rituximab, cyclophosphamide, doxorubicin, vincristine and prednisone therapy: retrospective cohort study. *Leuk Lymphoma.* (2014) 55(12):2721–7. doi: 10.4132/KoreanJPathol.2011.45.4.361

33. Tierney JF, Stewart LA, Ghersi D, Burdett S, Sydes MR. Practical methods for incorporating summary time-to-event data into meta-analysis. *Trials* (2007) 8:16. doi: 10.1002/hon.2142

34. Xu YL, Wang HQ, Qian ZZ, Song Z, Zhou SY, Zhang HL, et al. Expression and prognostic value of regulatory T cells and M2 macrophages in diffuse large B-cell lymphoma tissues. *Zhonghua Zhong Liu Za Zhi.* (2013) 35(6):450–5.

35. Wang X, Li X, Zhang X, Zang L, Yang H, Zhao W, et al. Toll-like receptor 4-induced inflammatory responses contribute to the tumor-associated macrophages formation and infiltration in patients with diffuse large B-cell lymphoma. *Ann Diagn Pathol* (2015) 19(4):232–8. doi: 10.1016/j.anndiagpath.2015.04.008

36. Lee J, K wak Y, Kim C, Kim I. Association of CD57+ natural killer cells with better overall survival in DLBCL patients. *Korean J Path.* (2011) 45:361–70. doi: 10.1371/journal.pone.0170042

37. Marchesi F, Cirillo M, Bianchi A, Gately M, Olimpieri OM, Cerchiara E, et al. High density of CD68+/CD163+ tumour-associated macrophages (M2-TAM) at diagnosis is significantly correlated to unfavorable prognostic factors and to poor clinical outcomes in patients with diffuse large B-cell lymphoma. *Hematol Oncol* (2015) 33(2):110–2. doi: 10.18632/oncotarget.25334

38. Ghorab DS, Helaly AM, El Mahdi HS, Khatatbeh M, Ibrahiem AT. Prognostic role of tumor microenvironment in DLBCL and relation to patients' clinical outcome: A clinical and immunohistochemical study. *Anal Cell Pathol (Amst).* (2022) 2022:9993496. doi: 10.1016/j.ygyno.2017.07.007

39. Thomas J, Chandler J, Cumpston M, Li T, Page MJ, et al. Cochrane handbook for systematic reviews of interventions Version5.2.0. *Cochrane* (2022). Available at: www.training.cochrane.org/handbook.

40. Yin S, Huang J, Li Z, Zhang J, Luo J, Lu C, et al. The prognostic and clinicopathological significance of tumor-associated macrophages in patients with gastric cancer: a meta-analysis. *PloS One* (2017) 12(1):e0170042. doi: 10.7150/jca.46282

41. Wu SQ, Xu R, Li XF, Zhao XK, Qian BZ. Prognostic roles of tumor associated macrophages in bladder cancer: A system review and meta-analysis. *Oncotarget* (2018) 9 (38):25294–303. doi: 10.18632/oncotarget.25334

42. Yuan X, Zhang J, Li D, Mao Y, Mo F, Du W, et al. Prognostic significance of tumor-associated macrophages in ovarian cancer: A meta-analysis. *Gynecol Oncol* (2017) 147 (1):181–7. doi: 10.1186/s12916-016-0711-6

43. Zhao X, Qu J, Sun Y, Wang J, Liu X, Wang F, et al. Prognostic significance of tumor-associated macrophages in breast cancer: A meta-analysis of the literature. *Oncotarget* (2017) 8(18):30576–86. doi: 10.1007/s12325-017-0612-x

44. Xie W, Yan O, Liu F, Han Y, Wang H. Prognostic value of survivin in nasopharyngeal carcinoma: A systematic review and meta-analysis. *J Cancer.* (2021) 12 (14):4399–407. doi: 10.1158/1078-0432.CCR-07-0778

45. Xu X, Li Z, Liu J, Zhu F, Wang Z, Wang J, et al. The prognostic value of tumour-associated macrophages in non-hodgkin's lymphoma: A systematic review and meta-analysis. *Scand J Immunol* (2020) 91(1):e12814. doi: 10.3390/ijms22136995

46. Guo B, Cen H, Tan X, Ke Q. Meta-analysis of the prognostic and clinical value of tumor-associated macrophages in adult classical Hodgkin lymphoma. *BMC Med* (2016) 14(1):159. doi: 10.1158/1078-0432.CCR-16-0870

47. Salles G, Barrett M, Foà R, Maurer J, O'Brien S, Valente N, et al. Rituximab in B-cell hematologic malignancies: A review of 20 years of clinical experience. *Adv Ther* (2017) 34(10):2232–73. doi: 10.1002/cam4.886

48. Taskinen M, Karjalainen-Lindsberg ML, Nyman H, Eerola LM, Leppä S. A high tumor-associated macrophage content predicts favorable outcome in follicular lymphoma patients treated with rituximab and cyclophosphamide-doxorubicin-vincristine-prednisone. *Clin Cancer Res* (2007) 13(19):5784–9. doi: 10.1016/j.ccr.2014.05.016

49. Boutilier AJ, Elsawa SF. Macrophage polarization states in the tumor microenvironment. *Int J Mol Sci* (2021) 22(13):6995. doi: 10.1002/eji.201847888

50. Kalbasi A, Komar C, Tooker GM, Liu M, Lee JW, Gladney WL, et al. Tumor-derived CCL2 mediates resistance to radiotherapy in pancreatic ductal adenocarcinoma. *Clin Cancer Res* (2017) 23(1):137–48. doi: 10.1158/1078-0432.CCR-16-0870

51. Arakaki R, Yamasaki T, Kanno T, Shibasaki N, Sakamoto H, Utsunomiya N. CCL2 as a potential therapeutic target for clear cell renal cell carcinoma. *Cancer Med* (2016) 5 (10):2920–33. doi: 10.1371/journal.pone.0153550

52. Ries CH, Cannarile MA, Hoves S, Benz J, Wartha K, Runza V, et al. Targeting tumor-associated macrophages with anti-CSF-1R antibody reveals a strategy for cancer therapy. *Cancer Cell* (2014) 25(6):846–59. doi: 10.3892/ol.2020.12037

53. Maeda A, Digifico E, Andon FT, Mantovani A, Allavena P. Poly(I:C) stimulation is superior than imiquimod to induce the antitumoral functional profile of tumor-conditioned macrophages. *Eur J Immunol* (2019) 49(5):801–11. doi: 10.1186/s13045-021-01197-w

54. Jensen JL, Hope C, Asimakopoulos F. Deploying myeloid cells against myeloma. *Oncoimmunology* (2015) 5(3):e1090076. doi: 10.3109/10428194.2015.1007504

55. Zhang M, Hutter G, Kahn SA, Azad TD, Gholamin S, Xu CY, et al. Anti-CD47 treatment stimulates phagocytosis of glioblastoma by M1 and M2 polarized macrophages and promotes M1 polarized macrophages *In vivo*. *PloS One* (2016) 11(4):e0153550. doi: 10.1038/s41375-019-0573-y

56. Li DK, Wang W. Characteristics and clinical trial results of agonistic anti-CD40 antibodies in the treatment of malignancies. *Oncol Lett* (2020) 20(5):176. doi: 10.1002/hon.3050

57. Jiang Z, Sun H, Yu J, Tian W, Song Y. Targeting CD47 for cancer immunotherapy. *J Hematol Oncol* (2021) 14(1):180. doi: 10.1186/s13045-021-01197-w

58. Fayad L, Ansell SM, Advani R, Coiffier B, Stuart R, Bartlett NL, et al. Dacetuzumab plus rituximab, ifosfamide, carboplatin and etoposide as salvage therapy for patients with diffuse large B-cell lymphoma relapsing after rituximab, cyclophosphamide, doxorubicin, vincristine and prednisolone: A randomized, double-blind, placebo-controlled phase 2b trial. *Leuk Lymphoma.* (2015) 56(9):2569–78. doi: 10.1016/j.ccell.2020.03.015

frontiers | Frontiers in Immunology

TYPE Original Research
PUBLISHED 28 September 2023
DOI 10.3389/fimmu.2023.1258700

OPEN ACCESS

EDITED BY
Robert Ohgami,
The University of Utah, United States

REVIEWED BY
Oliver Seifert,
University of Stuttgart, Germany
Michael R. Green,
University of Texas MD Anderson Cancer Center, United States
Benjamí Oller Salvia,
Institut Químic de Sarrià, Spain

*CORRESPONDENCE
Harald Kolmar
Harald.Kolmar@TU-Darmstadt.de

RECEIVED 14 July 2023
ACCEPTED 07 September 2023
PUBLISHED 28 September 2023

CITATION
Schoenfeld K, Harwardt J, Habermann J, Elter A and Kolmar H (2023) Conditional activation of an anti-IgM antibody-drug conjugate for precise B cell lymphoma targeting.
Front. Immunol. 14:1258700.
doi: 10.3389/fimmu.2023.1258700

Conditional activation of an anti-IgM antibody-drug conjugate for precise B cell lymphoma targeting

Katrin Schoenfeld[1], Julia Harwardt[1], Jan Habermann[1], Adrian Elter[1] and Harald Kolmar[1,2]*

[1]Institute for Organic Chemistry and Biochemistry, Technical University of Darmstadt, Darmstadt, Germany, [2]Centre for Synthetic Biology, Technical University of Darmstadt, Darmstadt, Germany

Cancerous B cells are almost indistinguishable from their non-malignant counterparts regarding their surface antigen expression. Accordingly, the challenge to be faced consists in elimination of the malignant B cell population while maintaining a functional adaptive immune system. Here, we present an IgM-specific antibody-drug conjugate masked by fusion of the epitope-bearing IgM constant domain. Antibody masking impaired interaction with soluble pentameric as well as cell surface-expressed IgM molecules rendering the antibody cytotoxically inactive. Binding capacity of the anti-IgM antibody drug conjugate was restored upon conditional protease-mediated demasking which consequently enabled target-dependent antibody internalization and subsequent induction of apoptosis in malignant B cells. This easily adaptable approach potentially provides a novel mechanism of clonal B cell lymphoma eradication to the arsenal available for non-Hodgkin's lymphoma treatment.

KEYWORDS

B cell receptor, antibody-drug conjugate, masked antibody, conditional activated antibody, MMP-9, matriptase, B cell lymphoma

Introduction

Immunotherapies represent a broad and rapidly growing type of therapies having a substantial impact on cancer outcomes. Monoclonal antibodies (mAbs) are among the first groups of immunotherapies approved for anti-tumor treatment and are still of exceptional relevance in current treatment regimens (1). Rituximab, the first US Food and Drug Administration (FDA)-approved mAb implemented in oncology, has widely been administered in patients suffering from B cell non-Hodgkin's lymphoma (NHL). NHL is a heterogeneous group of neoplasms and the most frequently diagnosed adult hematological cancer, accounting for the seventh most common cancer and the ninth leading cause of cancer deaths in the US (2). Targeting the pan-B cell antigen CD20, rituximab exerts anti-tumor activity in four main ways, three of which rely on recruiting

effector mechanisms from the patient's immune system such as complement-dependent cytotoxicity (CDC), antibody-dependent cell-mediated cytotoxicity (ADCC) and antibody-dependent phagocytosis (ADP) (3). A fourth proposed mechanism of action is the induction of apoptosis through both caspase-dependent and -independent mechanisms (3, 4). Although rituximab in combination with chemotherapy has tremendously improved the chance of cure for NHL patients, the clinical effectiveness of rituximab is ultimately limited by the development of treatment resistance. Notably, only 40% of the patients initially responding to rituximab have the ability to respond again after relapse (5, 6).

The B cell receptor (BCR) complex plays a pivotal role in the adaptive immune response. Comprising a membrane-bound immunoglobulin (Ig) and a non-covalently linked heterodimer composed of Igα and Igβ it is expressed on the surface of B lymphocytes with each B cell clone possessing a unique BCR of Ig isotype IgA, IgD, IgE, IgG, or IgM (7, 8). Previous reports have demonstrated that malignant B cells frequently express IgM BCRs (9–12). A subtype of the diffuse large B cell lymphoma (DLBCL) is activated B cell-like DLBCL, where it has been reported that IgM-positivity of tumor correlates with a poor prognosis and a shorter overall survival for patients (10–12). Harnessing the fact that clonal B cell cancers in most cases express BCRs of one Ig isotype, it might be possible to selectively deplete malignant B cells of the IgM isotype while sparing the majority of B lymphocytes expressing other isotype or no BCRs. However, therapeutic antibodies directed against IgM may not fully function in the body due to the presence of soluble IgM molecules in large amounts. In order to address the problem of selectivity and potential target-mediated drug disposition, an IgMxHLA-DR bispecific antibody targeting two B cell antigens has recently been engineered which demonstrated significant *in vitro* anti-tumor activity as well as efficacy and tolerability in non-human primate studies (13).

Besides improving specificity via multispecific cancer targeting, masking strategies have been developed allowing for conditional activation of antibodies in tumor tissue (14–16). The approach requires the generation of a suitable masking unit which prevents antibody-antigen interaction either by steric hindrance, e.g. by fusion of a bulky mask, or by specific binding to the antibody paratope, such as an epitope-mimetic or anti-idiotypic antibody fragment (14, 16). Antibody activation through demasking is typically mediated by proteases, such as serine proteases (e.g. matriptase), matrix metalloproteinases (e.g. MMP-2/MMP-9) and cysteine proteases (e.g. cathepsin S) frequently overexpressed in tumor tissues (17–19). Previous masking attempts put forth antibody therapeutics with improved safety profiles, while retaining anti-disease activity (20–24). The versatile probody therapeutic technology platform developed by CytomX Therapeutics has been applied to target a variety of receptors including CTLA-4, EGFR, as well as molecules considered undruggable because of their broad tissue expression, such as CD71 and EpCAM (25–27). The conditionally activated probody-drug conjugate CX-2029 (anti-CD71) demonstrated tumor regression and was well tolerated in patients with advanced solid tumors (28).

To combat resistance of current mAb-based therapies and improve the potency of biomolecules, antibody-drug conjugates (ADC) feature ideal properties for precise and efficient tumor targeting (29, 30). The first-in-class ADC to be FDA-approved for therapy was gemtuzumab ozogamicin (Mylotarg), in 2000 for the treatment of CD33-positive acute myeloid leukemia (AML) (31). Since then, 14 ADCs received worldwide market approval, besides over 100 ADC candidates being investigated in clinical stages at present (32). ADCs are typically composed of mAbs covalently bound to potent cytotoxic payload through synthetic (cleavable) linkers. However, there is ongoing optimization of certain parameters, including mAb specificity, linker technology, drug potency as well as stoichiometry and placement of warheads (30, 32). The mechanism leading to ADC's anti-tumor effect includes binding of the ADC to its target antigen that triggers ADC internalization and intracellular release of the payload which eventually mediates cytotoxic effects. Hence, candidate ADCs must be carefully selected regarding numerous properties influencing safety and efficacy. Particularly, the antigen to be targeted by the ADC must fulfill certain characteristics such as overexpression on the surface of cancer cells with minimal expression in normal tissue and the potency to rapidly internalize upon ADC binding (32). Since B cell NHL is currently treated with either chemotherapy or immunotherapy or a combination of both, it is anticipated that ADCs can be rational for NHL control.

In this study, we developed a proteolytically activatable IgM-directed antibody-drug conjugate for precise targeting of IgM-positive B cell lymphoma (Figure 1). Starting with the immunization of a chicken with IgM from human serum, we isolated IgM binders by single-chain variable fragment (scFv) immune library screening using yeast surface display (YSD) in combination with fluorescence-activated cell sorting (FACS). After expression and characterization of isolated binders in scFv format, full-length antibodies in Fab-Fc format were generated. With respect to potential off-target effects on healthy IgM-expressing B cells and capturing of antibodies by soluble IgM in the blood stream, we identified the antigenic constant Ig domain, derived from the IgM antigen, for antibody masking. The masking unit was genetically fused to the N-terminus of the anti-IgM light chain (LC) via a dual-protease cleavable linker addressable by matrix metalloproteinase-9 (MMP-9) and matriptase since these proteases are described to be overexpressed in B cell lymphoma (33, 34). The IgM-targeting antibody was further conjugated with the highly toxic and clinically proven chemotherapeutic agent monomethyl auristatin E (MMAE) imparting cytotoxic properties to the molecule (32). The resulting masked anti-IgM ADC demonstrated no significant interactions with different types of B cells. However, unmasking resulted in specific targeting and efficient killing of IgM-positive lymphoma cells while largely sparing other lymphocytes from chemotherapeutic damage.

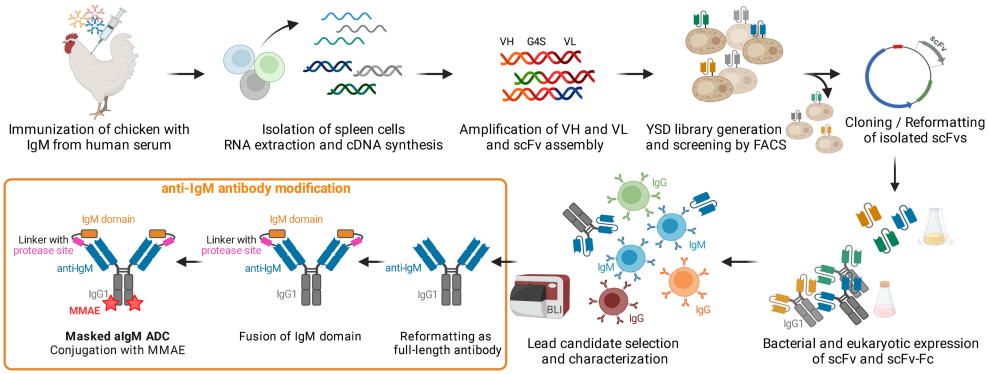

FIGURE 1
Concept Overview. Chicken immunization with IgM from human serum was followed by splenic RNA isolation and cDNA synthesis. Variable antibody domains were amplified and assembled as scFvs for yeast surface display and FACS. IgM binding scFvs were reformatted and cloned into bacterial and mammalian vectors for scFv/scFv-Fc expression. After selection and characterization of a lead candidate, the IgM binder was reformatted as full-length antibody, fused with the masking IgM domain and ultimately conjugated with MMAE resulting in a masked anti-IgM (aIgM) ADC. Created with BioRender.com.

Results

Design of protease-activated masked anti-IgM antibody-drug conjugates

Based on a chicken-derived anti-IgM (aIgM) antibody, we designed an antibody-drug conjugate that is masked to overcome potential off-target effects towards circulating IgM$^+$ B cells and interactions with soluble IgM in the blood stream (Figure 2). In our approach, the human IgM domain targeted by the antibody served as masking unit attached to the aIgM light chain. We assumed that the heavy chain CDRs are mainly responsible for antigen recognition as this was discovered in previous chicken-derived antibodies including common light chain approaches and is reinforced by the fact that chicken CDR3 of the VH tend to be longer and have much higher cysteine content leading to increased stability and complexity (36–39). Fusion of the masking unit was achieved via a synthetic linker (33 amino acids) comprising a dual-protease site (MMP site and MatA site) recognized by MMP-2/9 and matriptase (Figure 2A). Linker sequence and applicability to protease-activated antibodies in tumor context have been recently described by *Geiger et al.*, demonstrating a synergistic effect for the

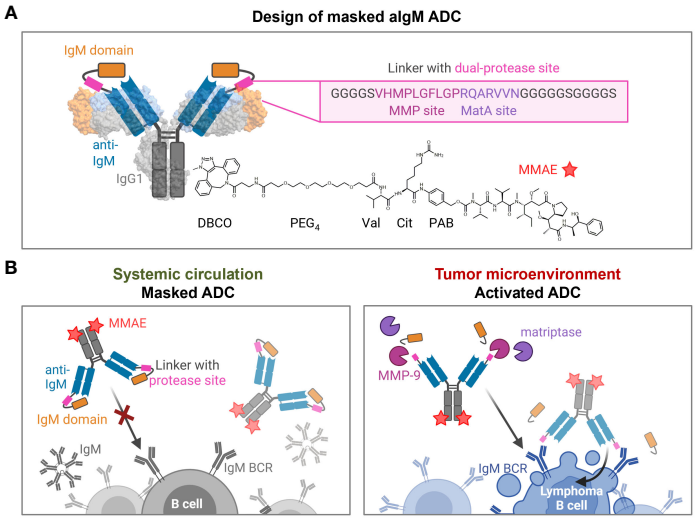

FIGURE 2
Design and mode of action of masked aIgM ADC. **(A)** Schematic representation of the masked aIgM ADC. The anti-IgM LC is (N-terminally) fused to an IgM domain via a linker with dual-protease site, the HC is (C-terminally) modified with DBCO-PEG$_4$-Val-Cit-PAB-MMAE. DBCO, Dibenzocyclooctyne; PEG, polyethylene glycol; Val, valine, Cit: citrulline; PAB, p-aminobenzyl alcohol; MMAE, monomethyl auristatin E. Surface representation rendered with UCSF ChimeraX (35) from PDB: 1IGT/7XQ8. **(B)** Conceptional mode of action of the masked anti-IgM ADC. In systemic circulation the masked aIgM ADC is not able to bind to either soluble pentameric IgM nor membrane-bound IgM. Once reaching the tumor microenvironment, tumor-specific proteases such as MMP-9 or matriptase hydrolyze the linker connecting the aIgM antibody and the masking IgM domain. The activated aIgM ADC regains binding ability leading to specific ADC uptake and killing of IgM$^+$ lymphoma B cells. Created with BioRender.com.

combination of the cleavage sites for MMP-2/9-matriptase compared to MatA site or MMP site linkers alone (21). For the generation of an ADC the mAb component was further provided with MMAE, since NHL is known to be sensitive to microtubule inhibitors (40, 41). The payload consists of DBCO, PEG_4 linker, Val-Cit dipeptide sequence as cathepsin substrate, p-aminobenzyl alcohol (PAB) self-immolative spacer and the cytotoxic payload MMAE. Site-specific coupling of DBCO-PEG_4-Val-Cit-PAB-MMAE was accomplished via a chemoenzymatic conjugation approach, resulting in a theoretical drug-to-antibody ratio (DAR) of two (detailed conjugation strategy described in section 'Cytotoxicity of masked and protease-activated CH2-aIgM ADC'). The aIgM ADC should remain masked in systemic circulation, but upon reaching the tumor microenvironment, upregulated protease activity promotes cleavage of the substrate linker and subsequent release of the blocking IgM domain (Figure 2B). Following antibody-directed binding to tumor target IgM isotype BCRs, the ADC is expected to be effectively internalized, followed by lysosomal degradation resulting in cleavage of the drug linker and intracellular release of the cytotoxic agent. Finally, MMAE binds to tubulin which inhibits its polymerization and ultimately triggers tumor cell death (42).

Generation of chicken-derived anti-IgM antibodies

In order to generate protease-activated anti-human IgM antibodies, we screened for IgM binders which are in a second step equipped with the epitope-bearing human IgM domain serving as antigenic affinity-based mask. Antibodies of IgM isotype play important roles in non-immune as well as antigen-induced immune reactions and constant domains of Ig heavy chain are broadly conserved in mammals (43–45). Hence, immunization of popularly chosen mammalian species such as mouse, rabbit or goat might not result in the desired immune response. Accordingly, chickens were considered for immunization as they are phylogenetic distant from humans and previous attempts succeeded in accessing antibodies against conserved epitopes on mammalian molecules (46, 47). Recently, we described the isolation of highly affine antibody fragments derived from immunized chickens using yeast surface display in combination with FACS (48–50). Applying this approach, we obtained high chicken antibody titers against human IgM and were able to enrich binders within two consecutive sorting rounds using 500 nM or 10 nM IgM from human serum, respectively (Supplementary Figures 1A, B). Sequence analysis of four yeast single clones emerging from the screening revealed four distinct scFv candidates (S5, S6, S8, S9). The four scFvs were heterologously expressed in *Escherichia coli* and were subjected to B cell binding assays. Antibody clone aIgM S8 was selected as lead candidate since it demonstrated affine binding to IgM^+ lymphocytes while IgM^- cells were not targeted indicating isotypic specificity (Supplementary Figure 2).

Generation and characterization of conditionally activated aIgM

The aIgM scFv S8 was reformatted as scFv-Fc fusion and as Fab-Fc full-length antibody. To investigate which of the four constant IgM domains aIgM S8 targets, biolayer interferometry (BLI) epitope binning was performed. To this end, His-tagged CH1-CH4 IgM domains were expressed separately in Expi293F™ cells and cell culture supernatants were immobilized on Ni-NTA biosensors. Association with aIgMscFv-Fc revealed specific and exclusive binding to IgM CH2 domain (Figure 3A). Consequently, simultaneous binding of full-length IgM and IgM CH2 domain should not be possible. This was confirmed by loading of biotinylated aIgMscFv-Fc onto SAX biosensors and stepwise association with equimolar concentrations of CH2 in antigens using 1,000 nM single IgM CH2 domain and 100 nM (pentameric) IgM from human serum (Figure 3B). The slightly increased binding signal detected when incubating with CH2, following the first IgM association can be ascribed to the small size of IgM CH2 (13 kDa) in comparison to the pentameric IgM molecule (970 kDa) allowing the single Ig domain to bind unoccupied paratopes which are sterically unavailable for pentameric IgM. Attempts to determine the affinity of aIgMscFv-Fc towards IgM CH2 failed as the off-rate turned out to be very low, nevertheless, implying high-affinity binding (Supplementary Figure 3A) . In a similar setup, a competition assay with B cells was performed using IgM^+ SUP-B8 and Ramos cells incubated with 100 nM aIgMscFv-Fc and varying concentrations of IgM CH2 (39-10,000 nM) (Figure 3C). In accordance with the BLI measurements, B cell binding decreased with increasing IgM CH2 concentration amounting to IC_{50} values of 143 nM and 135 nM for SUP-B8 and Ramos cells, respectively. Hence, BCRs of IgM isotype on the cell surface compete with the soluble IgM CH2 domain for scFv binding corroborating the notion that CH2 is the epitope-bearing IgM domain.

Taken together, these results indicate that human IgM CH2 domain suits as masking unit for the previously identified aIgM S8 antibody since pre-incubation of antibody with IgM CH2 efficiently impairs IgM binding in biolayer interferometric studies as well as on a cellular level with membrane-bound IgM.

For masking of aIgM S8 antibody the IgM CH2 domain was fused to the light chain by a linker with dual-protease site. The unmasked aIgM and masked aIgM antibody variant, referred to as CH2-aIgM, were expressed in Expi293F™ cells and purified via Protein A affinity chromatography. Integrity, size and purity of the proteins including stability of the linker during production and purification process were confirmed using reducing SDS-PAGE analysis (Figure 4A). Thermal stability investigated by SYPRO Orange revealed melting temperatures of 72.5°C and 71.5°C for the aIgM and CH2-aIgM, respectively (Supplementary Figure 4). Thus, no significant change in thermal stability was observed by attachment of the additional Ig domain. The functionality of the parental full-length aIgM concerning binding of IgM from human serum and IgM-derived CH2 domain was confirmed by BLI (Supplementary Figure 3B). In order to prove feasibility of

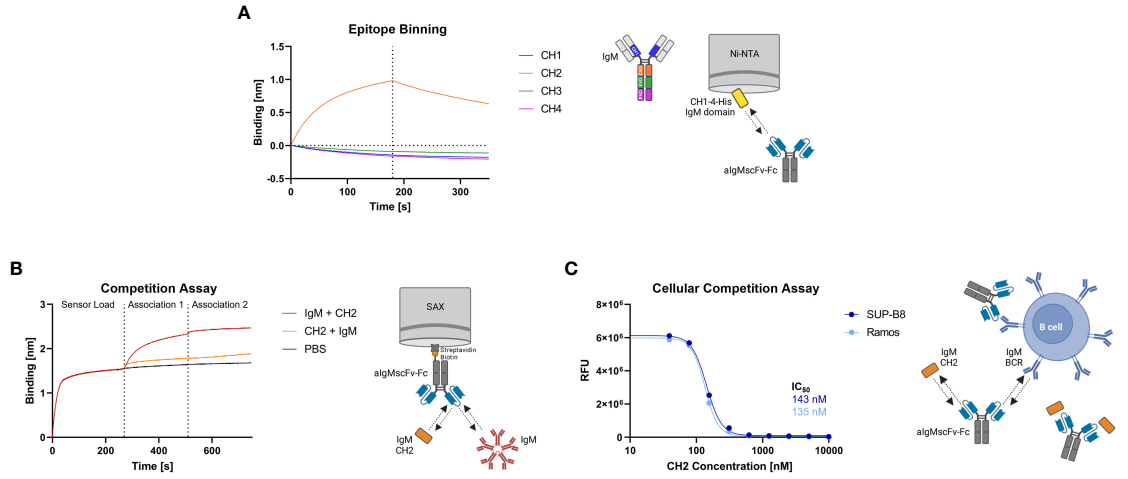

FIGURE 3
Epitope binning of aIgMscFv-Fc and CH2/IgM competition. **(A)** BLI-assisted epitope binning. The four His-tagged constant IgM domains of the HC (CH1, CH2, CH3 and CH4) were loaded onto Ni-NTA biosensor tips and associated with 150 nM aIgMscFv-Fc, followed by dissociation. **(B)** BLI-assisted competition assay. Biotinylated aIgMscFv-Fc was loaded onto SAX tips and IgM CH2/IgM from human serum were associated in sequence. **(C)** Cellular competition assay. IgM$^+$ SUP-B8 and Ramos B cells were incubated with 100 nM aIgMscFv-Fc and varying concentrations of IgM CH2 domain (39-10,000 nM). Detection was performed using anti-human IgG Fc-PE staining and flow cytometry.

reactivation of the aIgM binding capability in the masked antibody, CH2-aIgM was treated with either MMP-9 or matriptase. Linker proteolysis was analyzed by SDS-PAGE demonstrating successful and complete linker cleavage of the CH2-aIgM LC by both proteases which resulted in the aIgM LC migrating slightly higher in SDS gel electrophoresis than the unmasked aIgM LC due to residual linker amino acids, and the solitary CH2 domain (Figure 4A). Biolayer interferometry measurements were conducted to investigate, whether the binding capacity of CH2-aIgM is diminished and can in a next step be restored by protease cleavage. Therefore, aIgM, CH2-aIgM, protease treated CH2-aIgM and rituximab as an unrelated control were immobilized onto AHC biosensors and subsequently incubated with IgM from human serum. With CH2-aIgM loaded, association of IgM is completely impaired since the binding signal is comparable to rituximab control (Figure 4B). As previous experiments have shown that the dissociation rate of soluble IgM CH2 from the antibody is low, a Protein A purification step was systematically introduced after protease-mediated linker hydrolysis in subsequent assays in order to remove a large fraction of cleaved CH2 domain. MMP-9-cleaved, purified CH2-aIgM allows IgM association, although maximum binding capacity of aIgM may not fully be restored. This effect of reduced interaction might be traced back to remaining cleaved masking units blocking the aIgM paratope due to slow dissociation. Similar results were obtained in BLI experiments associating with different IgM concentrations (3.9-125 nM) for competition with cleaved CH2 masking moiety as well as in a reverse experimental setup immobilizing IgM to the biosensor and incubating with the respective antibody variants (Supplementary Figures 3C, D).

On-cell binding of masked and protease-activated CH2-aIgM

To investigate, whether the masked CH2-aIgM remains innate to IgM interaction when membrane-bound in a high copy number on cells and whether protease-activation of CH2-aIgM restores binding functionality, cell binding experiments were performed

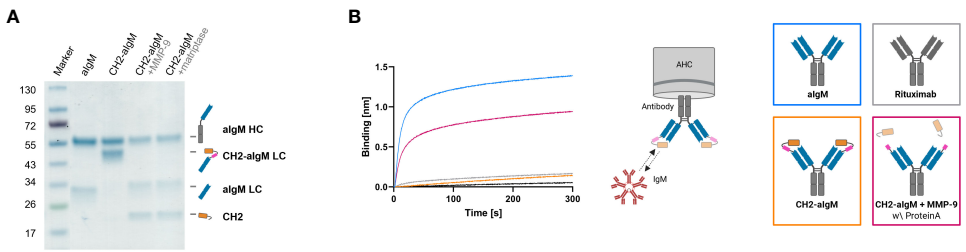

FIGURE 4
Protease-activation of CH2-masked aIgM. **(A)** Reducing SDS-PAGE of depicted antibodies with schematic representations of heavy and (masked) light chains. **(B)** BLI measurement. The four antibody constructs (Rituximab, aIgM, CH2-aIgM, Protein A purified CH2-aIgM+MMP-9) were loaded onto AHC biosensor tips and associated with 100 nM IgM from human serum.

using flow cytometry. SUP-B8 and Ramos B lymphoid cell lines derived from Burkitt lymphoma were used as IgM^+ cells while IgM^-/IgG^+ IM-9 B cells served as control (51–53). Cells were stained with 100 nM of respective antibody and PE-conjugated secondary antibody for detection. While aIgM represents maximum binding on IgM^+ SUP-B8 and Ramos cells, the masked variant CH2-aIgM shows 61-fold and 102-fold reduced cell binding, respectively (Figure 5A). Upon MMP-9 cleavage and Protein A purification of CH2-aIgM cell binding capacity is fully restored to a maximum binding comparable to the unmasked aIgM version. None of the antibodies showed unspecific interactions with IgM^-/IgG^+ IM-9 off-target cells. Furthermore, cell titration was conducted for determination of on-cell affinities for the masked and the proteolytically activated CH2-aIgM. Antibodies were applied to the cells in a serial dilution with concentrations ranging from 0.125 to 200 nM. Apparent binding affinities for aIgM amounted to 0.9 nM for SUP-B8 cells and 2.4 nM for Ramos cells, while titration of cleaved CH2-aIgM resulted in similar values of 1.5 nM and 2.6 nM for SUP-B8 and Ramos, respectively (Figure 5B). Besides comparable on-cell K_Ds of aIgM and protease treated CH2-aIgM, maximal binding levels are also restored. The masked CH2-aIgM displayed significantly reduced cell binding indicated by multiple-fold increased on-cell affinity values and decreased saturation binding levels (Figure 5B; Supplementary Figure 5A). Furthermore, interactions of aIgM and CH2-aIgM with PBMCs isolated from healthy human donor blood were scrutinized revealing binding of aIgM likely to the B cell subpopulation while the blocked aIgM antibody largely spares PBMCs (Supplementary Figure 5B). These results suggest that masking the aIgM antibody using a covalently linked blocking domain increases the likelihood of the mask remaining on the antibody due to loss of conformational degrees of freedom and high affinity, and thus significantly reduces binding of IgM. However, the MMP-9 treated CH2-aIgM revealed recovery in binding which indicates dissociation of the linker-cleaved CH2 domain from the antibody by reasons of competition with a high number of IgM BCRs in a cellular context (Figure 5). While covalent linkage of the CH2 domain shows efficient masking, presence of the cleaved masking unit reduces cell binding of the unmasked antibody to some extent (Supplementary Figure 6). This may be attributed to the relatively high concentration of masked antibody used (100 nM) and the slow dissociation kinetics of the masking CH2 domain.

Overall, transferring the features of the masked IgM antibody in a physiological setting, the blocked antibody is expected to be inert to interactions and interceptions related to IgM in systemic circulation while linker hydrolysis in the tumor microenvironment might result in localized unrestricted binding capacity and robust tumor targeting.

Cytotoxicity of masked and protease-activated CH2-aIgM ADC

For investigation of cytotoxicity mediated by an aIgM ADC and its masked variant CH2-aIgM ADC, both antibody versions were armed with MMAE generating ADCs with an expected DAR of two. Attachment of DBCO-PEG_4-Val-Cit-PAB-MMAE to the antibodies was accomplished site-specifically by a two-step approach of enzyme-assisted azide modification of the heavy chain's C-terminus which was endowed with a recognition sequence for lipoate-protein ligase A and click chemistry with DBCO-conjugated payload. Prior to cytotoxicity studies aIgM and CH2-masked aIgM were investigated towards internalization properties using our antibodies labeled with pH-dependent dye and flow cytometric analysis (54–56). In IgM^+ cell lines, the

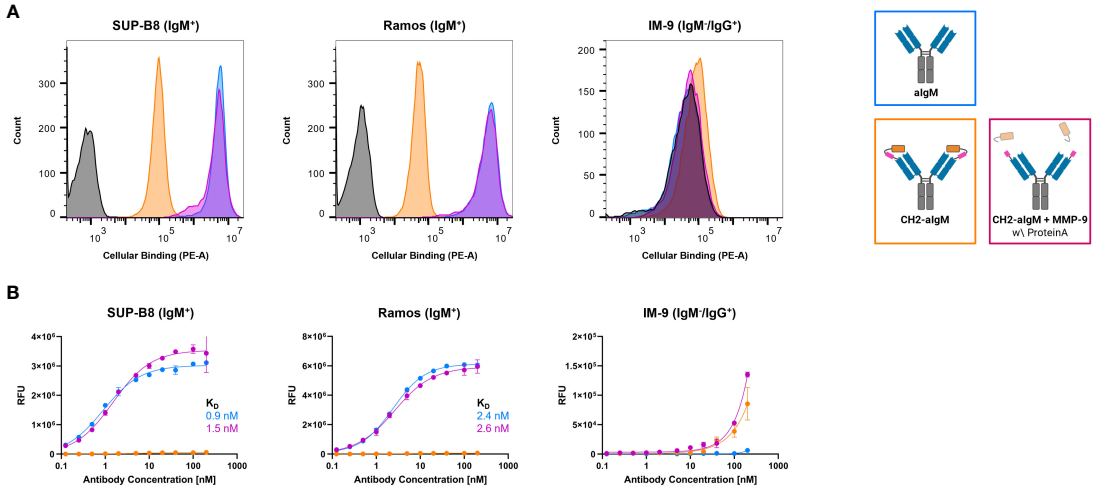

FIGURE 5
Cellular binding of unmasked and CH2-masked aIgM variants. Flow cytometry analysis of IgM^+ (SUP-B8, Ramos) and IgM^- (IM-9) B cells incubated with aIgM, CH2-aIgM and Protein A purified CH2-aIgM+MMP-9 antibodies and stained via anti-human IgG Fc-PE secondary detection antibody. **(A)** B cells were incubated with 100 nM of respective antibodies. Negative control samples (0 nM, black) represent cells stained with secondary detection antibody only. Histograms were created using FlowJoTM v10 Software (BD Life Sciences). **(B)** Cell titration of respective antibodies (0.125-200 nM) on B cells. On-cell K_Ds were determined using variable slope four-parameter fit. Results are shown as mean RFU, error bars represent standard deviation derived from experimental duplicates. Data is representative of three independent experiments.

proportion of endocytosed aIgM increased concentration-dependently reaching saturation in the single-digit nanomolar range while significantly less internalization was detected for CH2-aIgM (Figure 6). Internalization of aIgM and CH2-aIgM was barely measurable in IgM^- B cells. Data points of internalization measurement were removed for clarity but are available in the Supplementary Material for all investigated molecules (Supplementary Figure 7).

First, *in vitro* cytotoxicity studies were conducted with aIgM-MMAE, its masked variant CH2-aIgM-MMAE as well as a pre-cleaved, Protein A purified CH2-aIgM-MMAE version using on-target SUP-B8 and Ramos cells while IM-9 served as off-target cells. Consistent with the internalization properties of aIgM in target cells, IgM^+ cells were sensitive to aIgM ADC-induced cell death (Figure 6). The aIgM ADC displayed potent dose-dependent cell killing with EC_{50} values amounting to 0.43 nM and 0.66 nM for SUP-B8 and Ramos cells, respectively. No significant reduction in cell proliferation was observed by application of the aIgM-MMAE molecule to IM-9 B cells not expressing IgM. Paratope-masked aIgM ADC was unable to mediate cell death in any cell line, which we expected since no endogenous proteolytic activity was observed in cell culture supernatants supplemented with CH2-aIgM during 72 h of incubation (data not shown). Notably, MMP-9 and matriptase activity was detected in B cell lymphoma tumor tissue warranting the concept of protease-mediated antibody activation (33, 34). The activity of aIgM was mostly restored after linker hydrolysis since CH2-aIgM pre-treated with MMP-9 resulted in significantly decreased survival of IgM^+ cells. Comparing potencies of the parental unmasked ADC to the pre-cleaved CH2-aIgM, an approximately 5-fold reduced cytotoxic effect was observed on SUP-B8 cells, whilst on Ramos cells efficacy was fully recovered (Figure 6). Besides comparable induction of lymphoma cell killing in EC_{50} values, similar levels in maximal cell lysis were observed. MMP-9 treated unpurified CH2-aIgM ADC, revealed 8-9-fold increased half maximal effective doses compared to the parental unmasked ADC in target lymphoma cells (Supplementary Figure 8).

Next, we investigated whether apoptosis was triggered by aIgM-MMAE and CH2-aIgM-MMAE. To this end, cells expressing BCRs of IgM and IgG isotype were treated with the respective ADCs for 72 h and analyzed by Annexin V-FITC and propidium iodide (PI) staining using flow cytometry. Application of 50 nM aIgM-MMAE resulted in increased fractions of Annexin V-FITC-positive IgM^+ cells, indicating that apoptosis was induced by antibody-guided chemotherapeutic damage (Figure 7). SUP-B8 and Ramos cells being exposed to aIgM-MMAE showed approximately 4-fold and 26-fold increase in Annexin V-FITC positivity, respectively, compared to untreated control cells (0 nM). Previous investigations have postulated that MMAE induces cell death through a rarely studied mechanism termed mitotic catastrophe possibly being a prelude mechanism to apoptotic or necrotic cell death and further includes signs of autophagy (57–60). In contrast, CH2 masked aIgM ADC did not induce any killing detectable by Annexin V-FITC or PI staining. Likewise, IM-9 IgM^-/IgG^+ off-target cells remained unaffected during aIgM ADC treatment.

Discussion

Overcoming the limitations of treatment paradigms for B cell NHL, novel approaches of highly potent immunotherapies that work in concert with the host immune system such as bispecific T cell engaging antibodies and chimeric antigen receptor (CAR) T cells have been introduced (61–64). Great efforts have further been made in probing antibody-drug conjugates for lymphoma therapies. Brentuximab vedotin, Polatozumab vedotin and Loncastuximab tesirine represent FDA-approved ADCs to treat different types of B cell lymphoma, targeting antigens such as CD30, which is expressed by activated B cells, CD79b, and CD19, present on all B cell types apart from pre-proB cells and mature plasma cells (32, 65–67).

Besides selection of an appropriate antibody ensuring to reach the tumor target site without affecting healthy cells in the periphery, linker and cytotoxic payload are key design parameters in ADCs.

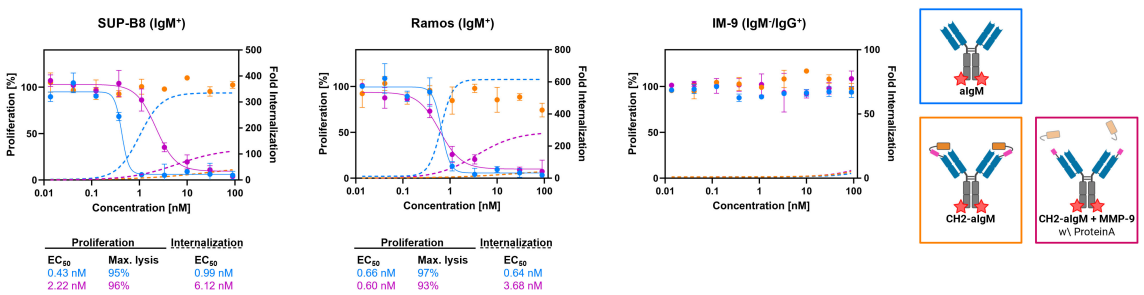

FIGURE 6
Internalization and cytotoxicity of unmasked and CH2-masked aIgM ADC variants towards B cells. For cytotoxicity studies IgM^+ (SUP-B8, Ramos) and IgM^- (IM-9) B cells were exposed to varying concentrations (0.014-90 nM) of aIgM, CH2-aIgM and Protein A purified CH2-aIgM+MMP-9 MMAE-conjugated antibodies for 72 h. Cell proliferation was normalized to untreated control cells (0 nM). For internalization studies pHAb-conjugated aIgM, CH2-aIgM and Protein A purified CH2-aIgM+MMP-9 (0.014-90 nM) were applied to B cells and incubated overnight. Fold internalization was defined by the ratio of relative fluorescence units (RFU) of the respective antibody sample and the untreated sample without antibody (0 nM). EC_{50}s were determined using variable slope four-parameter fit. Results are shown as mean, error bars represent standard deviation derived from experimental duplicates.

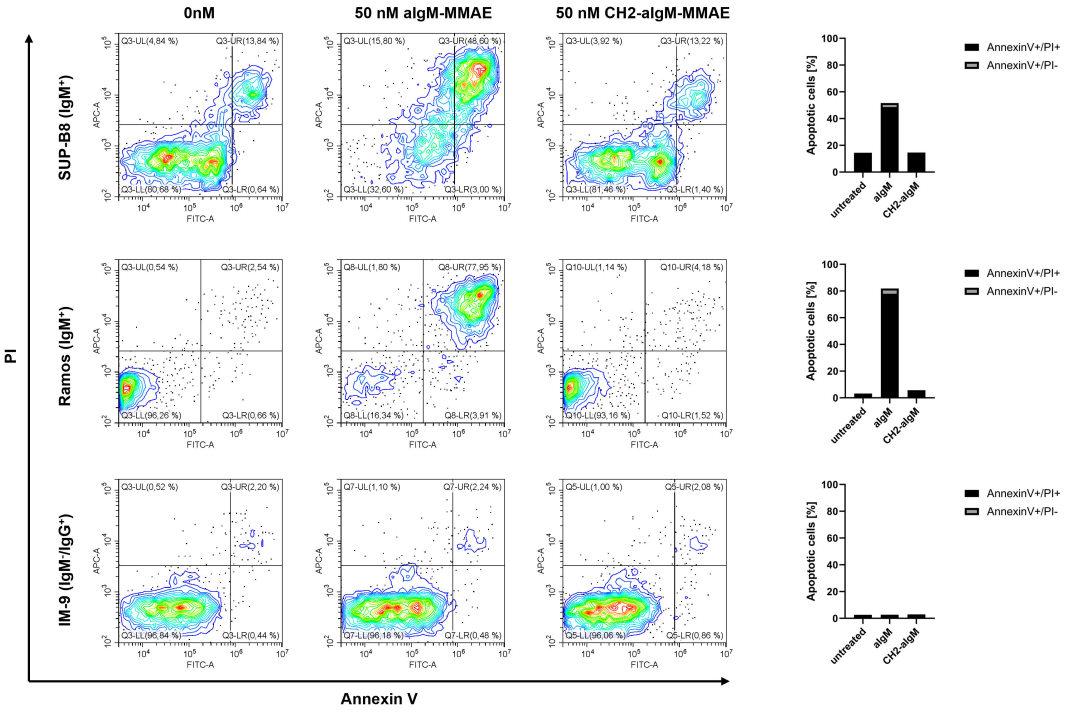

FIGURE 7
Apoptosis induction of aIgM and CH2-masked aIgM ADC in B cells. IgM$^+$ (SUP-B8, Ramos) and IgM$^-$ (IM-9) B cells were exposed to 0 nM, 50 nM of aIgM-MMAE and 50 nM CH2-aIgM-MMAE for 72 h. Cells were stained with Annexin V-FITC and propidium iodide (PI) and analyzed by flow cytometry. Percentage of Annexin V-FITC+/PI+ and Annexin V-FITC+/PI- (apoptotic cells) is depicted in right bar chart. Data is representative of two independent experiments.

Related to those criterions is the DAR which plays a pivotal role determining ADC's potency, safety, and pharmacokinetics. In general, higher drug loading comes along with increased anti-tumor activity. However, improvement in efficacy is limited and excessive cytotoxic payload may cause instabilities and aggregation and further lead to inferior pharmacokinetics such as in plasma clearance and tumor exposure (68, 69). *Bryant et al.* demonstrated that a DAR of 4 in a (trastuzumab) conjugate revealed highest potency *in vitro* and a significantly increased *in vivo* efficacy compared to the lower DAR conjugates (70). Referred to as the first approved mAb for cancer patients, auristatin-based rituximab ADCs have been developed with DARs of 7-7.5 and 4.2, respectively, both demonstrating potent therapeutic efficacy *in vitro* and *in vivo* (60, 71). Hence, further improvements may be reached for the CH2-masked aIgM ADC by examination of optimal drug loading but were out-of-scope for this proof-of-concept study.

To further promote safety and efficacy of ADCs several innovative approaches have been developed in the last decades. One of them includes the generation of a bispecific ADC that targets HER2 as tumor-associated antigen and CD63 rendering enhanced lysosomal delivery (72). Another appealing tool is introduced by CytomX Therapeutics with the probody platform expanding the availability of new targets for ADCs by antibody paratope masking and tumor-specific protease-activation. Probody-drug conjugates are supplied with a protease cleavable linker connected to a peptide mask limiting target engagement in normal tissue and circulation (73). CX-2029 targeting transferrin receptor 1 (CD71) attached to MMAE is currently being investigated in phase II clinical trials displaying translational and clinical activity at tolerable doses in patients (27, 73).

In this study, we present a novel conditionally activated anti-IgM antibody-drug conjugate for precise B cell lymphoma elimination. To this end, we isolated a chicken-derived IgM-specific antibody (aIgM), which was further fused to the epitope-holding IgM domain CH2 by a tumor-protease cleavable linker ultimately equipped with the cytotoxic payload MMAE. Efficient blockage of the tumor targeting moiety in CH2-aIgM was confirmed by biolayer interferometry. The masked antibody regained activity upon protease treatment, displaying affine binding to IgM from human serum. On a cellular level CH2-aIgM was inert to interact with IgM$^+$ B cells while the cleaved variant revealed excellent on-cell affinities comparable to the parental unmasked antibody regarding on-cell affinity constants in the low single-digit nanomolar range as well as maximum binding capacities. This allows penetration into the tumor microenvironment without being captured by soluble IgM or non-malignant IgM$^+$ B cells ultimately improving pharmacokinetic properties. Reaching the tumor target site, tumor-protease-mediated linker hydrolysis engenders high affinity targeting. The aIgM ADC demonstrated specific and effective receptor-mediated cellular uptake which was closely linked to killing of lymphoma cells exhibiting strong signs of apoptotic cell death. Cytotoxicity of the inactive ADC version was shown to be reduced since no cell killing was observed in the investigated concentration range, thus potentially preventing systemic side effects. CH2-aIgM is rendered active by proteases leading to regained toxicity towards malignant IgM$^+$ B

lymphocytes. Further animal studies are required to reveal whether the restrictive and potent *in vitro* anti-tumor efficacy of the antibody introduced in this study can be confirmed *in vivo*.

Our results further show that it is feasible to generate proteolytically activated antibody-drug conjugates against immunoglobulins of isotype (Ig)M for B cell lymphoma treatment. This novel strategy of Ig targeting in B cell-derived malignancies may be superior to conventional approaches in several respects. By addressing only a fraction of B cells, unwanted on-target off-tumor effects are reduced which is further enhanced through the masking functionality while conventional pan-B cell targeting results in patients suffering from B cell-aplasia induced immunosuppression (74). In case of the anti-CD20 antibody rituximab, various resistance mechanisms are existing such as tumor-dependent alterations e.g., antigen downregulation and antigenic modulation or host-dependent immunologic factors e.g., Fc receptor polymorphisms (75–79). Alternative attempts addressing the BCR include patient-specific anti-idiotypic peptides or antibodies against variable regions, however, laborious and time-consuming manufacturing may limit developability (80–83). We propose an alternative mechanism of tumor clearance providing the possibility to therapy relapsed or refractory NHL in the second- or third-line setting solely implying BCR sequencing to identify the disease-causing B cell clone. This concept would be effortlessly applicable to different kinds of B cell-derived malignancies as there are only four human Ig isotypes (IgM, IgG, IgD, IgA) expressed as BCRs, against which antibodies are already available and can in a next step be masked by the respective epitope-bearing Ig domains. As for the CH2-masked aIgM antibody, further protein or antibody engineering may be required to fine-tune the affinity, particularly concerning the off-rate of the blocking moiety to the antibody. In this *in vitro* study, the cleaved IgM CH2 masking unit not being removed from the assay sample associates to the aIgM paratope and thus hampers full functionality of the antibody in terms of (cell) binding and cytotoxicity requiring further purification to decrease the molar ratio of CH2 to corresponding aIgM antibody. In the body, demasking is mediated by proteases such as MMP-9 and matriptase described to be prognostic factors for B cell lymphoma when overexpressed (33, 34). The mechanisms of masking domain release may be shaped by multiple variables *in vivo*. Each individual binding event is a one-step reversible biomolecular process obeying the law of mass action. While interaction to cut CH2 is of monovalent nature, binding to IgM on B cells involves both antibody valences showing avidity effects. Moreover, unrestricted diffusion of the soluble masking domain in blood is opposed to spatial clustered B cell surface receptors effecting rebinding of aIgM which likely leads to local dilution of the masking domain ultimately resulting in preferred cell binding (84, 85). Contrary to synthetic peptide masks, the Ig domain used for paratope-blocking is of human origin reducing the risk of immunogenicity. However, aIgM is a chimeric antibody constituted of chicken-derived variable domains fused to human IgG1 constant domains. Hence, humanization is required to minimize immunogenicity in therapeutic applications. Our group recently developed a straightforward method to humanize avian-derived antibodies by CDR grafting onto a human germline framework based on Vernier residue randomization that could be applied for this purpose but is beyond the scope of this study (86, 87).

Taken together, our approach demonstrates a novel mechanism to specifically eradicate NHL B cells while preserving healthy human B lymphocytes that do not display IgM isotype BCRs. Constituting an inactive anti-IgM antibody-drug conjugate which is actuated in the proteolytic tumor environment, the molecule unites an enhanced safety profile due to tumor-proximity restricted activation and potent anti-tumor efficacy relying on a highly cytotoxic payload. Furthermore, our study provides a basis for the development of protease-activated anti-Ig ADCs for the treatment of B cell-driven pathologies.

Materials and methods

Chicken immunization and yeast library construction

Chicken immunization and scFv yeast surface display library generation were performed as described previously (48). In brief, an adult chicken (*Gallus gallus domesticus*) was immunized with IgM from human serum (Sigma Aldrich) on days 1, 14, 28, 35, and 56. The animal was sacrificed on day 63, followed by isolation of the spleen and total RNA extraction. The immunization process as well as splenic RNA isolation were executed by Davids Biotechnologie GmbH (Regensburg, Germany). For library construction, RNA was reverse transcribed to cDNA. Subsequently, genes encoding VH and VL were amplified and transferred into a YSD vector (pCT) via homologous recombination in yeast (*Saccharomyces cerevisiae* strain EBY100). Library generation in EBY100 cells was conducted according to Benatuil and colleagues (88). Cultivation and general handling of yeast cells are described elsewhere (48, 83).

Yeast library screening

Induction of gene expression and scFv surface presentation was achieved by inoculation of yeast cells in Synthetic Galactose minimal medium with Casein Amino Acids (SG-CAA) at an OD_{600} of 1.0 and incubation overnight at 30°C and 180 rpm. For library sorting, cells were harvested by centrifugation and washed with PBS+0.1% (w/v) BSA (PBS-B). Antigen staining was conducted with DyLight650™-labelled IgM from human serum (Sigma Aldrich) conjugated beforehand using 5-fold excess of DyLight650™ NHS Ester (Thermo Fisher Scientific). Simultaneously, staining for surface presentation using anti-cMyc antibody FITC-conjugated (Miltenyi Biotec; diluted 1:50) was performed for 30 min on ice. After another PBS-B washing step, the yeast library was screened using BD Influx cell sorter with corresponding BD FACS Sortware v1.0.

Expression and purification of scFv, scFv-Fc and Fab-Fc variants

Reformatting, expression and purification of scFvs was performed as described previously (89). Briefly, isolated yeast vectors were sequenced and scFv encoding genes were reformatted into a pET30 plasmid using golden gate assembly,

followed by recombinant expression in *E. coli* SHuffle® T7 Express (New England Biolabs). A two-step affinity purification was performed including IMAC and Strep-Tactin®XT purification, followed by buffer exchange against PBS. Production of Fc-fused scFvs and full-length antibodies (Fab-Fc) was conducted with pTT5-derived golden gate assembly vectors in Expi293F™ cells (Thermo Fisher Scientific). Expi293F™ cells were transiently transfected using ExpiFectamine™ 293 Transfection Kit (Thermo Fisher Scientific) following the manufacturer's protocol. For purification of Fc-containing antibody constructs, cell culture supernatants were collected five days post transfection, sterile filtered and applied to a HiTrap™ Protein A HP column (GE Healthcare) using an ÄKTA pure™ chromatography system (GE Healthcare). Buffer exchange against PBS or TBS was performed using a HiTrap™ Desalting column (GE Healthcare).

Cell lines

B cells including SUP-B8, IM-9 and Ramos cells were cultured at 37°C and 5% CO_2. All B cell lines were maintained in RPMI-1640 supplemented with 15% FBS and 1% Penicillin-Streptomycin and sub-cultured every 2-3 days. Expi293F™ cells were cultured in Expi293™ Expression Medium (Thermo Fisher Scientific), sub-cultured every 3-4 days and incubated at 37°C and 8% CO_2.

Protease-mediated protein hydrolysis

Recombinant human MMP-9 (Acro Biosystems) or recombinant human matriptase/ST14 catalytic domain (Bio-Techne) were used to cleave the dual-protease cleavable linker of CH2-aIgM. Prior to the protein hydrolysis reaction, MMP-9 was pre-activated with 1 mM 4-aminophenylmercuric acetate (APMA) overnight at 37°C. Proteins were dissolved in TBS pH 7.4, if necessary, by buffer exchange, ensuring suitable conditions for the MMP-9 and matriptase hydrolysis reaction. 0.25 mg of the respective antibody variant was mixed with 0.25 µg (0.1 mg/ml) of activated human MMP-9 or matriptase. Protein cleavage was performed at 37°C for 48 h. Complete linker hydrolysis was confirmed using SDS-PAGE under reducing conditions. Cleaved CH2-aIgM protein was further purified using Protein A spin columns (Protein A HP SpinTrap, Cytiva) in order to remove fractions of the masking IgM CH2 domain.

Thermal shift assay

Experiments to determine thermal stability were performed using a CFX Connect Real-Time PCR Detection System (BioRad) with a temperature gradient from 20°C to 95°C and 0.5°C/10 s. The derivatives of the melt curves were calculated with the corresponding BioRad CFX Maestro software to determine the melt temperature (Tm). All reactions were performed in PBS in presence of 0.1 mg/ml protein and SYPRO Orange (Thermo Fisher Scientific, diluted 1:100).

Biolayer interferometry

For biolayer interferometric measurements the Octet RED96 system (ForteBio, Sartorius) was used. Therefore, respective biosensor tips were soaked in PBS pH 7.4 for at least 10 min before assay start.

For epitope binning, Ni-NTA Biosensors (NTA, Sartorius) were loaded with cell culture supernatants of single His-tagged IgM domains expressed in Expi293F™ cells. All following steps were performed using kinetics buffer (KB, Sartorius). Association was measured for 180 s with 150 nM aIgMscFv-Fc followed by dissociation for 180 s.

For the CH2/IgM competition assay, High Precision Streptavidin biosensors (SAX, Sartorius) were loaded biotinylated aIgMscFv-Fc. After quenching in KB, two association steps of 250 s were conducted in sequence, a first association step using either 100 nM IgM from human serum (Sigma Aldrich) or 1,000 nM IgM CH2 was followed by a second association using 1,000 nM IgM CH2 or 100 nM serum, respectively.

For affinity determination of aIgMscFv-Fc and aIgMFab-Fc anti-human IgG Fc capture biosensors (AHC, Sartorius) were used to immobilize the aIgM antibodies. After a quenching step in KB, an association step using CH2-His with concentrations ranging from 31.25 to 500 nM or IgM from human serum (Sigma Aldrich) was performed followed by a dissociation step in KB. Association in KB served as reference and was subtracted prior to evaluation steps. Data analysis was performed using ForteBio data analysis software 9.0. Binding kinetics including the equilibrium constant K_D were determined using Savitzky-Golay filtering and 1:1 Langmuir model.

To confirm that the parental full-length aIgM antibody binds to IgM and IgM-derived CH2, aIgM antibody was loaded onto AHC biosensor tips, followed by quenching in KB, association with 50 nM IgM from human serum or 250 nM IgM CH2 and dissociation in PBS. In the same experimental setup, binding of aIgM, CH2-aIgM, non-purified and Protein A purified CH2-aIgM+MMP-9 and rituximab (control) were evaluated for IgM binding by association of 100 nM or 3.9-125 nM IgM from human serum. In a reverse experimental setup, biotinylated IgM from human serum was loaded onto SAX biosensor tips. After a quenching step in KB, 100 nM of the respective antibody variants were associated.

PBMC isolation

Peripheral blood mononuclear cells (PBMCs) were isolated from buffy coats from healthy human donors supplied by the Deutsche Rotes Kreuz (Frankfurt). To this end, 25 ml blood was mixed 1:1 with PBS +2% (w/v) FBS and PBMCs were purified using SepMate-50 tubes following the manufacturer's instructions (StemCell Technologies).

Cellular binding

Cellular binding of the antibodies was determined by affinity titration using IgM^+ SUP-B8 and Ramos cells. IgM^- (IgG^+) IM-9 cells were used to analyze unspecific cell binding. To this end, cells ($1.5x10^5$ cells/well) were washed with PBS-B and subsequently incubated with the respective antibody constructs in varying concentrations (for cell titration: 0.125-200 nM, serial dilution) for 30 min on ice. Followed by another PBS-B washing step, anti-human IgG Fc PE-conjugated secondary antibody (Thermo Fisher Scientific, diluted 1:50), anti-his AF647-conjugated secondary antibody (Thermo Fisher Scientific, diluted 1:50) or Streptavidin-APC conjugate (Thermo Fisher Scientific, diluted 1:50) was applied for 20 min on ice. After final washing with PBS-B, flow cytometry was performed using CytoFLEX S System (Beckman Coulter). The relative fluorescence units (RFU) were plotted against the respective logarithmic antibody concentration. The resulting curves were fitted with a variable slope four-parameter fit using GraphPad Prism.

Internalization assays

Investigations towards receptor-mediated antibody internalization were performed using pHAb Amine Reactive dye (Promega) according to the manufacturer's instructions. In brief, aIgM, CH2-aIgM, non-purified and Protein A purified CH2-aIgM +MMP-9 were conjugated with pHAb dyes and applied to B cells ($2x10^4$ cells/well) in different concentrations (0.014-90 nM) in a 96-well plate. After incubation overnight, cells were washed once with PBS and internalization was measured using flow cytometry. Fold internalization was determined by the ratio of relative fluorescence units (RFU) of the respective antibody sample and the untreated sample without antibody (0 nM). The resulting curves were fitted with a variable slope four-parameter fit and EC_{50}s were calculated using GraphPad Prism.

Generation of antibody-drug conjugates

Antibody-drug conjugates were generated via a two-step approach of enzymatic modification and click chemistry for conjugation of monomethyl auristatin E (MMAE) to the Fc fragment. Therefore, the C-terminus of the antibody heavy chain was genetically fused with a lipoic acid ligase acceptor peptide (LAP) serving as recognition sequence for lipoate-protein ligase A (LplA) from *Escherichia coli* (90). Lipoic acid ligase reaction was conducted with 0.1 equivalents (eq.) of a mutant lipoic acid ligase A ($LplA^{W37V}$) (91) accepting various carboxylic acid derivatives in the presence of 5 mM ATP, 5 mM Mg $(Ac)_2$ and 10-20 eq. azide-bearing lipoic acid derivative (synthesized in-house) in PBS pH 7.4 for 1h at 37°C. Covalent protein azide-functionalization was confirmed by hydrophobic interaction chromatography followed by click reaction with 5 eq. DBCO-PEG_4-Val-Cit-PAB-MMAE on Protein A resin (Protein A HP SpinTrap, Cytiva) overnight at 4°C. After acidic elution of ADC from Protein A column the buffer was exchanged to PBS pH 7.4.

Cytotoxicity assays

Cytotoxic effects of aIgM ADCs were evaluated by exposing IgM^+ lymphoma B cells or off-target (IgM^-) cells to different ADC concentrations. Cell viability was analyzed 72 h post ADC addition by a colorimetric method using CellTiter 96® AQ_{ueous} One Solution Cell Proliferation Assay (Promega). Briefly, cells were seeded ($1x10^4$ cells/well) in a 96-well plate with the desired antibody concentrations ranging from 0.014-90 nM in a serial dilution. After 72 h, MTS solution was added to the cells and plate was incubated for 2 h. Absorption was measured at 490 nm using CLARIOstar plus microplate reader (BMG LABTECH). Cell proliferation was normalized to untreated control cell absorption values. The resulting curves were fitted with a variable slope four-parameter fit and EC_{50}s were calculated using GraphPad Prism.

Apoptosis assays

For AnnexinV-FITC/PI staining ROTITEST® Annexin V (Carl Roth GmbH + Co. KG) was applied for apoptosis detection of B cells according to the manufacturer's instructions. The analysis was performed using CytoFLEX S System (Beckman Coulter).

Data availability statement

The raw data supporting the conclusions of this article will be made available by the authors, without undue reservation.

Ethics statement

Ethical approval was not required for the studies on animals because animal (chicken) immunization was performed by Davids Biotechnologie GmbH. Experimental procedures and animal care were in accordance with EU animal welfare protection laws and regulations.

Author contributions

KS: Conceptualization, Investigation, Data curation, Writing - original draft. JuH: Investigation, Writing - review & editing. JaH: Investigation, Writing - review & editing. AE: Conceptualization, Writing - review & editing. HK: Conceptualization, Project administration, Writing - original draft.

Funding

The authors declare financial support was received for the research, authorship, and/or publication of this article. Funding for this work was provided in part by the Ministry of Higher Education, Research and Arts of the State of Hesse under the LOEWE project "TRABITA".

Acknowledgments

The authors would like to thank Peter Bitsch for synthesis of azide-modified lipoic acid and Sebastian Harald Bitsch for the provision of LplA enzyme. We acknowledge support by the Deutsche Forschungsgemeinschaft (DFG – German Research Foundation) and the Open Access Publishing Fund of Technical University of Darmstadt.

Conflict of interest

The authors declare that the research was conducted in the absence of any commercial or financial relationships that could be construed as a potential conflict of interest.

Publisher's note

Supplementary material

The Supplementary Material for this article can be found online at: https://www.frontiersin.org/articles/10.3389/fimmu.2023.1258700/full#supplementary-material

References

1. Lu R-M, Hwang Y-C, Liu I-J, Lee C-C, Tsai H-Z, Li H-J, et al. Development of therapeutic antibodies for the treatment of diseases. *J BioMed Sci* (2020) 27:1. doi: 10.1186/s12929-019-0592-z

2. Siegel RL, Miller KD, Wagle NS, Jemal A. Cancer statistics, 2023. *CA Cancer J Clin* (2023) 73:17–48. doi: 10.3322/caac.21763

3. Pierpont TM, Limper CB, Richards KL. Past, present, and future of rituximab-the world's first oncology monoclonal antibody therapy. *Front Oncol* (2018) 8:163. doi: 10.3389/fonc.2018.00163

4. Hofmeister JK, Cooney D, Coggeshall KM. Clustered CD20 induced apoptosis: src-family kinase, the proximal regulator of tyrosine phosphorylation, calcium influx, and caspase 3-dependent apoptosis. *Blood Cells Molecules Dis* (2000) 26:133–43. doi: 10.1006/bcmd.2000.0287

5. Rezvani AR, Maloney DG. Rituximab resistance. *Best Pract Res Clin Haematol* (2011) 24:203–16. doi: 10.1016/j.beha.2011.02.009

6. Jazirehi AR, Vega MI, Bonavida B. Development of rituximab-resistant lymphoma clones with altered cell signaling and cross-resistance to chemotherapy. *Cancer Res* (2007) 67:1270–81. doi: 10.1158/0008-5472.CAN-06-2184

7. Su Q, Chen M, Shi Y, Zhang X, Huang G, Huang B, et al. Cryo-EM structure of the human IgM B cell receptor. *Science* (2022) 377:875–80. doi: 10.1126/science.abo3923

8. Kwak K, Akkaya M, Pierce SK. B cell signaling in context. *Nat Immunol* (2019) 20:963–9. doi: 10.1038/s41590-019-0427-9

9. D'Avola A, Drennan S, Tracy I, Henderson I, Chiecchio L, Larrayoz M, et al. Surface IgM expression and function are associated with clinical behavior, genetic abnormalities, and DNA methylation in CLL. *Blood* (2016) 128:816–26. doi: 10.1182/blood-2016-03-707786

10. Ruminy P, Etancelin P, Couronné L, Parmentier F, Rainville V, Mareschal S, et al. The isotype of the BCR as a surrogate for the GCB and ABC molecular subtypes in diffuse large B-cell lymphoma. *Leukemia* (2011) 25:681–8. doi: 10.1038/leu.2010.302

11. Cox MC, Di Napoli A, Scarpino S, Salerno G, Tatarelli C, Talerico C, et al. Clinicopathologic characterization of diffuse-large-B-cell lymphoma with an associated serum monoclonal IgM component. *PloS One* (2014) 9:e93903. doi: 10.1371/journal.pone.0093903

12. Cox MC, Marcheselli L, Scafetta G, Visco C, Hohaus S, Annibali O, et al. IgM-secreting diffuse large B-cell lymphoma: results of a multicentre clinicopathological and molecular study. *Leukemia* (2022) 36:2719–23. doi: 10.1038/s41375-022-01706-x

13. Ohashi T, Miyashita H, Nagata Y, Otsuka H, Suzuki H, et al. A Novel Anti-IgM/HLA-DR Bispecific Antibody for Treatment of Refractory B Cell Malignancies. *Blood* (2018) 132:1670. doi: 10.1182/blood-2018-99-117552

14. Lucchi R, Bentanachs J, Oller-Salvia B. The masking game: design of activatable antibodies and mimetics for selective therapeutics and cell control. *ACS Cent Sci* (2021) 7:724–38. doi: 10.1021/acscentsci.0c01448

15. Polu KR, Lowman HB. Probody therapeutics for targeting antibodies to diseased tissue. *Expert Opin Biol Ther* (2014) 14:1049–53. doi: 10.1517/14712598.2014.920814

16. Lin W-W, Lu Y-C, Chuang C-H, Cheng T-L. Ab locks for improving the selectivity and safety of antibody drugs. *J BioMed Sci* (2020) 27:76. doi: 10.1186/s12929-020-00652-z

17. Duffy MJ. Proteases as prognostic markers in cancer. *Clin Cancer Res* (1996) 2:613–8.

18. Rakash S. Role of proteases in cancer: A review. *Biotechnol Mol Biol Rev* (2012) 7:90–101. doi: 10.5897/BMBR11.027

19. Duffy MJ. The role of proteolytic enzymes in cancer invasion and metastasis. *Clin Exp Metastasis* (1992) 10:145–55. doi: 10.1007/BF00132746

20. Elter A, Yanakieva D, Fiebig D, Hallstein K, Becker S, Betz U, et al. Protease-activation of fc-masked therapeutic antibodies to alleviate off-tumor cytotoxicity. *Front Immunol* (2021) 12:715719. doi: 10.3389/fimmu.2021.715719

21. Geiger M, Stubenrauch K-G, Sam J, Richter WF, Jordan G, Eckmann J, et al. Protease-activation using anti-idiotypic masks enables tumor specificity of a folate receptor 1-T cell bispecific antibody. *Nat Commun* (2020) 11:3196. doi: 10.1038/s41467-020-16838-w

22. Naing A, Thistlethwaite F, de VEG, FA E, Uboha N, Ott PA, et al. CX-072 (pacmilimab), a Probody ® PD-L1 inhibitor, in advanced or recurrent solid tumors (PROCLAIM-CX-072): an open-label dose-finding and first-in-human study. *J Immunother Cancer* (2021) 9:e002447. doi: 10.1136/jitc-2021-002447

23. Etxeberria I, Bolaños E, Teijeira A, Garasa S, Yanguas A, Azpilikueta A, et al. Antitumor efficacy and reduced toxicity using an anti-CD137 Probody therapeutic. *Proc Natl Acad Sci U.S.A.* (2021) 118:e2025930118. doi: 10.1073/pnas.2025930118

24. Cattaruzza F, Nazeer A, To M, Hammond M, Koski C, Liu LY, et al. Precision-activated T-cell engagers targeting HER2 or EGFR and CD3 mitigate on-target, off-tumor toxicity for immunotherapy in solid tumors. *Nat Cancer* (2023) 4:485–501. doi: 10.1038/s43018-023-00536-9

25. Boustany LM, LaPorte SL, Wong L, White C, Vinod V, Shen J, et al. A probody T cell-engaging bispecific antibody targeting EGFR and CD3 inhibits colon cancer growth with limited toxicity. *Cancer Res* (2022) 82:4288–98. doi: 10.1158/0008-5472.CAN-21-2483

26. Gutierrez M, Friedman CF, Long GV, Ascierto PA, Melero I, Richards D, et al. 740P Anti-cytotoxic T-lymphocyte antigen-4 (CTLA 4) probody BMS-986249 ± nivolumab (NIVO) in patients (pts) with advanced cancers: Updated phase I results. *Ann Oncol* (2022) 33:S882. doi: 10.1016/j.annonc.2022.07.866

27. Singh S, Serwer L, DuPage A, Elkins K, Chauhan N, Ravn M, et al. Nonclinical efficacy and safety of CX-2029, an anti-CD71 probody-drug conjugate. *Mol Cancer Ther* (2022) 21:1326–36. doi: 10.1158/1535-7163.MCT-21-0193

28. Johnson M, El-Khoueiry A, Hafez N, Lakhani N, Mamdani H, Rodon J, et al. First-in-human study of the probody therapeutic CX-2029 in adults with advanced solid tumor Malignancies. *Clin Cancer Res* (2021) 27:4521–30. doi: 10.1158/1078-0432.CCR-21-0194

29. Alley SC, Okeley NM, Senter PD. Antibody-drug conjugates: targeted drug delivery for cancer. *Curr Opin Chem Biol* (2010) 14:529–37. doi: 10.1016/j.cbpa.2010.06.170

30. Fu Z, Li S, Han S, Shi C, Zhang Y. Antibody drug conjugate: the "biological missile" for targeted cancer therapy. *Signal Transduct Target Ther* (2022) 7:93. doi: 10.1038/s41392-022-00947-7

31. Sievers EL. Efficacy and safety of gemtuzumab ozogamicin in patients with CD33-positive acute myeloid leukaemia in first relapse. *Expert Opin Biol Ther* (2001) 1:893–901. doi: 10.1517/14712598.1.5.893

32. Samantasinghar A, Sunildutt NP, Ahmed F, Soomro AM, Salih AR, Parihar P, et al. A comprehensive review of key factors affecting the efficacy of antibody drug conjugate. *BioMed Pharmacother* (2023) 161:114408. doi: 10.1016/j.biopha.2023.114408

33. Sakata K, Satoh M, Someya M, Asanuma H, Nagakura H, Oouchi A, et al. Expression of matrix metalloproteinase 9 is a prognostic factor in patients with non-Hodgkin lymphoma. *Cancer* (2004) 100:356–65. doi: 10.1002/cncr.11905

34. Chou F-P, Chen Y-W, Zhao XF, Xu-Monette ZY, Young KH, Gartenhaus RB, et al. Imbalanced matriptase pericellular proteolysis contributes to the pathogenesis of Malignant B-cell lymphomas. *Am J Pathol* (2013) 183:1306–17. doi: 10.1016/j.ajpath.2013.06.024

35. Pettersen EF, Goddard TD, Huang CC, Meng EC, Couch GS, Croll TI, et al. UCSF ChimeraX: Structure visualization for researchers, educators, and developers. *Protein Sci* (2021) 30:70–82. doi: 10.1002/pro.3943

36. Wu L, Oficjalska K, Lambert M, Fennell BJ, Darmanin-Sheehan A, Ní Shúilleabháin D, et al. Fundamental characteristics of the immunoglobulin VH repertoire of chickens in comparison with those of humans, mice, and camelids. *J Immunol* (2012) 188:322–33. doi: 10.4049/jimmunol.1102466

37. Xu JL, Davis MM. Diversity in the CDR3 region of V(H) is sufficient for most antibody specificities. *Immunity* (2000) 13:37–45. doi: 10.1016/S1074-7613(00)00006-6

38. Krah S, Schröter C, Eller C, Rhiel L, Rasche N, Beck J, et al. Generation of human bispecific common light chain antibodies by combining animal immunization and yeast display. *Protein Eng Des Sel* (2017) 30:291–301. doi: 10.1093/protein/gzw077

39. Bogen JP, Carrara SC, Fiebig D, Grzeschik J, Hock B, Kolmar H. Design of a trispecific checkpoint inhibitor and natural killer cell engager based on a 2 + 1 common light chain antibody architecture. *Front Immunol* (2021) 12:669496. doi: 10.3389/fimmu.2021.669496

40. Bai R, Pettit GR, Hamel E. Dolastatin 10, a powerful cytostatic peptide derived from a marine animal. Inhibition of tubulin polymerization mediated through the vinca alkaloid binding domain. *Biochem Pharmacol* (1990) 39:1941–9. doi: 10.1016/0006-2952(90)90613-P

41. Chen H, Lin Z, Arnst KE, Miller DD, Li W. Tubulin inhibitor-based antibody-drug conjugates for cancer therapy. *Molecules* (2017) 22:1281. doi: 10.3390/molecules22081281

42. Johansson MP, Maaheimo H, Ekholm FS. New insight on the structural features of the cytotoxic auristatins MMAE and MMAF revealed by combined NMR spectroscopy and quantum chemical modelling. *Sci Rep* (2017) 7:15920. doi: 10.1038/s41598-017-15674-1

43. Han B, Yuan H, Wang T, Li B, Ma L, Yu S, et al. Multiple igH isotypes including IgD, subclasses of IgM, and IgY are expressed in the common ancestors of modern birds. *J Immunol* (2016) 196:5138–47. doi: 10.4049/jimmunol.1600307

44. Grönwall C, Vas J, Silverman GJ. Protective roles of natural IgM antibodies. *Front Immunol* (2012) 3:66. doi: 10.3389/fimmu.2012.00066

45. Díaz-Zaragoza M, Hernández-Ávila R, Viedma-Rodríguez R, Arenas-Aranda D, Ostoa-Saloma P. Natural and adaptive IgM antibodies in the recognition of tumor-associated antigens of breast cancer (Review). *Oncol Rep* (2015) 34:1106–14. doi: 10.3892/or.2015.4095

46. Larsson A, Bålöw RM, Lindahl TL, Forsberg PO. Chicken antibodies: taking advantage of evolution–a review. *Poult Sci* (1993) 72:1807–12. doi: 10.3382/ps.0721807

47. Davies EL, Smith JS, Birkett CR, Manser JM, Anderson-Dear DV, Young JR. Selection of specific phage-display antibodies using libraries derived from chicken immunoglobulin genes. *J Immunol Methods* (1995) 186:125–35. doi: 10.1016/0022-1759(95)00143-X

48. Grzeschik J, Yanakieva D, Roth L, Krah S, Hinz SC, Elter A, et al. Yeast surface display in combination with fluorescence-activated cell sorting enables the rapid isolation of antibody fragments derived from immunized chickens. *Biotechnol J* (2019) 14:e1800466. doi: 10.1002/biot.201800466

49. Bogen JP, Grzeschik J, Krah S, Zielonka S, Kolmar H. Rapid generation of chicken immune libraries for yeast surface display. *Methods Mol Biol* (2020) 2070:289–302. doi: 10.1007/978-1-4939-9853-1_16

50. Roth L, Grzeschik J, Hinz SC, Becker S, Toleikis L, Busch M, et al. Facile generation of antibody heavy and light chain diversities for yeast surface display by Golden Gate Cloning. *Biol Chem* (2019) 400:383–93. doi: 10.1515/hsz-2018-0347

51. Dussault N, Ducas E, Racine C, Jacques A, Paré I, Côté S, et al. Immunomodulation of human B cells following treatment with intravenous immunoglobulins involves increased phosphorylation of extracellular signal-regulated kinases 1 and 2. *Int Immunol* (2008) 20:1369–79. doi: 10.1093/intimm/dxn090

52. Carroll WL, Link MP, Cleary ML, Bologna S, Carswell C, Amylon MD, et al. Idiotype as a tumor-specific marker in childhood B cell acute lymphoblastic leukemia. *Blood* (1988) 71:1068–73. doi: 10.1182/blood.V71.4.1068.1068

53. Fahey JL, Buell DN, Sox HC. Proliferation and differentiation of lymphoid cells: studies with human lymphoid cell lines and immunoglobulin synthesis. *Ann N Y Acad Sci* (1971) 190:221–34. doi: 10.1111/j.1749-6632.1971.tb13537.x

54. Li Z, Wang M, Yao X, Li H, Li S, Liu L, et al. Development of novel anti-CD19 antibody-drug conjugates for B-cell lymphoma treatment. *Int Immunopharmacol* (2018) 62:299–308. doi: 10.1016/j.intimp.2018.06.034

55. Li Z, Wang M, Yao X, Luo W, Qu Y, Yu D, et al. Development of a novel EGFR-targeting antibody-drug conjugate for pancreatic cancer therapy. *Target Oncol* (2019) 14:93–105. doi: 10.1007/s11523-018-0616-8

56. Parameswaran N, Luo L, Zhang L, Chen J, DiFilippo FP, Androjna C, et al. CD6-targeted antibody-drug conjugate as a new therapeutic agent for T cell lymphoma. *Leukemia* (2023). doi: 10.1038/s41375-023-01997-8

57. Cunningham D, Parajuli KR, Zhang C, Wang G, Mei J, Zhang Q, et al. Monomethyl auristatin E phosphate inhibits human prostate cancer growth. *Prostate* (2016) 76:1420–30. doi: 10.1002/pros.23226

58. Portugal J, Mansilla S, Bataller M. Mechanisms of drug-induced mitotic catastrophe in cancer cells. *Curr Pharm Des* (2010) 16:69–78. doi: 10.2174/138161210789941801

59. Vakifahmetoglu H, Olsson M, Zhivotovsky B. Death through a tragedy: mitotic catastrophe. *Cell Death Differ* (2008) 15:1153–62. doi: 10.1038/cdd.2008.47

60. Wang Y, Zhang X, Fan J, Chen W, Luan J, Nan Y, et al. Activating autophagy enhanced the antitumor effect of antibody drug conjugates rituximab-monomethyl auristatin E. *Front Immunol* (2018) 9:1799. doi: 10.3389/fimmu.2018.01799

61. June CH, Sadelain M. Chimeric antigen receptor therapy. *N Engl J Med* (2018) 379:64–73. doi: 10.1056/NEJMra1706169

62. Schuster SJ, Svoboda J, Chong EA, Nasta SD, Mato AR, Anak Ö, et al. Chimeric antigen receptor T cells in refractory B-cell lymphomas. *N Engl J Med* (2017) 377:2545–54. doi: 10.1056/NEJMoa1708566

63. Jen EY, Xu Q, Schetter A, Przepiorka D, Shen YL, Roscoe D, et al. FDA approval: blinatumomab for patients with B-cell precursor acute lymphoblastic leukemia in morphologic remission with minimal residual disease. *Clin Cancer Res* (2019) 25:473–7. doi: 10.1158/1078-0432.CCR-18-2337

64. Falchi L, Vardhana SA, Salles GA. Bispecific antibodies for the treatment of B-cell lymphoma: promises, unknowns, and opportunities. *Blood* (2023) 141:467–80. doi: 10.1182/blood.2021011994

65. Chu Y, Zhou X, Wang X. Antibody-drug conjugates for the treatment of lymphoma: clinical advances and latest progress. *J Hematol Oncol* (2021) 14:88. doi: 10.1186/s13045-021-01097-z

66. Barreca M, Lang N, Tarantelli C, Spriano F, Barraja P, Bertoni F. Antibody-drug conjugates for lymphoma patients: preclinical and clinical evidences. *Explor Target Antitumor Ther* (2022) 3:763–94. doi: 10.37349/etat.2022.00112

67. Ku M, Chong G, Hawkes EA. Tumour cell surface antigen targeted therapies in B-cell lymphomas: Beyond rituximab. *Blood Rev* (2017) 31:23–35. doi: 10.1016/j.blre.2016.08.001

68. Hamblett KJ, Senter PD, Chace DF, Sun MM, Lenox J, Cerveny CG, et al. Effects of drug loading on the antitumor activity of a monoclonal antibody drug conjugate. *Clin Cancer Res* (2004) 10:7063–70. doi: 10.1158/1078-0432.CCR-04-0789

69. Adem YT, Schwarz KA, Duenas E, Patapoff TW, Galush WJ, Esue O. Auristatin antibody drug conjugate physical instability and the role of drug payload. *Bioconjug Chem* (2014) 25:656–64. doi: 10.1021/bc400439x

70. Bryant P, Pabst M, Badescu G, Bird M, McDowell W, Jamieson E, et al. *In vitro* and *in vivo* evaluation of cysteine rebridged trastuzumab-MMAE antibody drug conjugates with defined drug-to-antibody ratios. *Mol Pharm* (2015) 12:1872–9. doi: 10.1021/acs.molpharmaceut.5b00116

71. Law C-L, Cerveny CG, Gordon KA, Klussman K, Mixan BJ, Chace DF, et al. Efficient elimination of B-lineage lymphomas by anti-CD20-auristatin conjugates. *Clin Cancer Res* (2004) 10:7842–51. doi: 10.1158/1078-0432.CCR-04-1028

72. de Goeij BE, Vink T, ten Napel H, Breij EC, Satijn D, Wubbolts R, et al. Efficient payload delivery by a bispecific antibody-drug conjugate targeting HER2 and CD63. *Mol Cancer Ther* (2016) 15:2688–97. doi: 10.1158/1535-7163.MCT-16-0364

73. Boni V, Fidler MJ, Arkenau H-T, Spira A, Meric-Bernstam F, Uboha N, et al. Praluzatamab ravtansine, a CD166-targeting antibody-drug conjugate, in patients with advanced solid tumors: an open-label phase I/II trial. *Clin Cancer Res* (2022) 28:2020–9. doi: 10.1158/1078-0432.CCR-21-3656

74. Morrison VA. Immunosuppression associated with novel chemotherapy agents and monoclonal antibodies. *Clin Infect Dis* (2014) 59 Suppl 5:S360–4. doi: 10.1093/cid/ciu592

75. Beers SA, French RR, Chan HT, Lim SH, Jarrett TC, Vidal RM, et al. Antigenic modulation limits the efficacy of anti-CD20 antibodies: implications for antibody selection. *Blood* (2010) 115:5191–201. doi: 10.1182/blood-2010-01-263533

76. Czuczman MS, Olejniczak S, Gowda A, Kotowski A, Binder A, Kaur H, et al. Acquirement of rituximab resistance in lymphoma cell lines is associated with both global CD20 gene and protein down-regulation regulated at the pretranscriptional and posttranscriptional levels. *Clin Cancer Res* (2008) 14:1561–70. doi: 10.1158/1078-0432.CCR-07-1254

77. Beum PV, Kennedy AD, Williams ME, Lindorfer MA, Taylor RP. The shaving reaction: rituximab/CD20 complexes are removed from mantle cell lymphoma and chronic lymphocytic leukemia cells by THP-1 monocytes. *J Immunol* (2006) 176:2600–9. doi: 10.4049/jimmunol.176.4.2600

78. Dornan D, Spleiss O, Yeh R-F, Duchateau-Nguyen G, Dufour A, Zhi J, et al. Effect of FCGR2A and FCGR3A variants on CLL outcome. *Blood* (2010) 116:4212–22. doi: 10.1182/blood-2010–03–272765

79. Maeshima AM, Taniguchi H, Nomoto J, Maruyama D, Kim S-W, Watanabe T, et al. Histological and immunophenotypic changes in 59 cases of B-cell non-Hodgkin's lymphoma after rituximab therapy. *Cancer Sci* (2009) 100:54–61. doi: 10.1111/j.1349-7006.2008.01005.x

80. Torchia J, Weiskopf K, Levy R. Targeting lymphoma with precision using semisynthetic anti-idiotype peptibodies. *Proc Natl Acad Sci U.S.A.* (2016) 113:5376–81. doi: 10.1073/pnas.1603335113

81. Miller RA, Maloney DG, Warnke R, Levy R. Treatment of B-cell lymphoma with monoclonal anti-idiotype antibody. *N Engl J Med* (1982) 306:517–22. doi: 10.1056/NEJM198203043060906

82. Hamblin TJ, Cattan AR, Glennie MJ, MacKenzie MR, Stevenson FK, Watts HF, et al. Initial experience in treating human lymphoma with a chimeric univalent derivative of monoclonal anti-idiotype antibody. *Blood* (1987) 69:790–7. doi: 10.1182/blood.V69.3.790.790

83. Macarrón Palacios A, Grzeschik J, Deweid L, Krah S, Zielonka S, Rösner T, et al. Specific targeting of lymphoma cells using semisynthetic anti-idiotype shark antibodies. *Front Immunol* (2020) 11:560244. doi: 10.3389/fimmu.2020.560244

84. Goldstein B, Dembo M. Approximating the effects of diffusion on reversible reactions at the cell surface: ligand-receptor kinetics. *Biophys J* (1995) 68:1222–30. doi: 10.1016/S0006-3495(95)80298-5

85. Goldstein B, Posner RG, Torney DC, Erickson J, Holowka D, Baird B. Competition between solution and cell surface receptors for ligand. Dissociation of hapten bound to surface antibody in the presence of solution antibody. *Biophys J* (1989) 56:955–66. doi: 10.1016/S0006-3495(89)82741-9

86. Elter A, Bogen JP, Hinz SC, Fiebig D, Macarrón Palacios A, Grzeschik J, et al. Humanization of chicken-derived scFv using yeast surface display and NGS data mining. *Biotechnol J* (2021) 16:e2000231. doi: 10.1002/biot.202000231

87. Bogen JP, Elter A, Grzeschik J, Hock B, Kolmar H. Humanization of chicken-derived antibodies by yeast surface display. *Methods Mol Biol* (2022) 2491:335–60. doi: 10.1007/978-1-0716-2285-8_18

88. Benatuil L, Perez JM, Belk J, Hsieh C-M. An improved yeast transformation method for the generation of very large human antibody libraries. *Protein Eng Des Sel* (2010) 23:155–9. doi: 10.1093/protein/gzq002

89. Hinz SC, Elter A, Rammo O, Schwämmle A, Ali A, Zielonka S, et al. A Generic Procedure for the Isolation of pH- and Magnesium-Responsive Chicken scFvs for Downstream Purification of Human Antibodies. *Front Bioeng Biotechnol* (2020) 8:688. doi: 10.3389/fbioe.2020.00688

90. Puthenveetil S, Liu DS, White KA, Thompson S, Ting AY. Yeast display evolution of a kinetically efficient 13-amino acid substrate for lipoic acid ligase. *J Am Chem Soc* (2009) 131:16430–8. doi: 10.1021/ja904596f

91. Baruah H, Puthenveetil S, Choi Y-A, Shah S, Ting AY. An engineered aryl azide ligase for site-specific mapping of protein-protein interactions through photo-cross-linking. *Angew Chem Int Ed Engl* (2008) 47:7018–21. doi: 10.1002/anie.200802088

frontiers | Frontiers in Immunology

TYPE Original Research
PUBLISHED 14 November 2023
DOI 10.3389/fimmu.2023.1266265

OPEN ACCESS

EDITED BY
Shimin Hu,
University of Texas MD Anderson Cancer Center, United States

REVIEWED BY
Fabrizio Vianello,
University Hospital of Padua, Italy
Irma Olarte,
General Hospital of Mexico, Mexico
Zarir Karanjawala,
UC Davis Medical Center, United States

*CORRESPONDENCE
Giorgio Stassi
giorgio.stassi@unipa.it
Salvatrice Mancuso
salvatrice.mancuso@unipa.it

†These authors have contributed equally to this work and share first authorship

‡These authors have contributed equally to this work and share last authorship

RECEIVED 24 July 2023
ACCEPTED 17 October 2023
PUBLISHED 14 November 2023

CITATION
Turdo A, Gaggianesi M, D'Accardo C, Porcelli G, Bella SD, Cricchio D, Pillitteri I, Porcasi R, Lo Iacono M, Verona F, Modica C, Roozafzay N, Florena AM, Stassi G, Mancuso S and Todaro M (2023) EBF1, MYO6 and CALR expression levels predict therapeutic response in diffuse large B-cell lymphomas.
Front. Immunol. 14:1266265.
doi: 10.3389/fimmu.2023.1266265

EBF1, MYO6 and CALR expression levels predict therapeutic response in diffuse large B-cell lymphomas

Alice Turdo[1†], Miriam Gaggianesi[2†], Caterina D'Accardo[1], Gaetana Porcelli[1], Sebastiano Di Bella[2], Dario Cricchio[2], Irene Pillitteri[1], Rossana Porcasi[1], Melania Lo Iacono[1], Francesco Verona[1], Chiara Modica[2], Narges Roozafzay[1], Ada Maria Florena[1], Giorgio Stassi[2*], Salvatrice Mancuso[1*‡] and Matilde Todaro[1,3‡]

[1]Department of Health Promotion, Mother and Child Care, Internal Medicine and Medical Specialties (PROMISE), University of Palermo, Palermo, Italy, [2]Department of Surgical, Oncological and Stomatological Sciences (DICHIRONS), University of Palermo, Palermo, Italy, [3]A.O.U.P. "Paolo Giaccone", University of Palermo, Palermo, Italy

Background: Diffuse large B-cell lymphoma (DLBCL) is a hematological malignancy representing one-third of non-Hodgkin's lymphoma cases. Notwithstanding immunotherapy in combination with chemotherapy (R-CHOP) is an effective therapeutic approach for DLBCL, a subset of patients encounters treatment resistance, leading to low survival rates. Thus, there is an urgent need to identify predictive biomarkers for DLBCL including the elderly population, which represents the fastest-growing segment of the population in Western countries.

Methods: Gene expression profiles of n=414 DLBCL biopsies were retrieved from the public dataset GSE10846. Differentially expressed genes (DEGs) (fold change >1.4, p-value <0.05, n=387) have been clustered in responder and non-responder patient cohorts. An enrichment analysis has been performed on the top 30 up-regulated genes of responder and non-responder patients to identify the signatures involved in gene ontology (MSigDB). The more significantly up-regulated DEGs have been validated in our independent collection of formalin-fixed paraffin-embedded (FFPE) biopsy samples of elderly DLBCL patients, treated with R-CHOP as first-line therapy.

Results: From the analysis of two independent cohorts of DLBCL patients emerged a gene signature able to predict the response to R-CHOP therapy. In detail, expression levels of EBF1, MYO6, CALR are associated with a significant worse overall survival.

10.3389/fimmu.2023.1266265

Conclusions: These results pave the way for a novel characterization of DLBCL biomarkers, aiding the stratification of responder *versus* non-responder patients.

KEYWORDS

diffuse large B-cell lymphoma, R-CHOP, therapy resistance, elderly patients, gene expression signature, biomarkers of response

1 Introduction

Diffuse large B-cell lymphoma (DLBCL) is the most common subtype of non-Hodgkin's lymphoma and one of the highest mortality rates for all countries in the world within the elderly subjects (1). DLBCL is a heterogeneous disease at molecular and genetic level, characterized by a different biological behavior.

Although more than 50% of patients affected by DLBCL successfully respond to standard therapy, approximately 40% experience a relapse, making this neoplasia the leading cause of morbidity due to limited treatment options (2). Moreover, DLBCL commonly occurs in patients with comorbidities or in very elderly patients who warrants geriatric assessment prior treatment. Thus, a comprehensive examination of treatment efficacy versus the occurrence of side effects is required in order to predict tolerability, cardiotoxicity and the broad quality of life in frail patients (3).

Several studies have shown that the magnitude of clinical benefit rate in therapies for the treatment of DLBCL, which is mainly based on the use of immunotherapy in combination with chemotherapy (R-CHOP), reflects the molecular heterogeneity, including gene copy-number alterations and mutations (2, 4). Of note, in the last decades, the addition of rituximab to the standard CHOP therapy, significantly improved, by 10-15%, the overall survival of DLBCL patients (2).

Nonetheless comprehensive mechanisms underlying the refractoriness to R-CHOP have not been determined, several clinical parameters have been associated with treatment resistance and worse outcomes. The main prognostic model applied to DLBCL is based on the International Prognostic Index (IPI). The scoring system allows to stratify patients from low risk (0/1 score) to high risk (4/5 score) groups, depending on age, serum lactate dehydrogenase (LDH) levels, the eastern cooperative oncology group (ECOG) performance status, number of extranodal sites and Ann Arbor stage disease (5). Newly diagnosed DLBCL patients, treated with R-CHOP, are categorized according to the revised IPI, which facilitates the prognostic classification of patients (6).

Apart from the scoring system incorporating clinical parameters, advances in molecular characterization led to distinguish two different molecular subtypes of DLBCLs with a different biological behavior, the germinal center B-cell (GCB) lymphoma and the activated B-cell (ABC) lymphoma, this last associated with a poorer prognosis. These molecular subtypes of DLBCL are likewise arising from distinct cell of origin at diverse stages of lymphoid differentiation and specifically GCB from normal germinal-center B cells, while ABC from a post-germinal B cell (7).

Although several integrative approaches and models to detect patients at increased risk of relapse have been proposed, the identification of decisive driver biomarkers that can predict therapy response is still an unmet need. In the present study, in order to identify the gene expression profile of elderly (≥65-year-old) DLBCL patient's responders and non-responders to the therapy with CHOP and R-CHOP, we benefited from a publicly available dataset (GSE10846) (7). Using a multiplexed gene expression analysis, furtherly validated by immunohistochemical evaluation, it has been identified a gene signature predictive of therapeutic response, in an independent cohort of DLBCL patients. From the molecular analysis emerged that expression of EBF1, MYO6 and CALR is able to select patients with distinct outcomes. Here, we provided biomarkers that could be of clinical interest to stratify elderly DLBCL patients, predicting the response to standard therapy, and develop novel therapeutic strategies based on the knowledge acquired, regarding validated molecular targets.

2 Materials and methods

2.1 Study populations

DLBCL tumor specimens and patients' clinical data were obtained at the Hematology Unit, "P. Giaccone" Hospital of Palermo. Elderly patients (≥ 65-year-old) have been selected for the study and further classified in two cohorts of responder (n=13) and non-responder (n=6) to first-line R-CHOP therapy (validation cohort). A panel of hematologist and pathologist at the "P. Giaccone" Hospital followed the ESMO Clinical Practice Guidelines and Italian Society of Hematology guidelines for diagnosis, treatment and follow-up of DLBCL patients.

2.2 Statistical analysis

The training cohort (GSE10846, n=414) has been divided in two groups: patients treated with CHOP (n=181) and patients treated with R-CHOP (n=233). Patients' cohort has been filtered by age (≥ 65-year-old) (n=188) and subsequently divided in responder (n=94) and non-responder (n=94) (7).Differential expressed genes (DEGs) (fold change >1.4, p-value <0.05, κ=387) have been clustered in the

responder and non-responder groups and according to LDH levels. The activated B-cell (ABC) and germinal center B-cell (GCB) molecular subtypes have been reported as annotations.

Finally, the top 30 up-regulated genes of responder and non-responder patients have been used to perform enrichment analysis in order to identify the main signatures involved in gene ontology (MSigDB), considering molecular function, biological process and cellular component (p-value<10^{-7}). The signatures associated with the first 30 upregulated genes were also computed by the QIAGEN Ingenuity Pathway Analysis software.

The association between features and patients' overall survival was assessed by using Cox proportional- hazards model. Specifically, in the univariate analysis Cell of origin (COO), ECOG performance status, Extranodal Sites, IPI, LDH, sex and stage parameters were dichotomized according to (8, 9). The dichotomization of the identified signature was defined by using the median expression of each gene (*MYO6*, *EBF1* and *CALR*). In the multivariate analysis, we combined our signature with each previously described feature.

To generate the Kaplan-Meier curves of overall survival by using the GSE10846 dataset, the initial population was filtered by age (≥ 65-year-old). "High" and "Low" groups were defined by using the median expression of each gene (*MYO6*, *EBF1* and *CALR*) in the patient cohort.

All analyses were performed with R survival, survminer, and coxph libraries. Graphs were created by using the ggplot2 library.

2.3 RNA extraction and droplet digital PCR

Total RNA from FFPE tumor tissue specimens was isolated by using RNeasy FFPE Kit (Qiagen). 300 ng of total RNA was retro-transcribed with the high-capacity c-DNA reverse transcription kit (Applied Biosystem). In order to perform a four-gene multiplex assay, we used specific Droplet digital PCR (ddPCR- QX200 Droplet Reader) gene expression assays with FAM (*n=2*) and HEX (*n=2*) fluorophores. To optimize the multiplex reactions, from 100 to 300nM gene-specific primers have been used in combination with ddPCR supermix for probes (No-dUTP) and 25 ng of cDNA samples. Droplets were generated using the QX200 Droplet Generator (Bio-Rad) and dispensed into a 96 well-PCR plate. PCRs were performed in a ProFlex PCR System (Applied Biosystem) with the following protocol: 1x (95°C for 10 min), 50x (94°C for 30 sec, 56°C for 1 min), 1x (98°C for 10 min). After gene target amplification, samples were analyzed using QX200 Digital Droplet Reader (Bio-Rad). Gene expression analyses (copies/µl) were performed using QX Manager Software (1.2 Standard Edition) and normalized by using *GAPDH*.

2.4 Immunohistochemistry

FFPE lymphoma tissue specimens, stratified by age ≥ 65-year-old, were obtained from 11 responder patients and 4 non responder patients treated with R-CHOP.

Antigen retrieval was performed using the PT link system (Dako, Agilent Technologies, Santa Clara, CA, USA). Thereafter, sections were permeabilized with the 0.1% TRITON X-100 PBS for 10 min on ice, followed by 3% H_20_2 and 10% human serum blocking incubation.

All slides were exposed overnight at 4°C to primary antibodies against Calreticulin (CAL-R) (ab22683; mouse IgG1; Abcam, Cambridge Science Park, UK), Myosin VI (MYO6) (MUD-19; mouse IgG1, Sigma-Aldrich), and EBF-1 (HPA061169; rabbit; Sigma-Aldrich). Staining was revealed using a biotin-streptavidin system (Dako LSAB2 System-HRP) and detected with the DAB substrate chromogen system (Dako). Nuclei were counterstained with Mayer's Hematoxylin (Lillie's Modification) Histological Staining Reagent (Dako). Staining was analyzed using an Olympus BX60 microscope. Immunohistochemical analysis were quantified with Image J.

3 Results

3.1 The analysis of a large cohort of elderly DLBCL patients revealed a gene signature associated to prognosis

Diffuse large B-cell lymphoma (DLBCL) is a heterogeneous disease, causing high mortality in elderly patients. Despite the adverse effects, CHOP- and R-CHOP-based therapies result effective in the two-thirds of DLBCL patients, of which the rest portion experiences disease recurrence. Being DLBCL elderly patients the more susceptible to standard therapy side effects, in order to identify the genes predictive of therapy response, a gene expression analysis of 188 pretreatment biopsies of patients with an age ≥ 65 was retrieved from a publicly available dataset (GSE10846) (Figure 1A) (7).

Following unsupervised hierarchical clustering, the dichotomization of training cohort patients in responder and non-responder to CHOP and R-CHOP therapy allowed the identification of differentially expressed genes (DEGs) associated to a poor outcome (Figure 1B). The median age of the responder and non-responder cohorts of patients, to standard therapy, was comparable (74.04 *versus* 75.12-year-old) thus allowing the exclusion of age-related deaths. Of note, responder patients were mainly characterized by the GCB-like (62,5%) molecular subtype associated with a favorable outcome (Figure 1B). In accordance with well-established negative prognostic LDH parameter, responder DLBCL patients harbored lower LDH levels (1,0887 *versus* 1,8112) with respect to non-responder patients (Figure 1B; Supplementary Figures S1A, B). Analysis of gene expression profile, including 387 genes, of responder *versus* non-responder patients showed ten most differentially expressed genes (p-value ≤ 0.001) (Figure 1C; Supplementary Table 1). Specifically, *ATAD3A, CALR, CWF19L1, GALT, MAGEA9, MAPKI8IP3, PSLNR, SEPTIN7P13, SLC19A1* and *SLC38A5* resulted up-regulated in non-responder patients, while high expression levels of *EBF1, EDNRA, CCDC18, CCDC186, FYB, MALAT1, MIS18BP1, MYO6, THRAP3* and *TOP1*, characterized responder DLBCL patients (Figure 1C).

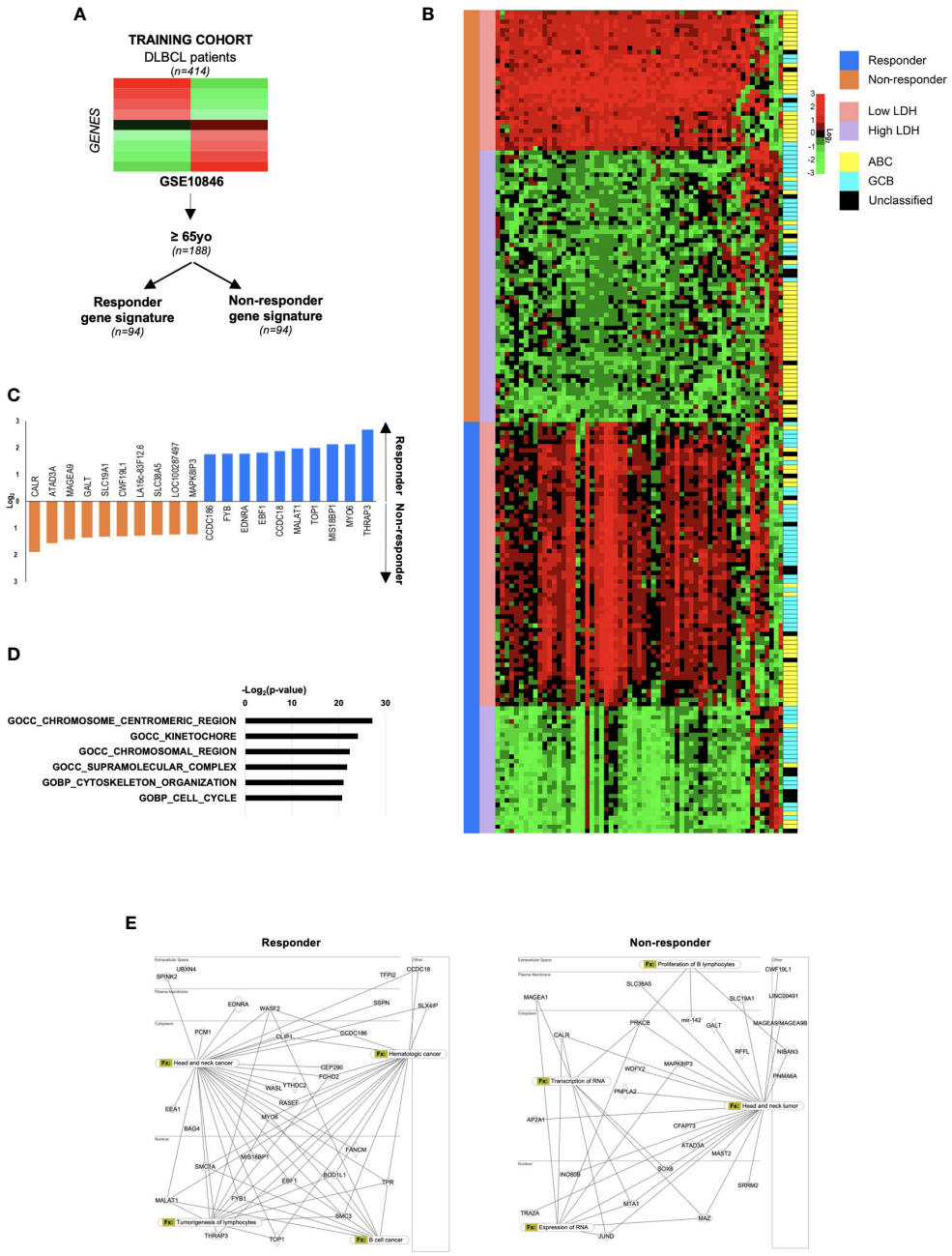

FIGURE 1
Gene expression analysis of a large cohort of DLBCL patients reveal a gene signature associated to prognosis. **(A)** Workflow chart indicating the process to select DLBCL responder and non-responder gene signatures in the training cohort of the GSE10846 database. **(B)** Heatmap of differential expressed genes (DEGs) (fold change >1.4, p-value <0.05, κ=387) in responder *versus* non responders DLBCL patients. The LDH levels and the molecular subtype classification are shown. **(C)** Top ten up-regulated genes (log2) in responder (blue) and non-responder (orange) DLBCL patient cohort. **(D)** Enrichment analysis in gene ontology (MSigDB) in responder and non-responder DLBCL patient cohort. **(E)** Protein network analysis, generated with DEGs listed in Supplementary Table 1 The networks were generated through the use of QIAGEN IPA (QIAGEN Inc., https://digitalinsights.qiagen.com/IPA), in responder and non-responder DLBCL patient cohort.

The enrichment analysis of top 30 upregulated genes computed with Molecular Signatures Database (MSigDB), revealed six signatures associated with cell cycle, cell division and cytoskeleton organization, which are related to B cell malignant neoplasia (Figures 1D, E; Supplementary Table 2). Together these data provide evidence that these gene signatures may select responder from non-responder patients, identifying patients with a better life expectancy.

10.3389/fimmu.2023.1266265

3.2 The expression levels of three genes predicted the response of DLBCL patients to R-CHOP therapy

In order to validate the expression levels of previously identified genes in dictating the dichotomization in life expectancy, we analyzed a cohort of naïve DLBCL patients, diagnosed and in follow-up at the Hematology/Oncology Unit of the "P. Giaccone" Hospital in Palermo, treated with R-CHOP as first -line therapy (validation cohort), selecting the frail cohort of DLBCL patients (≥ 65-year-old) (Table 1).

To overcome the low abundance and integrity of RNA content on formalin-fixed paraffin embedded (FFPE) biopsy samples, we adopted an implemented quantitative multiplex droplet digital PCR-based assay (Figure 1C; Figure 2A), from which emerged that two out ten DEGs, previously identified, *EBF1* and *MYO6* resulted up-regulated, at both mRNA and protein levels, in responder DLBCL patients (Figures 2B–D; Supplementary Figures 2A, B; Supplementary Table 3). Furthermore, the gene expression analysis of the ten upregulated genes, arisen from the non-responder included in the dataset (GSE10846), displayed an increasing trend of CALR mRNA levels, although not reaching statistical significance, which was paralleled by high protein expression levels (Figures 2B–D; Supplementary Table 4). These data indicate that EBF1, MYO6 and CALR could predict DLBCL patients' response to R-CHOP therapy and aid in the stratification of responder *versus* non-responder patients.

3.3 EBF1, MYO6 and CALR signature is associated with survival probability in DLBCL patients

To investigate the clinical significance of the identified signature, the magnitude of *EBF1*, *MYO6*, and *CARL* expression levels has been correlated to the survival data of ≥ 65-year-old DLBCL patients of the training cohort.

Transcriptome microarray analysis of a cohort of 154 DLBCL revealed a significant negative correlation between the signature $EBF1^{low}$, $MYO6^{low}$ and $CALR^{high}$ expression and survival probability of patients, assuming a more pronounced significance than single gene expression (Figure 3A). Univariate analysis denoted that $EBF1^{high}$, $MYO6^{high}$ and $CALR^{low}$ signature expression is an independent positive prognostic factor of overall survival showing a higher statistical significance over several important clinical parameters, such as ECOG performance status,

TABLE 1 Clinical parameters of patients with Diffuse Large B Cell Lymphoma (DLBCL) treated with rituximab, cyclophosphamide, doxorubicin, vincristine, and prednisone (R-CHOP) therapy.

Patient #	Age	Sex	Ann Arbor Stage	ECOG	Extranodal site	LDH	IPI	Responder
1	68	F	I	1	0	269	2	Yes
2	65	M	II	1	0	437	1	Yes
3	68	F	I	1	0	174	1	Yes
4	67	M	III	1	0	452	3	Yes
5	67	F	III	1	1	374	3	Yes
6	73	M	I	1	1	142	1	Yes
7	72	F	nd	nd	0	nd	nd	Yes
8	76	M	I	1	1	149	1	Yes
9	69	F	III	1	0	274	2	Yes
10	67	F	IV	1	0	985	3	Yes
11	69	F	IV	1	0	651	nd	Yes
12	79	M	IV	1	0	260	3	No
13	70	M	IV	2	1	511	5	No
14	71	M	IV	1	1	372	3	No
15	73	F	II	nd	nd	nd	1	No
16	73	F	nd	1	0	nd	1	Yes
17	69	M	nd	1	0	nd	3	Yes
18	65	M	nd	3	0	nd	4	No
19	70	F	nd	3	0	nd	2	No

Age is referred to the time of diagnosis. International prognostic Index (IPI) score varies from 0 to 5, according to the presence of prognostic factors. Responder patients to R-CHOP therapy are indicated with "Yes", while non-responder patients to R-CHOP therapy are indicated with "No".
Nd, not determined.

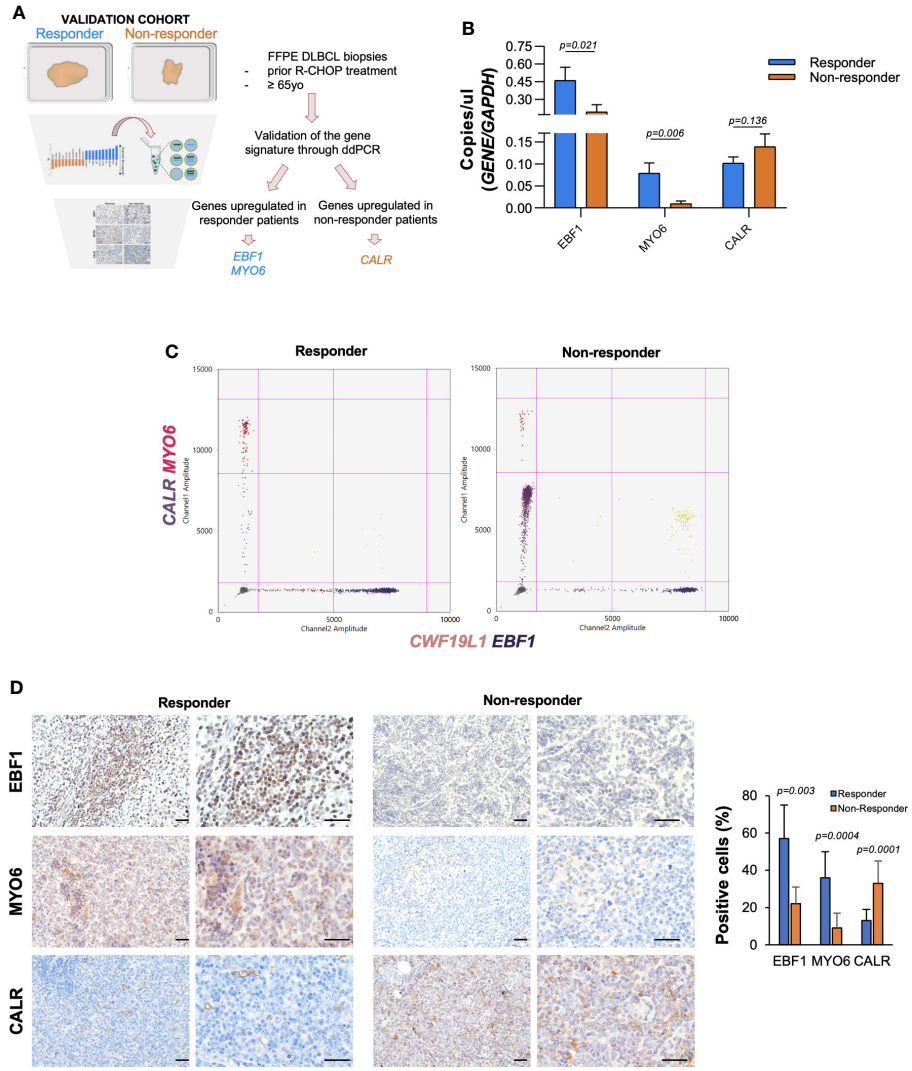

FIGURE 2
EBF1 and MYO6 result highly expressed in responder DLBCL patients whilst CALR high expression characterize non responder DLBCL patients. **(A)** Workflow chart indicating the validation of the identified signature in our cohort of FFPE DLBCL samples. **(B)** Absolute mRNA levels (copies/µl) of EBF1, MYO6 and CALR in responder and non-responder DLBCL patients (*n*=19). Data are represented as mean ± SEM of three independent experiments. **(C)** Representative droplet digital PCR (ddPCR) scatter plots showing single, double, triple or quadruple positive droplets for EBF1, MYO6, CALR and CWF19L1 of FFPE samples of responder (pt#1) and non-responder DLBCL patient (pt#14). **(D)** Representative IHC analysis for EBF1, MYO6 and CALR of patients as in **(C)** Scale bar is 100 µm.

extranodal sites and stage (Supplementary Figure 3A). Importantly, EBF1^{high}, MYO6^{high} and CALR^{low} signature expression significantly increased the prognostic value of ECOG performance status, extranodal sites, IPI, LDH and stage (Supplementary Figure 3B).

In line with the signature prognostic value, from the STRING network analysis emerged an implication of EBF1, MYO6, and CALR in the regulation of tumor progression together with the control of B lymphocyte gene transcription, intracellular vesicle transport and protein folding (Figure 3B; Supplementary Figure S3C). Being restricted the signature expression to DLBCLs as compared to non-tumoral lymphoid cells, a specific targeting of EBF1, MYO6 and CALR could be exploited for therapeutic intervention (Supplementary Figure S4A).

To investigate whether the *EBF1*, *MYO6* and *CALR* differential expression could be an age-independent signature to predict R-CHOP response, we assessed their expression levels in a heterogeneous age group, which revealed a comparable expression level in adults as well as elderly DLBCL patients (Figure 4A). Of note, beside in the over 65-year-old, EBF1^{low}, MYO6^{low} and CALR^{high} signature expression is able to dichotomize the response to R-CHOP treatment in under 65-year-old DLBCL patients (Figure 4B; Supplementary Figure S4B). Although EBF1^{high}, MYO6^{high} and CALR^{low} signature expression was an independent positive prognostic factor in under 65-year-old DLBCL patients, it did not increase the prognostic value of the selected clinical features in a multivariate analysis (Supplementary Figures 4C, D).

Our study unveils a robust predictive and prognostic signature able to determine the response to R-CHOP treatment in both under and over 65-year-old DLBCL patients. Notably, EBF1^{high},

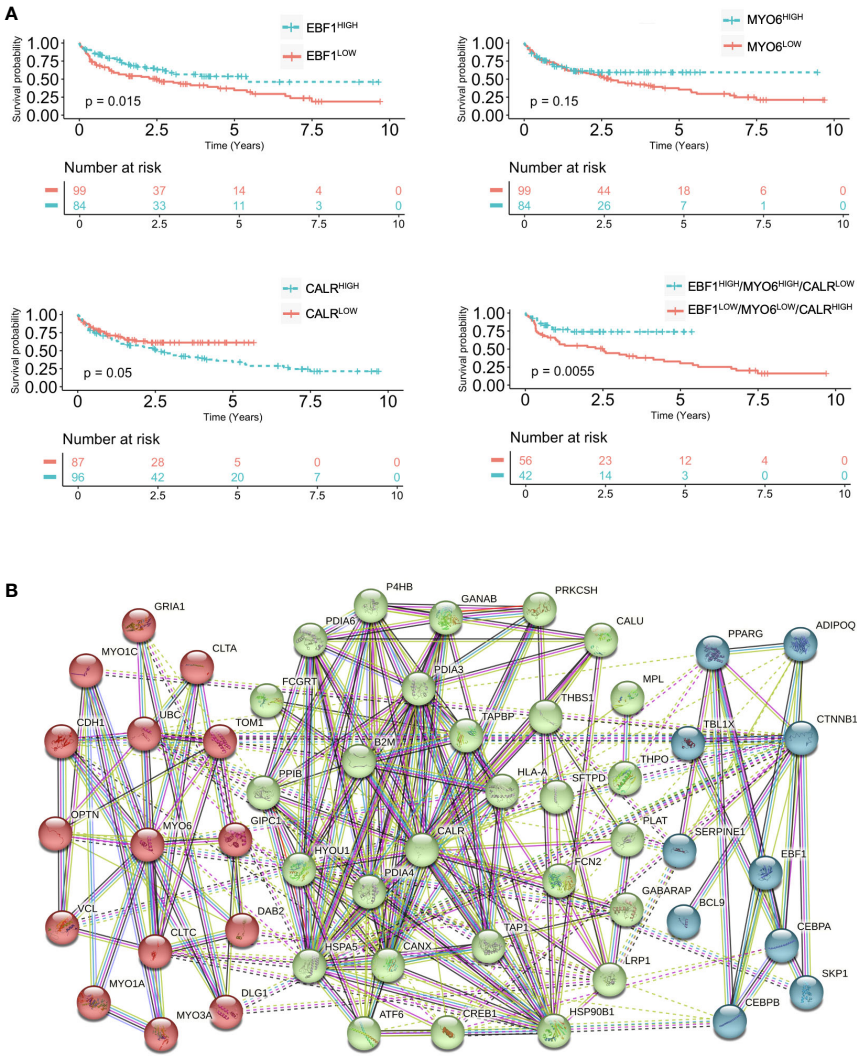

FIGURE 3
Expression of EBF1, MYO6 and CALR correlate with prognosis in DLBCL. **(A)** Kaplan Meier overall survival (OS) curves of elderly DLBCL patients (GSE10846) stratified by high or low EBF1, MYO6 and CALR expression levels. **(B)** Functional protein association network of EBF1, MYO6 and CALR based on STRING database.

MYO6^{high} and CALR^{low} signature expression ameliorates the prognostic power of the most important clinical parameters and, in particular, of the IPI clinical risk scoring system in the elderly patients.

4 Discussion

The clinical use of the so far identified gene signatures, mostly associated with tumor microenvironmental components, led to unsatisfied clinical outcomes of several DLBCL patients that remains poor (7, 10). Thus, it is becoming increasingly clear that the heterogeneity of patients, affected by DLBCL, has been underestimated, posing an urgent need to identify novel specific biomarkers for predicting the response to standard therapy.

Here, we found a new signature that significantly associates with the progression of disease that may be exploited for curative therapies in advanced DLBCLs. Droplet digital PCR and immunohistochemistry analysis of a cohort of ≥65-year-old naïve DLBCL patients revealed that EBF1, MYO6 and CALR expression levels stratify patients for the response to the standard R-CHOP therapy, regardless the IPI score, currently used in clinical settings. MYO6 is a motor protein, classified as unconventional myosin protein due to its reverse direction movement towards the actin filaments. MYO6 is involved in vesicular and macromolecules transport, cell migration and signaling (11). Albeit being implicated in prostate and breast cancer progression, here we uncover a novel role as favorable predictive biomarker in DLBCLs. CALR controls the protein folding by regulating the protein glucosylation-deglucosylation cycle and calcium homeostasis in the endoplasmic reticulum (12). CALR genetic alterations have been observed in several cancer types and correlated to a worse outcome. Specifically, CALR driver mutations has been described in myeloproliferative disorders but

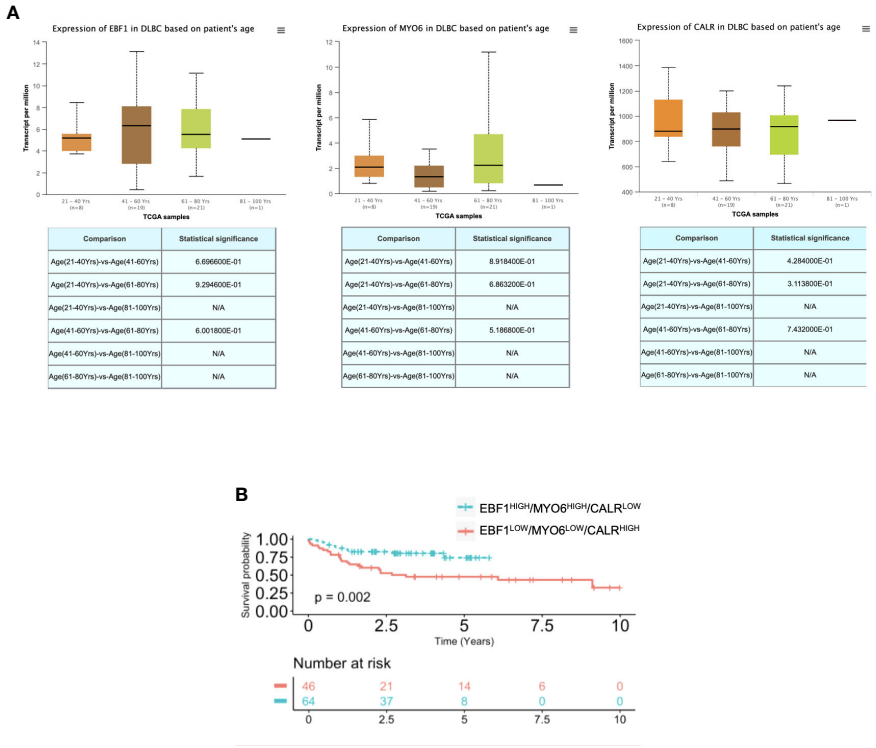

FIGURE 4
EBF1, MYO6 and CALR characterize DLBCL as compared to normal lymphoid tissues. **(A)** RNA seq expression data of EBF1, MYO6 and CALR in DLBCL patients at different age, retrieved from the TCGA database and analyzed by UALCAN. **(B)** Kaplan Meier overall survival (OS) curves of adult DLBCL patients (<65-year-old) (GSE10846) stratified by high or low EBF1, MYO6 and CALR expression levels. N/A stands for not available.

have not yet been associated to other hematological neoplasia (13, 14). Interestingly, the main driver mutations in CALR exon 9 change protein localization, from a cytoplasmic form to a membrane bound homodimers (15). Secretion of mutated CALR has also been observed in liquid biopsies samples as urine in bladder urothelial cancer patients (16). Our pioneer findings prospectively pose CALR as an extremely powerful biomarker in DLBCL patients and further analysis are necessary to clarify the mutational status of CALR also in DLBCL patients.

Being EBF1, together with E2A and Pax5, involved in the B-cell lineage commitment by regulating cell transcription, it has been also implicated in the development of B-cell-acute lymphoblastic leukemias (B-ALL) (17). EBF1 protein levels have been otherwise associated to better prognosis in colorectal cancer and cholangiocarcinoma and to a worse outcome in triple-negative breast cancer (18–20). The herein reported findings indicate that the *EBF1*^{low}/*MYO*^{low}/*CALR*^{high} gene expression foresees the failure in therapeutic response of patients associated with a low-intermediate IPI risk, airing this identified signature as significant prognostic power. While further studies are needed to investigate MYO6 regulation of lymphoma cell dynamics and to design novel therapeutic approaches, a monoclonal antibody targeting the neoepitope generated by mutated CALR in myeloproliferative disorders has been generated. This approach could be prospectively applied to DLBCL patients harboring alterations in *CALR* (21). To date, specific agonists of EBF1 are not clinically available, however, evidence showed that the inhibition of EBF1 may be influenced by Notch and IL-7 signaling, whose modulation by already accessible compounds could indirectly interfere with EBF1 (17). Our findings provide evidence that EBF1, likely by preserving B cell entity, is required together with MYO and CALR for R-CHOP response and significantly associates with patient overall survival.

High-grade DLBCLs requires more intensive therapies mainly characterized by the addition of other chemotherapeutic treatments. Although the major limitation of this study relies in the lack of functional validation of the newly identified genes, EBF1, MYO6 and CALR could be considered targetable candidates to aid advanced DLBCL management.

Data availability statement

The raw data supporting the conclusions of this article will be made available by the authors, without undue reservation.

Ethics statement

Ethical approval was not required for the studies involving humans because the study was performed on already published dataset and retrospective samples. The studies were conducted in

accordance with the local legislation and institutional requirements. For the human samples used in this study, a written informed consent was not required from the participants or the participants' legal guardians/next of kin in accordance with the national legislation and the institutional requirements.

Author contributions

AT: Conceptualization, Funding acquisition, Supervision, Writing – original draft, Writing – review & editing. MG: Conceptualization, Funding acquisition, Supervision, Writing – original draft, Writing – review & editing. CD'A: Methodology, Writing – review & editing. GP: Methodology, Writing – review & editing. SB: Methodology, Writing – review & editing. DC: Methodology, Writing – review & editing. IP: Resources, Writing – review & editing. RP: Resources, Writing – review & editing. MLI: Methodology, Writing – review & editing. FV: Methodology, Writing – review & editing. CM: Methodology, Writing – review & editing. NR: Methodology, Writing – review & editing. AF: Resources, Writing – review & editing. GS: Funding acquisition, Writing – review & editing, Writing – original draft. SM: Funding acquisition, Writing – review & editing, Writing – original draft. MT: Conceptualization, Funding acquisition, Writing – original draft, Writing – review & editing.

Funding

The author(s) declare financial support was received for the research, authorship, and/or publication of this article. The research leading to these results has received funding from AIRC under IG 2018 - ID. 21492 project and from PSN2015, 6.2, CUP176J17000470001 project to MT; from Department PROMISE - "Angelo Ferrante" project to AT, IP, AMF and SM; from Department DICHIRONS - PJ_PROGRIC2022_MIS1A project to MG; from Italian Ministry for University - PNRR M4C2I1.3-HEAL ITALIA project PE 00000019 CUP B73C22001310006 to GS and MT.

Acknowledgments

AT is a research fellow funded by "Programma Operativo Complementare" 2014-2020 from Regione Siciliana. AT and MG have been supported by FONDO FINALIZZATO ALLA RICERCA DI ATENEO (FFR) – 2023.

Conflict of interest

The authors declare that the research was conducted in the absence of any commercial or financial relationships that could be construed as a potential conflict of interest.

The author(s) declared that they were an editorial board member of Frontiers, at the time of submission. This had no impact on the peer review process and the final decision.

Publisher's note

Supplementary material

The Supplementary Material for this article can be found online at: https://www.frontiersin.org/articles/10.3389/fimmu.2023.1266265/full#supplementary-material

References

1. Hounsome L, Eyre TA, Ireland R, Hodson A, Walewska R, Ardeshna K, et al. Diffuse large B cell lymphoma (DLBCL) in patients older than 65 years: analysis of 3 year Real World data of practice patterns and outcomes in England. *Br J Cancer* (2022) 126(1):134–43. doi: 10.1038/s41416-021-01525-4

2. Coiffier B, Lepage E, Briere J, Herbrecht R, Tilly H, Bouabdallah R, et al. CHOP chemotherapy plus rituximab compared with CHOP alone in elderly patients with diffuse large-B-cell lymphoma. *N Engl J Med* (2002) 346(4):235–42. doi: 10.1056/NEJMoa011795

3. Handforth C, Clegg A, Young C, Simpkins S, Seymour MT, Selby PJ, et al. The prevalence and outcomes of frailty in older cancer patients: a systematic review. *Ann Oncol* (2015) 26(6):1091–101. doi: 10.1093/annonc/mdu540

4. Schmitz R, Wright GW, Huang DW, Johnson CA, Phelan JD, Wang JQ, et al. Genetics and pathogenesis of diffuse large B-cell lymphoma. *N Engl J Med* (2018) 378 (15):1396–407. doi: 10.1056/NEJMoa1801445

5. International Non-Hodgkin's Lymphoma Prognostic Factors P. A predictive model for aggressive non-Hodgkin's lymphoma. *N Engl J Med* (1993) 329(14):987–94. doi: 10.1056/NEJM199309303291402

6. Sehn LH, Berry B, Chhanabhai M, Fitzgerald C, Gill K, Hoskins P, et al. The revised International Prognostic Index (R-IPI) is a better predictor of outcome than the standard IPI for patients with diffuse large B-cell lymphoma treated with R-CHOP. *Blood* (2007) 109(5):1857–61. doi: 10.1182/blood-2006-08-038257

7. Lenz G, Wright G, Dave SS, Xiao W, Powell J, Zhao H, et al. Stromal gene signatures in large-B-cell lymphomas. *N Engl J Med* (2008) 359(22):2313–23. doi: 10.1056/NEJMoa0802885

8. Risueno A, Hagner PR, Towfic F, Fontanillo C, Djebbari A, Parker JS, et al. Leveraging gene expression subgroups to classify DLBCL patients and select for clinical benefit from a novel agent. *Blood* (2020) 135(13):1008–18. doi: 10.1182/blood.2019002414

9. Ruppert AS, Dixon JG, Salles G, Wall A, Cunningham D, Poeschel V, et al. International prognostic indices in diffuse large B-cell lymphoma: a comparison of IPI, R-IPI, and NCCN-IPI. *Blood* (2020) 135(23):2041–8. doi: 10.1182/blood.2019002729

10. Feng P, Li H, Pei J, Huang Y, Li G. Identification of a 14-gene prognostic signature for diffuse large B cell lymphoma (DLBCL). *Front Genet* (2021) 12:625414. doi: 10.3389/fgene.2021.625414

11. Wang D, Zhu L, Liao M, Zeng T, Zhuo W, Yang S, et al. MYO6 knockdown inhibits the growth and induces the apoptosis of prostate cancer cells by decreasing the

phosphorylation of ERK1/2 and PRAS40. *Oncol Rep* (2016) 36(3):1285–92. doi: 10.3892/or.2016.4910

12. Fucikova J, Spisek R, Kroemer G, Galluzzi L. Calreticulin and cancer. *Cell Res* (2021) 31(1):5–16. doi: 10.1038/s41422-020-0383-9

13. Mozes R, Gango A, Sulak A, Vida L, Reiniger L, Timar B, et al. Calreticulin mutation specific CAL2 immunohistochemistry accurately identifies rare calreticulin mutations in myeloproliferative neoplasms. *Pathology* (2019) 51(3):301–7. doi: 10.1016/j.pathol.2018.11.007

14. Jutzi JS, Marneth AE, Jimenez-Santos MJ, Hem J, Guerra-Moreno A, Rolles B, et al. CALR-mutated cells are vulnerable to combined inhibition of the proteasome and the endoplasmic reticulum stress response. *Leukemia* (2023) 37(2):359–69. doi: 10.1038/s41375-022-01781-0

15. Varricchio L, Falchi M, Dall'Ora M, De Benedittis C, Ruggeri A, Uversky VN, et al. Calreticulin: challenges posed by the intrinsically disordered nature of calreticulin to the study of its function. *Front Cell Dev Biol* (2017) 5:96. doi: 10.3389/fcell.2017.00096

16. Kageyama S, Isono T, Matsuda S, Ushio Y, Satomura S, Terai A, et al. Urinary calreticulin in the diagnosis of bladder urothelial carcinoma. *Int J Urol* (2009) 16 (5):481–6. doi: 10.1111/j.1442-2042.2009.02287.x

17. Lukin K, Fields S, Hartley J, Hagman J. Early B cell factor: Regulator of B lineage specification and commitment. *Semin Immunol* (2008) 20(4):221–7. doi: 10.1016/j.smim.2008.07.004

18. Qiu Z, Guo W, Dong B, Wang Y, Deng P, Wang C, et al. EBF1 promotes triple-negative breast cancer progression by surveillance of the HIF1alpha pathway. *Proc Natl Acad Sci U.S.A.* (2022) 119(28):e2119518119. doi: 10.1073/pnas.2119518119

19. Shen Z, Chen Y, Li L, Liu L, Peng M, Chen X, et al. Transcription Factor EBF1 Over-Expression Suppresses Tumor Growth in *vivo* and *in vitro* via Modulation of the PNO1/p53 Pathway in Colorectal Cancer. *Front Oncol* (2020) 10:1035. doi: 10.3389/fonc.2020.01035

20. Armartmuntree N, Murata M, Techasen A, Yongvanit P, Loilome W, Namwat N, et al. Prolonged oxidative stress down-regulates Early B cell factor 1 with inhibition of its tumor suppressive function against cholangiocarcinoma genesis. *Redox Biol* (2018) 14:637–44. doi: 10.1016/j.redox.2017.11.011

21. Tvorogov D, Thompson-Peach CAL, Fosselteder J, Dottore M, Stomski F, Onnesha SA, et al. Targeting human CALR-mutated MPN progenitors with a neoepitope-directed monoclonal antibody. *EMBO Rep* (2022) 23(4):e52904. doi: 10.15252/embr.202152904

frontiers | Frontiers in Immunology

TYPE Original Research
PUBLISHED 12 December 2023
DOI 10.3389/fimmu.2023.1277695

OPEN ACCESS

EDITED BY
Shimin Hu,
University of Texas MD Anderson Cancer Center, United States

REVIEWED BY
Shuiyan Wu,
Children's Hospital of Soochow University, China
Walter Hanel,
The Ohio State University, United States

*CORRESPONDENCE
XiongPeng Zhu
xiongpengzhu@163.com

RECEIVED 15 August 2023
ACCEPTED 15 November 2023
PUBLISHED 12 December 2023

CITATION
Zhang C, Lin Q, Li C, Qiu Y, Chen J and Zhu X (2023) Comprehensive analysis of the prognostic implication and immune infiltration of CISD2 in diffuse large B-cell lymphoma.
Front. Immunol. 14:1277695.
doi: 10.3389/fimmu.2023.1277695

Comprehensive analysis of the prognostic implication and immune infiltration of CISD2 in diffuse large B-cell lymphoma

ChaoFeng Zhang[1,2,3], Qi Lin[4], ChunTuan Li[1], Yang Qiu[3], JingYu Chen[3] and XiongPeng Zhu[1*]

[1]Department of Haematology, Quanzhou First Hospital Affiliated to Fujian Medical University, Quanzhou, China, [2]Department of Hematology and Rheumatology, The Affiliated Hospital of Putian University, Putian, China, [3]The School of Basic Medicine, Putian University, Putian, China, [4]Department of Pharmacy, The Affiliated Hospital of Putian University, Putian, China

Background: Diffuse large B-cell lymphoma (DLBCL) is the most common B-cell lymphoma in adults. CDGSH iron sulfur domain 2 (CISD2) is an iron–sulfur protein and plays a critical role of cell proliferation. The aberrant expression of CISD2 is associated with the progression of multiple cancers. However, its role in DLBCL remains unclear.

Methods: The differential expression of CISD2 was identified via public databases, and quantitative real-time PCR (qRT-PCR) and western blot were used to identifed the expression of CISD2. We estimated the impact of CISD2 on clinical prognosis using the Kaplan-Meier plotter. Meanwhile, the drug sensitivity of CISD2 was assessed using CellMiner database. The 100 CISD2-related genes from STRING obtained and analyzed using the LASSO Cox regression. A CISD2 related signature for risk model (CISD2Risk) was established. The PPI network of CISD2Risk was performed, and functional enrichment was conducted through the DAVID database. The impacts of CISD2Risk on clinical features were analyzed. ESTIMATE, CIBERSORT, and MCP-counter algorithm were used to identify CISD2Risk associated with immune infiltration. Subsequently, Univariate and multivariate Cox regression analysis were applied, and a prognostic nomogram, accompanied by a calibration curve, was constructed to predict 1-, 3-, and 5-years survival probabilities.

Results: CISD2 was upregulated in DLBCL patients comparing with normal controls via public datasets, similarly, CISD2 was highly expressed in DLBCL cell lines. Overexpression of CISD2 was associated with poor prognosis in DLBCL patients based on the GSE31312, the GSE32918, and GSE93984 datasets ($P<0.05$). Nine drugs was considered as a potential therapeutic agents for CISD2. By using the LASSO cox regression, twenty seven genes were identified to construct CISD2Risk, and biological functions of these genes might be involved in apoptosis and P53 signaling pathway. The high CISD2Risk value had a worse prognosis and therapeutic effect ($P<0.05$). The higher stromal score, immune score, and ESTIMATE score were associated with lowe CISD2Risk value, CISD2Risk was negatively correlated with several immune infiltrating cells (macrophages M0 and M1, CD8 T cells, CD4 naïve T cells, NK cell, etc) that

might be correlated with better prognosis. Additionally, The high CISD2Risk was identified as an independent prognostic factor for DLBCL patients using both univariate and multivariate Cox regression. The nomogram produced accurate predictions and the calibration curves were in good agreement.

Conclusion: Our study demonstrates that high expression of CISD2 in DLBCL patients is associated with poor prognosis. We have successfully constructed and validated a good prognostic prediction and efficacy monitoring for CISD2Risk that included 27 genes. Meanwhile, CISD2Risk may be a promising evaluator for immune infiltration and serve as a reference for clinical decision-making in DLBCL patients.

KEYWORDS

diffuse large B cell lymphoma, CISD2, prognosis, immune infiltration, risk model

Introduction

Diffuse large B-cell lymphoma (DLBCL) is the most common subtype of non-Hodgkin lymphoma (NHL) (1, 2), accounting for approximately 30–40% of NHL cases. DLBCL is a clinically and biologically heterogeneous disease with variable responses to treatment and prognoses (1–3). R-CHOP (rituximab, cyclophosphamide, doxorubicin, vincristine, and prednisone) has become the standard treatment for DLBCL due to its clinical efficacy and well-established safety (3). There are some risk stratifications, such as activated B-cell (ABC) origin, BCL2/MYC double-expression, and high International Prognostic Index (IPI) score (3, 4), that are associated with poor prognosis, aggressive disease behavior, or resistance to R-CHOP in DLBCL patients. Improved understanding of the factors influencing DLBCL prognosis is crucial for refining risk stratification, tailoring treatment approaches, and ultimately enhancing clinical benefit and overall survival (3, 5).

CDGSH iron-sulfur domain-containing protein 2 (CISD2), also known as mitoNEET, is anchored to the mitochondrial outer membrane (MOM) (6, 7). It believes that CISD2 is associated with lifespan and health span (8), and overexpression of CISD2 might restrain age-associated degeneration of the skin, skeletal muscles, neurons, and cardiac system in aging (7, 9). CISD2 is also involved in the development and progression of multiple cancer types, including breast cancer (10), lung cancer (11), and colorectal cancer (12). Upregulation of CISD2 has often been correlated with aggressive tumor characteristics such as increased tumor size and advanced clinical stage (7, 13, 14). In tumorigenesis, CISD2 can regulate cancer cell growth, proliferation, invasion, biosynthesis, and progression through various cellular processes, including mitochondrial iron metabolism, redox regulation, lipid metabolism, and cellular stress response (7, 9). Moreover, inhibition of CISD2 could improve the chemosensitivity of tumors through increasing cell autophagy and ferroptosis (15, 16). However, knowledge about the biological function of CISD2 in DLBCL is meager.

This study aimed to depict the expression profiles of CISD2 and to analyze its prognostic role and immune infiltration in DLBCL through bioinformatics analysis and to clarify its probable mechanisms. We indicated that high CISD2 acted as a biomarker and an indicator of an adverse prognosis among patients with DLBCL. Taken together, these findings provided evidence that CISD2 is important in the occurrence and development of DLBCL and suggested that CISD2 may be a new biomarker and a novel therapeutic target for DLBCL.

Materials and methods

Data collection

The public electronic datasets extracted from The Cancer Genome Atlas (TCGA-DLBC) (n = 47), Genotype-Tissue Expression (GTEx) (n = 444), which were downloaded from UCSC Xena (https://xena.ucsc.edu/), and the Gene Expression Omnibus (GEO, https://www.ncbi.nlm.nih.gov/geo/), including GSE83632 (17) (n = 163), GSE31312 (18) (n = 498), GSE32918 (19) (n = 172), GSE93984 (20) (n = 88), GSE117556 (21) (n = 928), and GSE181063 (22) (n = 1311). The general information and clinical metadata were obtained and provided in Supplementary Table S1. Three healthy volunteers were recruited in our institution, and peripheral blood mononuclear cell (PBMC) were extracted, this protocol was approved by the ethics committee of Quanzhou First Hospital Affiliated to Fujian Medical University (No. [2023]K096).

Cell lines culture and expression validation

The lymphoblastoid cell line GM12878 (BeNa, China), DLBCL cell lines DB (Procell, China), SUDHL4 (Meisen, China), and SUDHL2 (A gift from Eatern-Sounth University), were used and cultured in RPMI-1640 (Biosharp, China) supplemented with 10%

fetal bovine serum (FBS, Gibco, USA), 1% streptomycin, and penicillin (Gibco, USA). The expression of CISD2 in cell lines was validated through quantitative real-time polymerase chain reaction (qRT-PCR) and western blotting analysis. First, the total RNA was extracted using TRIzol reagent (Invitrogen, US) and reverse-transcribed into complementary DNA (cDNA) for qRT-PCR following the manufacturer's instructions. The primer sequences of CISD2 and β-actin (As an endogenous control) used in the experiment are illustrated in Supplementary Table S2. Second, the protein was collected using RIPA buffer (Beyotime, China) with 1% PMSF (Beyotime, China), and the concentration of protein was measured using a BCA protein assay kit (Beyotime, China). Then, the extracted protein was loaded onto a 12.5% SDS-PAGE gel (Meilunbio, China) and transferred onto Polyvinylidene fluoride (PVDF) membranes. The membranes were incubated with the anti-CISD2 primary antibody (1:1000, Proteintech, China) at 4° C overnight. After the membranes were incubated with goat anti-mouse IgG (1:10000, Beyotime, China) At room temperature, the level of protein was detected using BeyoECL Plus (Beyotime, China) and quantified using Fiji (version 2.9, fiji.sc).

Expression analysis and survival analysis

The differential expression of CISD2 between DLBCL patients and healthy donors was generated using the TCGA-DLBC, GTEx, and GSE83632 datasets. The protein expression of CISD2 was explored through The Human Protein Altas (HPA, https://www.proteinatlas.org). And the receiver operating characteristic (ROC) curve was plotted for the performance of distinguishing between them. Meanwhile, we attempted to investigate the prognostic role of CISD2 in multiple GEO datasets, including GSE31312, GSE32918, and GSE93984 datasets, using the survival package.

Drug sensitivity assessment

CellMiner database (www.discover.nci.nih.gov) (23) was used to assess the drug sensitivity analysis, RNA expression data (RNA: RNA-seq) and drug data (Compound activity: DTP NCI-60), which the drugs were selected though approving by clinical trial and FDA, were downloaded. The Pearson correlation coefficient between CISD2 expression and drugs was calculated and screened (|Pearson| > 0.03 and $P < 0.01$) using impute and limma (24) packages.

Development of a CISD2-related risk model

The TOP 100 CISD2-related genes were downloaded from the Search Tool for the Retrieval of Interacting Genes/Proteins (STRING, https://version-12-0.string-db.org/, Version 12.0) with at least a medium confidence score (0.400). Based on the GSE117556 dataset, these genes were inputted into the least absolute shrinkage and selection operator (LASSO) Cox regression using the glmnet package (25), a CISD2 related signature for risk stratification (CISD2Risk) was developed and determined, and the risk score was generated: risk score = $\Sigma\beta_i x_i$.

Performance assessment for CISD2Risk

Aiming to elucidate CISD2Risk-related biological function and interaction, we imported genes of CISD2Risk to STRING and performed the protein-protein interaction (PPI) network, in which the association was represented via a confidence score greater than 0.400 and a P-value less than 0.05. Next, we uploaded these genes to the Database for Annotation, Visualization and Integrated Discovery (DAVID) (26), and Gene Ontology (GO) (27) and Kyoto Encyclopedia of Genes and Genome (KEGG) analysis (28) were executed. Based on the GSE117556 as training datasets and the GSE181063 as validation datasets, expression analysis, survival analysis, univariate Cox analysis, and multivariate Cox analysis were adopted to appraise the association of the CISD2Risk and clinical characteristics with OS.

CISD2Risk associated with immune infiltration

To explore the potential immune infiltration contributing to CISD2Risk, we qualified the tumor microenvironment, including the stroma score, immune score, and estimate score, using the estimate package (29). The cell type identification by estimating relative subsets of RNA transcripts (CIBERSORT) algorithm (30) was used to evaluate 22 types of immune cell infiltration in the GSE117556 and GSE181063 datasets, and the difference between the CISD2Risk value and the abundances of immune cells was estimated. And the Microenvironment Cell Populations-counter (MCP-counter) algorithm (31) that could allow use of the transcriptome data to quantify the absolute abundance of 8 immune cells and 2 stromal cells was analyzed.

Prognostic implication of CISD2Risk

Meanwhile, we developed the nomograms using the rms package, and the time-dependent receiver operating characteristic (ROC) curves were plotted to determine the prognostic accuracy of the CISD2Risk using the timeROC package (32), and the probability of 1-, 3-, and 5-year OS can be obtained. A calibration curve was used to visualize the deviation of predicted probabilities from what actually happened. The concordance index (C-index) was used to measure the predictive accuracy of the nomogram.

Statistical analysis

Data are expressed as the mean ± standard deviation (SD). Comparisons between two groups were analyzed using the Student's t-test (two-tailed). Comparisons among groups were analyzed using a one-Way ANOVA followed by the Tukey test. All

analyses were performed with R programming (version 4.2.1). $P < 0.05$ was considered to indicate a statistically significant difference.

Results

Upregulated CISD2 expression in DLBCL

Figure 1 illustrates the workflow in this study. Based on TIMER2.0 (http://timer.cistrome.org), we found that CISD2 expression was upregulated in numerous tumors (7) (Supplementary Figure S1A), including lung adenocarcinoma (LUAD) (33), breast cancer (BRCA) (10, 34), and liver cancer (LIHC) (35). Due to the lack of normal control, the whole blood cohort was often used as a reference to TCGA-DLBC. After excluding Epstein Barr virus (EBV) transformed lymphocytes, a total of 337 whole blood specimens were enrolled. In the comparison of gene expression between TCGA tumor and GTEx normal datasets (Figures 2A). CISD2 expression was dramatically increased in DLBCL samples in TCGA-DLBC compared with 337 whole blood specimens in GTEx dataset($P < 0.05$, Figure 2B). We also analyzed CISD2 expression patterns in the GSE83632 datasets, which enrolls 76 DLBCL patients and 87 healthy controls (HCs). As shown in Figures 2C, D, the result showed CISD2 expression in DLBCL was higher than in HCs ($P < 0.05$). In order to assess the performance of the CISD2 expression for the predictor variable. First, comparing TCGA-DLBC with whole blood samples in GTEx dataset, the area under the curve (AUC) of the ROC curve was 0.818 (95% CI: 0.780-0.856, Figure 2E). Meanwhile, the AUC value of 0.8274 (95% CI: 0.759-0.896, Figure 2F) was showed in the GSE83632 dataset. On the other hand, using HPA dataset, the protein expression of CISD2 in lymphoma tissues were higher than lymph node tissues

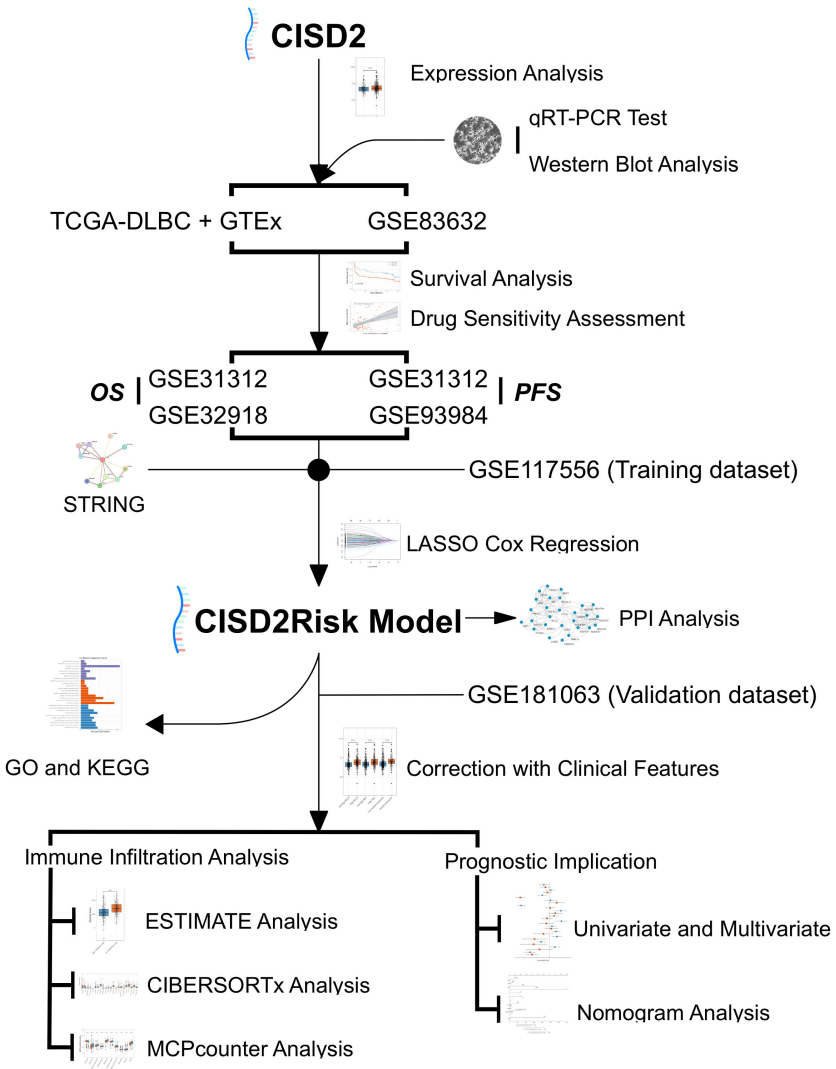

FIGURE 1
Study flowchart. DLBCL, Diffuse large B-cell lymphoma; GO, Gene Ontology; GSE, Gene Expression Omnibus Series; GTEx, The Genotype-Tissue Expression; KEGG, the Kyoto Encyclopedia of Genes and Genomes; LASSO, the least absolute shrinkage and selection operator regression; MCP-counter, Microenvironment Cell Populations-counter; OS, over survival; PFS, progression-free survival; PPI, Protein-protein interaction; qRT-PCR, real-time reverse transcription-PCR; STRING, the Retrieval of Interacting Genes/Proteins; TCGA, The Cancer Genome Atlas.

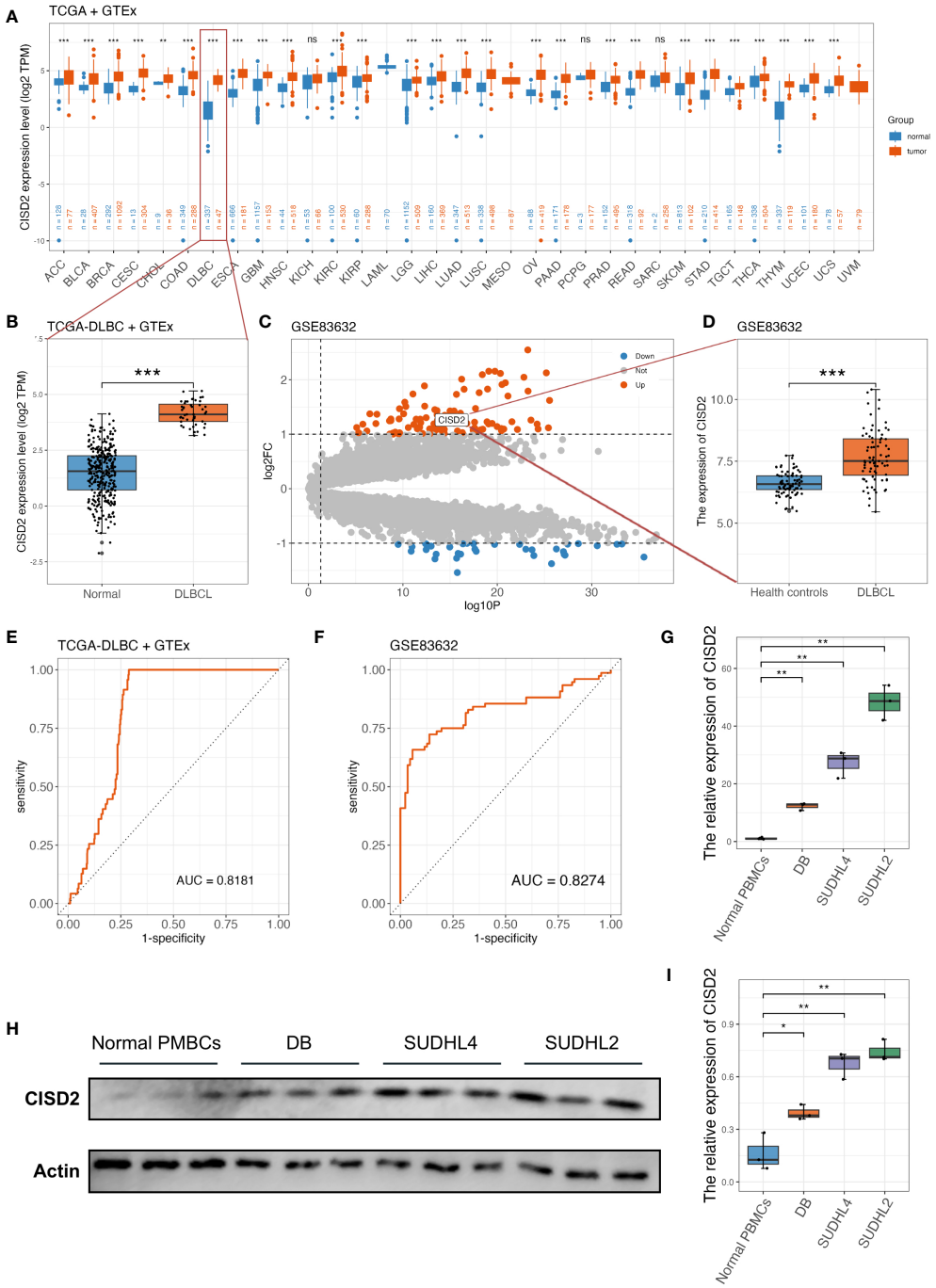

FIGURE 2
The upregulated expression of CISD2 in DLBCL. **(A)** The gene expression profile of CISD2 in different types of tumors and its homologous normal tissues, data was extracted from TCGA and GTEx. **(B)** CISD2 expression in DLBCL tissue (TCGA-DLBC, n = 47) compared with the whole blood excluded EBV transformed lymphocytes in GTEx cohort (n = 337). **(C)** The volcano plot based on GSE83632 datasets, CISD2 was located in the area of upregulation, adjust *P* value < 0.05 and fold change < 1. **(D)** CISD2 expression in DLBCL whole blood samples (n = 76) compared with healthy controls (n = 87) based on GSE83632 dataset. The ROC curves and AUC for evaluating the prediction accuracy of CISD2 in the network analysis of TCGA-DLBC and GTEx gene expression datasets **(E)**, and GSE83632 dataset **(F)**. The expression of CISD2 in different B lymphocyte cell lines, including normal PBMCs, SUDHL2, SUDHL4, and DB. A qRT-PCR analysis **(G)**, and a WB analysis **(H, I)**. AUC, area under curve; DLBCL, Diffuse large B-cell lymphoma; GSE, Gene Expression Omnibus Series; GTEx, The Genotype-Tissue Expression; PBMC, peripheral blood mononuclear cell; qRT-PCR, real-time reverse transcription-PCR; ROC, receiver operating characteristic; WB, western blotting. *** *P* < 0.001, ** *P* < 0.01, * *P* < 0.05, ns, not signifcance.

(Supplementary Figure S1B). For further comparison of CISD2 expression among B-cell lines, first, CISD2 expression of DLBCL cell lines, including DB, SUDHL4, and SUDHL2, was upregulated compared with normal B cell lines (GM12878) through WB analysis (Supplementary Figures S1C, D) and qRT-PCR analysis (Supplementary Figure S1E). Second, the PBMCs extracted from three healthy volunteers, comparison with DLBCL cell lines, the CISD2 expression in PBMCs downregulated using qRT-PCR and

WB analysis($P < 0.05$, Figures 2G–I). These evidences indicated that CISD2 has auxiliary diagnostic significance in distinguishing DLBCL samples from normal samples.

Prognostic role of CISD2 expression in DLBCL

To determine whether CISD2 could have a novel prognostic value in DLBCL, we analyzed its prognostic significance in DLBCL patients using a Kaplan-Meier (KM) curve based on GEO datasets. As shown in Figures 3A, C, upregulated CISD2 expression was associated with poor over survival (OS) in both the GSE31312 dataset (Hazard Ratio (HR) = 0.746, 95% CI: 0.594-0.938, $P = 0.01$) and the GSE32918 dataset (HR = 0.688, 95% CI: 0.492-0.962, $P = 0.028$) by the KM survival curve analysis. Also, DLBCL with high CISD2 expression showed remarkably worse progression-free survival (PFS) than low CISD2 expression in both the GSE31312 dataset (HR = 0.774, 95% CI: 0.614-0.976, $P = 0.028$) and the GSE93984 dataset (HR = 0.297, 95% CI: 0.086-1.029, $P = 0.009$) (Figures 3B, D). For each of the above datasets, patients were stratified into two groups using the median CISD2 expression level as a cutoff and were eliminated if OS or PFS were lower than one month. This suggests that CISD2 expression may influence the prognosis of patients with DLBCL.

Drug sensitivity assessment of CISD2

Using the CellMiner database (23), the results showed that AM-5992, Ribavirin, Chelerythrine, KPT-9274, Palbociclib, LEE-011, Hydroxyurea, PX-316, and Nelarabine were positively correlated with CISD2 expression (Figure 3E, Supplementary Table S3). Meanwhile, the scatter plots were provided in Supplementary

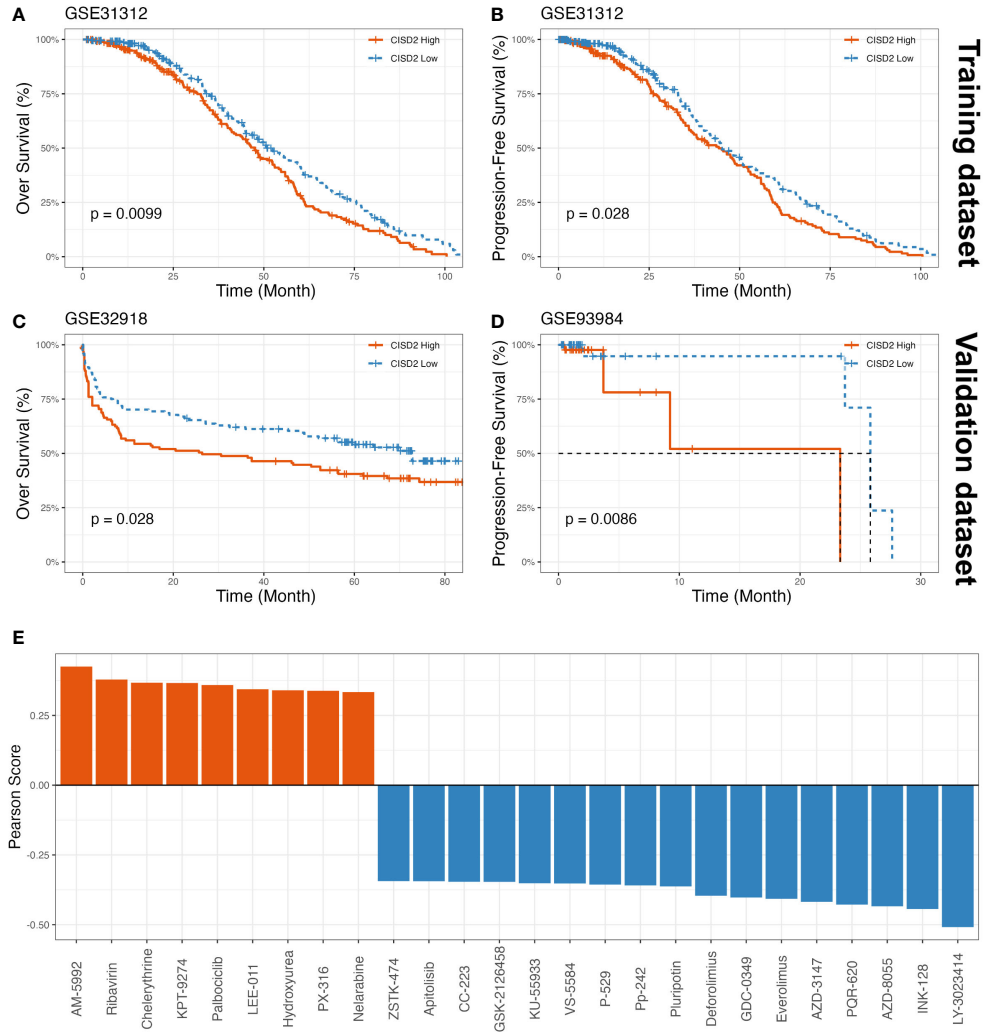

FIGURE 3
The prognostic value of CISD2 expression in DLBCL and drug sensitivity assessment of CISD2. The KM curves showed OS **(A)** and PFS **(B)** based on GSE31312 as training datasets, on the other part, the KM curves showed OS based on GSE32918 as a validation dataset **(C)**, and PFS based on GSE93984 as a validation dataset **(D)**. **(E)** The drug sensitivity analysis was showed, a total of 9 drugs were positively associated with CISD2 expression, and 17 drugs suggested negative correlation though CellMiner database. GSE, Gene Expression Omnibus Series; KM, Kaplan–Meier; OS, over survival; PFS, progression-free survival.

Figure S2. These findings indicated that these small molecule compounds may be potential therapeutic agents for CISD2.

Development of the CISD2Risk

To in-depth explore the biological function of CISD2 and its related genes in DLBCL, we collected 100 CISD2-related genes from the STRING website (Supplementary Figure S3). A total of 928 patients in the GSE117556 (21) were applied for investigation into their potential effectiveness in this study. After excluding patients with OS times of less than one month, 844 patients were enrolled. The levels of CISD2 related genes were inputted into LASSO Cox regression analysis (Figures 4A, B). Twenty-seven genes, including *CISD2*, *BID*, *NDUFA9*, *NDUFS5*, *NDUFB9*, *BCL2*, *NDUFA7*, *MCL1*, *PMAIP1*, *PIK3C3*, *CYCS*, *UQCRB*, *NDUFS1*, *HRK*, *UVRAG*, *BBC3*, *PIK3R4*, *CISD3*, *NDUFB1*, *NRBF2*, *NDUFB4*, *FXC1*, *TMEM49*, *TIMM10*, *NDUFB2*, *BCL2L1*, and *BCL2L11* were evaluated (Figure 4C). Therefore, the CISD2Risk was: CISD2Risk = 0.2485 × *CISD2* -0.0610 × *BID* -0.0224 × *NDUFA9* + 0.0176 × *NDUFS5* + 0.2460 × *NDUFB9* + 0.1057 × *BCL2* + 0.04074 × *NDUFA7* + 0.2673 × *MCL1* + 0.1250 × *PMAIP1* + 0.1510 × *PIK3C3* + 0.1428 × *CYCS* + 0.1468 × *UQCRB* + 0.0598 × *NDUFS1* + 0.0390 × *HRK* - 0.2614 × *UVRAG* - 0.0441 × *BBC3* + 0.2380 × *PIK3R4* + 0.1201 × *CISD3* - 0.1192 × *NDUFB1* + 0.0746 × *NRBF2* -0.1411 × *NDUFB4* + 0.0350 × *FXC1* - 0.3655 × *TMEM49* - 0.0525 × *TIMM10* - 0.1292 × *NDUFB2* - 0.1168 × *BCL2L1* - 0.0537 × *BCL2L11*. The PPI network of 27 genes extracted from CISD2Risk was visualized using the Cytoscape software (36) (version 3.9.1, Figure 4D).

Enrichment analysis of CISD2Risk genes in DLBCL

Enrichment analysis of GO enrichment and KEGG pathways was performed based on the CISD2Risk genes. We found enrichment in GO in terms of a few biological processes (BP), such as aerobic respiration, mitochondrial respiratory chain complex I assembly, and apoptotic processes. The main top enrichment cellular component (CC) was the mitochondrion, mitochondrial inner membrane, and mitochondrial outer membrane. And molecular function (MF) enrichment involved protein binding, NADH dehydrogenase (ubiquinone) activity, and BH3 domain binding, as shown in Figure 4E and Supplementary Table S4. The KEGG pathway analysis showed that oxidative phosphorylation, apoptosis, autophagy, and the P53 signaling pathway are involved (Figure 4F, Supplementary Table S5).

Association between CISD2Risk and clinical features in DLBCL

Next, we examined the impact of CISD2Risk in DLBCL. Dividing into two groups by the median CISD2Risk value, we found that a high CISD2Risk group was closely related to the relatively poor prognosis of patients with DLBCL in the GSE117556 dataset that enrolled 844 DLBCL patients as a training dataset ($P < 0.05$, Figure 5A), and 1058 DLBCL patients in the GSE181063 dataset (Validation dataset) that excluded patients with OS times of less than one month ($P < 0.05$, Figure 5E). Sha et al. (21) had defined the molecular high-grade (MHG) subtype of patients with DLBCL that identifies an activated aggressiveness and a poor prognosis (3, 21, 37). In this study, the highest CISD2Risk value in MHG subtype was shown both the GSE117556 and the GSE181063 datasets ($P < 0.05$, Figures 5B, F). Generally, the prognosis of DLBCL patients in ABC subtype is inferior to that of the germinal center B cell like (GCB) subtype (38, 39), the CISD2Risk value in ABC subtype DLBCL was higher than GCB subtype DLBCL ($P < 0.05$, Figures 5B, F). Similarly, high CISD2Risk patients in ABC, GCB, and MHG DLBCL cases revealed an unfavorable prognosis, compared to low CISD2Risk patients (Supplementary Figures S4A–C). We had found that a higher CISD2Risk value in DLBCL patients with raised lactate dehydrogenase (LDH) (greater than 245 U/L) than patients with normal LDH ($P < 0.05$, Figures 5C, G). As previously described (40), the IPI score was divided into high and low IPI groups with a value of two as the cut-off, DLBCL patients with high IPI exhibited a significantly higher CISD2Risk value ($P < 0.05$, Figures 5D, H), and CISD2Risk valu play a good prognostic role of DLBCL patients both IPI >= 2 and IPI < 2 group (Supplementary Figures S4D, E). The clinical effectiveness of treatment for DLBCL is often divided into four categories: complete response (CR), partial response (PR), stable disease (SD), and progressive disease (PD), DLBCL patients achieved PD exhibited higher CISD2Risk value than DLBCL patients achieved CR or PR ($P < 0.05$, Figure 5I), we also set patients achieved CR and PR as clinical effectiveness and the others considered as clinical ineffectiveness (41), the result was demonstrated that the DLBCL patients achieved clinical effectiveness manifested lower CISD2Risk value than that achieved clincial ineffectiveness ($P < 0.05$, Figure 5J). On the other part, DLBCL cases with low CISD2Risk value were often obtained a curative treatment ($P < 0.05$, Figures 5K). Several studies revealed the poor prognosis of MYC and BCL2 and/or BCL6 overexpression in DLBCL, known as double-expressor DLBCL (21, 42). We also reported the overexpression of MYC and BCL2 in DLBCL cases were possiblely associated with CISD2Risk value, and the double-expressor DLBCL exhibited the high CISD2Risk value ($P < 0.05$, Figure 5L). These evidences indicated CISD2Risk value was associated with adverse clinical outcomes in DLBCL patients. Subsequencely, we investigated the correlation among included genes in CISD2Risk both the training and validation datasets (Figures 5M, N), the results demonstrated that the correlations were similar, indicating that CISD2Risk had relative stability. In addition, CISD2 is related to aging, we divided into two groups based on age, neither greater nor less than 60 years, there was no difference between CISD2 expression and age (Supplementary Figures S5A–D). And a high CISD2Risk group was closely related to the relatively poor prognosis of DLBCL patients with different age group (Supplementary Figures S5E–H). These results suggested that the prognosis of CISD2Risk was not affected by different ages.

Relationship between the CISD2Risk and immune infiltration in DLBCL

The tumor immune microenvironment significantly affects the therapeutic effect and prognosis of multiple tumor (43, 44). We introduced the ESTIMATE algorithm to infer the fraction of

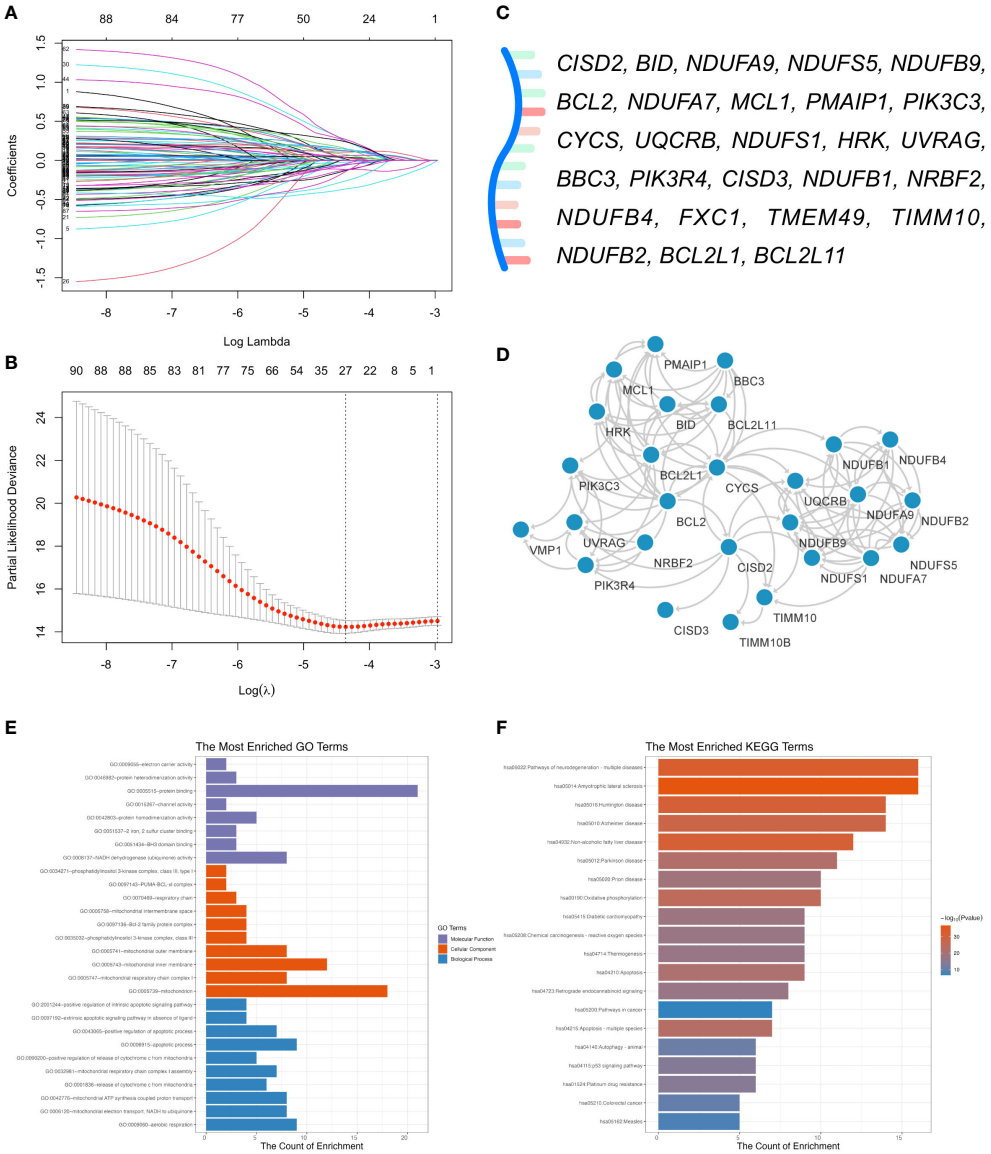

FIGURE 4
Development of the CISD2 risk model (CISD2Risk). **(A)** The LASSO Cox regression profiles of the CISD2Risk. **(B)** The 27 genes selected using LASSO Cox regression analysis, the two dotted vertical lines were drawn at the optimal scores by lamba.minimum criteria and lamba.1se. **(C)** There were 27 genes enrolled: *CISD2, BID, NDUFA9, NDUFS5, NDUFB9, BCL2, NDUFA7, MCL1, PMAIP1, PIK3C3, CYCS, UQCRB, NDUFS1, HRK, UVRAG, BBC3, PIK3R4, CISD3, NDUFB1, NRBF2, NDUFB4, FXC1, TMEM49, TIMM10, NDUFB2, BCL2L1,* and *BCL2L11*. **(D)** The PPI network of 27 genes enrolled in DLBCL patients visualized by the Cytoscape software (version 3.9.1). **(E)** GO enrichment analysis of 27 genes enrolled. **(F)** KEGG pathway analysis of 27 genes enrolled. DLBCL, Diffuse large B-cell lymphoma; GO, Gene Ontology; GSE, Gene Expression Omnibus Series; KEGG, Kyoto Encyclopedia of Genes and Genomes; LASSO, least absolute shrinkage and selection operator; PPI, protein-protein interaction; STRING, Search Tool for the Retrieval of Interacting Genes/Proteins.

stromal and immune cells in tumour samples based on single sample gene set enrichment analysis (ssGSEA). A higher stromal ($P < 0.05$, Figures 6A, D) or immune scores ($P < 0.05$, Figures 6B, E) suggested greater density of stromal or immune cells in the tumour immune microenvironment of DLBCL patients with low CISD2Risk value the ESTIMATE scores that represent the sum of the stromal or immune scores, which can infer tumour purity associated with poor prognosis (29, 45), were negatively correlated with CISD2Risk value (46, 47) ($P < 0.05$, Figures 6C, F). The CIBERSORT algorithm (30) was used to estimate the distribution and proportion of 22 immune cell types in DLBCL. The gene expression profiles of the GSE117556 and GSE181063 datasets were inputted into CIBERSORTx (http://cibersortx.stanford.edu). As demonstrated in Figures 6G, H, both the GSE117556 and GSE181063 datasets, there were a represented abundance of CD8 T cells, CD4 naïve T cells, macrophages M0, macrophages M1, neutrophils, and activated mast cells had significantly negative correlations with CISD2Risk values ($P < 0.05$). On the contrary, three cells that include naïve B cells, memory B cells, and plasma cells had significantly positive correlations with CISD2Risk value ($P < 0.05$). MCP-counter algorithm (31) aims to estimate immune infiltration by fibroblasts, endothelial cells, and eight immune cells

10.3389/fimmu.2023.1277695

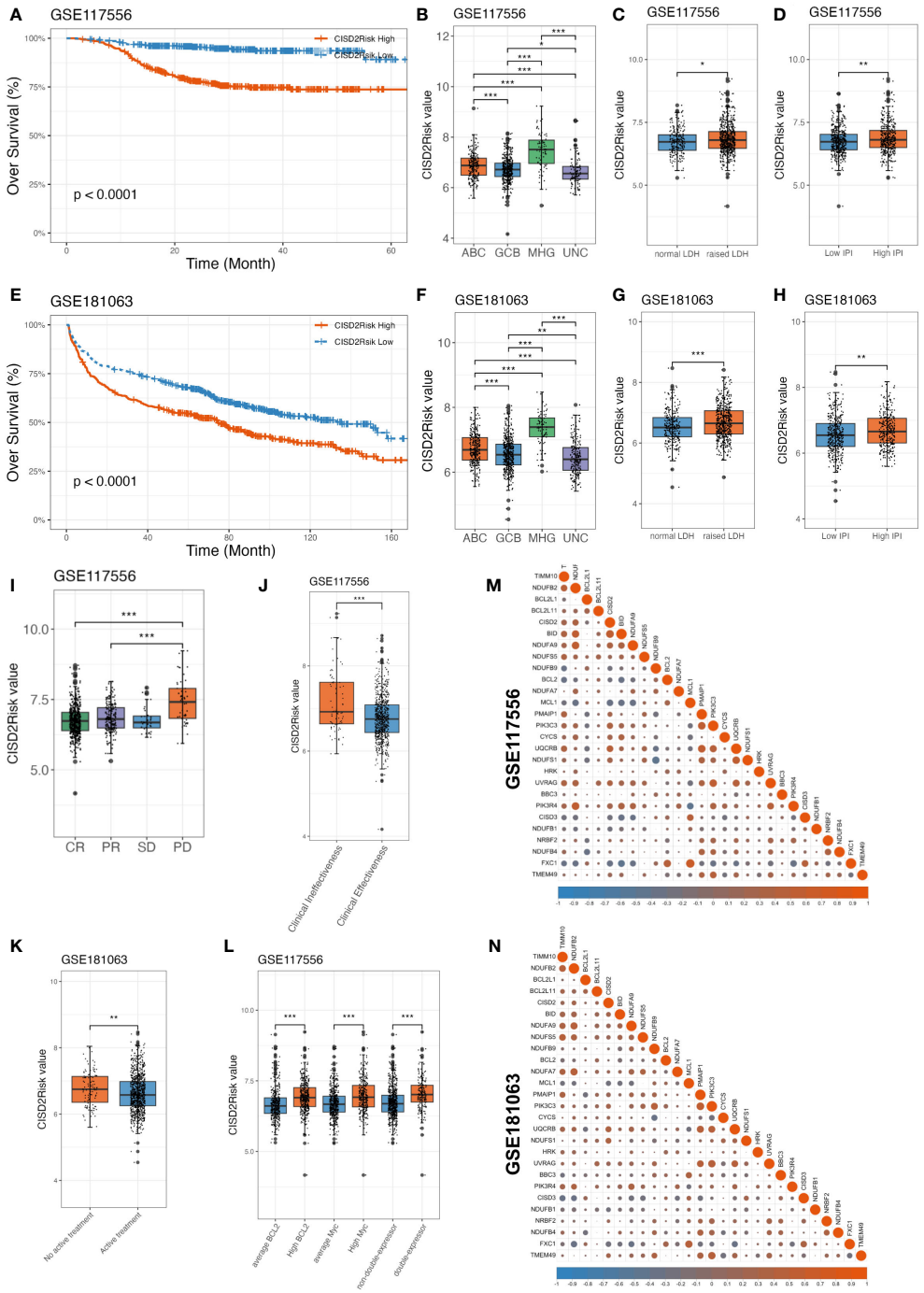

FIGURE 5
Association between CISD2 expression and clinical features in DLBCL. CISD2Risk was divided into high- and low- groups according to the median based on GSE117556 (training dataset) and GSE181063 (validation dataset). **(A, E)** The KM curves showed that high CISD2Risk group had poor OS. **(B, F)** Comparison among CISD2Risk values of different molecular subgroup. **(C, G)** Comparison between CISD2Risk values of normal and raised LDH. **(D, H)** Comparison between CISD2Risk values of low and high IPI. **(I, J)** Comparison between CISD2Risk values of clinical effectiveness and clinical ineffectiveness based on GSE117556 dataset. **(K)** Comparison between CISD2Risk values of inactive treatment and active treatment DLBCL cases based on GSE181063 dataset. **(L)** Comparison among CISD2Risk values of MYC, BCL2, and double-expressor based on GSE117556 dataset. **(M, N)**. The correlation analysis of 27 genes enrolled by CISD2Risk. CR, complete response; DLBCL, Diffuse large B-cell lymphoma; GSE, Gene Expression Omnibus Series; IPI, international prognostic index; KM, Kaplan–Meier; LDH, lactate dehydrogenase; OS, over survival; PD, progressive disease; PR, partial response; SD, stable disease. *** P < 0.001, ** P < 0.01, * P < 0.05.

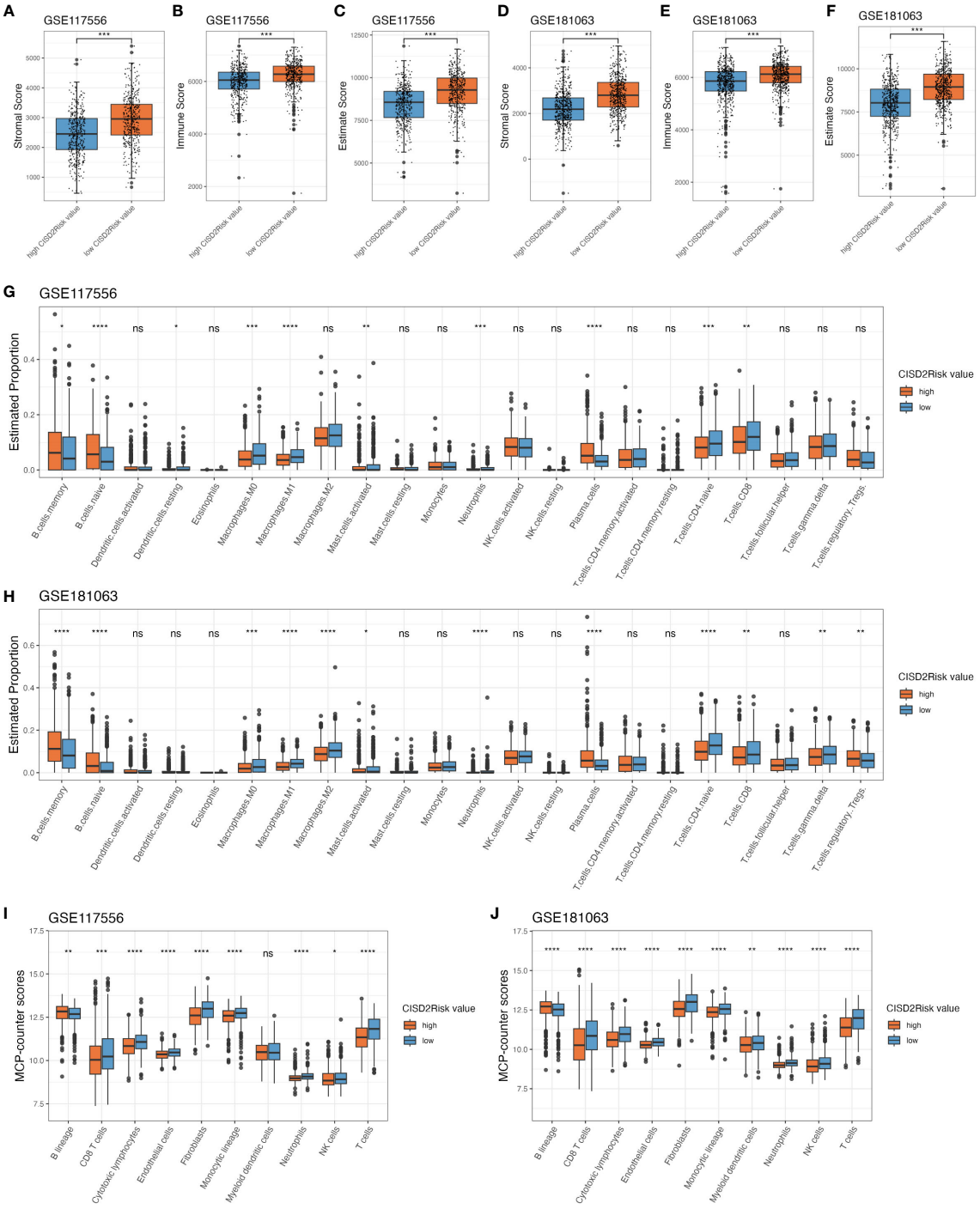

FIGURE 6
The immune infiltration associations about CISD2Risk in DLBCL based on GSE117556 and GSE1810163 datasets. First, estimate algorithm used to qualitify the tumour microenvironment. **(A, D)** Comparison between the stromal scores of high and low CISD2Risk value, **(B, E)** Comparison between the immune scores of high and low CISD2Risk value, **(C, F)** Comparison between the estimate scores of high and low CISD2Risk value. Second, CIBERSORT algorithm used to evaluate 22 types of immune cell infiltration, **(G, H)** Comparison between the estimate proportion in 22 types of immune cell of high and low CISD2Risk value. Third, MCP-counter algorithm used to analyse 8 types of immune cell, **(I, J)** Comparison between the MCP-counter scores in 8 types of immune cell of high and low CISD2Risk value. CIBERSORT, cell type identification by estimating relative subsets of RNA transcripts; DLBCL, Diffuse large B-cell lymphoma; MCP-counter, Microenvironment Cell Populations-counter. **** P < 0.0001, *** P < 0.001, ** P < 0.01, * P < 0.05, ns, not signifcance.

using transcriptomic data. We found that the high CISD2Risk value was associated with significantly decreased abundances of six immune cells, inclinding CD8 T cells, T cells, Natural killer (NK) cells, cytotoxic lymphocytes, neutrophils, and monocytic lineage, while fibroblasts and endothelial cells showed the similar trend both the training and validation datasets. On the other hand, compared with the low CISD2Risk value, the high CISD2Risk exhibited increased proportion of B lineage, as shown in Figures 6I, J.

Prognostic implication of CISD2Risk in DLBCL

IPI scoring is a widely used tool to assess the prognosis and predict outcomes for patients with DLBLC, the factors considered in the IPI include ages, clinical stage, elevated serum LDH, Eastern Cooperative Oncology Group Performance Status (ECOG PS), and extranodal sites of disease. To investigate the prognostic values of CISD2Risk in DLBCL, we employed these variables included gender, cell of original (COO), molecular subgroup (21, 22), IPI, double-expressor and status of CISD2Risk divided into high and low levels by median of CISD2Risk value, into univariate and multivariate Cox regression analysis. As shown in Figure 7, the results showed that the status of CISD2Risk could be an independent prognostic factor for OS both the GSE117556 (Figure 7A) and the GSE181063 (Supplementary Figure S6). A forrest plot exploring multiple clinical features for PFS in the GSE117556 dataset was provided, CISD2Risk was also an independent prognostic indicator for PFS (Figure 7B).

Construction and validation of the nomogram in DLBCL

We built a prognostic nomogram in DLBCL to anticipate the 1-, 3-, and 5-years OS based on prognostic factors such as age, gender, COO, molecular subgroup (21, 22), IPI, ECOG PS, clinical stage, LDH, extranodal, double-expressor and status of CISD2Risk in the GSE117556 dataset (Figure 8A), that the higher total points in the nomogram indicated worse survival. And the C-index of the nomogram was 0.746 (95% CI: 0.743-0.749). While a survival prediction nomogram in the validation dataset was constructed (Supplementary Figure S7A) and C-index was 0.732 (95% CI: 0.730-0.734). The calibration curves (The training dataset showed at Figure 8B, The valication dataset showed at Supplementary Figure S4B) were visualized and indicated acceptable agreement between the predicted survival rate and the actual survival rate, suggesting that these nomograms we constructed might favorably predict the prognosis of patients with DLBCL. The AUC of time-dependent ROC curves (Figures 8C, D, and Supplementary Figures S4C–E) were presented in Supplementary Table S6. These data suggested that the prognostic nomogram constructed by these clinical features and CISD2Risk had a good prediction ability on the prognosis of DLBCL patients.

Discussion

At present, emerging evidence demonstrates that the pathogenesis of DLBCL is complicated and consistent with aberrant gene expression that affects cell growth (48), invasiveness (49), angiogenesis (50), and apoptosis (51). It is reasonable for us to believe that CISD2 may play a significant role in DLBCL. Using public databases (17–22), we found upregulated CISD2 as an appropriate diagnostic factors and a unfavorable prognostic indicator in DLBCL. Recent studies demonstrated that a clinical risk model included multiple genes is helpful to better implement the eligible diagnostic and the favorably prognostic criteria in DLBCL patients (52–55). Here, we developed a CISD2-related risk model (CISD2Risk) based on CISD2 related genes using LASSO Cox regression analysis in the GSE117556 dataset, and performed external validation (GSE181063 dataset) for its performance. Our results showed that CISD2Risk revealed a good ability to predict survival, and was an independent prognostic factor of DLBCL patients.

There are eight genes (BUB1B, CISD2, KLOTHO, PAWR, PPARG, PTEN, SIRT1, and SIRT6) listed as pro-longevity genes in mammals by the Human Aging Genomic Resources (HAGR) (56). Several studies have showed that some pro-longevity genes (such as PTEN, SIRT1, and SIRT6) influenced the occurrence and development, the drug resistance of DLBCL (57–59). However, the biological function of CISD2 in DLBCL is still unclear. Knockout of CISD2 in mice could cause a number of age-related phenotypes in multiple organs and lead to premature aging (6, 7), suggesting that CISD2 might play a critical role in controlling lifespan. Mechanically, CISD2 could regulate Ca^{2+} homeostasis and

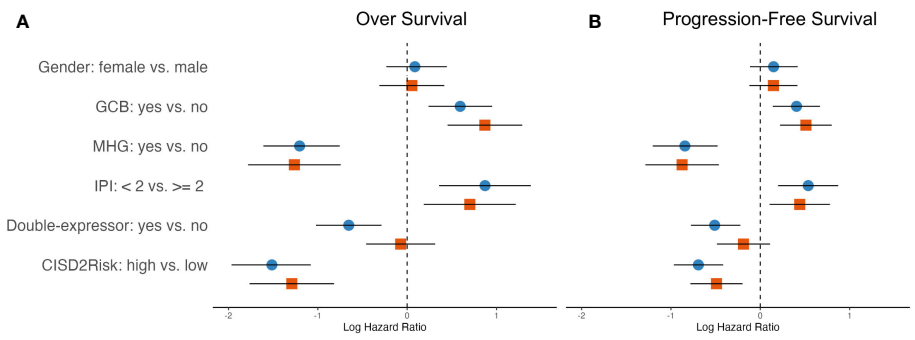

FIGURE 7
The hazard ratios of clinical features integrated into the OS and PFS showed in the forest plots in DLBCL using univariate and multivariate cox regression analysis based on the training dataset, **(A)** left, OS; **(B)** right, PFS; blue and circle, univariate Cox regression analysis; red and square, multivariate Cox regression analysis. OS, over survival; PFS, progression-free survival.

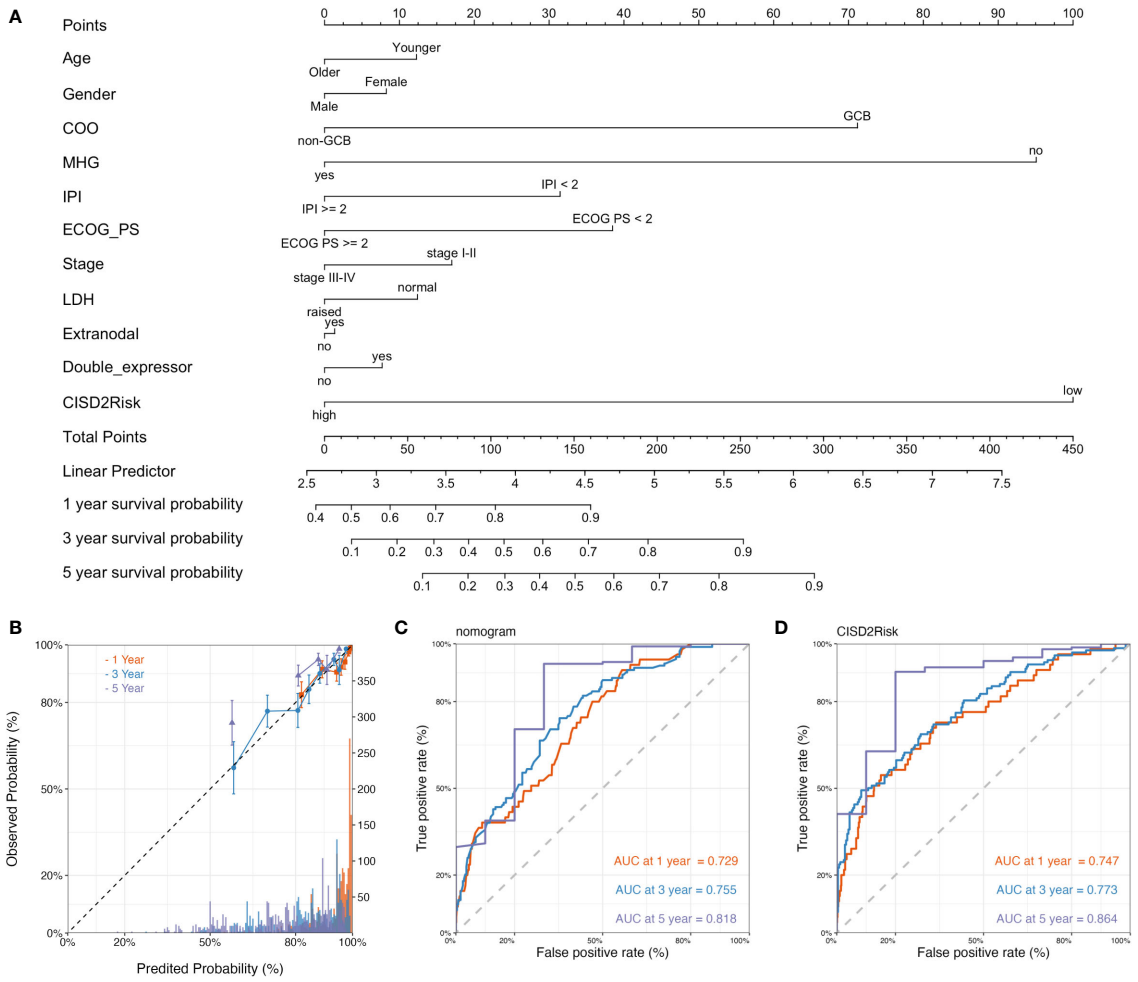

FIGURE 8
The construction and validation of the nomogram. **(A)** The nomogram plot of the GSE117556 dataset showed the prediction of clinical features including age, gender, COO, molecular subgroup, IPI, ECOG PS, clinical stage, LDH, extranodal, double-expressor, CISD2Risk, and 1-year, 3-year, and 5-year survival probability. **(B)** The calibration curve of 1-year, 3-years, and 5-year survival probability of DLBCL patients, The dashed line represented a perfect uniformity between predicted probability and observed probability. The time-dependent ROC curves for nomogram **(C)** and CISD2Risk **(D)** at 1-year, 3-year, and 5-year for DLBCL, respectively. COO, cell of original; DLBCL, Diffuse large B-cell lymphoma; ECOG PS, Eastern Cooperative Oncology Group performance status; GSE, Gene Expression Omnibus Series; IPI, international prognostic index; LDH, lactate dehydrogenase; ROC, receiver operating characteristic.

maintain mitochondrial function (8, 60). Currently, the role of CISD2 in cancers causes more interest. Sun et al. (13) showed that CISD2 expression was negatively correlated with the survival of patients with glioma, and inhibition of CISD2 might activate BECN-1-mediated autophagy to reduce the proliferation of glioma cells. Cervical cancer patients with higher CISD2 expression had shorter OS and were associated with pelvic lymph node metastasis (61). Upregulation of CISD2 in lung adenocarcinoma (ADC) specimens compared with their adjacent normal counterparts was found (33), and was associated with increased antioxidant capacity in response to elevated ROS levels during the formation and progression of lung cancer (33). In this study, we also found that CISD2 was upregulated in DLBCL compared with NCs, and CISD2 expression was negatively associated with survival, indicating that CISD2 may be involved in the pathologic progression of DLBCL. Numerous studies (6–9) indicated that CISD2 regulates age-associated disorders. The expression of CISD2 could be activated at a late-life stage of aged mice pharmaceutically, hesperetin considered as CISD2 activator enhanced CISD2 expression in order to slow down aging and promote longevity (9). It highlights the urgent need to explore the potential therapeutic strategy for cancer and age-associated diseases based on CISD2 manner. In this study, different age in DLBCL did not affect the CISD2 expression ($P > 0.05$), suggesting that CISD2 might play a role in promoting the development of DLBCL. We also assessed the drug sensitivity, AM-5992, Ribavirin, Chelerythrine, KPT-9274, Palbociclib, LEE-011, Hydroxyurea, PX-316, and Nelarabine were potential therapeutic role for DLBCL.

CISD2 is localized on MOM, ER, and mitochondrial-associated ER membrane (MAM) (7, 9), which is closely related to its biological functions. Natasha et al. indicated that CISD2 could be a physical interaction between BCL2 and BECN1 to antagonize

autophagy in response to nutrient stress; the BCL2-CISD2 complex is a requirement for BCL2-mediated depression of ER Ca^{2+} stores (62). It was suggested that CISD2 might be involved in multiple biological processes as an interaction or intermediate. For further investigation of the biological function of CISD2 in DLBCL, we collected 100 CISD2-related genes from STRING and identified 27 genes using LASSO Cox regression analysis. CISD2Risk was developed based on these genes using the GSE117556 datasets. GO and KEGG enrichment analysis of 27 genes revealed that CISD2Risk might be likely to be involved in apoptosis and the P53 signaling pathway and localize on the mitochondrial inner membrane and outer membrane, suggesting that it may participate in mitochondrial apoptosis. Several studies showed that apoptosis proteins such as P53 (63, 64), BCL2 (65–67), and MCL1 (68), directly and indirectly involved in the intrinsic or extrinsic apoptotic pathways in the regulation of pathophysiology and chemotherapy resistance in DLBCL (5, 51, 67, 69).

The efficacy of CISD2Risk was verified from multiple clinical aspects, CISD2Risk showed a good performance associated with clinical factors stratification. MHG is supposed to be an aggressive B-cell lymphoma and show an inferior response to RCHOP treatment (3, 21, 37). In this study, the MHG DLBCL patients exhibited highest CISD2Risk value which indicated a poor prognosis. MHG DLBCL has distinct molecular features with concurrent activation of MYC and BCL2 (21, 42). DLBCL patients with double-expressor that defined by the coexpression of MYC and BCL-2 have a poor prognosis after standard chemoimmunotherapy (21, 42). DLBCL patients with double-expressor has a higher CISD2Risk value than that with non-double-expressor in this study. Also, DLBCL patients with high CISD2Risk value was associated with raised LDH or high IPI level, which might be considered as a predictor of clinical outcomes traditionally (3, 21, 70). Meanwhile, DLBCL patients who were responsed to clinical treatment showed a relatively lower CISD2Risk value. These evidences revealed that a high CISD2Risk value might lead to poor clinical outcomes.

The tumor microenvironment has been considered an important biological aspect of development and occurrence in DLBCL (71–73), which includes multiple immunemodulating mechanisms (73). The stromal cells are well known to be recruited by tumor cells and regulate tumor development, and the immune cells respond to tumor cells by causing inflammatory responses; all of them are involved in the development and occurrence of tumors through immunoregulatory mechanisms (73, 74). We explored the stromal and immune cells in DLBCL using the ESTIMATE algorithm. The high CISD2Risk values were negatively associated with stromal scores, immune scores, and ESTIMATE scores between the training and validation datasets, suggesting poor prognosis and high tumor purity in DLBCL.

Hence, understanding the types and roles of immune cells related to CISD2Risk is crucial to targeting and improving the precise treatment of DLBCL, the CIBERSORT algorithm (30) can be used to accurately estimate the immune composition of the 22 closely related types of immune cells. We found that CISD2Risk value were inversely associated with the infiltration levels of activated mast cells, neutrophils, CD8 T cells, CD4 naïve T cells, macrophages M0, and M1, as well as a positively associated with a high proportion of B cells in DLBCL. Traditionally, Macrophages that acting as sentinels of the tumor microenvironment are extensively involved in the regulation of immune response and homeostasis (75, 76). Macrophages M0 can be polarized into either M1 or M2, activated M1 macrophages produces various pro-inflammatory cytokines to cause tumor damage (76), while M2 decrease inflammation and encourage tissue repair. A high numbers M0, M1 macrophages correlated with better survival in DLBCL (75, 77), and these data are consistent with our data. A lot of studies reported the lower amount of CD4 T cells and CD8 T cells in the lymphoma microenvironment correlated with poor survival (73, 77–79). CD4 naïve T cell is considered essential to guarantee immune competence throughout life, can be activated after interaction with antigen Major Histocompatibility Complex (MHC) and differentiated into memory, effector, and suppressor cells (71, 73). It believed that activated CD4 memory T cell was associated with better survival and overcame some of the chemotherapy resistance (80, 81). CD8 T cells as a key players might have defective cytotoxicity in the process of targeting cancer cells (73, 79). CD8 T cells infiltrating DLBCL that been correlated with better prognosis are highly activated and lack an exhausted phenotype (82). B cells as immunomodulatory cells, positive mediators, and antigen-presenting cells play a role in modulating the immune response to cancer (83). We found that DLBCL with high CISD2Risk value exhibited increased B cell infiltrations in accord with several studies (47, 77, 84, 85). B cells are part of the adaptive immune system and can produce antibodies against cancer cells. There are some studies demonstrated a robust B cell response may indicate an active immune reaction against the tumor. The increased B cells within tumour microenvironment (TME) may reflect an attempt by the immune system to mount an anti-tumor response. On the other hand, inflammatory signals which may be activated by TME of DLBCL can attract immune cells, including B cells, and these immune cells may participate in a proinflammatory response, which can sometimes promote tumor growth and aggressiveness (71, 81, 86). It had been reported that DLBCL recruited T cells and monocytes via CCL5 to support B cells survival and proliferation (87). According to COO, DLBCL was pathologically divided into ABC, GCB, and unclassifiable (UNC) subtypes, the aberrant memory B cells (MBs) might be the true COO for ABC subtype DLBCL (88). The correlation between CISD2Risk and activated B cells may be explained by the pathological features of DLBCL (47, 88). Next, the MCP-counter algorithm (31) can be used to analyze gene expression profiles to estimate the expression levels of multiple tumor-infiltrating lymphocytes. The high CISD2Risk was associated with significantly decreased abundances of NK cells. NK cells recognize and kill cancer cells via releasing cytolytic granules. When DLBCL patients were treated with RCHOP, low amount of NK cell count was associated with shorter PFS and decreased OS compared to patients with high amount of NK cells (89, 90), these data are consistent with our data. These findings suggested CISD2Risk might be used to estimate the anti-tumor immunity of

DLBCL patients, but the immune regulation of CISD2Risk needs further investigation.

Additionally, CISD2Risk has effectively and independently determined the prognosis of patients with DLBCL through univariate and multivariate Cox regression. Hence, a novel nomogram was developed that exhibited superior discrimination ability for the prediction of prognosis in DLBCL patients and could be used to guide routine OS for DLBCL patients. Time-dependent ROC curve analysis of the CISD2Risk value revealed a relatively accurate ability to predict OS. Recently, several studies showed some clinical prediction model for DLBCL. A ferroptosis-based risk scoring model of 16 genes for patients with DLBCL was constructed and had good efficacy in predicting survival compared to clinical characteristics (52), similar to Chen et al.'s study (91). Likewise, an immune score model including 22 genes could predict the survival of DLBCL patients and be more accurate than the IPI and Revised International Prognostic Index (R-IPI) (77). 15 differentially expressed genes (DEGs) among metabolic subtypes were used to build a predictive model that could evaluate survival and drug sensitivity in DLBCL patients (78). Different from other risk models (52, 77, 78, 91), we built a risk model based on CISD2 and its related genes, which also has excellent prediction ability in line with those.

Some limitations existed in this study. First, the biological function of CISD2 need to be explored using *in vitro* and *in vivo* experiments. Specifically, the practical effect of drugs that selected should be assessed. Second, both the construction and validation of CISD2Risk were based on retrospective public data; the reliability and applicability of CISD2Risk need to be verified by some clinical experiments. Third, GO and KEGG enrichment analysis of 27 genes revealed that CISD2Risk might be involved in apoptosis, the P53 signaling pathway, and so on; however, the underlying mechanism of these genes needs to be explored in the future.

Conclusion

In conclusion, our study indicated that upregulated CISD2 was correlated with a poor prognosis. Meanwhile, we developed a CISD2Risk for DLBCL patients that was validated in an independent dataset. CISD2Risk showed better ability of clinical prediction to prognosis. Additionally, CISD2Risk had a capacity for estimation for anti-tumor immunity in DLBCL, suggesting CISD2Risk could be a predictor for clinical prognosis as well as a clinical evaluator for immunotherapy.

Data availability statement

The datasets presented in this study can be found in online repositories. The names of the repository/repositories and accession number(s) can be found in the article/Supplementary Material.

Ethics statement

The studies involving human participants were reviewed and approved by the ethics committee of Quanzhou First Hospital Affiliated to Fujian Medical University (No. [2023]K096).

Author contributions

CZ: Funding acquisition, Methodology, Visualization, Writing – original draft. QL: Data curation, Investigation, Visualization, Writing – original draft. CL: Writing – review & editing. YQ: Investigation, Writing – original draft. JC: Investigation, Writing – original draft. XZ: Writing – review & editing.

Funding

The author(s) declare financial support was received for the research, authorship, and/or publication of this article. This study was supported by the General Program of the Natural Science Foundation of Fujian Province, China (No. 2022J011435).

Acknowledgments

We thank all the participants who contributed to our study.

Conflict of interest

The authors declare that the research was conducted in the absence of any commercial or financial relationships that could be construed as a potential conflict of interest.

Publisher's note

Supplementary material

The Supplementary Material for this article can be found online at: https://www.frontiersin.org/articles/10.3389/fimmu.2023.1277695/full#supplementary-material

References

1. Swerdlow SH, Campo E, Pileri SA, Harris NL, Stein H, Siebert R, et al. The 2016 revision of the World Health Organization classification of lymphoid neoplasms. *Blood* (2016) 127:2375–90. doi: 10.1182/blood-2016-01-643569

2. Sehn LH, Salles G. Diffuse large B-cell lymphoma. *N Engl J Med* (2021) 384:842–58. doi: 10.1056/NEJMra2027612

3. Sarkozy C, Sehn LH. Management of relapsed/refractory DLBCL. *Best Pract Res Clin Haematol* (2018) 31:209–16. doi: 10.1016/j.beha.2018.07.014

4. Wight JC, Chong G, Grigg AP, Hawkes EA. Prognostication of diffuse large B-cell lymphoma in the molecular era: Moving beyond the IPI. *Blood Rev* (2018) 32:400–15. doi: 10.1016/j.blre.2018.03.005

5. Miao Y, Medeiros LJ, Li Y, Li J, Young KH. Genetic alterations and their clinical implications in DLBCL. *Nat Rev Clin Oncol* (2019) 16:634–52. doi: 10.1038/s41571-019-0225-1

6. Shen Z-Q, Huang Y-L, Teng Y-C, Wang T-W, Kao C-H, Yeh C-H, et al. CISD2 maintains cellular homeostasis. *BBA Mol Cell Res* (2021) 1868:118954. doi: 10.1016/j.bbamcr.2021.118954

7. Liao H-Y, Liao B, Zhang H-H. CISD2 plays a role in age-related diseases and cancer. *BioMed Pharmacother* (2021) 138:111472. doi: 10.1016/j.biopha.2021.111472

8. Wang C-H, Kao C-H, Chen Y-F, Wei Y-H, Tsai T-F. Cisd2 mediates lifespan: Is there an interconnection among Ca^{2+} homeostasis, autophagy, and lifespan? *Free Radic Res* (2014) 48:1109–14. doi: 10.3109/10715762.2014.936431

9. Yeh C-H, Shen Z-Q, Lin C-C, Lu C-K, Tsai T-F. Rejuvenation: turning back time by enhancing CISD2. *Int J Mol Sci* (2022) 23:14014. doi: 10.3390/ijms232214014

10. Holt SH, Darash-Yahana M, Sohn YS, Song L, Karmi O, Tamir S, et al. Activation of apoptosis in NAF-1-deficient human epithelial breast cancer cells. *J Cell Sci* (2016) 129:155–65. doi: 10.1242/jcs.178293

11. Shao F, Li Y, Hu W, Yu J, Wu H, Ying K, et al. Downregulation of CISD2 has prognostic value in non-small cell lung cancer and inhibits the tumorigenesis by inducing mitochondrial dysfunction. *Front Oncol* (2021) 10:595524. doi: 10.3389/fonc.2020.595524

12. Wang J, Hu J, Wang M, Yuan H, Xing Y, Zhou X, et al. CISD2 promotes proliferation of colorectal cancer cells by inhibiting autophagy in a Wnt/β-catenin-signaling-dependent pathway. *Biochem Genet* (2022) 61:615–627. doi: 10.1007/s10528-022-10267-8

13. Sun A-G, Meng F-G, Wang M-G. CISD2 promotes the proliferation of glioma cells via suppressing beclin-1-mediated autophagy and is targeted by microRNA-449a. *Mol Med Rep* (2017) 16:7939–48. doi: 10.3892/mmr.2017.7642

14. Zhang F, Cai H-B, Liu H-Z, Gao S, Wang B, Hu Y-C, et al. High expression of CISD2 in relation to adverse outcome and abnormal immune cell infiltration in glioma. *Dis Markers* (2022) 2022:8133505. doi: 10.1155/2022/8133505

15. Li B, Wei S, Yang L, Peng X, Ma Y, Wu B, et al. CISD2 promotes resistance to sorafenib-induced ferroptosis by regulating autophagy in hepatocellular carcinoma. *Front Oncol* (2021) 11:657723. doi: 10.3389/fonc.2021.657723

16. Kim EH, Shin D, Lee J, Jung AR, Roh J-L. CISD2 inhibition overcomes resistance to sulfasalazine-induced ferroptotic cell death in head and neck cancer. *Cancer Lett* (2018) 432:180–90. doi: 10.1016/j.canlet.2018.06.018

17. Azzaoui I, Uhel F, Rossille D, Pangault C, Dulong J, Le Priol J, et al. T-cell defect in diffuse large B-cell lymphomas involves expansion of myeloid-derived suppressor cells. *Blood* (2016) 128:1081–92. doi: 10.1182/blood-2015-08-662783

18. Frei E, Visco C, Xu-Monette ZY, Dirnhofer S, Dybkær K, Orazi A, et al. Addition of rituximab to chemotherapy overcomes the negative prognostic impact of cyclin E expression in diffuse large B-cell lymphoma. *J Clin Pathol* (2013) 66:956–61. doi: 10.1136/jclinpath-2013-201619

19. Barrans SL, Crouch S, Care MA, Worrillow L, Smith A, Patmore R, et al. Whole genome expression profiling based on paraffin embedded tissue can be used to classify diffuse large B-cell lymphoma and predict clinical outcome. *Br J Haematol* (2012) 159:441–53. doi: 10.1111/bjh.12045

20. Kuo H-P, Ezell SA, Schweighofer KJ, Cheung LWK, Hsieh S, Apatira M, et al. Combination of ibrutinib and ABT-199 in diffuse large B-cell lymphoma and follicular lymphoma. *Mol Cancer Ther* (2017) 16:1246–56. doi: 10.1158/1535-7163.MCT-16-0555

21. Sha C, Barrans S, Cucco F, Bentley MA, Care MA, Cummin T, et al. Molecular high-grade B-cell lymphoma: defining a poor-risk group that requires different approaches to therapy. *J Clin Oncol* (2019) 37:202–12. doi: 10.1200/JCO.18.01314

22. Painter D, Barrans S, Lacy S, Smith A, Crouch S, Westhead D, et al. Cell-of-origin in diffuse large B-cell lymphoma: Findings from the UK's population-based Haematological Malignancy Research Network. *Br J Haematol* (2019) 185:781–4. doi: 10.1111/bjh.15619

23. Reinhold WC, Sunshine M, Liu H, Varma S, Kohn KW, Morris J, et al. CellMiner: A web-based suite of genomic and pharmacologic tools to explore transcript and drug patterns in the NCI-60 cell line set. *Cancer Res* (2012) 72:3499–511. doi: 10.1158/0008-5472.CAN-12-1370

24. Ritchie ME, Phipson B, Wu D, Hu Y, Law CW, Shi W, et al. Limma powers differential expression analyses for RNA-sequencing and microarray studies. *Nucleic Acids Res* (2015) 43:e47. doi: 10.1093/nar/gkv007

25. Friedman J, Hastie T, Tibshirani R. Regularization paths for generalized linear models via coordinate descent. *J Stat Soft* (2010) 33:1–22. doi: 10.18637/jss.v033.i01

26. Sherman BT, Hao M, Qiu J, Jiao X, Baseler MW, Lane HC, et al. DAVID: A web server for functional enrichment analysis and functional annotation of gene lists (2021 update). *Nucleic Acids Res* (2022) 50:W216–21. doi: 10.1093/nar/gkac194

27. Gene Ontology Consortium. Gene ontology consortium: going forward. *Nucleic Acids Res* (2015) 43:D1049–1056. doi: 10.1093/nar/gku1179

28. Kanehisa M, Furumichi M, Sato Y, Kawashima M, Ishiguro-Watanabe M. KEGG for taxonomy-based analysis of pathways and genomes. *Nucleic Acids Res* (2023) 51: D587–92. doi: 10.1093/nar/gkac963

29. Yoshihara K, Shahmoradgoli M, Martínez E, Vegesna R, Kim H, Torres-Garcia W, et al. Inferring tumour purity and stromal and immune cell admixture from expression data. *Nat Commun* (2013) 4:2612. doi: 10.1038/ncomms3612

30. Newman AM, Steen CB, Liu CL, Gentles AJ, Chaudhuri AA, Scherer F, et al. Determining cell type abundance and expression from bulk tissues with digital cytometry. *Nat Biotechnol* (2019) 37:773–82. doi: 10.1038/s41587-019-0114-2

31. Becht E, Giraldo NA, Lacroix L, Buttard B, Elarouci N, Petitprez F, et al. Estimating the population abundance of tissue-infiltrating immune and stromal cell populations using gene expression. *Genome Biol* (2016) 17:218. doi: 10.1186/s13059-016-1070-5

32. Blanche P, Dartigues J-F, Jacqmin-Gadda H. Estimating and comparing time-dependent areas under receiver operating characteristic curves for censored event times with competing risks. *Stat Med* (2013) 32:5381–97. doi: 10.1002/sim.5958

33. Li S-M, Chen C-H, Chen Y-W, Yen Y-C, Fang W-T, Tsai F-Y, et al. Upregulation of CISD2 augments ROS homeostasis and contributes to tumorigenesis and poor prognosis of lung adenocarcinoma. *Sci Rep* (2017) 7:11893. doi: 10.1038/s41598-017-12131-x

34. Sohn Y-S, Tamir S, Song L, Michaeli D, Matouk I, Conlan AR, et al. NAF-1 and mitoNEET are central to human breast cancer proliferation by maintaining mitochondrial homeostasis and promoting tumor growth. *Proc Natl Acad Sci U.S.A.* (2013) 110:14676–81. doi: 10.1073/pnas.1313198110

35. Chen B, Shen S, Wu J, Hua Y, Kuang M, Li S, et al. CISD2 associated with proliferation indicates negative prognosis in patients with hepatocellular carcinoma. *Int J Clin Exp Pathol* (2015) 8:13725–38.

36. Shannon P, Markiel A, Ozier O, Baliga NS, Wang JT, Ramage D, et al. Cytoscape: A software environment for integrated models of biomolecular interaction networks. *Genome Res* (2003) 13:2498–504. doi: 10.1101/gr.1239303

37. Xu-Monette ZY, Zhang H, Zhu F, Tzankov A, Bhagat G, Visco C, et al. A refined cell-of-origin classifier with targeted NGS and artificial intelligence shows robust predictive value in DLBCL. *Blood Adv* (2020) 4:3391–404. doi: 10.1182/bloodadvances.2020001949

38. Hunter E, McCord R, Ramadass AS, Green J, Westra JW, Mundt K, et al. Comparative molecular cell-of-origin classification of diffuse large B-cell lymphoma based on liquid and tissue biopsies. *Trans Med Commun* (2020) 5:5. doi: 10.1186/s41231-020-00054-1

39. Li H-B, Wang D, Zhang Y, Shen D, Che Y-Q. IGFBP3 enhances treatment outcome and predicts favorable prognosis in ABC-DLBCL. *J Oncol* (2023) 2023:1388041. doi: 10.1155/2023/1388041

40. Choi YW, Ahn MS, Choi J-H, Lee HW, Kang SY, Jeong SH, et al. High expression of Bcl-2 predicts poor outcome in diffuse large B-cell lymphoma patients with low international prognostic index receiving R-CHOP chemotherapy. *Int J Hematol* (2016) 103:210–8. doi: 10.1007/s12185-015-1911-0

41. Crump M, Neelapu SS, Farooq U, Van Den Neste E, Kuruvilla J, Westin J, et al. Outcomes in refractory diffuse large B-cell lymphoma: Results from the international SCHOLAR-1 study. *Blood* (2017) 130:1800–8. doi: 10.1182/blood-2017-03-769620

42. Hashmi AA, Iftikhar SN, Nargus G, Ahmed O, Asghar IA, Shirazi UA, et al. Double-expressor phenotype (BCL-2/c-MYC co-expression) of diffuse large B-cell lymphoma and its clinicopathological correlation. *Cureus* (2021) 13:e13155. doi: 10.7759/cureus.13155

43. Luo C, Nie H, Yu L. Identification of aging-related genes associated with prognostic value and immune microenvironment characteristics in diffuse large B-cell lymphoma. *Oxid Med Cell Longev* (2022) 2022:1–30. doi: 10.1155/2022/3334522

44. Wu J, Li L, Zhang H, Zhao Y, Zhang H, Wu S, et al. A risk model developed based on tumor microenvironment predicts overall survival and associates with tumor immunity of patients with lung adenocarcinoma. *Oncogene* (2021) 40:4413–24. doi: 10.1038/s41388-021-01853-y

45. Wu Z, Guan Q, Han X, Liu X, Li L, Qiu L, et al. A novel prognostic signature based on immune-related genes of diffuse large B-cell lymphoma. *Aging* (2021) 13:22947–62. doi: 10.18632/aging.203587

46. Wang L, Yuan W, Li L, Shen Z, Geng Q, Zheng Y, et al. Immunogenomic-based analysis of hierarchical clustering of diffuse large cell lymphoma. *J Immunol Res* (2022) 2022:9544827. doi: 10.1155/2022/9544827

47. Cui Y, Leng C. A glycolysis-related gene signatures in diffuse large B-Cell lymphoma predicts prognosis and tumor immune microenvironment. *Front Cell Dev Biol* (2023) 11:1070777. doi: 10.3389/fcell.2023.1070777

48. Stirm K, Leary P, Bertram K, Núñez NG, Wüst D, Boudesco C, et al. Tumor cell-derived IL-10 promotes cell-autonomous growth and immune escape in diffuse large B-cell lymphoma. *Oncoimmunology* (2021) 10:2003533. doi: 10.1080/2162402X.2021.2003533

49. Xing X, Wang X, Liu M, Guo Q, Wang H. Ras interacting protein 1 facilitated proliferation and invasion of diffuse large B-cell lymphoma cells. *Cancer Biol Ther* (2023) 24:2193114. doi: 10.1080/15384047.2023.2193114

50. Liu Y, Wang J, Shen X, Li L, Zhang N, Wang X, et al. A novel angiogenesis-related scoring model predicts prognosis risk and treatment responsiveness in diffuse large B-cell lymphoma. *Clin Exp Med* (2023) 23:3781–3797. doi: 10.1007/s10238-023-01127-9

51. Leveille E, Johnson NA. Genetic events inhibiting apoptosis in diffuse large B cell lymphoma. *Cancers* (2021) 13:2167. doi: 10.3390/cancers13092167

52. Xiong D, Li M, Zeng C. Construction and validation of a risk scoring model for diffuse large B-cell lymphoma based on ferroptosis-related genes and its association with immune infiltration. *Transl Oncol* (2022) 16:101314. doi: 10.1016/j.tranon.2021.101314

53. Wright GW, Huang DW, Phelan JD, Coulibaly ZA, Roulland S, Young RM, et al. A probabilistic classification tool for genetic subtypes of diffuse large B cell lymphoma with therapeutic implications. *Cancer Cell* (2020) 37:551–568.e14. doi: 10.1016/j.ccell.2020.03.015

54. Pasqualucci L, Dalla-Favera R. Genetics of diffuse large B-cell lymphoma. *Blood* (2018) 131:2307–19. doi: 10.1182/blood-2017-11-764332

55. Zhang C, Lin Q, Li C, Chen Z, Deng M, Weng H, et al. Analysis of endoplasmic reticulum stress-related gene signature for the prognosis and pattern in diffuse large B cell lymphoma. *Sci Rep* (2023) 13:13894. doi: 10.1038/s41598-023-38568-x

56. Tacutu R, Thornton D, Johnson E, Budovsky A, Barardo D, Craig T, et al. Human Ageing Genomic Resources: New and updated databases. *Nucleic Acids Res* (2018) 46:D1083–90. doi: 10.1093/nar/gkx1042

57. Zhou Z, Ma D, Li P, Wang P, Liu P, Wei D, et al. Sirt1 gene confers Adriamycin resistance in DLBCL via activating the PCG-1α mitochondrial metabolic pathway. *Aging* (2020) 12:11364–85. doi: 10.18632/aging.103174

58. Yang J, Li Y, Zhang Y, Fang X, Chen N, Zhou X, et al. Sirt6 promotes tumorigenesis and drug resistance of diffuse large B-cell lymphoma by mediating PI3K/Akt signaling. *J Exp Clin Cancer Res* (2020) 39:142. doi: 10.1186/s13046-020-01623-w

59. Zheng S, Ma J, Li J, Pang X, Ma M, Ma Z, et al. Lower PTEN may be associated with CD8+ T cell exhaustion in diffuse large B-cell lymphoma. *Hum Immunol* (2023) 84:551–60. doi: 10.1016/j.humimm.2023.07.007

60. Yeh C-H, Chou Y-J, Kao C-H, Tsai T-F. Mitochondria and calcium homeostasis: Cisd2 as a big player in cardiac ageing. *Int J Mol Sci* (2020) 21:9238. doi: 10.3390/ijms21239238

61. Liu L, Xia M, Wang J, Zhang W, Zhang Y, He M. CISD2 expression is a novel marker correlating with pelvic lymph node metastasis and prognosis in patients with early-stage cervical cancer. *Med Oncol* (2014) 31:183. doi: 10.1007/s12032-014-0183-5

62. Chang NC, Nguyen M, Shore GC. BCL2-CISD2: An ER complex at the nexus of autophagy and calcium homeostasis? *Autophagy* (2012) 8:856–7. doi: 10.4161/auto.20054

63. Xu-Monette ZY, Wu L, Visco C, Tai YC, Tzankov A, Liu W, et al. Mutational profile and prognostic significance of TP53 in diffuse large B-cell lymphoma patients treated with R-CHOP: Report from an International DLBCL Rituximab-CHOP Consortium Program Study. *Blood* (2012) 120:3986–96. doi: 10.1182/blood-2012-05-433334

64. Wang XJ, Jeffrey Medeiros null L, Bueso-Ramos CE, Tang G, Wang S, Oki Y, et al. P53 expression correlates with poorer survival and augments the negative prognostic effect of MYC rearrangement, expression or concurrent MYC/BCL2 expression in diffuse large B-cell lymphoma. *Mod Pathol* (2017) 30:194–203. doi: 10.1038/modpathol.2016.178

65. Tsuyama N, Sakata S, Baba S, Mishima Y, Nishimura N, Ueda K, et al. BCL2 expression in DLBCL: Reappraisal of immunohistochemistry with new criteria for therapeutic biomarker evaluation. *Blood* (2017) 130:489–500. doi: 10.1182/blood-2016-12-759621

66. Dunleavy K, Wilson WH. Differential role of BCL2 in molecular subtypes of diffuse large B-cell lymphoma. *Clin Cancer Res* (2011) 17:7505–7. doi: 10.1158/1078-0432.CCR-11-2372

67. Donati G, Ravà M, Filipuzzi M, Nicoli P, Cassina L, Verrecchia A, et al. Targeting mitochondrial respiration and the BCL2 family in high-grade MYC-associated B-cell lymphoma. *Mol Oncol* (2022) 16:1132–52. doi: 10.1002/1878-0261.13115

68. Wenzel S-S, Grau M, Mavis C, Hailfinger S, Wolf A, Madle H, et al. MCL1 is deregulated in subgroups of diffuse large B-cell lymphoma. *Leukemia* (2013) 27:1381–90. doi: 10.1038/leu.2012.367

69. Ngoi NYL, Choong C, Lee J, Bellot G, Wong AL, Goh BC, et al. Targeting mitochondrial apoptosis to overcome treatment resistance in cancer. *Cancers* (2020) 12:574. doi: 10.3390/cancers12030574

70. Nowakowski G, Chiappella A, Hong F, Gascoyne RD, Scott DW, Macon WR, et al. Potential factors that impact lenalidomide/R-CHOP efficacy in previously untreated diffuse large B-cell lymphoma in the ROBUST and ECOG-ACRIN 1412 studies. *Blood* (2019) 134:4092–2. doi: 10.1182/blood-2019-123083

71. Autio M, Leivonen S-K, Brück O, Mustjoki S, Jørgensen JM, Karjalainen-Lindsberg M-L, et al. Immune cell constitution in the tumor microenvironment predicts the outcome in diffuse large B-cell lymphoma. *Haematologica* (2020) 106:718–29. doi: 10.3324/haematol.2019.243626

72. Ennishi D. The biology of the tumor microenvironment in DLBCL: Targeting the "Don't Eat Me" signal. *J Clin Exp Hematop* (2021) 61:210–5. doi: 10.3960/jslrt.21015

73. Takahara T, Nakamura S, Tsuzuki T, Satou A. The immunology of DLBCL. *Cancers (Basel)* (2023) 15:835. doi: 10.3390/cancers15030835

74. Mun J-Y, Leem S-H, Lee JH, Kim HS. Dual relationship between stromal cells and immune cells in the tumor microenvironment. *Front Immunol* (2022) 13:864739. doi: 10.3389/fimmu.2022.864739

75. Yin C, Zhang J, Shen M, Gu Z, Li Y, Xue W, et al. Matrix metallopeptidase 14: A candidate prognostic biomarker for diffuse large B-cell lymphoma. *Front Oncol* (2020) 10:1520. doi: 10.3389/fonc.2020.01520

76. Li Y-L, Shi Z-H, Wang X, Gu K-S, Zhai Z-M. Tumor-associated macrophages predict prognosis in diffuse large B-cell lymphoma and correlation with peripheral absolute monocyte count. *BMC Cancer* (2019) 19:1049. doi: 10.1186/s12885-019-6208-x

77. Ma S-Y, Tian X-P, Cai J, Su N, Fang Y, Zhang Y-C, et al. A prognostic immune risk score for diffuse large B-cell lymphoma. *Br J Haematol* (2021) 194:111–9. doi: 10.1111/bjh.17478

78. Hou J, Guo P, Lu Y, Jin X, Liang K, Zhao N, et al. A prognostic 15-gene model based on differentially expressed genes among metabolic subtypes in diffuse large B-cell lymphoma. *Pathol Oncol Res* (2023) 29:1610819. doi: 10.3389/pore.2023.1610819

79. Raskov H, Orhan A, Christensen JP, Gögenur I. Cytotoxic CD8+ T cells in cancer and cancer immunotherapy. *Br J Cancer* (2021) 124:359–67. doi: 10.1038/s41416-020-01048-4

80. Das RK, Vernau L, Grupp SA, Barrett DM. Naïve T-cell Deficits at Diagnosis and after Chemotherapy Impair Cell Therapy Potential in Pediatric Cancers. *Cancer Discovery* (2019) 9:492–9. doi: 10.1158/2159-8290.CD-18-1314

81. Chen W, Liang W, He Y, Liu C, Chen H, Lv P, et al. Immune microenvironment-related gene mapping predicts immunochemotherapy response and prognosis in diffuse large B-cell lymphoma. *Med Oncol* (2022) 39:44. doi: 10.1007/s12032-021-01642-3

82. Greenbaum AM, Fromm JR, Gopal AK, Houghton AM. Diffuse large B-cell lymphoma (DLBCL) is infiltrated with activated CD8+ T-cells despite immune checkpoint signaling. *Blood Res* (2022) 57:117–28. doi: 10.5045/br.2022.2021145

83. Yuen GJ, Demissie E, Pillai S. B lymphocytes and cancer: A love-hate relationship. *Trends Cancer* (2016) 2:747–57. doi: 10.1016/j.trecan.2016.10.010

84. Sun J, Zhu X, Zhao Y, Zhou Q, Qi R, Liu H. CHN1 is a novel prognostic marker for diffuse large B-cell lymphoma. *Pharmgenomics Pers Med* (2021) 14:397–408. doi: 10.2147/PGPM.S301718

85. He J, Chen Z, Xue Q, Sun P, Wang Y, Zhu C, et al. Identification of molecular subtypes and a novel prognostic model of diffuse large B-cell lymphoma based on a metabolism-associated gene signature. *J Transl Med* (2022) 20:186. doi: 10.1186/s12967-022-03393-9

86. Brummel K, Eerkens AL, de Bruyn M, Nijman HW. Tumour-infiltrating lymphocytes: From prognosis to treatment selection. *Br J Cancer* (2023) 128:451–8. doi: 10.1038/s41416-022-02119-4

87. Mueller CG, Boix C, Kwan W-H, Daussy C, Fournier E, Fridman WH, et al. Critical role of monocytes to support normal B cell and diffuse large B cell lymphoma survival and proliferation. *J Leukoc Biol* (2007) 82:567–75. doi: 10.1189/jlb.0706481

88. Venturutti L, Melnick AM. The dangers of déjà vu: Memory B cells as the cells of origin of ABC-DLBCLs. *Blood* (2020) 136:2263–74. doi: 10.1182/blood.2020005857

89. Chu Y, Lamb M, Cairo MS, Lee DA. The future of natural killer cell immunotherapy for B cell non-Hodgkin lymphoma (B cell NHL). *Curr Treat Options Oncol* (2022) 23:381–403. doi: 10.1007/s11864-021-00932-2

90. Kim SJ, Sohn I, Do I-G, Jung SH, Ko YH, Yoo HY, et al. Gene expression profiles for the prediction of progression-free survival in diffuse large B cell lymphoma: Results of a DASL assay. *Ann Hematol* (2014) 93:437–47. doi: 10.1007/s00277-013-1884-0

91. Chen H, He Y, Pan T, Zeng R, Li Y, Chen S, et al. Ferroptosis-related gene signature: A new method for personalized risk assessment in patients with diffuse large B-cell lymphoma. *Pharmgenomics Pers Med* (2021) 14:609–19. doi: 10.2147/PGPM.S309846

frontiers | Frontiers in Oncology

TYPE Original Research
PUBLISHED 01 February 2024
DOI 10.3389/fonc.2024.1282323

OPEN ACCESS

EDITED BY
Robert Ohgami,
The University of Utah, United States

REVIEWED BY
Guido Gini,
Azienda Ospedaliero Universitaria Ospedali Riuniti, Italy
Irma Olarte,
Hospital General de México Dr. Eduardo Liceaga, Mexico

*CORRESPONDENCE
Mi-Hai Park
bestway00@skku.edu
Dok Hyun Yoon
dhyoon@amc.seoul.kr

†These authors have contributed equally to this work and share first authorship

RECEIVED 24 August 2023
ACCEPTED 16 January 2024
PUBLISHED 01 February 2024

CITATION
Cho J-Y, Jang S-C, Kang D-W, Lee E-K, Koh H, Yoon DH and Park M-H (2024) A nationwide analysis of the treatment patterns, survival, and medical costs in Korean patients with relapsed or refractory diffuse large B-cell lymphoma.
Front. Oncol. 14:1282323.
doi: 10.3389/fonc.2024.1282323

A nationwide analysis of the treatment patterns, survival, and medical costs in Korean patients with relapsed or refractory diffuse large B-cell lymphoma

Jeong-Yeon Cho[1†], Suk-Chan Jang[1†], Dong-Won Kang[1], Eui-Kyung Lee[1], Hyein Koh[2], Dok Hyun Yoon[3*] and Mi-Hai Park[1*]

[1]School of Pharmacy, Sungkyunkwan University, Suwon, Gyeonggi-do, Republic of Korea, [2]Novartis, Seoul, Republic of Korea, [3]Department of Oncology, Asan Medical Center, University of Ulsan College of Medicine, Seoul, Republic of Korea

Background: Approximately one-third of patients with diffuse large B-cell lymphoma (DLBCL) are refractory to treatment or experience relapse after initial therapy. Unfortunately, treatment options for older patients and those who experience relapse or become refractory to hematopoietic stem cell transplantation (HSCT) are limited. This nationwide population-based study aimed to identify treatment patterns, survival times, and treatment costs in patients with relapsed/refractory DLBCL (R/R DLBCL).

Materials and methods: Between 2011 and 2020, data on patients with R/R DLBCL were retrieved from the Korean Health Insurance Review & Assessment Service, encompassing the entire population. We identified the treatment patterns for each treatment line using a Sankey diagram and calculated the median time to the subsequent treatment in line. Median overall and progression-free survival times were estimated using the Kaplan–Meier survival curves. Finally, the medical costs incurred during DLBCL treatment were calculated for each treatment line and the costs related to HSCT were summarized at the episode level.

Results: A total of 864 patients with R/R DLBCL who received second-line treatment were identified, and a regimen of ifosfamide, carboplatin, and etoposide (ICE) was administered the most. Among them, 353 were refractory or relapsed cases that were treated with third-line treatments. The median times for second-line to third-line, third-line to fourth-line, fourth-line to fifth-line, and fifth-line to sixth-line treatment failures gradually decreased (3.93, 2.86, 1.81, and 1.38 months, respectively). The median overall survival time was 8.90 and 4.73 months following the second-line and third-line treatments, respectively. In the third-line treatment setting, the patients did not show a significant difference in survival time after HSCT. The median medical cost was $39,491 across all treatment lines including the cost of HSCT which was $22,054.

Conclusion: The treatment patterns in patients with R/R DLBCL, especially at third-line treatments and thereafter, were complicated, and their prognosis was poor despite the high medical costs. Novel and effective treatment options are expected to improve the prognosis and alleviate the economic burden of patients with R/R DLBCL.

KEYWORDS

diffuse large B-cell lymphoma, hematopoietic stem cell transplantation, treatment patterns, survival, medical costs

1 Introduction

Diffuse large B-cell lymphoma (DLBCL) accounts for approximately 30% of non-Hodgkin lymphoma (NHL) cases, with an age-adjusted incidence of 5.0 cases per 100,000 person-years worldwide (1, 2). Although DLBCL affects patients of all ages, it is most common in patients aged > 60 years (3). The rituximab, cyclophosphamide, hydroxydaunorubicin, oncovin, and prednisone (R-CHOP) regimen was introduced as a standard first-line treatment in 2002, and a polatuzumab-vedotin combination regimen with rituximab, cyclophosphamide, hydroxydaunorubicin, and prednisone (R-CHP) was recently introduced as a first-line treatment (4, 5). However, approximately one-third of patients experience relapse or disease progression after first-line treatment, and 83% of progression occurs within the first 3 years of treatment (6). For patients with relapsed/refractory DLBCL (R/R DLBCL), high-dose therapy with autologous hematopoietic stem cell transplantation (HDT/HSCT) is recommended (7, 8). However, no clear treatment options are available for patients ineligible for HSCT because of older age, frailty, lack of response to second-line treatment, or failure to collect stem cells (9). Furthermore, the treatment strategy is less apparent in these patients, particularly after the failure of a second-line treatment (10). Although not yet widely available, the introduction of bispecific antibody therapies and chimeric antigen receptor (CAR) T-cell therapies for patients with R/R DLBCL is anticipated to expand treatment options, potentially improving prognoses and alleviating the economic burden on these patients (11–15).

A previous study in the United States reported that rituximab-based regimens were the most prevalent, with 25% of patients receiving HSCT as a second-line treatment (16). Another study demonstrated that the median survival of patients with R/R DLBCL was 13.4 months after the initiation of second-line treatment in an outpatient setting (17). Nevertheless, only a few studies have reported on the survival times and treatment patterns of patients with R/R DLBCL, particularly those who have received second- to third-line treatments in real-world settings. In addition, studies using nationwide Korean data on these patients are limited, and treatment patterns differ from country to country depending on the reimbursement system. Therefore, we aimed to identify the treatment patterns and survival of patients with R/R DLBCL and analyze the economic burden using Korean claims data from the Health Insurance Review and Assessment Service (HIRA).

2 Materials and methods

2.1 Study design and data source

We performed a retrospective observational study using the HIRA claims data, which contain data on more than 98% of the nationwide population in South Korea (18). The data included patient characteristics such as age, sex, prescribed medications, medical procedures reimbursed by the National Health Insurance Service (NHIS), and disease codes according to the Korean Classification of Disease 7th version (KCD-7), which is a modified version of the International Classification of Disease 10th version (ICD-10). In Korean claims data, the overall positive predictive value of diagnosis using ICD-10 codes is 82% (19). Data from January 1, 2011, to February 28, 2020, were analyzed in our study, and the enrollment period during which patients with DLBCL were identified was from January 1, 2013, to December 31, 2019.

Abbreviations: CAR, chimeric antigen receptor; CCI, Charlson Comorbidity Index; CI, confidence interval; DHAP, dexamethasone, cytarabine, and cisplatin; DLBCL, Diffuse large B-cell lymphoma; ESHAP, etoposide, methylprednisolone, cytarabine, and cisplatin; HDT/HSCT, high-dose therapy with autologous hematopoietic stem cell transplantation; HIRA, Health Insurance Review and Assessment Service; ICE, ifosfamide, carboplatin, and etoposide; ICD-10, International Classification of Disease 10th version; IQR, interquartile range; KCD-7, Korean Classification of Disease 7th version; KRW, Korean Won; MINE, mesna, ifosfamide, mitoxantrone, and etoposide; NHIS, National Health Insurance Service; NHL, non-Hodgkin lymphoma; OS, overall survival; R-CHOP, rituximab, cyclophosphamide, hydroxydaunorubicin, oncovin, and prednisone; R-CHP, rituximab, cyclophosphamide, hydroxydaunorubicin, and prednisone; R/R DLBCL, relapsed/refractory DLBCL; SD, standard deviation; TTNT, time to the next treatment; USD, United States Dollar.

2.2 Study population and eligibility criteria

The target population for this study was patients with R/R DLBCL, defined as those who received second-line treatments. Patients who died without receiving second-line treatments were excluded. Prior to the selection of patients with R/R DLBCL, we constructed a cohort of patients who were newly diagnosed with DLBCL during the index period from January 1, 2013, to December 31, 2019, using their diagnosis codes and medical history claims for diffuse large B-cell lymphoma (DLBCL) (ICD-10 codes C83.3). The index date was defined as the first record of a newly diagnosed DLBCL. To exclude confounding diseases and overcome the limitations of our data, we excluded patients who met the following criteria: (1) patients who had a history of DLBCL within 5 years before the index date (washout period); (2) patients who had a history of confounding lymphomas, such as small cell B-cell lymphoma (C83.0), mantle cell lymphoma (C83.1), lymphoblastic lymphoma (C83.5), Burkitt lymphoma (C83.7), other non-follicular lymphomas (C83.8), primary mediastinum large B-cell lymphoma (C85.2), and solid cancer (C00–C80) during the study period; (3) patients with confounding medical histories, such as a history of HSCT before the index date; (4) patients with no treatment records after the index date; (5) patients who had a record of DLBCL within 2 years before the index date or who had a record of salvage chemotherapy regimens as the first-line treatment. This last criterion was created to account for patients with washout periods of less than five years prior to study inclusion.

To select eligible patients with R/R DLBCL, the treatment regimen was defined by combining the drugs administered for each medical episode. The specific medications and regimens used are summarized in Table S1. Moreover, we determined whether the treatment regimen for each medical episode was the same as that of the previous regimen based on the combination of drugs. Treatments targeting central nervous system diseases, such as the administration of intrathecal methotrexate or modifications in corticosteroid prescriptions, were considered independent of the line of treatment. We then used both treatment regimens and gaps between treatment episodes to classify the treatment line. First-line treatment was defined as prescribed medications for 12 weeks from the first record of newly diagnosed DLBCL (17). Second-line treatment was defined as the first record of switching the treatment regimen from first-line treatment. Each treatment line was defined similarly. However, if patients received the HDT regimen before HSCT, the HDT and HSCT were considered consecutive within the same treatment line (HDT/HSCT). Follow-up began from the date of each line of treatment and continued until death or the end of the study (February 28, 2020), during which time only patients with claims data were selected. All patients were followed-up for at least 60 days.

2.3 Outcomes and measurement

Baseline characteristics included age, sex, and comorbidities within 1 year before the index date. Age groups were stratified based on the eligibility for HSCT according to the local reimbursement criteria, which were up to 65 years of age during the study period. We assessed treatment patterns using the medical records of each patient to identify their treatment lines and survival data.

We calculated the median time to the next treatment (TTNT) for each treatment line and estimated the patients' overall survival (OS), which was defined as the time from initiating each line of treatment until death. The claims data of the HIRA contained only "in-hospital" deaths. Therefore, if mortality was only marked by the "in-hospital death" code, patient survival rates would be highly overestimated. To address this limitation, we defined "out-of-hospital" death as the date of the last claims filed for patients with no further records for 6 months, a method that has been adopted in previous research and validated in high-mortality cancer patients (20, 21). We then assessed the survival outcomes from the first date of each line of treatment. In addition to OS, progression-free survival was defined as the survival time from the date of relapse or refractory disease diagnosis to the initiation of a subsequent line of treatment or death.

Medical costs incurred during DLBCL treatment were summarized for each treatment line. In contrast, the costs related to HSCT were summarized at the episode level to determine the total economic burden. We also calculated cumulative medical costs while considering censoring (22) to show the difference in disease-related costs between patients who received third-line treatments and those who did not. Costs in South Korean Won (KRW) were converted to United States Dollar (USD) at the 2020 exchange rate of 1,086.3 KRW/USD.

2.4 Statistical analysis

Descriptive analyses were performed to assess patient demographics, survival, treatment patterns, and medical costs. Categorical variables were expressed as counts and percentages of patients in each category, whereas continuous variables were expressed as mean and standard deviation (SD) or median and interquartile range (IQR). The Charlson Comorbidity Index (CCI) was estimated to include the risk for the severity of the underlying disease before diagnosis (23, 24). Survival analysis was performed to estimate the survival probability over time and calculate the survival time. The median survival time of patients with R/R DLBCL was computed using the Kaplan–Meier curve with a 95% confidence interval (CI). All analyses were performed using SAS version 9.4 (SAS Institute, Cary, NC, USA).

3 Results

3.1 Baseline characteristics of patients with R/R DLBCL

A total of 21,353 patients were diagnosed with DLBCL between January 2013 and December 2019, and 4,931 eligible patients with newly diagnosed DLBCL were identified. Among them, 4,067 patients were excluded because they did not receive second-line treatment including 922 patients who died of progressive disease or other causes. Finally, 864 patients who experienced relapsed or refractory DLBCL

and received second-line treatments were selected for this study (Figure 1). The baseline characteristics of the patients included in this study are presented in Table 1. The median (IQR) age of the population was 63 (53–71) years; more than half of the patients met the age criteria for HSCT (55.79%), and the male patients (n = 522, 60.42%) outnumbered the female patients.

3.2 Treatment patterns of R/R DLBCL

Figure 2 displays the treatment patterns of the patients with R/R DLBCL. Of the 864 patients, 821 (95.02%) received R-CHOP-based regimens as the first-line treatment and 32 underwent HDT/HSCT as a consolidation therapy (Table S1). In terms of second-line treatments, 363 (42.01%) patients received an ifosfamide, carboplatin, and etoposide (ICE) regimen, of whom 42 additionally underwent HDT/HSCT. Other second-line treatments included the etoposide, methylprednisolone, cytarabine, and cisplatin (ESHAP) (16.09%) and dexamethasone, cytarabine, and cisplatin (DHAP) regimens (15.39%). Regarding third-line treatments, 82 patients (23.23%) received the DHAP regimen, 21.81% received ICE, and 14.16% received the mesna, ifosfamide, mitoxantrone, and etoposide (MINE) regimen. During the follow-up period, 212 patients (24.54%) underwent HSCT.

3.3 Time to next treatments and survival of R/R DLBCL patients

The median time from diagnosis to a second-line treatment was 9.33 months (Table 2). Among the 864 patients with R/R DBLCL, 353 experienced progression after second-line treatments and received third-line treatments. The median time from a second-line to a third-line treatment was 3.93 months. Among them, 330 (93.48%) received salvage chemotherapy (58 patients with HDT/HSCT and 272 without HDT/HSCT). A total of 114 and 42 patients experienced third- and fourth-line treatment failures, respectively. The median times for third-line to fourth-line, fourth-line to fifth-line, and fifth-line to sixth-line treatment failures gradually decreased (2.86, 1.81, and 1.38 months, respectively). Most patients received salvage chemotherapy in each line of treatment (93.48%, 85.09%, and 73.81%, respectively). The median OS time was 8.90 months after a second-line treatment and 4.73 months after a third-line treatment (Figures 3A, B). Regardless of the previous administration of HSCT, third-line treatments did not significantly differ in terms of median OS times (3.31 vs. 4.83 months, p = 0.242) (Figure 3C).

3.4 Economic burden of R/R DLBCL patients

The total lifetime medical cost across all treatment lines for R/R DLBCL was $39,491, and the cost related to HSCT was $22,054 (Table 3). The cost for patients who experienced second-line failures was $42,706, whereas it was $34,182 for those who did not encounter second-line failure (Table S2). The median cost of each treatment line was the highest from diagnosis to second-line treatment ($32,468). Among subsequent treatment lines, the cost from second-line to third-line treatment was the highest ($21,058), followed by costs from third-, fourth-, and fifth-line treatments to subsequent-line treatments. After the failure of second-line treatments, the cumulative cost for patients who received third-line treatments was higher than that of patients who did not receive third-line treatment from the fifth month onwards (Figure S1 and Table S3).

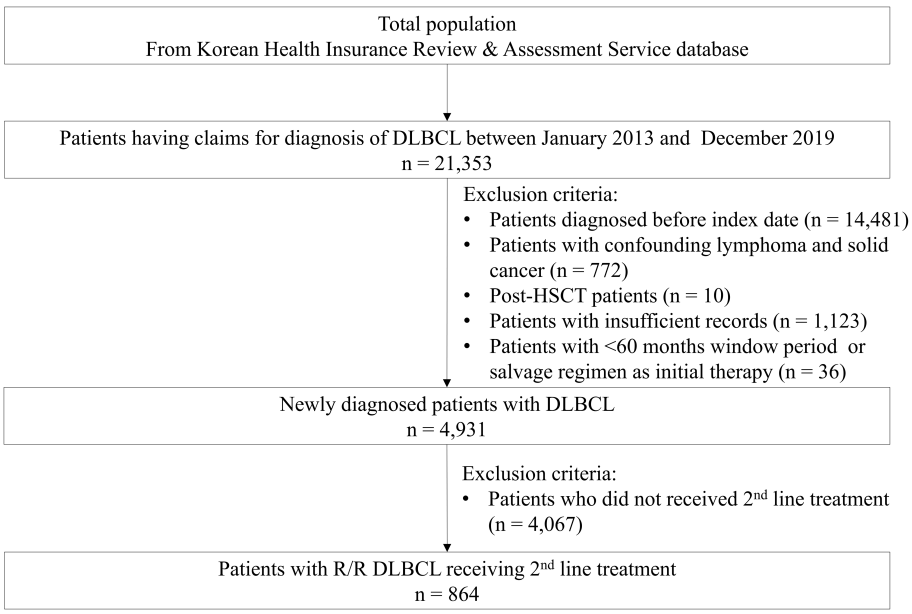

FIGURE 1
Flow chart of the selection process for eligible patients with R/R DLBCL.

TABLE 1 Baseline characteristics of patients with R/R DLBCL.

Variables	Second-line treatment (N = 864)	Third-line treatment (N = 353)
Age, median (IQR)	63 (53–71)	60 (50–68)
Age group, n (%) [a]		
< 65	482 (55.79)	222 (62.89)
≥ 65	382 (44.21)	131 (37.11)
Sex, n (%)		
Male	522 (60.42)	223 (63.17)
Female	342 (39.58)	130 (36.83)
CCI, median (IQR)	5.00 (4.00–8.00)	5.00 (4.00–8.00)
Comorbidities, n (%)		
Diabetes	368 (42.59)	150 (42.49)
Hypertension	405 (46.88)	155 (43.91)
Heart disease [b]	74 (8.56)	32 (9.07)

[a]Age eligibility for HSCT according to the local reimbursement criterion: < 65 years.
[b]Heart disease was defined by ICD-10 codes I21 (acute MI), I22 (STEMI), I43 (cardiomyopathy), and I50 (HF).
HSCT, hematopoietic stem cell transplantation; R/R DLBCL, relapsed or refractory diffuse large B-cell lymphoma; CCI, Charlson comorbidity index.

4 Discussion

In this nationwide population-based study, we estimated the treatment patterns, survival times, and treatment costs for patients with R/R DLBCL. Our findings revealed a lack of clear treatment patterns for these patients, with the ICE, ESHAP, and DHAP regimens being the most commonly administered, in that specific order. The median OS of patients with R/R DLBCL was 8.90 months and the progression-free survival time was 4.47 months. Additionally, we determined that the median treatment cost for these patients was $39,491 over their lifetime. As the patients experienced multiple treatment failures and received subsequent lines of therapy, a decreasing trend in TTNT was observed. Although TTNTs decreased remarkably in subsequent treatment stages, the decrease in cost was relatively minor.

The treatment of R/R DLBCL remains a clinical challenge. R-CHOP has been the standard first-line treatment for DLBCL for more than 20 years (25, 26), and a polatuzumab-vedotin combination regimen has recently been introduced (4). However, an established effective treatment for patients with R/R DLBCL, particularly those who cannot undergo transplantation, remains lacking (27). Similar to a previous study (28), approximately one-fourth of the patients in this study received HSCT, and many patients only underwent salvage chemotherapy due to the lack of treatment options for DLBCL within the reimbursement criteria in Korea.

Although several studies have analyzed the survival of patients with DLBCL, few have investigated patients experiencing relapsed or refractory disease. The median OS of 6.3 months presented by Crump et al. (29) was similar to that in our study, considering that they focused on patients who received only salvage chemotherapy. However, this study reported only OS after a second-line treatment, whereas our study holds significance for presenting OS following a third-line treatment in patients with second-line failure. Another study investigated outpatient chemotherapy in patients with R/R

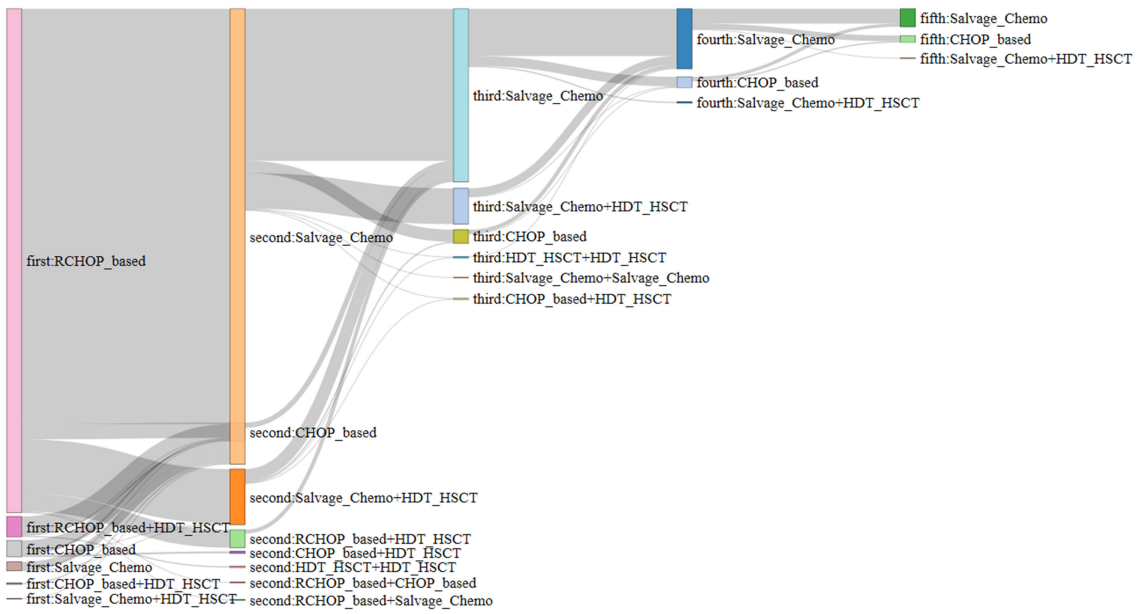

FIGURE 2
Treatment patterns for patients with R/R DLBCL.

TABLE 2 Time to next treatments and survival of R/R DLBCL patients.

	Patients with R/R DLBCL
Median follow-up time, months (IQR)	*7.62 (3.55–15.33)*
Median time to next treatment, months (IQR)	
Time from diagnosis to second-line treatment (n = 864)	9.33 (5.98–16.46)
Time from second-line treatment to third-line treatment (n = 864)	3.93 (2.00–9.89)
Time from third-line treatment to fourth-line treatment (n = 353)	2.86 (1.38–6.64)
Time from fourth-line treatment to fifth-line treatment (n= 114)	1.81 (1.08–3.19)
Time from fifth-line treatment to sixth-line treatment (n = 42)	1.38 (0.95–4.34)
Overall survival	
Median time from second-line treatment, months (95% CI), (n = 864)	*8.90 (8.08, 9.63)*
% proportion of censored patients	*34.38*
Median time from third-line treatment, months (95% CI), (n = 353)	4.73 (4.17, 5.72)
% proportion of censored patients	21.81
Progression-free survival	
Median time from second-line treatment, months (95% CI), (n = 864)	*4.47 (3.88, 5.06)*
% proportion of censored patients	*25.46*
% proportion of death before progression	*33.68*
Median time from third-line treatment, months (95% CI), (n = 353)	3.12 (2.73, 3.61)
% proportion of censored patients	17.85
% proportion of death before progression	49.86
Number of patients who received HSCT, n (%) (n = 864)	212 (24.54)
Autologous HSCT	210 (24.31)
Allogenic HSCT	9 (1.04)

HSCT, hematopoietic stem cell transplantation; R/R DLBCL, relapsed or refractory diffuse large B-cell lymphoma.

DLBCL; however, our study adds value by including both inpatients and outpatients (17). We also presented OS with a focus on HDT combined with HSCT, which is recommended as a second-line treatment for patients with chemotherapy-sensitive DLBCL (7). Patients with R/R DLBCL who underwent HSCT exhibited a better prognosis than those who did not (30). However, because the prognosis for relapse after HSCT is poor, similar to other second-line options, HSCT should be carefully considered.

The median TTNTs rapidly shortened after the first relapse or refractory diagnosis and continued to decrease until the sixth-line treatment. In other words, as the disease progressed, the response to the drug decreased, resulting in a rapid occurrence of refractoriness or relapse. Although the TTNTs continued to decrease until the sixth-line treatment, the medical costs were similar, indicating that the cost per unit time was higher on the next subsequent treatment line than on the prior treatments and that the economic burden increased as the treatment failed. This was presumably because of the absence of other anticancer therapy and the availability of only salvage chemotherapy; therefore, the medical expenses required to provide care for patients eventually increased. A previous study reported that patients who experienced relapse spent significantly more on medical costs than those who did not experience relapse (31). From the perspective of each treatment line, the higher cost of each treatment line compared with that of the next treatment line could be attributed to the TTNT. A previous study demonstrated that the cost of the treatment for relapse after 3 months was higher than that of relapse within 3 months (31). Although several studies have estimated the medical costs in patients with DLBCL, most of them only demonstrated the medical costs for treating DLBCL and not for R/R DLBCL. In a study evaluating the medical costs in patients with R/R DLBCL, a similarly high cost was observed (31). However, their assessment was confined to the initial few years post-diagnosis; therefore, we supplemented this by calculating the total lifetime costs. Patients who experienced relapse after the second-line treatment spent more disease-related costs across all time points than that patients who did not experience relapse.

This study had several limitations. Although the study lacked clinical information, such as patients' disease stages and treatment lines, we classified their treatment regimens and lines based on the drugs in each of their claims and the intervals between claims. Therefore, it is possible that some treatment lines were misclassified, which may have affected the TTNT and medical expenses. In addition, patients with R/R DLBCL who did not receive second-line treatment because of relapse or refractory disease may have been excluded. Third, the claims data did not allow us to identify non-covered drugs. Therefore, treatment costs may have been underestimated. Another limitation of this study was that we could not include newly introduced therapies because of the limited study period. For instance, starting in April 2022 in South Korea, CAR T-cell therapies were reimbursed for patients who experienced failure with second-line treatment and those who faced failure after HSCT (32). Since these therapies have shown clinical benefits through trials to improve the prognosis of patients with R/R DLBCL (11–13), they are likely to affect treatment patterns after reimbursement (33). However, CAR T-cell therapies could not be included because they were introduced after the study period (34). With the recent approval of other CAR T-cell and bispecific antibody therapies (14, 15), the treatment paradigm for patients with R/R DLBCL is expected to change in the future, and further long-term follow-up studies, including novel therapies, should be conducted after data accumulation. Therefore, although our data did not include newly introduced therapies, our results remain valuable because they offer insights into the population to which new treatments will be applied.

Despite these limitations, our study had significant strengths. We assessed the clinical and economic burden of patients with R/R

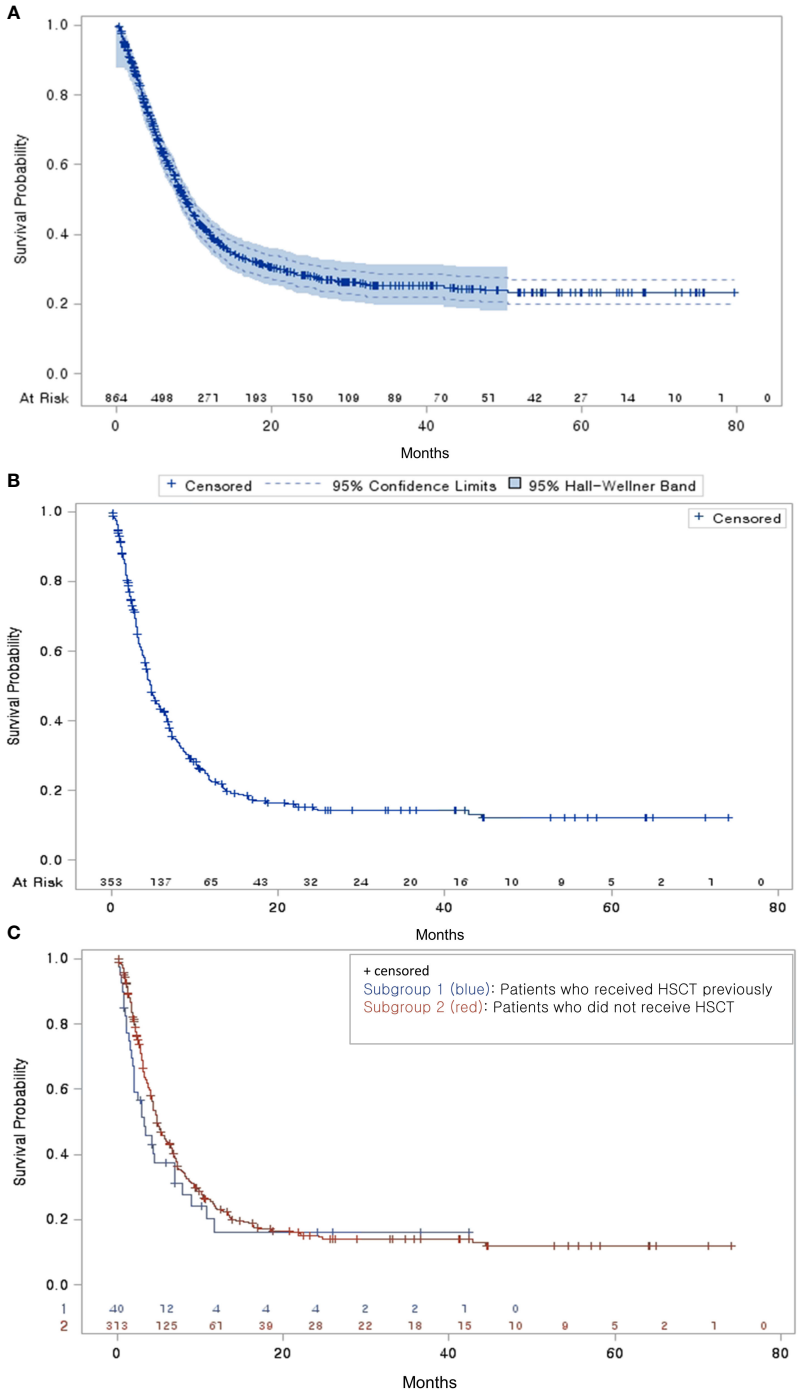

FIGURE 3
Overall survival probability **(A)** Overall survival of patients with R/R DLBCL who received second-line treatment **(B)** Overall survival of third-line treatment patients from the end of their second-line treatment **(C)** Overall survival of third-line treatment patients by HSCT subgroup.

DLBCL using long-term real-world data derived from the nationwide HIRA database encompassing the entire national population. In addition, this study adequately evaluated the disease burden of patients by focusing on those with R/R DLBCL. Unlike previous studies that reported only treatment regimen ratios (16, 17, 35), our study demonstrated the flow of regimens using a Sankey diagram and reported their complexities.

5 Conclusion

Complex treatment patterns, poor prognoses, and high medical costs have been reaffirmed by the results of previous studies on patients with R/R DLBCL, especially those who received third-line treatments. This high clinical and economic burden in patients with R/R DLBCL may be due to limited treatment options following

TABLE 3 Economic burden of patients with R/R DLBCL.

	Patients with R/R DLBCL
Total medical cost, median (IQR) (n = 864)	$39,491 (21,451–62,732)
Total inpatient cost	$31,069 (15,791–52,685)
Total medical cost related to HSCT	$22,054 (15,804–32,040)
Medical costs for each treatment line, median (IQR)	
From diagnosis to second-line treatment (n = 864)	$32,468 (26,174–41,667)
From second-line treatment to third-line treatment (n = 864)	$21,058 (11,456–38,154)
From third-line treatment to fourth-line treatment (n = 353)	$21,017 (10,197–39,718)
From fourth-line treatment to fifth-line treatment (n= 114)	$18,228 (8,658–35,140)
From fifth-line treatment to sixth-line treatment (n = 42)	$16,147 (2,778–32,631)

R/R DLBCL, relapsed or refractory diffuse large B-cell lymphoma; IQR, interquartile range; 1 USD = 1086.30 KRW (2020 exchange rate).

second-line treatments. Establishing appropriate policies and novel treatment options that will provide excellent response rates is expected to improve prognosis and alleviate the economic burden of patients with R/R DLBCL.

Data availability statement

Publicly available datasets were analyzed in this study. This data can be found here: Data from the Korean National Health Insurance Service (M20200325409) were obtained after appropriate authorization approval. (https://opendata.hira.or.kr/).

Ethics statement

The Institutional Review Board of Sungkyunkwan University approved this retrospective study (SKKU-2020-01-010). Written informed consent from the participant's legal guardian/next of kin was not required to participate in this study in accordance with the national legislation and institutional requirements. The studies were conducted in accordance with the local legislation and institutional requirements. The ethics committee/institutional review board waived the requirement of written informed consent for participation from the participants or the participants' legal guardians/next of kin because As participants' personal information was anonymized, the institutional review board waived the need for informed consent for this study.

Author contributions

J-YC: Conceptualization, Data curation, Formal analysis, Investigation, Methodology, Writing – original draft. S-CJ: Conceptualization, Formal analysis, Investigation, Writing – original draft, Writing – review & editing. D-WK: Investigation, Writing – original draft. E-KL: Supervision, Writing – review & editing. HK: Conceptualization, Writing – review & editing. DHY: Conceptualization, Validation, Writing – review & editing. M-HP: Conceptualization, Funding acquisition, Project administration, Supervision, Writing – review & editing.

Funding

The author(s) declare financial support was received for the research, authorship, and/or publication of this article. This study was funded by Novartis.

Conflict of interest

Author HK was employed by the company Novartis.

The remaining authors declare that the research was conducted in the absence of any commercial or financial relationships that could be construed as a potential conflict of interest.

The authors declare that this study received funding from Novartis. The funder was not involved in the study design, collection, analysis, interpretation of data, the writing of this article or the decision to submit it for publication.

Publisher's note

Supplementary material

The Supplementary Material for this article can be found online at: https://www.frontiersin.org/articles/10.3389/fonc.2024.1282323/full#supplementary-material

References

1. Teras LR, DeSantis CE, Cerhan JR, Morton LM, Jemal A, Flowers CR. 2016 Us lymphoid Malignancy statistics by world health organization subtypes. *CA: Cancer J Clin* (2016) 66(6):443–59. doi: 10.3322/caac.21357

2. Sehn LH, Salles G. Diffuse large B-cell lymphoma. *N Engl J Med* (2021) 384 (9):842–58. doi: 10.1056/NEJMra2027612

3. Le Guyader-Peyrou S, Orazio S, Dejardin O, Maynadié M, Troussard X, Monnereau A. Factors related to the relative survival of patients with diffuse large B-cell lymphoma in a population-based study in France: does socio-economic status have a role? *Haematologica* (2017) 102(3):584. doi: 10.3324/haematol.2016.152918

4. Tilly H, Morschhauser F, Sehn LH, Friedberg JW, Trneny M, Sharman JP, et al. Polatuzumab vedotin in previously untreated diffuse large B-cell lymphoma. *N Engl J Med* (2022) 386(4):351–63. doi: 10.1056/NEJMoa2115304

5. Pfreundschuh M, Kuhnt E, Trumper L, Osterborg A, Trneny M, Shepherd L, et al. Chop-like chemotherapy with or without rituximab in young patients with good-prognosis diffuse large-B-cell lymphoma: 6-year results of an open-label randomised study of the mabthera international trial (Mint) group. *Lancet Oncol* (2011) 12 (11):1013–22. doi: 10.1016/S1470-2045(11)70235-2

6. Coiffier B, Thieblemont C, Van Den Neste E, Lepeu G, Plantier I, Castaigne S, et al. Long-term outcome of patients in the lnh-98.5 trial, the first randomized study comparing rituximab-chop to standard chop chemotherapy in dlbcl patients: A study by the groupe D'etudes des lymphomes de L'adulte. *Blood* (2010) 116(12):2040–5. doi: 10.1182/blood-2010-03-276246

7. Philip T, Guglielmi C, Hagenbeek A, Somers R, van der Lelie H, Bron D, et al. Autologous bone marrow transplantation as compared with salvage chemotherapy in relapses of chemotherapy-sensitive non-Hodgkin's lymphoma. *N Engl J Med* (1995) 333(23):1540–5.

8. Merryman RW, Kim HT, Zinzani PL, Carlo-Stella C, Ansell SM, Perales MA, et al. Safety and efficacy of allogeneic hematopoietic stem cell transplant after Pd-1 blockade in relapsed/refractory lymphoma. *Blood* (2017) 129(10):1380–8. doi: 10.1182/blood-2016-09-738385

9. Zelenetz AD, Gordon LI, Chang JE, Christian B, Abramson JS, Advani RH, et al. Nccn guidelines® Insights: B-cell lymphomas, version 5.2021: featured updates to the nccn guidelines. *J Natl Compr Cancer Netw* (2021) 19(11):1218–30. doi: 10.6004/jnccn.2021.0054

10. Gisselbrecht C, Van Den Neste E. How I manage patients with relapsed/refractory diffuse large B cell lymphoma. *Br J Haematol* (2018) 182(5):633–43. doi: 10.1111/bjh.15412

11. Neelapu SS, Locke FL, Bartlett NL, Lekakis LJ, Miklos DB, Jacobson CA, et al. Axicabtagene ciloleucel car T-cell therapy in refractory large B-cell lymphoma. *N Engl J Med* (2017) 377(26):2531–44. doi: 10.1056/NEJMoa1707447

12. Schuster SJ, Bishop MR, Tam CS, Waller EK, Borchmann P, McGuirk JP, et al. Tisagenlecleucel in adult relapsed or refractory diffuse large B-cell lymphoma. *N Engl J Med* (2019) 380(1):45–56. doi: 10.1056/NEJMoa1804980

13. Abramson JS, Palomba ML, Gordon LI, Lunning MA, Wang M, Arnason J, et al. Lisocabtagene maraleucel for patients with relapsed or refractory large B-cell lymphomas (Transcend nhl 001): A multicentre seamless design study. *Lancet* (2020) 396(10254):839–52. doi: 10.1016/S0140-6736(20)31366-0

14. Dickinson MJ, Carlo-Stella C, Morschhauser F, Bachy E, Corradini P, Iacoboni G, et al. Glofitamab for relapsed or refractory diffuse large B-cell lymphoma. *N Engl J Med* (2022) 387(24):2220–31. doi: 10.1056/NEJMoa2206913

15. Hutchings M, Mous R, Clausen MR, Johnson P, Linton KM, Chamuleau MED, et al. Dose escalation of subcutaneous epcoritamab in patients with relapsed or refractory B-cell non-hodgkin lymphoma: an open-label, phase 1/2 study. *Lancet* (2021) 398(10306):1157–69. doi: 10.1016/S0140-6736(21)00889-8

16. Morrison VA, Shou Y, Bell JA, Hamilton L, Ogbonnaya A, Raju A, et al. Evaluation of treatment patterns and survival among patients with diffuse large B-cell lymphoma in the USA. *Future Oncol (London England)* (2019) 15(9):1021–34. doi: 10.2217/fon-2018-0788

17. Danese MD, Griffiths RI, Gleeson ML, Dalvi T, Li J, Mikhael JR, et al. Second-line therapy in diffuse large B-cell lymphoma (Dlbcl): treatment patterns and outcomes in older patients receiving outpatient chemotherapy. *Leuk Lymphoma* (2017) 58 (5):1094–104. doi: 10.1080/10428194.2016.1228924

18. Peabody JW, Lee S-W, Bickel SR. Health for all in the Republic of Korea: one country's experience with implementing universal health care. *Health Policy* (1995) 31 (1):29–42. doi: 10.1056/NEJM199512073332305

19. Park EC. *Evaluation and Consideration Methods of Consistency between Health Insurance Claims Diagnostic Codes and Medical Records*. Wonju, Gangwon-do, Republic of Korea: Korean Health Insurance Review & Assessment Service (2017).

20. Lee JS, Hong JH, Sun S, Won HS, Kim YH, Ahn MS, et al. The impact of systemic treatment on brain metastasis in patients with non-small-cell lung cancer: A retrospective nationwide population-based cohort study. *Sci Rep* (2019) 9(1):18689. doi: 10.1038/s41598-019-55150-6

21. Jang SC, Kwon SH, Min S, Jo AR, Lee EK, Nam JH. Optimal indicator of death for using real-world cancer patients' Data from the healthcare system. *Front Pharmacol* (2022) 13:906211. doi: 10.3389/fphar.2022.906211

22. Zhao H, Tian L. On estimating medical cost and incremental cost-effectiveness ratios with censored data. *Biometrics* (2001) 57(4):1002–8. doi: 10.1111/j.0006-341x.2001.01002.x

23. Quan H, Li B, Couris CM, Fushimi K, Graham P, Hider P, et al. Updating and validating the charlson comorbidity index and score for risk adjustment in hospital discharge abstracts using data from 6 countries. *Am J Epidemiol* (2011) 173(6):676–82. doi: 10.1093/aje/kwq433

24. Charlson ME, Pompei P, Ales KL, MacKenzie CR. A new method of classifying prognostic comorbidity in longitudinal studies: development and validation. *J Chronic Dis* (1987) 40(5):373–83. doi: 10.1016/0021-9681(87)90171-8

25. Tilly H, Gomes da Silva M, Vitolo U, Jack A, Meignan M, Lopez-Guillermo A, et al. Diffuse large B-cell lymphoma (Dlbcl): esmo clinical practice guidelines for diagnosis, treatment and follow-up. *Ann Oncol* (2015) 26 Suppl 5:v116–25. doi: 10.1093/annonc/mdv304

26. Coiffier B, Lepage E, Briere J, Herbrecht R, Tilly H, Bouabdallah R, et al. Chop chemotherapy plus rituximab compared with chop alone in elderly patients with diffuse large-B-cell lymphoma. *N Engl J Med* (2002) 346(4):235–42. doi: 10.1056/NEJMoa011795

27. Nowakowski GS, Blum KA, Kahl BS, Friedberg JW, Baizer L, Little RF, et al. Beyond rchop: A blueprint for diffuse large B cell lymphoma research. *J Natl Cancer Inst* (2016) 108(12):djw257. doi: 10.1093/jnci/djw257

28. Sehn LH, Gascoyne RD. Diffuse large B-cell lymphoma: optimizing outcome in the context of clinical and biologic heterogeneity. *Blood* (2015) 125(1):22–32. doi: 10.1182/blood-2014-05-577189

29. Crump M, Neelapu SS, Farooq U, Van Den Neste E, Kuruvilla J, Westin J, et al. Outcomes in refractory diffuse large B-cell lymphoma: results from the international scholar-1 study. *Blood* (2017) 130(16):1800–8. doi: 10.1182/blood-2017-03-769620

30. Nabhan C, Klink A, Lee CH, Laney JR, Yang Y, Purdum AG. Overall survival (Os) and transplantation (Asct) utilization in real-world patients with relapsed/refractory diffuse large B-cell lymphoma (Rr-Dlbcl). *Am Soc Clin Oncol* (2018) 36:7545. doi: 10.1200/JCO.2018.36.15_suppl.7545

31. Purdum A, Tieu R, Reddy SR, Broder MS. Direct costs associated with relapsed diffuse large B-cell lymphoma therapies. *Oncologist* (2019) 24(9):1229–36. doi: 10.1634/theoncologist.2018-0490

32. Prasad V. Immunotherapy: tisagenlecleucel - the first approved car-T-cell therapy: implications for payers and policy makers. *Nat Rev Clin Oncol* (2018) 15 (1):11–2. doi: 10.1038/nrclinonc.2017.156

33. Roschewski M, Longo DL, Wilson WH. Car T-cell therapy for large B-cell lymphoma—Who, When, and How? *Mass Med Soc* (2022) p:692–6. doi: 10.1056/NEJMe2118899

34. Chow VA, Shadman M, Gopal AK. Translating anti-cd19 car T-cell therapy into clinical practice for relapsed/refractory diffuse large B-cell lymphoma. *Blood* (2018) 132 (8):777–81. doi: 10.1182/blood-2018-04-839217

35. Ren J, Asche CV, Shou Y, Galaznik A. Economic burden and treatment patterns for patients with diffuse large B-cell lymphoma and follicular lymphoma in the USA. *J Comp Eff Res* (2019) 8(6):393–402. doi: 10.2217/cer-2018-0094

frontiers | Frontiers in Oncology

TYPE Brief Research Report
PUBLISHED 08 February 2024
DOI 10.3389/fonc.2024.1304144

OPEN ACCESS

EDITED BY
Robert Ohgami,
The University of Utah, United States

REVIEWED BY
Jaine Katharine Blayney,
Queen's University Belfast, United Kingdom
Irma Olarte,
Hospital General de México Dr. Eduardo Liceaga, Mexico

*CORRESPONDENCE
Sungwon Lim
sungwon@imprimedicine.com

RECEIVED 29 September 2023
ACCEPTED 16 January 2024
PUBLISHED 08 February 2024

CITATION
Callegari AJ, Tsang J, Park S, Swartzfager D, Kapoor S, Choy K and Lim S (2024) Multimodal machine learning models identify chemotherapy drugs with prospective clinical efficacy in dogs with relapsed B-cell lymphoma. *Front. Oncol.* 14:1304144. doi: 10.3389/fonc.2024.1304144

Multimodal machine learning models identify chemotherapy drugs with prospective clinical efficacy in dogs with relapsed B-cell lymphoma

A. John Callegari[1], Josephine Tsang[1], Stanley Park[1], Deanna Swartzfager[1], Sheena Kapoor[1], Kevin Choy[2] and Sungwon Lim[1]*

[1]ImpriMed Inc., Mountain View, CA, United States, [2]Department of Oncology, Blue Pearl Seattle Veterinary Specialist, Kirkland, WA, United States

Dogs with B-cell lymphoma typically respond well to first-line CHOP-based chemotherapy, but there is no standard of care for relapsed patients. To help veterinary oncologists select effective drugs for dogs with lymphoid malignancies such as B-cell lymphoma, we have developed multimodal machine learning models that integrate data from multiple tumor profiling modalities and predict the likelihood of a positive clinical response for 10 commonly used chemotherapy drugs. Here we report on clinical outcomes that occurred after oncologists received a prediction report generated by our models. Remarkably, we found that dogs that received drugs predicted to be effective by the models experienced better clinical outcomes by every metric we analyzed (overall response rate, complete response rate, duration of complete response, patient survival times) relative to other dogs in the study and relative to historical controls.

KEYWORDS

chemotherapy, machine learning, personalized & precision medicine (PPM), lymphoma, artificial intelligence - AI, rescue therapy, salvage therapy

Introduction

Diffuse large B cell lymphoma (DLBCL) is the most commonly occurring lymphoma in both dogs and humans (1, 2). In both species, the tumors are typically highly responsive to first-line combination therapies that include cyclophosphamide, doxorubicin, vincristine, and prednisone (CHOP). There is not yet a standard of care for either dogs or humans when patients relapse after first-line therapy (2, 3). Patients may be reinduced with first-line therapy or treated with one of several different rescue therapies (salvage therapies). Thus, in

both humans and dogs there is an unmet need for support in identifying the most effective treatment option in the event of relapse.

To help veterinary oncologists rapidly identify the most effective treatments for dogs with lymphoid malignancies like DLBCL, we developed machine learning (ML) models that predict clinical outcomes for 10 different chemotherapy drugs commonly used to treat these malignancies (3). The models predict outcomes derived from medical records by integrating information from two tumor profiling technologies known to yield actionable information with a high frequency: multicolor flow cytometry (4, 5) and ex vivo drug sensitivity testing (3, 6–8). Flow cytometry provides quantitative information about immune cell composition, cell size, and cell granularity at the single-cell level, while ex vivo drug sensitivity testing directly quantifies the cytotoxic effects of different drugs using live tumor cells. ML models like ours, which integrate data from multiple tumor profiling modalities, are termed "multimodal" ML models. Because these models have the potential to increase the accuracy of ML-based precision oncology tools and the frequency with which these tools provide actionable clinical guidance, the development of multimodal ML models is a highly active area of research (9–11).To our knowledge, the study presented here is the first to report on prospective clinical outcomes for cancer patients treated with the assistance of a multimodal ML tool (10).

Results

We used ML models to generate a prediction report that was provided to oncologists at multiple sites in the US beginning in June of 2020. The report was sent 7 days after live tumor biopsies were received for profiling at our testing facility. In the report, tumor response predictions were presented for each drug on a scale of 0 to 1, with 1 representing the highest likelihood of a positive clinical response (partial response or complete response). We found that there was an approximate correspondence between a prediction score of 0.5 and a 50% probability of a positive response (3). The report provided written guidance on how to interpret the predictions but did not specify how the information should be used to modify treatment plans. Thus, clinicians were free to combine their clinical expertise with the additional information in the prediction report.

The reports were provided to veterinary oncologists at multiple clinics in the US and treatment outcomes were then collected and analyzed. Our primary endpoint for analysis of patient outcomes was patient survival time, but for this study we also analyzed duration of complete response, complete response rate, and overall response rate. Because of the high prevalence of B-cell lymphoma and the short duration of response to therapy in relapsed patients with this cancer type [106 days (12)], patients with relapsed B-cell lymphoma were among the first patients in our population for whom we were able to accumulate a statistically relevant number of prospective survival outcomes. For the current study, we analyzed a cohort of 60 dogs that had relapsed from a prior therapy or therapies at the time that our prediction report was provided (Supplementary Figure 1).

Performance of the prediction report was quantified using a matching score analysis commonly employed in human clinical trials where patients are stratified by the degree of matching between recommended and administered drug treatments (13–18). For each dog, the degree to which treatments matched the prediction report was summarized using a matching score similar to those described previously (13–18). The matching score was calculated as the percentage of all administered drug treatments assigned a prediction score greater than 0.5 in our prediction report. We found that the matching scores for this cohort were generally very high, with a median value of 87.5% (Supplementary Figure 2).

To examine the relationship between matching scores and clinical outcomes, we split the cohort into two groups at the median matching score value and analyzed outcomes in the two groups (17). One group comprised the lower-matching half of the population while the other group comprised the higher-matching half of the population. A detailed discussion of dichotomization methods is included below in the methods section.

Baseline patient and tumor characteristics were similar in the two matching groups (Supplementary Table 1), but clinical outcomes were better in the high matching group for every metric we analyzed. Using the Kaplan-Meier estimator to analyze the interval between receipt of the prediction report and death of the patient (Figure 1A), we found that patients in the high matching group experienced significantly longer survival times ($p < 0.001$ for the logrank test), with a median survival time of 270 days in the high matching group and 83 days in the low matching group.

Patients in the high matching group experienced both a higher CR rate (CRR) and a higher overall response rate (ORR) than patients in the low matching group (Figure 1B) (CRR: 53.3% high, 13.3% low, $p = 0.002$; ORR: 70.0% high, 46.6% low, $p = 0.12$). In patients that experienced a CR, Kaplan-Meier analysis indicated that duration of CR was longer in the high matching group than in the low matching group (Figure 1C) ($p = 0.10$ for the logrank test). The statistical power of this survival curve comparison is limited because only five patients in the low matching group experienced a CR. The median duration of a CR was 200 days for the high matching group as compared to 48 days for the low matching group. Thus, the longer survival experienced by the high matching group was accompanied by a similarly extended period of good health during which the lymphoma was in complete remission.

To determine if matching scores were influenced by the drugs predicted to be effective in the report, we analyzed the frequency with which the prediction report contained scores above 0.5 for the chemotherapy drugs in the high matching and low matching groups (Figure 1D). No statistically significant difference was found between the relative frequency of these predictions in the two groups for any drug. Thus, matching scores in the low matching group cannot be explained by properties of the drugs predicted to be effective for the dogs in that group. This analysis also suggests that the drug sensitivity of the two matching groups was similar at the population level and that any differences in clinical outcomes were likely attributable to personalization of the drug selection process.

To isolate the effect of matching score from other variables that might confound our analysis of patient survival times, we corrected

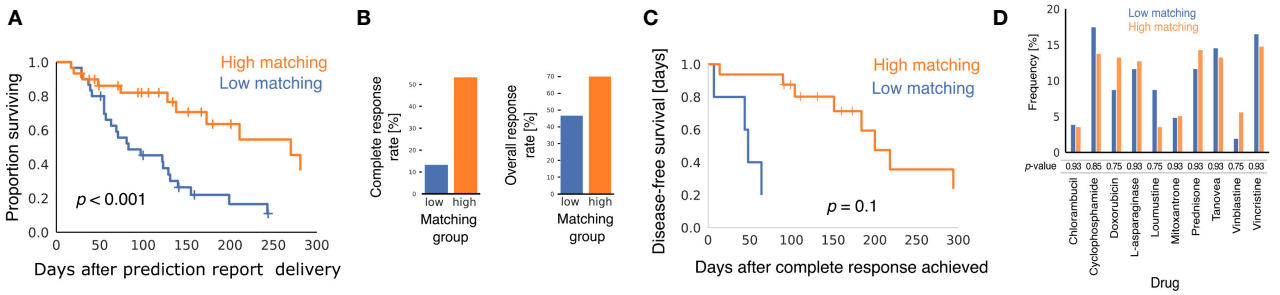

FIGURE 1
Comparison of clinical outcomes in low matching and high matching groups. **(A)** Kaplan-Meier curves showing survival of dogs after oncologists were provided with multimodal ML predictions. All causes of mortality are included. *p*-value was calculated using the logrank test. **(B)** Bar graphs showing CRR and ORR for the two matching score groups. *p*-values from Fisher's exact test were $p = 0.002$ for CRR and $p = 0.12$ for ORR. **(C)** Kaplan-Meier curves showing disease-free survival after CR for the subset of dogs that experienced CR after their oncologists received multimodal ML predictions (n = 5 for low matching and n = 16 for high matching). *p*-value was calculated using the logrank test. **(D)** Bar graph showing the relative frequencies with which different chemotherapy drugs were predicted to elicit a positive response for dogs in the two matching groups. *p*-values are from the two-sample Z-test with correction for multiple hypothesis testing using the Benjamini-Hochberg method.

for tumor grade, cancer stage, and cancer substage using multivariate Cox regression. In both univariate and multivariate Cox regression models, matching score group was the best predictor of patient survival with a hazard ratio (HR) of 0.31 (95% CI 0.15-0.65) in a univariate model and HR of 0.28 (95% CI 0.14-0.59) in a multivariate model (Table 1). Thus, consistent with the baseline patient characteristics shown in Supplementary Table 1, the markedly longer survival seen in the high matching group cannot easily be explained by the presence of more advanced or aggressive disease in the low matching group.

Discussion

The clinical outcome advantage of the high matching group relative to the low matching group was observed with every metric examined (ORR, CRR, durations of CRs, survival times) and after correcting for potentially confounding variables using multivariate Cox modeling. The clinical outcome advantage was also evident in all four metrics when we compared high matching group outcomes to historical controls (Table 2). Both ORR and CRR values observed in the high matching group were higher than historical control values (ORR: 70% this study, 48% controls; CRR: 53% this study, 27% controls) (19). The median duration of CR of 200 days that we observed in the high matching group was longer than a historical control value of 106 days taken from the mean of 15 rescue therapy studies (12). Thus, the patients in our study group that received treatments matching their multimodal ML predictions to a high degree experienced approximately double the frequency of CR and double the duration of CR compared to historical values reported in the literature. Although patient survival is not uniformly reported in the canine rescue therapy literature, we estimated that historical median survival time after relapse to be 110 days (see methods section for details), which is substantially lower than the value of 270 days that we observed in the high matching group.

To compare the clinical performance of our precision oncology platform with results from other platforms, we compiled mortality hazard ratios (HRs) from a sample of prospective matching score studies in the published literature (Table 3) (13–18). A low HR means that reduced mortality was observed for patients in the high matching group. The HR that we report here (0.28, 95% CI 0.14-0.59) is comparable to that of the most performant precision oncology platform in the sample of published values (HR 0.24, 95% CI 0.078–0.76). Among the studies shown in Table 3, our study is the only to use computer-automated predictions rather than recommendations from human experts.

TABLE 1 Cox proportional hazards models of patient survival.

	Univariate				Multivariate		
covariate	coef	HR (95% CI)	P-value	concordance	coef	HR (95% CI)	P-value
grade	-0.11	0.90 (0.27-2.98)	0.861	0.49	0.33	1.4 (0.41-4.7)	0.604
substage	0.63	1.8 (0.85-4.14)	0.121	0.55	0.96	2.6 (1.1-6.1)	0.027
stage	-0.13	0.87 (0.57-1.34)	0.535	0.52	-0.23	0.80 (0.49-1.3)	0.357
matching group	-1.16	0.31 (0.15-0.65)	0.002	0.57	-1.26	0.28 (0.14-0.59)	<0.001

TABLE 2 Comparison of high matching group outcomes to internal and historical controls.

metric	high matching group	low matching group internal control	historical control[a]
complete response rate [%]	53*	13*	27
overall response rate [%]	70**	47**	48
median duration of complete response [days]	200	48	106
median survival after relapse [days]	270	83	~110

p-value comparisons between high and low matching groups calculated using Fisher's exact: *p = 0.002, **p = 0.12. [a]See main text for information on historical controls.

The results reported here strongly support the efficacy of combining clinical knowledge with multimodal ML decision support to optimize rescue therapy outcomes for canine patients with relapsed B-cell lymphoma. We are actively researching application of this technology in human oncology and the impact of tumor mutation profiling data on ML model performance.

Methods

Study design

Multimodal ML models were initially developed during a preclinical research stage and then provided to veterinary oncologists throughout the US. The preclinical research was reported in a previous study (3) and clinical research is reported here. An open cohort study design was used to assess the performance of clinical decision support provided by multimodal ML models. Enrollment began in June of 2020 and is continuing at the time of this publication. Informed consent was obtained from pet owners using a form that was approved by the clinical review boards and ethical review committees of participating veterinary hospitals. Veterinary oncologists at multiple sites in the US collected live-cell tumor biopsies from dogs with lymphoid malignancies as described below. Tumor samples were profiled at ImpriMed labs, generating inputs for multimodal ML models. ML prediction reports were provided to oncologists in pdf format with an average turnaround time of seven days from receipt of samples in the labs. Chemotherapy was administered by veterinary oncologists according to the standards used at their treatment sites. Medical records were requested 3 months after delivery of the prediction report and then periodically after that to increase the length of the outcome observation interval. The stopping point for this study was chosen when we estimated that sufficient time had elapsed from the beginning of the enrollment period to assess patient survival in a statistically relevant number of patients.

Tumor biopsy

Fine-needle aspirates (FNAs) from enlarged lymph nodes were collected at oncology clinics and shipped to the ImpriMed testing lab via overnight courier and processed within 24-72 hours of collection. Cells were maintained at a high level of viability during shipping using ImpriMed Transport Media (ImpriMed Inc., Mountain View, CA) that was optimized for this purpose.

Inclusion criteria

For this study, we included dogs with B-cell lymphoma that had relapsed from prior cytotoxic chemotherapy when their oncologists were provided with ML prediction reports. Relapse status was reported to us by participating oncologists or determined by inspection of medical records. We performed immunophenotyping and clonality testing on all tumor samples internally at our A2LA-accredited testing lab. Patients were included in this study that were determined to have a clonal rearrangement of a B-cell receptor using PARR and to have the following immunophenotype using flow cytometry: ($CD21^+$ or $CD79a^+$)$CD34^-CD14^-CD3^-CD5^-$. Only dogs that were treated with 3 or more anticancer drug administrations after reception of the prediction report were included. This final

TABLE 3 Mortality hazard ratios for high matching group patients in a sample of different precision oncology publications.

year	study	HR	95% CI	n patients
2023	Shaya et al. (13)	0.24	0.078–0.76	18
2023	*this study*	0.28	0.14-0.59	60
2019	Sicklick et al. (14)	0.44	0.19-1.1	69
2019	Rodon et al. (15)	0.48	0.28–0.84	69
2022	Louie et al. (16)	0.54	0.28–1.03	80
2019	Rodon et al. (15)	0.56	0.25–1.3	38
2016	Wheler et al. (17)	0.65	0.43–1.0	188
2022	Charo et al. (18)	0.65	0.34 to 1.25	113

inclusion criterion was added to improve the accuracy of the matching scores by guaranteeing a minimal sample size for the calculation. Cohort selection statistics are shown in Supplementary Figure 1. The patients who met all of these inclusion criteria had prediction reports delivered to oncologists on their behalf between June 26th, 2020 and November 1st, 2022. Biopsy samples and medical records for patients in the study cohort were provided by 31 veterinarians at 29 clinics in 14 states. Of the 31 veterinarians, 29 were board-certified oncologists, 1 was an oncology resident, and 1 was a general practitioner.

Tumor profiling

The sensitivity of live tumor cells to 13 different drugs was quantified using a high-throughput ex vivo assay as previously described (3). Tumor cells were profiled at the single-cell level using multicolor flow cytometry and a panel of 9 primary antibodies as previously described (3).

Collection of clinical information

Baseline patient characteristics (Supplementary Table 1) were collected at the time of biopsy or soon afterwards from service request forms or a web portal. Tumor grades were determined by individual oncology practices and may refer to cytology or histopathology results. Patient medical charts and electronic health record exports were emailed to us by oncology clinics three months or more after the biopsy date. Medical records were inspected and drug treatments, tumor responses, and death/euthanasia events were manually entered into spreadsheets. Tumor response annotations were classified into four categories progressive disease (PD), stable disease (SD), partial response (PR), or complete response (CR). We found that some clinicians used RECIST (20) to objectively assign response categories while others recorded qualitative clinical assessments. Medical records collected and analyzed in this fashion were used both to create clinical outcome labels for training ML models and to quantify health outcomes occurring after delivery of ML predictions.

ML model development

Binary drug response labels were generated from medical records as previously described (3). Briefly, drug treatments followed by SD or PD clinical tumor responses were assigned a value of 0 and drug treatments followed PR or CR were assigned a value of 1. ML models were trained to predict the binary drug response labels for a set of commonly used drugs using features from flow cytometry and ex vivo drug sensitivity assays as previously described (3). Models were updated periodically over the course of the study by retraining existing models with additional data (continual ML) and by adding models for drugs that had previously lacked sufficient data for model development. Continuous accrual of additional training samples was a consequence of our open cohort study design and resulted in an increasing number of samples independently and identically drawn from the same population of dogs. The first generation of models was trained to predict clinical outcomes for 7 different chemotherapy drugs using training data from 463 dogs with known clinical outcomes. During this study, the number of individual drug prediction models increased to 10 and the number of training samples increased to 842 dogs. The models in release v1.0 were random forest models generated using the caret (21) and ranger (22) libraries. The models in releases v2.0 and above were generated using the scikit-learn (23), BayesOpt (24), XGBoost (25), and imbalanced-learn (26) libraries and were either random forest models, elastic net logistic regression models, or voting ensembles composed of multiple different ML models. Predictions for the low and high matching groups were evenly distributed in time, resulting in a similar utilization of the different model versions in the two matching groups (Supplementary Figure 3).

Matching score calculation

Matching score was determined by calculating the percentage of the drug treatments received by a dog that corresponded to drugs with a prediction score above 0.5 in the prediction report:

$$matching\ score = 100 \times \frac{treatments\ with\ prediction\ score > 0.5}{total\ number\ of\ treatments}$$

Only treatments occurring after delivery of the prediction report were included in the calculation. For the purposes of this analysis, a treatment was defined as a 1 week course of a drug that was administered more than once per week, or a single administration of a drug that was given weekly or at lower frequency. To illustrate calculation of the matching score, consider a dog that received 6 weeks of prednisone treatments given twice per week, and 2 infusions of rabacfosadine (trade name Tanovea-CA1) separated by a three week interval. If the dog's prediction scores for prednisone and rabacfosadine were 0.3 and 0.7 respectively, then the dog received 2 rabacfosadine treatments that matched the ML predictions and 6 prednisone treatments that did not match the ML predictions for a total of 8 treatments. Thus, the matching score for this dog would be 100 * 2/8 = 25%.

Our matching score calculation was slightly different than the calculation most frequently found in the precision oncology literature (13–18). We introduced a modification to the calculation to prevent the score from biasing our outcome statistics towards positive clinical outcomes in the high matching group. Matching score is typically calculated by dividing the number of drugs given that match actionable biomarkers by the total number of actionable biomarkers. When we implemented this standard matching score for our study, we discovered that the high matching group experienced better clinical outcomes even when we shuffled the drug recommendations. In retrospect, it is easy to see why the standard matching score calculation introduces a bias

towards positive clinical outcomes in the high matching group. Patients who lived longer tended to receive a greater number of different drugs by virtue of the fact that the oncologist had more time for empirical therapy (i.e. to try more drugs). Thus, any matching score that rewards the total number of drugs administered will bias towards healthier patients regardless of the performance of the precision oncology platform. We eliminated this inherent bias by including the total number of drugs administered in the denominator of our calculation.

Dichotomization by matching score

Several methods were found in the precision oncology literature for choosing the threshold value used to dichotomize the study cohort into low matching and high matching groups. In the studies we examined, four used the arbitrary threshold value of 50% (13, 14, 16, 27), three adjusted the threshold to create the greatest difference in outcomes between the high and low matching groups (14, 15, 18), and one study used the median matching score (17). We chose the median matching score as the threshold for dichotomization of our cohort because this method offers no opportunity for investigator bias introduced by testing multiple hypotheses about the appropriate threshold value. The clinical outcome advantage associated with higher matching scores was not dependent on the method of dichotomization (Supplementary Figure 4).

Analysis of clinical outcomes

Clinical outcomes data were analyzed using custom Python scripts and statistical functions from Python libraries. Supplementary Table 1 was automatically generated using the TableOne library (28). The lifelines library (29) was used for Kaplan-Meier statistics and logrank testing. The scipy library (30) was used to compute Fisher's exact test. The statsmodels (31) library was used to calculate the two-sample Z-test and Benjamini-Hochberg corrections.

Cox proportional hazards modeling

The lifelines library (29) was used for univariate and multivariate Cox regression. Confounding variables were chosen based on prior evidence of prognostic significance. The proportional hazards assumption of time invariance was verified for each variable using the check_assumptions() method of the CoxPHFitter class. Models were fit using default parameters for the CoxhPHFitter class (baseline_estimation_method = 'breslow', penalizer = 0.0, strata = None, l1_ratio = 0.0, n_baseline_knots = None, knots = None, breakpoints = None). Confidence intervals and p-values were generated by CoxhPHFitter during model fitting. Concordance for the multivariate model was 0.62. Concordance values for univariate models are shown in Table 1.

Estimation of survival after relapse for historical control

We estimated that the historical median survival time after initiation of rescue therapy is roughly 110 days by subtracting median time to relapse from median overall survival time [the mean values from 14 published studies were used to derive this estimate (19)].

Data availability statement

The raw data supporting the conclusions of this article will be made available by the authors, without undue reservation.

Ethics statement

The animal studies were approved by the Institutional Review Board and/or Ethics Committee of the BluePearl Science and SAGE Veterinary Centers (protocol code IMVLSA1223.18). The studies were conducted in accordance with the local legislation and institutional requirements. Written informed consent was obtained from the owners for the participation of their animals in this study.

Author contributions

AC: Conceptualization, Data curation, Formal analysis, Investigation, Methodology, Software, Visualization, Writing – original draft, Writing – review & editing. JT: Investigation, Methodology, Writing – review & editing. SP: Data curation, Project administration, Writing – review & editing. DS: Data curation, Writing – review & editing. SK: Investigation, Methodology, Writing – review & editing. KC: Conceptualization, Investigation, Methodology, Writing – review & editing. SL: Conceptualization, Data curation, Funding acquisition, Investigation, Methodology, Project administration, Resources, Supervision, Writing – review & editing.

Funding

The author(s) declare that no financial support was received for the research, authorship, and/or publication of this article.

Acknowledgments

We would like to thank the following doctors for providing tumor samples and medical records used in this study: KC (Seattle Veterinary Specialists Blue Pearl Kirkland, WA), Dr. Christine Oakley (Veterinary Cancer Group of San Fernando Valley, CA),

Dr. Naoko Sogame (SAGE Redwood Veterinary Centers, CA), Dr. Carrie DeRegis (Pieper Veterinary Middletown, CT), Dr. Conor McNeill (Hope Advanced Veterinary Center, VA), Dr. Sarah Collette (Upstate Vet Emergency + Specialty Asheville, NC), Dr. Crystal Garnett (VCA Animal Specialty Group San Diego, CA), Dr. Christine Swanson (BluePearl Pet Hospital Grand Rapids, MI), Dr. Krystal Harris (Central Texas Veterinary Specialty & Emergency Hospital Round Rock, TX), Dr. Kelly Carlsten (Bridger Veterinary Specialists, MT), Dr. David Heller (VCA California Veterinary Specialists Ontario, CA), Dr. Emi Ohashi (VCA Animal Specialty Group, CA), Dr. Evan Sones (Animal Cancer Care Clinic Orlando, FL), Dr. Ivan Martinez (Upstate Vet Emergency + Specialty Greenville, SC), Dr. Jennifer Baez (BluePearl Pet Hospital Langhorne, PA), Dr. Lisa Parshley (Olympia Veterinary Specialists, WA), Dr. Ian Muldowney (Fetch Specialty and Cancer Veterinary Centers, FL), Dr. Dana Connell (Upstate Vet Emergency + Specialty Asheville, NC), Dr. Gabrielle Carter (VCA California Veterinary Specialists Carlsbad, CA), Dr. Sara Fiocchi (Veterinary Cancer Group Orange County, CA), Dr. Cecile Siedlecki (PETS Referral Center, CA), Dr. Bonnie Smith (Veterinary Specialty Services Manchester, MO), Dr. Avenelle Turner (Metropolitan Animal Specialty Hospital, CA), Dr. Erica Faulhaber (Four Seasons Veterinary Specialists, CO), Dr. David Proulx (VCA California Veterinary Specialists Carlsbad, CA), Dr. Karen Oberthaler (Treeline Veterinary Cancer Care, CO), Dr. Amanda Smith (Bridge Animal Referral Center, WA), Dr. Theresa Arteaga (Animal Cancer Center, CA), Dr. Sarah McMillan (Hope Advanced Veterinary Center, VA), Dr. Suzanne Rau (Metropolitan Veterinary Associates, CA), Dr. Mary Klein (Southwest Veterinary Oncology, AZ).

Conflict of interest

The technology reported on here has been commercialized by ImpriMed, Inc. AC, JT, SP, SK, and SL are employees of ImpriMed. DS is an independent contractor for ImpriMed and KC is a consultant for ImpriMed.

Publisher's note

Supplementary material

The Supplementary Material for this article can be found online at: https://www.frontiersin.org/articles/10.3389/fonc.2024.1304144/full#supplementary-material

References

1. Morton LM, Wang SS, Devesa SS, Hartge P, Weisenburger DD, Linet MS. Lymphoma incidence patterns by WHO subtype in the United States, 1992-2001. *Blood* (2006) 107:265–76. doi: 10.1182/blood-2005-06-2508

2. Vail DM, Thamm DH, Liptak JM. Hematopoietic tumors. *Withrow and MacEwen's Small Animal Clinical Oncology (6th Edition).* (2019), 688–772. doi: 10.1016/B978-0-323-59496-7.00033-5

3. Bohannan Z, Pudupakam RS, Koo J, Horwitz H, Tsang J, Polley A, et al. Predicting likelihood of *in vivo* chemotherapy response in canine lymphoma using ex vivo drug sensitivity and immunophenotyping data in a machine learning model. *Vet Comp Oncol* (2021) 19:160–71. doi: 10.1111/vco.12656

4. Riondato F, Comazzi S. Flow cytometry in the diagnosis of canine B-cell lymphoma. *Front Vet Sci* (2021) 8:600986. doi: 10.3389/fvets.2021.600986

5. Comazzi S, Riondato F. Flow cytometry in the diagnosis of canine T-cell lymphoma. *Front Vet Sci* (2021) 8:252. doi: 10.3389/fvets.2021.600963

6. Blom K, Nygren P, Alvarsson J, Larsson R, Andersson CR. Ex vivo assessment of drug activity in patient tumor cells as a basis for tailored cancer therapy. *SLAS Technol* (2016) 21:178–87. doi: 10.1177/2211068215598117

7. Blom K, Nygren P, Larsson R, Andersson CR. Predictive value of ex vivo chemosensitivity assays for individualized cancer chemotherapy: A meta-analysis. *SLAS Technol* (2017) 22:306–14. doi: 10.1177/2472630316686297

8. Koo J, Choi K, Lee P, Polley A, Pudupakam RS, Tsang J, et al. Predicting dynamic clinical outcomes of the chemotherapy for canine lymphoma patients using a machine learning model. *Vet Sci* (2021) 8:301. doi: 10.3390/vetsci8120301

9. Acosta JN, Falcone GJ, Rajpurkar P, Topol EJ. Multimodal biomedical AI. *Nat Med* (2022) 28:1773–84. doi: 10.1038/s41591-022-01981-2

10. Boehm KM, Khosravi P, Vanguri R, Gao J, Shah SP. Harnessing multimodal data integration to advance precision oncology. *Nat Rev Cancer* (2022) 22:114–26. doi: 10.1038/s41568-021-00408-3

11. Perez-Lopez R, Reis-Filho JS, Kather JN. A framework for artificial intelligence in cancer research and precision oncology. *NPJ Precis Oncol* (2023) 7:1–3. doi: 10.1038/s41698-023-00383-y

12. Zandvliet M. Canine lymphoma: a review. *Vet Q* (2016) 36:76–104. doi: 10.1080/01652176.2016.1152633

13. Shaya J, Kato S, Adashek JJ, Patel H, Fanta PT, Botta GP, et al. Personalized matched targeted therapy in advanced pancreatic cancer: a pilot cohort analysis. *NPJ Genomic Med* (2023) 8:1–8. doi: 10.1038/s41525-022-00346-5

14. Sicklick JK, Kato S, Okamura R, Schwaederle M, Hahn ME, Williams CB, et al. Molecular profiling of cancer patients enables personalized combination therapy: the I-PREDICT study. *Nat Med* (2019) 25:744–50. doi: 10.1038/s41591-019-0407-5

15. Rodon J, Soria J, Berger R, Miller WH, Rubin E, Kugel A, et al. Genomic and transcriptomic profiling expands precision cancer medicine: the WINTHER trial. *Nat Med* (2019) 25:751–8. doi: 10.1038/s41591-019-0424-4

16. Louie BH, Kato S, Kim KH, Jeong Lim LJ, Okamura R, Eskander RN, et al. Pan-cancer molecular tumor board experience with biomarker-driven precision immunotherapy. *NPJ Precis Oncol* (2022) 6:1–8. doi: 10.1038/s41698-022-00309-0

17. Wheler JJ, Janku F, Naing A, Li Y, Stephen B, Zinner R, et al. Cancer therapy directed by comprehensive genomic profiling: A single center study. *Cancer Res* (2016) 76:3690–701. doi: 10.1158/0008-5472.CAN-15-3043

18. Charo LM, Eskander RN, Sicklick J, Kim KH, Lim HJ, Okamura R, et al. Real-world data from a molecular tumor board: improved outcomes in breast and gynecologic cancers patients with precision medicine. *JCO Precis Oncol* (2022) 6: e2000508. doi: 10.1200/PO.20.00508

19. Bennett P, Williamson P, Taylor R. Review of canine lymphoma treated with chemotherapy—Outcomes and prognostic factors. *Vet Sci* (2023) 10:342. doi: 10.3390/vetsci10050342

20. Nguyen SM, Thamm DH, Vail DM, London CA. Response evaluation criteria for solid tumours in dogs (v1.0): a Veterinary Cooperative Oncology Group (VCOG) consensus document. *Vet Comp Oncol* (2015) 13:176–83. doi: 10.1111/vco.12032

21. Kuhn M. Building predictive models in R using the caret package. *J Stat Software* (2008) 28:1–26. doi: 10.18637/jss.v028.i05

22. Wright MN, Ziegler A. ranger: A fast implementation of random forests for high dimensional data in C++ and R. *J Stat Software* (2017) 77:1–17. doi: 10.18637/jss.v077.i01

23. Pedregosa F, Varoquaux F, Gramfort A, Michel V, Thirion B, Grisel O, et al. Scikit-learn: machine learning in python. *J Mach Learn Res* (2011) 12:2825–30. doi: 10.48550/arXiv.1201.0490

24. Martinez-Cantin R. BayesOpt: a Bayesian optimization library for nonlinear optimization, experimental design and bandits. *J Mach Learn Res* (2014) 15:3735–9.

25. Chen T, Guestrin C. XGBoost: A scalable tree boosting system, in: *Proceedings of the 22nd ACM SIGKDD International Conference on Knowledge Discovery and Data Mining 785–794 (Association for Computing Machinery, 2016)* (2016) San Francisco: KDD, Knowledge Discovery and Data Mining. doi: 10.1145/2939672.2939785

26. Lemaitre G, Nogueira F, Aridas CK. "Imbalanced-learn: a python toolbox to tackle the curse of imbalanced datasets in machine learning." *J Mach Learn Res* (2017) 18(17):1–5.

27. Kato S, Kim K, Lim HJ, Boichard A, Nikanjam M, Weihe E, et al. Real-world data from a molecular tumor board demonstrates improved outcomes with a precision N-of-One strategy. *Nat Commun* (2020) 11:4965. doi: 10.1038/s41467-020-18613-3

28. Pollard TJ, Johnson AEW, Raffa JD, Mark RG. tableone: An open source Python package for producing summary statistics for research papers. *JAMIA Open* (2018) 1:26–31. doi: 10.1093/jamiaopen/ooy012

29. Davidson-Pilon C. lifelines: survival analysis in Python. *J Open Source Software* (2019) 4:1317. doi: 10.21105/joss.01317

30. Virtanen P, Gommers R, Oliphant TE, Haberland M, Reddy T, Cournapeau D, et al. SciPy 1.0: fundamental algorithms for scientific computing in Python. *Nat Methods* (2020) 17:261–72. doi: 10.1038/s41592-019-0686-2

31. Seabold S, Perktold J. Statsmodels: econometric and statistical modeling with python. *Proc 9th Python Sci Conf* (2010), 92–6. doi: 10.25080/Majora-92bf1922-011

frontiers | Frontiers in Oncology

TYPE Original Research
PUBLISHED 12 February 2024
DOI 10.3389/fonc.2024.1363385

OPEN ACCESS

EDITED BY
Shimin Hu,
University of Texas MD Anderson Cancer Center, United States

REVIEWED BY
Yi Miao,
Nanjing Medical University, China
Shih-Sung Chuang,
Chi Mei Medical Center, Taiwan

*CORRESPONDENCE
Jin Seok Kim
hemakim@yuhs.ac

RECEIVED 30 December 2023
ACCEPTED 29 January 2024
PUBLISHED 12 February 2024

CITATION
Kim YR, Shin HJ, Yhim H-Y, Yang D-H, Park Y, Lee JH, Lee W-S, Do YR, Mun Y-C, Kim DS and Kim JS (2024) Clinical significance of bone marrow involvement by immunoglobulin gene rearrangement in *de novo* diffuse large B-cell lymphoma: a multicenter retrospective study. *Front. Oncol.* 14:1363385. doi: 10.3389/fonc.2024.1363385

Clinical significance of bone marrow involvement by immunoglobulin gene rearrangement in *de novo* diffuse large B-cell lymphoma: a multicenter retrospective study

Yu Ri Kim[1], Ho Jin Shin[2], Ho-Young Yhim[3], Deok-Hwan Yang[4], Yong Park[5], Ji Hyun Lee[6], Won-Sik Lee[7], Young Rok Do[8], Yeung-Chul Mun[9], Dae Sik Kim[10] and Jin Seok Kim[11]*

[1]Division of Hematology, Department of Internal Medicine, Yonsei University College of Medicine, Gangnam Severance Hospital, Seoul, Republic of Korea, [2]Division of Haematology-Oncology, Department of Internal Medicine, Pusan National University School of Medicine, Busan, Republic of Korea, [3]Division of Haematology-Oncology, Department of Internal Medicine, Jeonbuk National University Medical School, Jeonju, Republic of Korea, [4]Division of Haematology-Oncology, Department of Internal Medicine, Chonnam National University Hwasun Hospital, Jeollanam-do, Republic of Korea, [5]Division of Hematology-Oncology, Department of Internal Medicine, Korea University Anam Hospital, Seoul, Republic of Korea, [6]Department of Internal Medicine, Dong-A University College of Medicine, Busan, Republic of Korea, [7]Division of Haematology-Oncology, Department of Internal Medicine, Inje University Busan Paik Hospital, Busan, Republic of Korea, [8]Division of Hemato-Oncology, Department of Internal Medicine, Keimyung University Dongsan Medical Center, Daegu, Republic of Korea, [9]Department of Internal Medicine, Ewha Women's University College of Medicine, Seoul, Republic of Korea, [10]Division of Hematology-Oncology, Department of Internal Medicine, Korea University Guro Hospital, Seoul, Republic of Korea, [11]Division of Hematology, Department of Internal Medicine, Yonsei University College of Medicine, Severance Hospital, Seoul, Republic of Korea

Background: Bone marrow (BM) involvement is an indicator of a poor prognosis in diffuse large B-cell lymphoma (DLBCL); however, few studies have evaluated the role of immunoglobulin gene rearrangement (IgR) in detecting BM involvement.

Methods: We evaluated the clinical characteristics and treatment outcomes of patients with DLBCL based on histological BM involvement or positive BM IgR using polymerase chain reaction or next-generation sequencing. We also investigated the role of consolidative upfront autologous hematopoietic stem cell transplantation (ASCT) in patients with DLBCL and BM involvement.

Results: Among 624 patients, 123 (19.7%) with histological BM involvement and 88 (17.5%) with positive IgR in histologically negative BM had more advanced disease characteristics. Overall (OS) and progression-free (PFS) survival was better for patients with negative BM histology and negative IgR than that in patients with histological BM involvement ($P = 0.050$ and $P < 0.001$, respectively) and positive IgR with negative BM histology ($P = 0.001$ and $P = 0.005$, respectively). Survival rates did not differ among 82 (13.1%) patients who were treated with upfront ASCT and had histological BM involvement or positive IgR with negative BM histology. The survival outcomes were worse for patients who

were not treated with upfront ASCT and for those with histological BM involvement or positive IgR, than for those with negative BM histology and negative IgR.

Conclusion: Patients diagnosed with DLBCL and BM involvement based on histology or IgR had aggressive clinical features and poor survival. Upfront ASCT mitigated poor prognosis due to BM involvement.

KEYWORDS

diffuse large B-cell lymphoma, bone marrow involvement, immunoglobulin gene rearrangement, progression-free survival, transplantation

1 Introduction

Although the treatment outcomes of diffuse large B-cell lymphoma (DLBCL) have improved with the development of new drugs, relapse is frequent and associated with dismal outcomes (1, 2). Bone marrow (BM) involvement is classified as extranodal and stage 4, which increases the international prognostic index (IPI) and is directly linked to shorter survival (3–5). The reported incidence of BM involvement is 11%-36% and the classic definition of BM involvement is abnormal lymphoma cells in BM aspirates or biopsies (3, 4, 6). However, minimal BM involvement of malignant lymphoma cells often generates false negative results because a histological diagnosis is very difficult in the absence of significant morphological changes (7–9). Bone marrow involvement can be diagnosed using 18F-FDG PET, but only within a limited range, and diagnostic rates vary depending on the lymphoma subtype (10–13). These problems have been addressed using the polymerase chain reaction (PCR) to detect immunoglobulin gene rearrangement (IgR) in BM samples because B-cell non-Hodgkin lymphoma (NHL) undergoes clonal IgR (9, 14). Clonal immunoglobulin heavy chain (IGH) and kappa chain (IGK) gene rearrangement could help the diagnostic process when histological findings are inconclusive. Moreover, gene rearrangement can be a helpful indicator during follow-up, as well as for diagnoses (15, 16). Patients with negative histological BM can be classified based on whether they test positive for IgR and negative for BM histology which indicates a more accurately determined advanced stage and a poorer prognosis (14, 17). Immunoglobulin gene rearrangement has mostly been detected using PCR; however, next-generation sequencing (NGS) has also been recently used (18). Detecting BM involvement in patients newly diagnosed with DLBCL indicates poor prognosis; to that end, IgR tests have been applied in a few studies to detect BM involvement in patients DLBCL treated with R-CHOP (rituximab, cyclophosphamide, doxorubicin, vincristine, and prednisolone) chemotherapy (14, 19–21).

Patients newly diagnosed with DLBCL accompanied by negative BM histology and poor outcomes of current standard treatment should be tested for IgR to precisely diagnose BM involvement. New treatment approaches should also be applied such as high-intensity chemotherapy to overcome BM involvement as a poor prognostic factor (5). Here, we investigated the clinical characteristics and treatment outcomes of upfront consolidative ASCT as part of a high-intensity chemotherapeutic regimen in patients with DLBCL and BM involvement determined by histological or molecular biological methods.

2 Materials and methods

This study enrolled patients from nine institutions in Korea who were newly diagnosed with DLBCL based on the World Health Organization classification (22) and histological BM involvement between 2010 and 2019. The study was conducted according to the guidelines of the Declaration of Helsinki, and approved by the Institutional Review Board of Severance Hospital (4-2019-0579 Aug 5, 2019) and each institution.

The control group comprised patients from Severance Hospital who were newly diagnosed with DLBCL and were tested for IgR regardless of BM involvement status within the same period. The exclusion criteria were disease transformation from indolent follicular lymphoma, primary central nervous system lymphoma, cutaneous DLBCL, primary mediastinal B-cell lymphoma, and human immunodeficiency virus-associated DLBCL. All patients were administered with R-CHOP as first-line chemotherapy. Upfront consolidative ASCT was considered for patients with Ann Arbor stages III or IV and elevated lactic dehydrogenase (LDH) levels who achieved complete (CR) or partial (PR) remission after R-CHOP chemotherapy. The international prognostic index (IPI) score was calculated as described (23). Responses were assessed based on the Cheson criteria (24).

2.1 Histological diagnosis of bone marrow involvement

We obtained aspirates and BM biopsies from the posterior superior iliac crest from all enrolled patients before starting chemotherapy for DLBCL. Bone marrow involvement was diagnosed based on histological criteria and immunochemical staining for B-cell markers (3, 8). Concordant BM involvement was defined as BM involvement of DLBCL, while discordant involvement was defined as involvement of small and low-grade lymphoma cells (3). The present study investigated only concordant BM involvement. Thirteen patients had discordant BM involvement without DLBCL involvement, and these patients were classified as negative. Cells of origin were classified based on the Hans algorithm using immunochemical staining (25).

2.2 Immunoglobulin gene rearrangement test to diagnose bone marrow involvement

We assessed clonal gene rearrangement in BM aspirates from 504 patients. The assays included BIOMED-2 multiplex primer sets in five master mixes that targeted the IGH and two master mixes that target the IGK locus. Fragment analysis was applied to fluorescence-labeled PCR products using an ABI 3130 DNA sequencer (Thermo Fisher Scientific Inc., Waltham, MA, USA) and GeneMapper 3.2 software (Thermo Fisher Scientific Inc.). Next-generation sequencing (NGS) was applied from April 2017 using LymphoTrack® IGH FR1 and IGK Assays (Invivoscribe Technologies Inc., San Diego, CA, USA). After PCR amplification, libraries were purified using the Agencourt AMPure XP system (Beckman Coulter, Inc., Brea, CA, USA). Quantified libraries were sequenced on a MiSeq system using MiSeq Reagent Kit v2 (Illumina Inc., San Diego, CA, USA). Bioinformatics were analyzed using LymphoTrack® Dx MiSeq Data Analysis version 2.4.3 (Invivoscribe Technologies, Inc.). The cut-offs for clonality and clonotype sequences were determined as described by the manufacturers. We assessed IgR in patients without histological BM involvement. Positive IgR was defined as positive IGH and/or IGK gene rearrangement. The sensitivity of PCR is 10^{-3} and that of NGS is 10^{-4}.

2.3 Statistical analysis

Overall survival (OS) was determined as elapsed time between the dates of diagnosis and death, regardless of the cause. Surviving patients were censored at the last date of follow-up. Progression-free survival (PFS) was defined as elapsed time between the dates of diagnosis to progression, relapse, or death from any cause. Survival was analyzed using Kaplan-Meier curves, and pairs of groups were compared using log-rank tests. A Cox proportional hazard model was used for multivariate analysis. The multicollinearity of all variables in univariate analyses was assessed as tolerance and a variance inflation factor using linear regression analysis. Values with $P < 0.05$ in all analyses were considered statistically significant. All data were statistically analyzed using SPSS for Windows, version 23.0 (IBM Corp., Armonk, NY, USA).

Results

2.4 Patients' characteristics

Among 624 patients newly diagnosed with DLBCL, 123 (19.7%) had histological BM involvement. Among 501 patients without histological BM involvement, 88 (17.5%) were IgR positive, 29 (5.7%) and 26 (5.1%) had positive IGH and IGK rearrangement, respectively, and 33 (6.5%) had rearranged IGH and IGK (Figure 1). Patients with histological BM involvement or positive IgR with negative BM histology tended to be older ($P = 0.02$ and $P < 0.001$, respectively). Moreover, these patients had advanced-stage DLBCL with extranodal involvement at more than one site and elevated LDH, as well as significantly higher IPI scores than patients who were negative for both (Table 1). We tested 276 (55.1%) patients for clonal IgR using PCR. Fifty (50/276, 18.1%) patients showed positive results by PCR, whereas 38 (16.9%) of 225 patients had positive results of NGS. The rates of positivity rates did not significantly differ between the two test methods ($P = 0.814$).

2.5 Treatment outcomes according to bone marrow involvement

Among the registered patients who received R-CHOP chemotherapy as the first-line treatment, 587 responded. A CR was achieved in 465 (79.2%) of 587 evaluable patients, which included 93 (78.2%) of 119) with histological BM involvement. These findings did not significantly differ from those of patients without BM involvement ($P = 0.428$). Meanwhile, 56 (70.0%) of 80 evaluable patients with positive IgR achieved CR. This was significantly lower than the 316 (76.5%) of 388 patients without histologic and molecular BM involvement ($P = 0.032$). The median follow-up was 32 (range: 1-108) months, and the 3-year OS and PFS rates were 80.4% and 69.5%, respectively (Figures 2A, B). The 3-year OS and PFS were 74.9% and 56.0% in patients with histological BM involvement and 72.4% and 62.4% in those with positive IgR and negative BM histology. These were lower than the survival outcomes of patients with negative IgR and BM histology (83.9% and 75.7%, respectively; (Figures 3A, B).

2.6 Treatment outcomes according to autologous hematopoietic stem cell transplantation

Upfront consolidative ASCT was administered to 82 (13.1%) patients after they completed frontline R-CHOP chemotherapy. Among them, 53 (64.6%) had histological BM involvement, 10

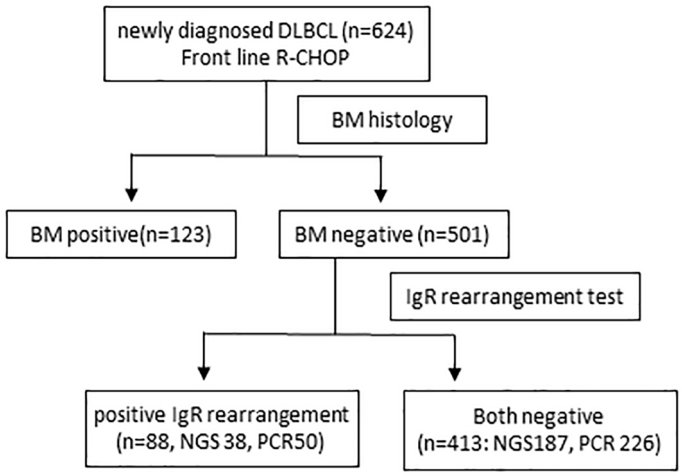

FIGURE 1
Flowchart of patients. BM, bone marrow; DLBCL, diffuse large B-cell lymphoma; IgR, immunoglobulin gene rearrangement R-CHOP, rituximab, cyclophosphamide, doxorubicin, vincristine, and prednisolone.

(12.2%) had positive IgR and negative BM histology, and 19 (23.2%) did not have histological BM involvement and were IgR negative. Treatment outcomes were analyzed according to upfront ASCT in patients with advanced-stage and elevated LDH levels. The OS and PFS rates were better for patients who were administered upfront ASCT than for patients who were not (P = 0.010 and P = 0.004, respectively). The OS and PFS outcomes of patients who received upfront ASCT to minimize selection bias associated with treatment intensity did not significantly differ according to histological BM involvement (P = 0.388 and P = 0.663, respectively) or positive IgR (P = 0.685 and P = 0.528, respectively; Figures 4A, B). The 3-year OS and PFS rates among patients who did not receive upfront ASCT were poorer for those with BM involvement than for those without (65.0% *vs.* 85.1%, P = 0.001, and 49.2% *vs.* 77.0%, P < 0.001, respectively). The OS and PFS rates were also lower for patients with positive IgR than for those without histological BM

TABLE 1 Clinical characteristics of 624 patients according to BM involvement or immunoglobulin gene rearrangement.

Characteristics	BM negative (n=413) No. (%)	BM positive (n=123) No. (%)	Clonal IgR[a] (n=88) No. (%)	Comparison between two factors p-value		
				BM negative vs BM positive	BM negative vs clonal IgR	BM positive vs clonal IgR
Age, median (range) years	61 (19–86)	56 (19–85)	66 (41–89)	0.02	<0.001	<0.001
Male patients	236 (57.1)	64 (52.0)	54 (61.4)	0.352	0.479	0.206
ECOG 2-4	28 (6.8)	28 (22.8)	15 (17.0)	<0.001	0.005	0.387
Stage III or IV	177 (42.9)	123 (100)	58 (65.9)	<0.001	<0.001	<0.001
Extranodal sites >1	114 (27.6)	93 (75.6)	38 (43.2)	<0.001	0.005	<0.001
LDH, elevated	186 (45.0)	110/122 (90.2)	54/88 (61.4)	<0.001	0.007	<0.001
Non-GCB subtype	278 (67.3)	62/93 (66.7)	66/88 (75.0)	0.903	0.166	0.254
DEL	102 (24.7)	21/74 (28.4)	36/88 (40.9)	0.561	0.004	0.102
Upfront ASCT	19 (4.6)	53 (43.1)	10 (11.4)	<0.001	0.022	<0.001
IPI				<0.001	<0.001	<0.001
Low/Low-intermediate	293 (70.9)	26 (21.1)	43 (45.3)			
High-intermediate/High	120 (29.1)	97 (78.9)	52 (54.7)			

[a]This patient was IgR positive and BM histology negative. ASCT, autologous hematopoietic stem cell transplantation.
BM, bone marrow; DEL, double expressor lymphoma; ECOG, Eastern Cooperative Oncology Group;IgR, Immunoglobulin gene rearrangements; GCB, germinal center B-cell; IPI, International prognostic index; LDH, Lactate dehydrogenase.

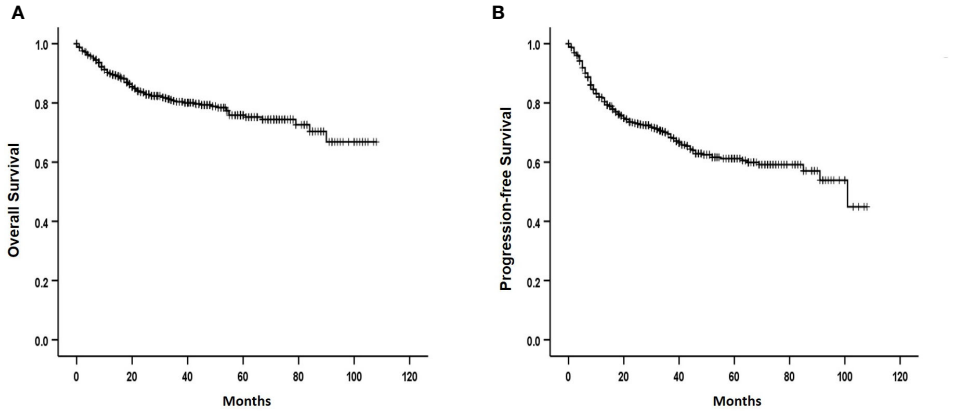

FIGURE 2
Overall **(A)** and progression-free **(B)** survival of patients.

involvement and negative IgR (72.0% *vs.* 85.1%, $P < 0.001$ and 60.6% *vs.* 77.0%, $P < 0.001$, respectively; Figures 4C, D).

2.7 Univariate analysis of prognostic factors associated with poor survival

We assessed the results of the univariate analysis of patients who were not treated with upfront ASCT. The following factors were significantly associated with poor prognosis: age ≥ 60 years, poor performance status, advanced disease stage, involvement of at least one lymph node, elevated LDH, histological BM involvement, positive IgR, non-germinal center B-cell (GCB) subtype, and IPI. The multivariate analysis associated poor OS and PFS with elevated LDH ($P < 0.001$ and $P = 0.001$, respectively), poor performance status ($P = 0.004$ and $P = 0.05$, respectively), and positive IgR ($P = 0.001$ and P = 0.004, respectively; Table 2). In contrast, age was the only prognostic factor among patients who received upfront ASCT (P = 0.001 and P = 0.036, respectively).

3 Discussion

The present study findings revealed that the clinical characteristics of patients with DLBCL and positive IgR in BM samples (besides those with traditional histological BM involvement) who received R-CHOP chemotherapy, resembled those of patients with advanced-stage lymphoma. Moreover, these patients did not respond well to R-CHOP first-line treatment and had poor OS and PFS. Therefore, tests for IgR should be applied to precisely predict the prognosis of patients with negative BM histology.

BM involvement of DLBCL cells showed an unfavorable gene signature, which was related to tumor cell proliferation, migration, and immune escape. These could explain high-risk clinical features and poor prognosis (5). However, differentiating the histological diagnosis of BM involvement of malignant lymphoma cells can be challenging particularly in patients with small amount of lymphoma cells. The IgR test could be helpful under such circumstances. The IgR results were positive in 13%–16% of

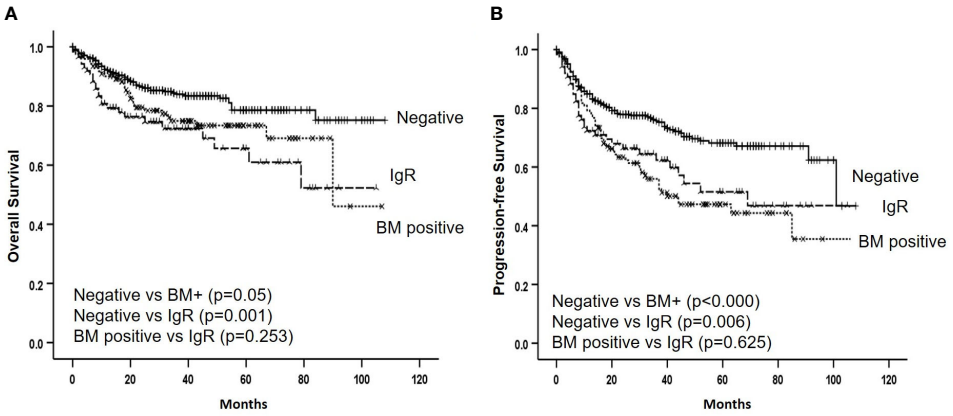

FIGURE 3
Overall **(A)** and progression-free **(B)** survival according to bone marrow involvement by histology and immunoglobulin gene rearrangement. BM, bone marrow, IgR, immunoglobulin gene rearrangement.

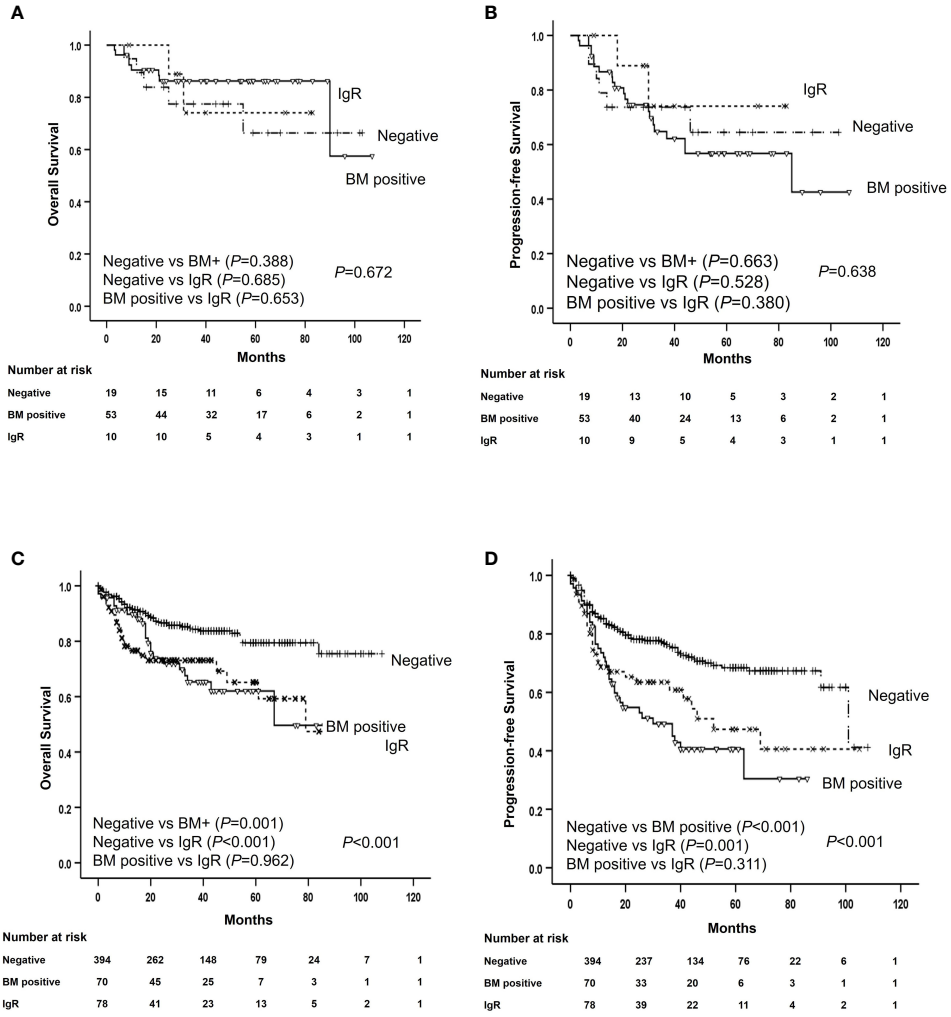

FIGURE 4
Survival of patients with and without ASCT according to histological bone marrow involvement and IGR. Overall and progression-free survival of patients with **(A, B)** and without **(C, D)** ASCT according to histological bone marrow involvement and immunoglobulin gene rearrangement. ASCT, autologous stem cell transplantation; BM, bone marrow; IgR, immunoglobulin gene rearrangement; OS, overall survival; PFS, progression-free survival.

patients with DLBCL who were diagnosed with histologically normal BM and these patients did not survive for long (14, 20). Here, we found positive IgR in 17.5% of patients with negative histological BM involvement, which was similar to previous findings. Without IgR tests, these patients would have been classified as having no BM involvement and the disease stage would have been lowered. Therefore, routine IgR tests of BM samples should be recommended to evaluate the molecular BM involvement of DLBCL cells.

A higher proportion of patients with histological BM involvement had a more advanced disease stage, more frequent extranodal involvement, and more elevated LDH than patients with positive IgR and negative BM histology. Patients with histological BM involvement were classified as having stage 4 disease or a high IPI score at the time of diagnosis. However, patients with positive IgR might not be classified as having an advanced disease stage and might have been down-staged because histological BM involvement was not found. Therefore, the clinical characteristics of patients with histological BM involvement differed from those with only positive IgR with negative BM histology. Nevertheless, we found that the differences in OS and PFS between patients with histological BM involvement and those with positive IgR and negative BM histology were not significant. In addition, the multivariate analysis identified positive IgR as an important prognostic factor associated with poor OS and PFS in patients who were not treated with upfront ASCT.

The most useful tool for assessing clonality in patients with NHL until recently was BIOMED-2 PCR assays. These had been widely used as they were standardized and deemed suitable for technically routine test environments (26). However, PCR is limited by being unsuitable for samples with poor DNA quality, such as formalin-fixed paraffin-embedded (FFPE) samples, which could produce false negative results (15, 18). However, small amplicons and FFPE samples can be analyzed using NGS (18). We compared the ability of PCR and NGS to detect clonality and found no significant differences.

TABLE 2 Prognostic factors of OS and PFS among patients who did not receive upfront ASCT.

	OS		PFS	
Univariate analysis				
Variable	HR (95% CI)	p-value	HR (95% CI)	p-value
Age ≥60	1.890 (1.253-2.852)	0.002	1.683 (1.227-2.308)	0.001
Male	1.026 (0.694-1.516)	0.898	1.287 (0.941-1.760)	0.114
ECOG ≥2	3.474 (2.183-5.531)	<0.001	2.918 (1.973-4.315)	<0.001
Stage 3,4	2.207 (1.463-3.331)	<0.001	3.015 (2.150-4.226)	<0.001
Extranodal >1	2.501 (1.697-3.686)	<0.001	3.067 (2.257-4.167)	<0.001
LDH, elevated	3.706 (2.344-5.860)	<0.001	2.856 (2.046-3.987)	<0.001
BM involvement	1.929 (1.203-3.094)	0.006	2.211 (1.539-3.179)	<0.001
IgR	2.699 (1.752-4.159)	<0.000	2.289 (1.608-3.259)	<0.001
GCB vs non-GCB	1.501 (0.966-2.333)	0.071	1.533 (1.082-2.174)	0.016
DEL	1.149 (0.734-1.799)	0.544	1.066 (0.749-1.517)	0.722
IPI	3.282 (2.202-4.894)	<0.000	3.404 (2.491-4.651)	<0.001
Multivariate analysis				
IgR	2.145 (1.379-3.337)	0.001	1.711 (1.186-2.468)	0.004
LDH, elevated	2.862 (1.760-4.655)	<0.001	1.887 (1.292-2.755)	0.001
ECOG≥2	2.200 (1.379-3.737)	0.004	1.589 (1.000-2.524)	0.050
Extranodal >1			2.128 (1.480-3.061)	<0.001

BM, bone marrow; CI, confidence interval; ECOG, Eastern Cooperative Oncology Group; GCB, Germinal center B-cell; HR, hazard ratio; IgR, Immunoglobulin gene rearrangement; DEL, double expressor lymphoma; IPI, International prognostic index; LDH, lactic dehydrogenase.

Although histological BM involvement is considered a poor prognostic factor, a standardized treatment approach has not yet been established. Furthermore, patients with positive IgR have not been studied. High-intensity chemotherapy, such as fractionated cyclophosphamide, vincristine, doxorubicin, and dexamethasone alternating with high-dose methotrexate and cytarabine (rituximab-hyper-CVAD/MA) or dose-adjusted etoposide, prednisone, vincristine, cyclophosphamide, doxorubicin, and rituximab (EPOCH-R) might overcome poor prognoses, and treatment outcomes are better than those of R-CHOP in high-risk patients with DLCBL (5). Consolidative upfront ASCT might also be considered as a different approach to high-intensity chemotherapy for DLBCL because it can eradicate PCR-detectable NHL cells and consequently reduce recurrence (27). Upfront ASCT in the rituximab era improves PFS in high-risk patients with DLBCL (28, 29). Based on this, we investigated whether upfront ASCT could mitigate the poor prognosis of patients with DLBCL and BM involvement. According to Korean reimbursement guidelines, consolidative upfront ASCT in clinical practice can be recommended for patients with elevated LDH and stage III/IV DLBCL at the time of diagnosis who respond to front-line R-CHOP chemotherapy. However, the present study was retrospective, and as a result, patients with good treatment response and performance might have been selected to receive upfront ASCT. Accordingly, the patients were divided into groups with and without upfront ASCT when analyzing the prognostic factors associated with survival to minimize bias associated with the intensity of treatment. Analysis of all enrolled patients showed that survival was shorter for patients with histological BM involvement or positive IgR with negative BM histology than for those without histological BM involvement and negative IgR. The results of the multivariate analysis showed that patients with poor performance status, elevated LDH, or positive IgR who did not receive upfront ASCT tended to have poor OS and PFS. These results indicated that upfront ASCT plays an important role in overcoming a poor prognosis due to histological BM involvement or positive IgR with negative BM histology. The routine application of upfront ASCT consolidation after R-CHOP is not considered standard care in all countries. However, we suggest that upfront ASCT for high-risk patients with DLBCL and BM involvement should be considered at least in those countries with access to novel target agents.

This study had the following limitations. First, this was a retrospective study and not a prospective randomized study. To overcome this limitation, we registered as many patients as possible from nine institutions in Korea. Another limitation was the absence of regular follow-up data for IgR tests, although they were applied at the time of diagnosis. Based on the concept of minimal residual disease, follow-up tests for IgR are underway and will be examined through further follow-up studies. Although IgR tests could not discriminate infiltration by a high- or low-grade component, the poor prognostic impact of IgR positivity for patients with DLBCL nevertheless generated meaningful information. Despite these

limitations, our findings were meaningful insofar as we used PCR and NGS to investigate the role of IgR, in addition to histological BM involvement, in a large cohort of patients with DLBCL and analyzed their clinical characteristics and treatment outcomes.

In conclusion, tests to detect IgR BM allowed a more detailed classification of the prognosis of patients who were negative for histological BM involvement. Patients who did not receive upfront ASCT could not overcome the poor prognosis associated with BM involvement. Our results suggested that ASCT could mitigate the poor prognosis of not only patients with histological BM involvement but also those with positive IgR and negative BM histology. Accordingly, these findings require validation through future prospective studies.

Data availability statement

The raw data supporting the conclusions of this article will be made available by the authors, without undue reservation.

Ethics statement

The studies involving humans were approved by Ethical Review Committee of Severance Hospital. The studies were conducted in accordance with the local legislation and institutional requirements. The ethics committee/institutional review board waived the requirement of written informed consent for participation from the participants or the participants' legal guardians/next of kin because this is a retrospective cohort study.

Author contributions

YK: Conceptualization, Data curation, Formal analysis, Funding acquisition, Investigation, Methodology, Resources, Software, Validation, Visualization, Writing – original draft, Writing – review & editing. HS: Data curation, Resources, Writing – original draft, Writing – review & editing. H-YY: Data curation, Resources, Writing – original draft, Writing – review & editing. D-HY: Data curation, Resources, Writing – original draft, Writing – review & editing. YP: Data curation, Resources, Writing – original draft, Writing – review & editing. JL: Data curation, Resources, Writing – original draft, Writing – review & editing. W-SL: Data curation, Resources, Writing – original draft, Writing – review & editing. YD: Data curation, Resources, Writing – original draft, Writing – review & editing. Y-CM: Data curation, Resources, Writing – original draft, Writing – review & editing. DK: Data curation, Resources, Writing – original draft, Writing – review & editing. JK: Conceptualization, Data curation, Formal analysis, Funding acquisition, Investigation, Methodology, Project administration, Resources, Software, Supervision, Validation, Visualization, Writing – original draft, Writing – review & editing.

Funding

The author(s) declare financial support was received for the research, authorship, and/or publication of this article. This work was supported by the National Research Foundation of Korea(NRF) grant funded by the Ministry of Science and ICT of Korea (No. NRF-2022R1A2C1013495). This study was supported by a faculty research grant of Yonsei University College of Medicine (6–2020–0092).

Acknowledgments

The authors acknowledge the patients, medical staff, and physicians who participated in this study.

Conflict of interest

The authors declare that the research was conducted in the absence of any commercial or financial relationships that could be construed as a potential conflict of interest.

Publisher's note

References

1. Pfreundschuh M, Kuhnt E, Trümper L, Osterborg A, Trneny M, Shepherd L, et al. CHOP-like chemotherapy with or without rituximab in young patients with good-prognosis diffuse large-B-cell lymphoma: 6-year results of an open-label randomised study of the MabThera International Trial (MInT) Group. *Lancet Oncol* (2011) 12 (11):1013–22. doi: 10.1016/S1470-2045(11)70235-2

2. Coiffier B, Thieblemont C, Van Den Neste E, Lepeu G, Plantier I, Castaigne S, et al. Long-term outcome of patients in the LNH-98.5 trial, the first randomized study comparing rituximab-CHOP to standard CHOP chemotherapy in DLBCL patients: a study by the Groupe d'Etudes des Lymphomes de l'adulte. *Blood* (2010) 116(12):2040–5. doi: 10.1182/blood-2010-03-276246

3. Sehn LH, Scott DW, Chhanabhai M, Berry B, Ruskova A, Berkahn L, et al. Impact of concordant and discordant bone marrow involvement on outcome in diffuse large B-cell lymphoma treated with R-CHOP. *J Clin Oncol* (2011) 29(11):1452–7. doi: 10.1200/JCO.2010.33.3419

4. Campbell J, Seymour JF, Matthews J, Wolf M, Stone J, Juneja S. The prognostic impact of bone marrow involvement in patients with diffuse large cell lymphoma varies according to the degree of infiltration and presence of discordant marrow involvement. *Eur J Haematol* (2006) 76(6):473–80. doi: 10.1111/j.1600-0609.2006.00644.x

5. Yao Z, Deng L, Xu-Monette ZY, Manyam GC, Jain P, Tzankov A, et al. Concordant bone marrow involvement of diffuse large B-cell lymphoma represents a

distinct clinical and biological entity in the era of immunotherapy. *Leukemia* (2018) 32 (2):353–63. doi: 10.1038/leu.2017.222

6. Chung R, Lai R, Wei P, Lee J, Hanson J, Belch AR, et al. Concordant but not discordant bone marrow involvement in diffuse large B-cell lymphoma predicts a poor clinical outcome independent of the International Prognostic Index. *Blood* (2007) 110 (4):1278–82. doi: 10.1182/blood-2007-01-070300

7. Wang J, Weiss LM, Chang KL, Slovak ML, Gaal K, Forman SJ, et al. Diagnostic utility of bilateral bone marrow examination: significance of morphologic and ancillary technique study in Malignancy. *Cancer* (2002) 94(5):1522–31. doi: 10.1002/cncr.10364

8. Conlan MG, Bast M, Armitage JO, Weisenburger DD. Bone marrow involvement by non-Hodgkin's lymphoma: the clinical significance of morphologic discordance between the lymph node and bone marrow. *Nebraska Lymphoma Study Group J Clin Oncol* (1990) 8(7):1163–72. doi: 10.1200/JCO.1990.8.7.1163

9. Talaulikar D, Dahlstrom JE. Staging bone marrow in diffuse large B-cell lymphoma: the role of ancillary investigations. *Pathology* (2009) 41(3):214–22. doi: 10.1080/00313020902756295

10. Elstrom R, Guan L, Baker G, Nakhoda K, Vergilio JA, Zhuang H, et al. Utility of FDG-PET scanning in lymphoma by WHO classification. *Blood* (2003) 101(10):3875–6. doi: 10.1182/blood-2002-09-2778

11. Pakos EE, Fotopoulos AD, Ioannidis JP. 18F-FDG PET for evaluation of bone marrow infiltration in staging of lymphoma: a meta-analysis. *J Nucl Med* (2005) 46 (6):958–63.

12. Adams HJ, Kwee TC, Fijnheer R, Dubois SV, Nievelstein RA, de Klerk JM. Bone marrow 18F-fluoro-2-deoxy-D-glucose positron emission tomography/computed tomography cannot replace bone marrow biopsy in diffuse large B-cell lymphoma. *Am J Hematol* (2014) 89(7):726–31. doi: 10.1002/ajh.23730

13. Yoo KH. Staging and response assessment of lymphoma: a brief review of the Lugano classification and the role of FDG-PET/CT. *Blood Res* (2022) 57(S1):75–8. doi: 10.5045/br.2022.2022055

14. Mitterbauer-Hohendanner G, Mannhalter C, Winkler K, Mitterbauer M, Skrabs C, Chott A, et al. Prognostic significance of molecular staging by PCR-amplification of immunoglobulin gene rearrangements in diffuse large B-cell lymphoma (DLBCL). *Leukemia* (2004) 18(6):1102–7. doi: 10.1038/sj.leu.2403376

15. Langerak AW, van Krieken JH, Wolvers-Tettero IL, Kerkhof E, Mulder AH, Vrints LW, et al. The role of molecular analysis of immunoglobulin and T cell receptor gene rearrangements in the diagnosis of lymphoproliferative disorders. *J Clin Pathol* (2001) 54(7):565–7. doi: 10.1136/jcp.54.7.565

16. Arnold A, Cossman J, Bakhshi A, Jaffe ES, Waldmann TA, Korsmeyer SJ. Immunoglobulin-gene rearrangements as unique clonal markers in human lymphoid neoplasms. *N Engl J Med* (1983) 309(26):1593–9. doi: 10.1056/NEJM198312293092601

17. Kokovic I, Jezersek Novakovic B, Novakovic S. Diagnostic value of immunoglobulin kappa light chain gene rearrangement analysis in B-cell lymphomas. *Int J Oncol* (2015) 46(3):953–62. doi: 10.3892/ijo.2014.2790

18. Scheijen B, Meijers RWJ, Rijntjes J, van der Klift MY, Möbs M, Steinhilber J, et al. Next-generation sequencing of immunoglobulin gene rearrangements for clonality assessment: a technical feasibility study by EuroClonality-NGS. *Leukemia* (2019) 33 (9):2227–40. doi: 10.1038/s41375-019-0508-7

19. Seo JY, Hong J, Chun K, Jeong J, Cho H, Kim KH, et al. Prognostic significance of PCR-based molecular staging in patients with diffuse large B-cell lymphoma treated with R-CHOP immunochemotherapy. *Leuk Lymphoma* (2017) 58(2):357–65. doi: 10.1080/10428194.2016.1190967

20. Arima H, Maruoka H, Nasu K, Tabata S, Kurata M, Matsushita A, et al. Impact of occult bone marrow involvement on the outcome of rituximab plus cyclophosphamide, doxorubicin, vincristine and prednisone therapy for diffuse large B-cell lymphoma. *Leuk Lymphoma* (2013) 54(12):2645–53. doi: 10.3109/10428194.2013.788697

21. Kang YH, Park CJ, Seo EJ, Huh J, Kim SB, Kang YK, et al. Polymerase chain reaction-based diagnosis of bone marrow involvement in 170 cases of non-Hodgkin lymphoma. *Cancer* (2002) 94(12):3073–82. doi: 10.1002/cncr.10584

22. Swerdlow SH, Campo E, Harris NL, Jaffe ES, Pileri SA, Stein H, et al. *WHO Classification of Tumours of Haematopoietic and Lymphoid Tissues. 4th ed*. International Agency for Research on Cancer (2008).

23. International Non-Hodgkin's Lymphoma Prognostic Factors Project. A predictive model for aggressive non-Hodgkin's lymphoma. *N Engl J Med* (1993) 329 (14):987–94. doi: 10.1056/NEJM199309303291402

24. Cheson BD, Fisher RI, Barrington SF, Cavalli F, Schwartz LH, Zucca E, et al. Recommendations for initial evaluation, staging, and response assessment of Hodgkin and non-Hodgkin lymphoma: the Lugano classification. *J Clin Oncol* (2014) 32 (27):3059–68. doi: 10.1200/JCO.2013.54.8800

25. Hans CP, Weisenburger DD, Greiner TC, Gascoyne RD, Delabie J, Ott G, et al. Confirmation of the molecular classification of diffuse large B-cell lymphoma by immunohistochemistry using a tissue microarray. *Blood* (2004) 103(1):275–82. doi: 10.1182/blood-2003-05-1545

26. Langerak AW, Groenen PJ, Brüggemann M, Beldjord K, Bellan C, Bonello L, et al. EuroClonality/BIOMED-2 guidelines for interpretation and reporting of Ig/TCR clonality testing in suspected lymphoproliferations. *Leukemia* (2012) 26(10):2159–71. doi: 10.1038/leu.2012.246

27. Zwicky CS, Maddocks AB, Andersen N, Gribben JG. Eradication of polymerase chain reaction detectable immunoglobulin gene rearrangement in non-Hodgkin's lymphoma is associated with decreased relapse after autologous bone marrow transplantation. *Blood* (1996) 88(9):3314–22. doi: 10.1182/blood.V88.9.3314.bloodjournal8893314

28. Stiff PJ, Unger JM, Cook JR, Constine LS, Couban S, Stewart DA, et al. Autologous transplantation as consolidation for aggressive non-Hodgkin's lymphoma. *N Engl J Med* (2013) 369(18):1681–90. doi: 10.1056/NEJMoa1301077

29. Kim YR, Yoon SO, Kim SJ, Cheong JW, Chung H, Lee JY, et al. Upfront autologous hematopoietic stem cell transplantation for high-risk patients with double-expressor diffuse large B cell lymphoma. *Ann Hematol* (2020) 99(9):2149–57. doi: 10.1007/s00277-020-04043-0

frontiers | Frontiers in Immunology

TYPE Clinical Trial
PUBLISHED 26 February 2024
DOI 10.3389/fimmu.2024.1293931

OPEN ACCESS

EDITED BY
Robert Ohgami,
The University of Utah, United States

REVIEWED BY
Nabil Hajji,
Imperial College London, United Kingdom
Francesco Vallania,
Freenome Inc., United States

*CORRESPONDENCE
Víctor Sánchez-Margalet
margalet@us.es
Luis de la Cruz-Merino
luis.cruz.sspa@juntadeandalucia.es

†These authors have contributed equally to this work and share first authorship

‡These authors share senior authorship

RECEIVED 13 September 2023
ACCEPTED 12 February 2024
PUBLISHED 26 February 2024

CITATION
Hontecillas-Prieto L, García-Domínguez DJ, Palazón-Carrión N, Martín García-Sancho A, Nogales-Fernández E, Jiménez-Cortegana C, Sánchez-León ML, Silva-Romeiro S, Flores-Campos R, Carnicero-González F, Ríos-Herranz E, de la Cruz-Vicente F, Rodríguez-García G, Fernández-Álvarez R, Martínez-Banaclocha N, Gumà-Padrò J, Gómez-Codina J, Salar-Silvestre A, Rodríguez-Abreu D, Gálvez-Carvajal L, Labrador J, Guirado-Risueño M, Provencio-Pulla M, Sánchez-Beato M, Marylene L, Álvaro-Naranjo T, Casanova-Espinosa M, Rueda-Domínguez A, Sánchez-Margalet V and de la Cruz-Merino L (2024) CD8+ NKs as a potential biomarker of complete response and survival with lenalidomide plus R-GDP in the R2-GDP-GOTEL trial in recurrent/refractory diffuse large B cell lymphoma.
Front. Immunol. 15:1293931.
doi: 10.3389/fimmu.2024.1293931

CD8+ NKs as a potential biomarker of complete response and survival with lenalidomide plus R-GDP in the R2-GDP-GOTEL trial in recurrent/refractory diffuse large B cell lymphoma

Lourdes Hontecillas-Prieto[1,2,3,4†], Daniel J. García-Domínguez[2,3†], Natalia Palazón-Carrión[4,5], Alejandro Martín García-Sancho[6], Esteban Nogales-Fernández[4,5], Carlos Jiménez-Cortegana[2], María L. Sánchez-León[4], Silvia Silva-Romeiro[4], Rocío Flores-Campos[4], Fernando Carnicero-González[7], Eduardo Ríos-Herranz[8], Fátima de la Cruz-Vicente[9], Guillermo Rodríguez-García[9], Rubén Fernández-Álvarez[10], Natividad Martínez-Banaclocha[11], Josep Gumà-Padrò[12], José Gómez-Codina[13], Antonio Salar-Silvestre[14], Delvys Rodríguez-Abreu[15], Laura Gálvez-Carvajal[16], Jorge Labrador[17], María Guirado-Risueño[18], Mariano Provencio-Pulla[19], Margarita Sánchez-Beato[20], Lejeune Marylene[21], Tomás Álvaro-Naranjo[22], María Casanova-Espinosa[23], Antonio Rueda-Domínguez[23], Víctor Sánchez-Margalet[1,2,3*‡] and Luis de la Cruz-Merino[3,4,5*‡]

[1]Clinical Biochemistry Service, Virgen Macarena University Hospital, University of Seville, Seville, Spain, [2]Department of Medical Biochemistry and Molecular Biology and Immunology, Medical School, Virgen Macarena University Hospital, University of Seville, Seville, Spain, [3]Institute of Biomedicine of Seville, Virgen Macarena University Hospital, CSIC, University of Seville, Seville, Spain, [4]Clinical Oncology Service, Hospital Universitario Virgen Macarena, University of Seville, Seville, Spain, [5]Department of Medicine, University of Seville, Seville, Spain, [6]Department of Hematology, Hospital Universitario de Salamanca, IBSAL, CIBERONC, University of Salamanca, Salamanca, Spain, [7]Department of Hematology, Hospital San Pedro de Alcántara de Cáceres, Cáceres, Spain, [8]Department of Hematology, Hospital Universitario de Valme, Seville, Spain, [9]Department of Hematology, Hospital Universitario Virgen del Rocío, Seville, Spain, [10]Department of Hematology, Cabueñes Hospital, Gijón, Spain, [11]Oncology Dept., Dr. Balmis General University Hospital, Alicante Institute for Health and Biomedical Research (ISABIAL), Alicante, Spain, [12]Department of Clinical Oncology, Hospital Universitari Sant Joan de Reus URV, IISPV, Reus, Spain, [13]Department of Clinical Oncology, Hospital Universitario La Fé, Valencia, Spain, [14]Department of Hematology, Hospital del Mar, Barcelona, Spain, [15]Department of Clinical Oncology, Hospital Universitario Insular, Las Palmas de Gran Canaria, Spain, [16]Department of Medical Oncology Intercenter Unit, Regional and Virgen de la Victoria University Hospitals, IBIMA, Málaga, Spain, [17]Department of Hematology, Research Unit, Hospital Universitario de Burgos, Burgos, Spain, [18]Department of Clinical Oncology, Hospital General Universitario de Elche, Elche, Spain, [19]Department of Medical Oncology, Hospital Universitario Puerta de Hierro-Majadahonda, Facultad de Medicina, Universidad Autónoma de Madrid, IDIPHISA, Madrid, Spain, [20]Department of Medical Oncology, Lymphoma Research Group, Hospital Universitario Puerta de Hierro-Majadahonda, IDIPHISA, CIBERONC, Madrid, Spain, [21]Department of Pathology,

Plataforma de Estudios Histológicos, Citológicos y de Digitalización, Hospital de Tortosa Verge de la Cinta, IISPV, URV, Tortosa, Tarragona, Spain, [22]Department of Pathology, Hospital de Tortosa Verge de la Cinta, Catalan Institute of Health, Institut d'Investigació Sanitària Pere Virgili (IISPV), Tortosa, Tarragona, Spain, [23]Department of Hematology/Clinical Oncology, Hospital Costa del Sol, Marbella, Spain

Background: Diffuse large B cell lymphoma (DLBCL) is the most common non-Hodgkin lymphoma worldwide. DLBCL is an aggressive disease that can be cured with upfront standard chemoimmunotherapy schedules. However, in approximately 35-40% of the patients DLBCL relapses, and therefore, especially in this setting, the search for new prognostic and predictive biomarkers is an urgent need. Natural killer (NK) are effector cells characterized by playing an important role in antitumor immunity due to their cytotoxic capacity and a subset of circulating NK that express CD8 have a higher cytotoxic function. In this substudy of the R2-GDP-GOTEL trial, we have evaluated blood CD8+ NK cells as a predictor of treatment response and survival in relapsed/refractory (R/R) DLBCL patients.

Methods: 78 patients received the R2-GDP schedule in the phase II trial. Blood samples were analyzed by flow cytometry. Statistical analyses were carried out in order to identify the prognostic potential of CD8+ NKs at baseline in R/R DLBCL patients.

Results: Our results showed that the number of circulating CD8+ NKs in R/R DLBCL patients were lower than in healthy donors, and it did not change during and after treatment. Nevertheless, the level of blood CD8+ NKs at baseline was associated with complete responses in patients with R/R DLBCL. In addition, we also demonstrated that CD8+ NKs levels have potential prognostic value in terms of overall survival in R/R DLBCL patients.

Conclusion: CD8+ NKs represent a new biomarker with prediction and prognosis potential to be considered in the clinical management of patients with R/R DLBCL.

Clinical trial registration: https://www.clinicaltrialsregister.eu/ctr-search/search?query=2014-001620-29 EudraCT, ID:2014-001620-29.

KEYWORDS

DLBCL, B cell lymphoma, recurrent/refractory disease, immune system, natural killer, CD8+ NK, biomarker, R2-GDP-GOTEL

Introduction

Lymphoproliferative diseases comprise a diverse and heterogeneous group of malignancies (1). Diffuse large B-cell lymphoma (DLBCL) is the most common non-Hodgkin lymphoma (NHL) subtype, accounting 30%-40% of lymphoid malignancies (2). Chemoimmunotherapy with R-CHOP (rituximab, cyclophosphamide, doxorubicin, vincristine, and prednisone) and R-CHOP-like schedules remains the upfront standard of care in DLBCL. However, one-third of DLBCL patients will relapse having a poor outcome, especially the cases with refractory disease to frontline or subsequent therapies (2). Although new strategies as chimeric antigen receptor T-cells (CART), bispecific monoclonal antibodies and new combinations with anti-CD19 (tafasitamab) plus lenalidomide or antibody drug conjugates (polatuzumab) plus bendamustine and rituximab are increasing the therapeutic armamentarium in relapsed/refractory (R/R) DLBCL (3), the search of new reliable predictive and prognostic biomarkers that could guide clinical management and eventually point to new therapeutic targets is extremely relevant and necessary.

Antitumor immune cells in peripheral blood have gained increasing relevance and interest, particularly natural killer cells (NKs). NK population is responsible for immune surveillance and represents major component of innate immunity against virus infected cells or malignant cells (4). NKs are effector cells characterized by exerting strong cytotoxicity against tumor cells and play an important role in the efficacy of rituximab-based therapy due to their ability to induce antibody-dependent cell cytotoxicity (ADCC) (5, 6). In DLBCL patients, some studies have evaluated NKs in peripheral blood. Indeed, NK cell count was associated with response and event free survival independently of adverse age-adjusted International Prognostic Index (7). In this line, low baseline NK cell count has also been associated with shorter progression-free survival (8). In these studies, NKs were defined as CD3-CD16 + 56+. Nevertheless, NKs express a large number of surface antigens (9); and, consequently, many subsets of NKs have been described in human peripheral blood (10, 11). One of the most promising and underexplored subsets of NKs in cancer are those that express CD8+ at lower levels than T cells (12, 13). The CD8 expression on NKs seems to be associated with a higher cytotoxic function compared with CD8- NK cells in healthy humans (14, 15), and in avian CD8 identify the lytic NK (16). Moreover, CD8+ NKs are capable of sequential lysis of multiple target cells (12). Regarding their relevance in human diseases, CD8+ NKs have been found to exert a suppressive effect in relapsing remitting multiple sclerosis (13). In chronic human immunodeficiency virus (HIV) patients an initial loss of this subset of NKs has been described, followed by a phenotypic change in CD8- NKs to become CD8+ in the progression of the disease (9). Moreover, high CD8+ NKs have been associated with slower disease progression exhibiting a more functional profile (17). Finally, it has been reported that CD8+ NKs mediate the autologous cytotoxicity of myeloid leukemic cells from patients in clinical remission after autologous stem-cell transplantation (18) and of acute myeloid leukemia patients in complete remission after chemotherapy alone *in vitro* (19).

Recently in the GOTEL clinical trial in R/R DLBCL, we found that the number of circulating myeloid-derived suppressor cells (MDSCs) after the third cycle of treatment was a good immunological biomarker associated with both survival (2, 20) and clinical benefit (21). However, the number of basal circulating MDSCs did not predict survival or clinical benefit. As a result, we have continued to search for blood biomarkers of treatment response in this clinical trial. As CD8+ NK cells seem to have a high cytotoxic function against tumor cells, we analyzed this subset of NKs in patients treated with R-GDP plus lenalidomide in the R2-GDP-GOTEL phase II trial and evaluated their prognostic impact at baseline. The results obtained showed that CD8+ NKs, but not CD8- NKs, are associated with complete responses and, more importantly, with overall survival (OS), representing a promising new biomarker with prediction and prognosis potential in R/R DLBCL.

Materials and methods

Study design

79 patients diagnosed with R/R DLBCL were enrolled in this multicenter (78 patients were finally considered in the intention to treat (ITT) analysis due to the voluntary withdrawal of one patient), open-label, single-arm R2-GDP-GOTEL phase II clinical trial study (EudraCT Number: 2014-001620-29) (21). The main baseline characteristics of the patients are summarized in Supplementary Table 1 and the progress of patients through the trial are summarized in Supplementary Figure 1A. The study was conducted in compliance with the International Ethical Guidelines for Biomedical Research Involving Human Subjects, the Declaration of Helsinki, good clinical practice guidelines, and local laws. The study protocol and any subsequent amendments were approved by Seville Provincial Ethics Committee for Research with Drug.

Lenalidomide plus R-GDP treatment

R/R DLBCL patients received the R2-GDP schedule, based on lenalidomide in combination with R-GDP. After a first run-in phase period the following schedule was administered: intravenous rituximab 375 mg/m^2 on day (D)1, intravenous cisplatin 60 mg/m^2 D1, intravenous gemcitabine 750 mg/m^2 D1 and D8, oral dexamethasone 20 mg D1–3, subcutaneous granulocyte colony stimulating factor (G-CSF) 30 million units international (MUI) D2–6 and D9–14 in combination with oral lenalidomide 10 mg D1–14, in cycles every 3 weeks. If after the 3rd cycle there was no progression of disease, a maximum of 6 induction cycles were administered. Patients that reached clinical benefit after at least 3 cycles of treatment could enter a maintenance phase with lenalidomide 10 mg (or the last dose administered in the induction phase) D1–21 in cycles every 4 weeks. The maintenance phase was intended to continue until progression, unacceptable toxicity, patient voluntary withdrawal, or when two positron emission tomography (PET) confirmed metabolic complete response after 2 years of treatment.

Response evaluation and outcome

Evaluation of the response to treatment allowed us to define patients in complete response (CR), partial response (PR), stable disease (SD) or patients with progression of the disease (PD). Tumor response was evaluated according to the International Working Group Criteria (22) using computed tomography after the third induction cycle and PET in the following 4 weeks after the last cycle of the induction phase, and the response to treatment was calculated as Best Overall Response.

Immunophenotyping

NKs and other immune cells were studied in peripheral blood from R/R DLBCL patients during the R2-GDP-GOTEL study at three time-points: basal, cycle 3 and end of induction (EOI). Blood samples were collected in EDTA-K3 tubes and cell populations were determined by flow cytometry analysis using the BD FACSCanto II™ flow cytometry system with the monoclonal antibodies (mAbs) and protocols recommended by Becton Dickinson Immunocytometry Systems (BDIS, San Jose, CA, USA). mAbs are listed in Supplementary Table 2 and the phenotypes for immune cell studies are described in Supplementary Table 3.

Lymphocyte subpopulations were analyzed by BD Multi-test 6-Color TBNK (Becton Dickinson). NK cells were gated by selecting the CD3- and CD16 + 56+ cells, and then analyzed as CD8- and CD8+ (Supplementary Figure 1B).

Statistical analysis

Mann–Whitney and One-way tests were used to evaluate differences between two or more groups, respectively. Paired samples *t*-test was applied to compare the mean level of expression within the same specimens. Overall survival was analyzed using the Kaplan–Meier estimator, and the differences were evaluated using the log-rank test. This survival analysis was performed to determine the survival of all patients according to the levels of CD8 positive or negative NKs. The Spearman's Rank test and principal component analysis were used to determine the relationship between different variables. Receiver operator characteristic curve (ROC) analysis was conducted to calculate the area under the curve (AUC). To calculate the ROC curve, all patients were used and compared those with CR compared to the rest of the patients in the study. Uni- and multivariate Cox regression analyses were used with all study patients to estimate hazard ratios (HRs) and the influence of CD8 positive and negative NK variables on survival time, independent of treatment response. All statistical analyses in the study were performed using the software's GraphPad Prism (6.01), JMP (V.10), and SPSS (V.25.0). The average of samples with SD is presented in all experiments. For all analyses, *p*-values of ≤0.05 were considered statistically significant.

Results

Baseline clinical characteristics of R/R DLBCL patients

A total of 78 patients were finally considered in the ITT analysis. In terms of clinical characteristics, the median age was 66 (range 23-86) years, and of the total number of patients 41 were male (51.9%) and 38 female (48.1%). Thirty-three patients (41.8%) were primary refractory DLBCL defined as in the SCHOLAR-1 study (23), and thirty-six samples (64.3%) were classified as non-germinal center B-cell (GCB) and 20 (35.7%) samples as GCB subtype, by Hans algorithm. Of the total patients included, 29 (36.7%) achieved CR, 18 (22.8%) patients had PR, 6 (7.6%) had SD and 25 (31.6%) showed PD. The main baseline characteristics of the patients are summarized in Supplementary Table 1. In addition, 10 women and 10 men with a similar median age (68.2 years) to the patients were recruited as healthy donors.

Blood CD8+ NK level does not change during the treatment of R/R DLBCL patients

In order to understand the potential roles of CD8+ NK cell subpopulation, we first compared their basal blood levels in R/R DLBCL patients with those in healthy donors. Circulating CD8+ NK levels were significantly lower in R/R DLBCL patients compared with healthy donors ($p<0.0001$). Moreover, CD8- NKs and total NKs were also lower in patients ($p=0.0271$ and $p=0.0005$ respectively) (Figure 1A). Next, both subpopulations were compared before (baseline), during (Cycle 3) and after treatment (EOI) in R/R DLBCL patients, finding that the levels of CD8- NKs were significantly higher than CD8+ NKs levels at all sampling stages (Figure 1B). Finally, we studied how the levels of CD8+ NKs evolved during the treatment. There were no differences neither CD8+ NK nor CD8- NK subpopulations before, during and after treatment in paired samples (Figure 1C). In addition, the same results were observed when the analyses were with all samples (Supplementary Figure 2). In this study, CD8+ NKs are the minority subset of circulating NKs observed in R/R DLBCL patients, and the treatment did not modify their levels.

High-circulating CD8+ NK levels at baseline were associated with complete response to treatment

Once the number of circulating CD8+ NKs was assessed, we performed a detailed analysis of the number of CD8+ NKs in relation to clinical parameters. No significant differences in CD8+ NK levels were observed between the tumor molecular subtype in DLBCL (GCB and no GCB by Hans algorithm), or between patients with or without refractory disease (Supplementary Figure 3). There was also no significant difference neither between elderly and non-elderly patients, nor between men and women (Supplementary Figure 3). In addition, results shown in CD8- NKs and total NKs did not change significantly in either of the clinical parameters studied (Supplementary Figure 3).

When response to treatment was analyzed, R/R DLBCL patients with CR had a significant higher level of basal CD8+ NKs than patients with PD ($p=0.0006$) (Figure 2A), whereas there were no differences in treatment response in CD8- NK subpopulation (Figure 2A). To rule out that the result obtained from CD8+ NK cells with response to treatment was based on confounding factors, we performed an analysis between the clinical characteristic of the patients and response to treatment. No association was observed

10.3389/fimmu.2024.1293931

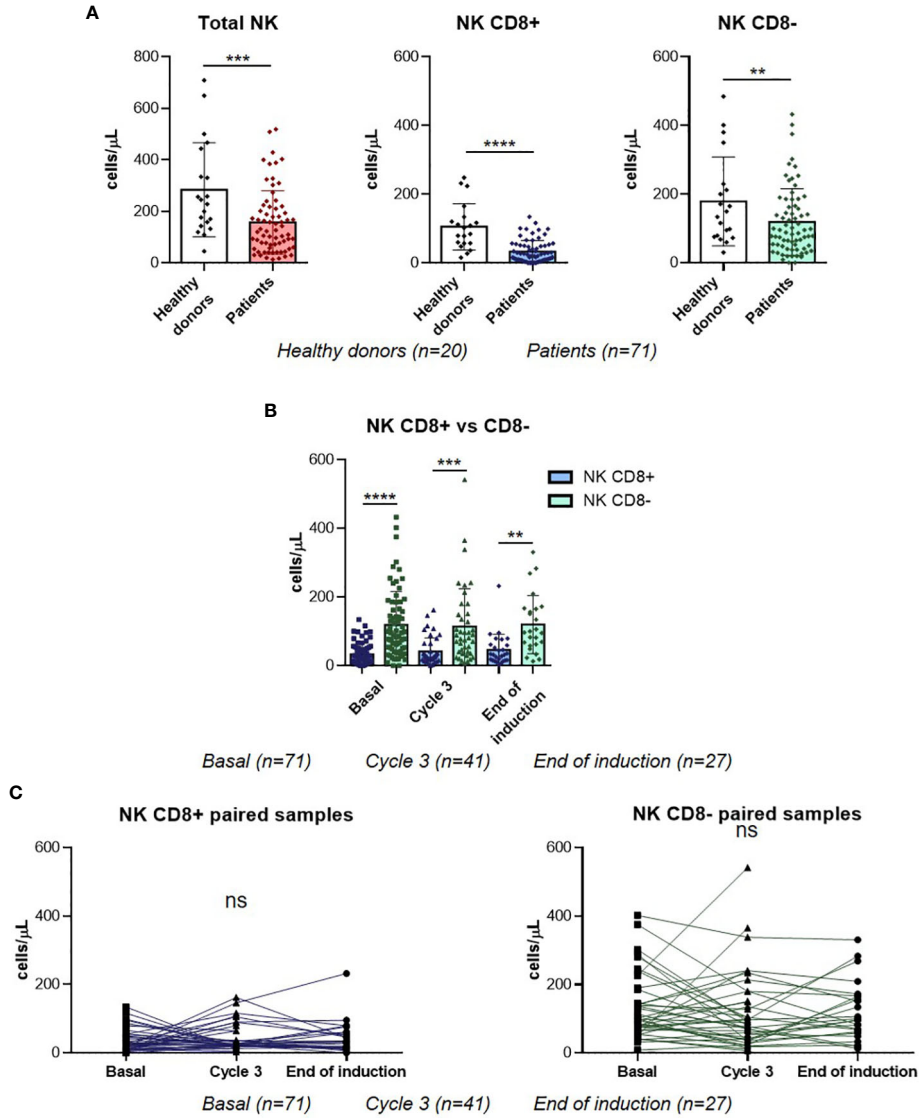

FIGURE 1
NK populations in R/R DLBCL patients. **(A)** Comparison of total NKs, CD8+ NK and CD8- NK basal levels between healthy donors and R/R DLBCL patients. **(B)** CD8+ NK and CD8- NK levels comparison at three time-points in all samples. **(C)** CD8+ NK and CD8- NK levels comparison at three time-points in paired samples. For all the analyses, $*P \leq 0.05$, $**P \leq 0.01$, $***P \leq 0.001$ and $****P \leq 0.0001$. ns, not significant.

with age, gender, molecular subtypes and refractory disease (Supplementary Figure 4A).

Since clinical response was associated with different levels of CD8 + NKs prior to therapy at basal point, we aimed to further analyze the direct relationship of this promising biomarker with response to treatment in these patients. We next performed a multivariate analysis with pro- and anti-tumor immune cells from CR and PD groups. However, in those patients with PD, levels of CD8+ NKs did not correlate with any immune cell studied at baseline (Supplementary Figures 4B, C). Instead, a positive correlation was observed between CD8+ NKs and CD4 and CD8+ T cells (p=0.0155 and p=0.0025) and gamma delta (γδ) T cells (CD3+C4-CD8-) (p=0.0209) in patients with CR before treatment (Figure 2B). Nevertheless, there was no correlation with other antitumor immune cells such as activated T cells or the immunosuppressive MDSCs (Figures 2B, C). Principal component analysis in CR patients also showed a positive relationship between CD8+ NKs, CD8+ and γδ T cells (Figure 2D). Together, high-circulating CD8+ NK levels at baseline are associated with CR in R/R DLBCL patients. In addition, in those CR patients, the CD8+ NK subpopulation correlates with the antitumor immune response.

CD8+ NK cells are potential predictive and prognostic factors to R2-GDP treatment in R/R DLBCL patients

Given the CD8+ NK association with treatment response, we investigated the prognostic potential at baseline in lymphoma patients. The area under the curve (AUC) of CD8+ and CD8-

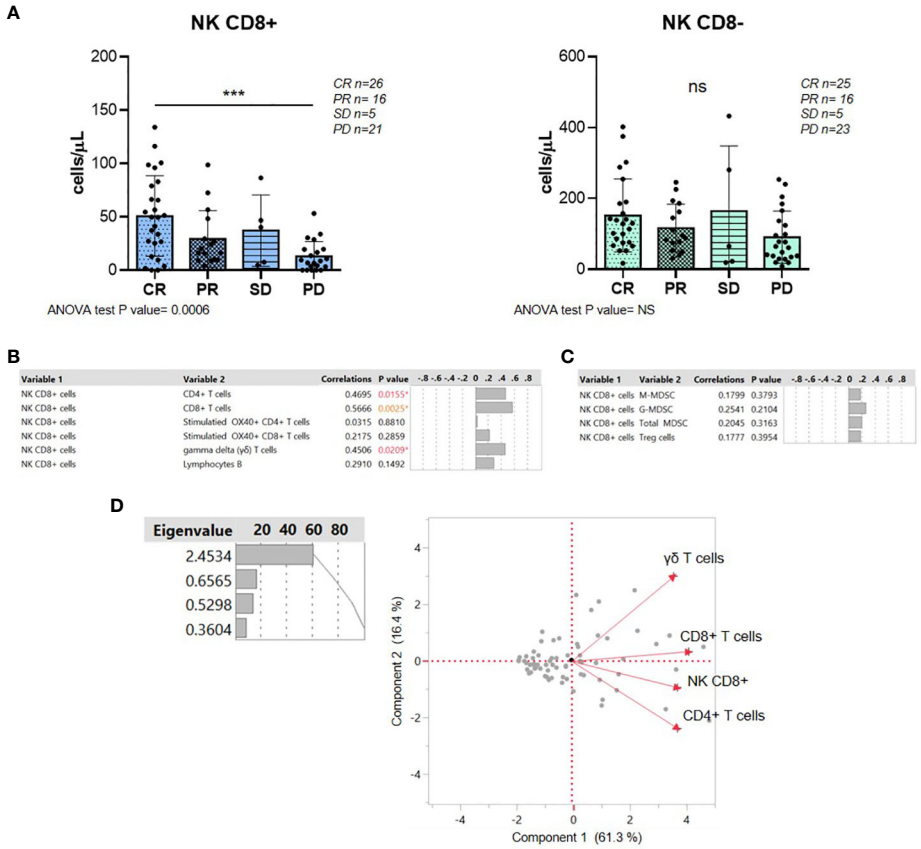

FIGURE 2
High levels of circulating CD8+ NKs were associated with a complete response to treatment. **(A)** Analysis of CD8+ and CD8- NK levels according to R/R DLBCL patients' response to treatment. **(B)** Multivariate correlations between CD8+ NKs and protumor immune cells in R/R DLBCL patients with CR. **(C)** Multivariate correlations between CD8+ NKs and antitumor immune cells in R/R DLBCL patients with CR. **(D)** Principal component analysis represented by biplot showed the positive relations between NK CD8+ and CD4+, CD8+ and γδ T cells. For all the analyses, $*P \leq 0.05$, $**P \leq 0.01$, $***P \leq 0.001$ and $****P \leq 0.0001$. ns, not significant.

NKs was 0.698 (95% confidence interval [CI], 0.563–0.833; p=0.004) and 0.629 (95% CI, 0.491–0.766; p=0.066), respectively (Figure 3A). In the CD8+ NK subset, the cutoff value of the predictive score at the optimum point was 24.8, the specificity was 34.1%, and the sensitivity was 76.9% (Supplementary Table 4). Therefore, ROC curve analyses indicated that CD8+ NK levels at baseline are a good predictor of treatment response in R/R DLBCL patients but not the CD8- NK subset. Then, we analyzed the relationship between OS and CD8+ NK levels by Kaplan–Meier test using the ROC curve cutoff level 24.8. We observed that patients with high levels of CD8+ NKs showed a higher survival rate than patients with low CD8+ NK levels (p=0.0209) (Figure 3B). However, there were no differences in survival in CD8- NK population (p=0.2487) (Figure 3B). In addition, two groups were performed, both for CD8+ NKs and CD8- NKs, depending on whether the patients had a longer or shorter survival than 24 months. Significant high levels of CD8+ NK subset at baseline were found in those patients with an OS >24 months compared with those patients with an OS <24 months (p=0.0142); whereas there were no changes in OS at 24 months in CD8- NKs (p=0.0974) (Figure 3C). Finally, we also examined the prognostic role of CD8+ NKs by Cox-regression analysis of OS. Here, the patients with primary refractory disease (a critical prognosis factor in DLBCL patients) and the levels of two CD8 NK subpopulations were explored. Uni- and multivariate analysis showed that only CD8+ NK was strongly associated with OS in an independent manner to the primary refractory disease (p=0.012 and p=0.036, respectively) (Figure 3D). These results indicate that the basal levels of circulating CD8+ NKs can be used as an emerging non-invasive and independent biomarker with prognostic and predictive potential.

Discussion

NKs are cytotoxic lymphocytes with an important antitumor function acting as the first line of defense in tumor surveillance. These effector cells exert natural cytotoxicity against tumor cells by inhibiting their proliferation, migration, or colonization of distant tissues (24, 25). Thus, understanding the role of innate immunity in cancer, and NKs, in particular, is attracting increasing attention. This has led to the discovery of various NK subsets with different immune functions such as CD8+ NKs. We hypothesized that

10.3389/fimmu.2024.1293931

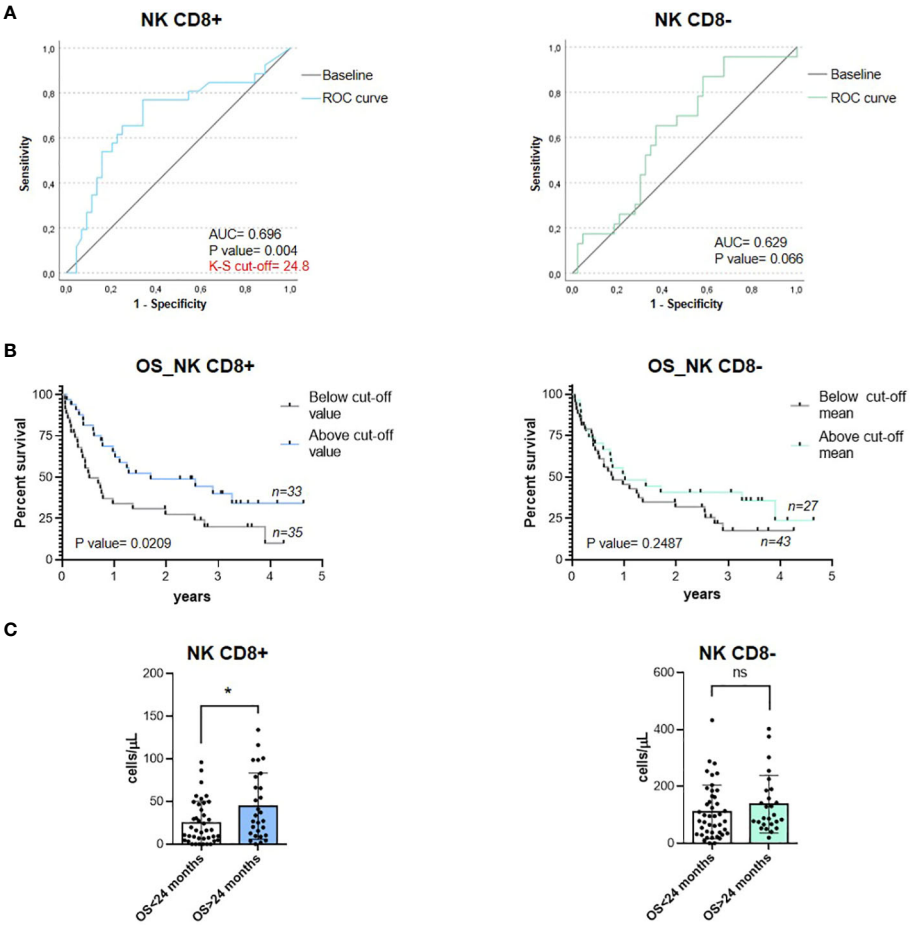

D

Overall Survival (24 months)

	Univariate Cox Regression		Multivariate Cox Regression	
	HR (95% CI)	P value	HR (95% CI)	P value
Refractory disease	2,028 (1,153-3,568)	0.014	2,149 (1,141-4,045)	0.018
NK CD8+ cells	0,985 (0,973-0,997)	0.012	0,985 (0,971-0,999)	0.036
NK CD8- cells	1,577 (0,994-1,001)	0.231	1,001 (0,996-1,005)	0.784

FIGURE 3
Circulating CD8+ NKs were a prognostic value for predicting the response to treatment and overall survival of R/R DLBCL patients. **(A)**. ROC curve analyses of both subsets of NKs at baseline for the prognosis of treatment response in R/R DLBCL patients. **(B)**. Kaplan–Meier curves of overall survival according to the levels of circulating CD8+ NKs and CD8- NKs in R/R DLBCL patients. **(C)**. Levels of CD8+ NKs and CD8- NKs in patients with OS >24 months and OS <24 months. **(D)**. Cox-regression analysis of CD8 NK cells subpopulations and primary refractory disease in patients. For all the analyses, $*P \leq 0.05$, $**P \leq 0.01$, $***P \leq 0.001$ and $****P \leq 0.0001$. ns, not significant.

circulating CD8+ NKs may provide a potential information regarding disease progression in R/R DLBCL patients. To elucidate the role of CD8+ NKs in peripheral blood in R/R DLBCL patients, we first observed that the levels of the two subtypes are different, with higher percentage of CD8- NKs. Moreover, a significant decreased number of circulating CD8+ NKs as well as in CD8- NKs and total NKs was found in R/R DLBCL patients compared to healthy donors. These observations are in line with other studies in cancer in which a decrease in the NK cell numbers is often reported (26, 27). However, before, during and after treatment the levels of both CD8 NK subsets did not change, which are in concordance with Waidhauser J. et al., who also showed no significant changes before and after chemotherapy in the count of NKs in solid tumors (28). Thus, no influence of treatment on the CD8 NK subsets may be identified.

Then, we addressed the question whether the peripheral blood profiles of both NK (CD8- and CD8+) populations were correlated with clinical status. Although both subsets of NKs were clearly altered in R/R DLBCL patients as compared to healthy controls, no major shifts were observed in relation to tumor phenotype, refractory disease, gender, or age of patients. However, differences in NK subsets at baseline were related to treatment response. Those patients with CR had significant higher basal levels of CD8+ NKs than those patients in which the disease progressed, whereas no differences in treatment response in CD8- NK subpopulation were observed. In patients with DLBCL, peripheral blood NKs (CD3-CD16+ and/or CD56+) count was associated with treatment response (7). In this study, responders to induction treatment (complete remission, uncertain complete remission or partial remission) had higher levels of total NKs than non-responders

(7). To the best of our knowledge, this is the first time that CD8+ NKs demonstrate its potential value as a predictive factor for treatment response in cancer.

In addition to the relationship between CD8+ NKs and response to treatment, we also evidenced a positive interaction between CD8+ NK and some circulating immune cell in responder patients, but not in those patients that progressed on treatment. NKs play a role in antitumor immunity because of both their cytotoxic capacity and their ability to modulate the immune response. Indeed, through cytokines and chemokines production, NKs impact the function of B and T cells responses, dendritic cells, macrophages or neutrophils (29) hindering tumor cell growth, whereas MDSCs promote tumor growth and progression (30, 31). In fact, it has been described that circulating NKs were positively correlated to T and B lymphocytes in cancer (27). Therefore, the correlation with only immune cells that also hinder tumor cell growth in patients with CR would suggest the presence of an antitumor environment that induce a better response to treatment in these patients.

Given that CD8 expression in NKs implies a higher cytotoxic activity (14–16, 18, 19) and they are associated with slower disease progression in HIV patients (17), the prognostic potential of CD8+ NK at baseline were explored. The analyses showed that CD8+ NKs are useful as biomarkers regarding the treatment response in R/R DLBCL patients. In addition, patients with higher levels of CD8+ NKs showed a higher survival rate than patients with low CD8+ NK levels. Since patients in this clinical trial were treated with anti-CD20 (rituximab), which has high affinity for Fc gamma receptors, including FcγRIIIa (expressed on the surface of NKs), clinical results may be explained at least in part by an enhanced FcγRIIIa-mediated ADCC. In this context, recent data of treatment of DLBCL patients with tafasitamab (anti-CD19) and lenalidomide demonstrated an enhanced NK-cell–mediated antibody ADCC by tafasitamab *in vitro* (32–34). We have found that treatment with anti-CD20 and lenalidomide is very effective in those patients with higher level of CD8+ NKs. Therefore, a possible mechanism of treatment response may be the increased ADCC in this subpopulation of NKs (CD8+) potentiated by lenalidomide, what could also partially elucidate the immune effects and mechanism of action of lenalidomide and other immunomodulatory drugs (IMIDs). Nevertheless, this mechanism remains speculative and further studies are needed to confirm this hypothesis. Besides, new therapeutic choices in R/R DLBCL, including NK-CART, reinforces the value and potential clinical applicability of our results.

Finally, in the light of the multivariate analysis, the significant correlation between OS and CD8+ NKs was independent of other relevant clinical parameters such as primary refractory disease, which may point to CD8+ NKs as a molecular factor with a relevant prognostic value in DLBCL.

In conclusion, the search for immune biomarkers is critically important for identifying patients who may be more likely to benefit from cancer therapies. Nevertheless, the discovery of new biomarkers poses challenges, as integrating new biomarkers into clinical practice effectively and accurately in daily practice is a challenge. In line with this, we previously found in this clinical trial that circulating MDSCs along the course of antineoplastic treatment are a promising biomarker in the clinical management of these patients (2, 21), although these immune cells could not predict survival or clinical benefit measured before treatment. Here instead we have demonstrated that the number of circulating CD8+ NKs at baseline is a favorable predictor of survival outcomes and complete response to treatment in patients with R/R DLBCL. Therefore, it could be used as a potential non-invasive predictive and prognostic biomarker. Moreover, our study reveals the existence of novel NK cell subsets displaying different functions in R/R DLBCL patients. Finally, the identification of CD8+ NKs as a unique marker in this tumor may represent an important advance in our understanding of lymphomas, especially DLBCL. Further studies are required to validate this potential biomarker, and to be analyzed in other lymphoma subtypes, due to its biological heterogeneity, and in other cancer types.

Author's note

Disclosures provided by the authors are available with this article at doi: 10.1158/1078-0432.CCR-22-0588.

Data availability statement

The original contributions presented in the study are included in the article/Supplementary Material. Further inquiries can be directed to the corresponding authors.

Ethics statement

The studies involving humans were approved by Seville Provincial Ethics Committee for Research with Drug. The studies were conducted in accordance with the local legislation and institutional requirements. The participants provided their written informed consent to participate in this study. Written informed consent was obtained from the individual(s) for the publication of any potentially identifiable images or data included in this article.

Author contributions

LH-P: Conceptualization, Data curation, Formal Analysis, Investigation, Supervision, Writing – original draft. DG-D: Conceptualization, Formal Analysis, Investigation, Supervision, Visualization, Writing – original draft. NP-C: Investigation, Writing – review & editing. AG-S: Investigation, Writing – review & editing. EN-F: Investigation, Writing – review & editing. CJ-C: Investigation, Writing – review & editing. MS-L: Investigation, Writing – review & editing. SS-R: Investigation, Validation, Writing – review & editing. RF-C: Investigation, Visualization, Writing – review & editing. FC-G: Investigation, Writing – review & editing. ER-H: Investigation, Writing – review & editing. FC-V: Investigation, Writing – review & editing. GR-G:

Investigation, Writing – review & editing. RF-Á: Investigation, Writing – review & editing. NM-B: Investigation, Writing – review & editing. JG-P: Investigation, Writing – review & editing. JG-C: Investigation, Writing – review & editing. AS-S: Investigation, Writing – review & editing. DR-A: Investigation, Writing – review & editing. LG-C: Investigation, Writing – review & editing. JL: Investigation, Writing – review & editing. MG-R: Investigation, Writing – review & editing. MP-P: Investigation, Writing – review & editing. MS-B: Investigation, Writing – review & editing. LM: Investigation, Writing – review & editing. TÁ-N: Investigation, Writing – review & editing. MC-E: Investigation, Writing – review & editing. AR-D: Investigation, Writing – review & editing. VS-M: Conceptualization, Formal Analysis, Investigation, Supervision, Writing – original draft. LC-M: Writing – original draft, Funding acquisition, Investigation, Supervision, Writing – original draft.

Funding

The author(s) declare that financial support was received for the research, authorship, and/or publication of this article. This research was funded by the Spanish Lymphoma Oncology Group (GOTEL) with the financial support of Celgene (Investigator Initiated Trials Program); no grant numbers applicable. LH-P is supported by the Consejería de Salud y Familias, Junta de Andalucía (RH-0047-2021) and Miguel Servet Researcher Fellow from the Instituto de Salud Carlos III. DG-D is supported by the VII Plan Propio de Investigacioín y Transferencia of Universidad de Sevilla [Contrato de Acceso (II.4)/VII PPIT-US]. CJ-C is supported by the Margarita Salas fellowship, granted by the University of Seville (Seville, Spain).

Acknowledgments

We want to thank Irene Borreguero and Clara M. Rosso-Fernández from the CTU-HUVR, Clinical Trial Unit, Hospital Universitario Virgen del Rocío, Spanish Clinical Research and Clinical Trial Platform (SCReN, PT13/PT17/PT20/0017/0012/00123)S, and specially to the patients and their families for their commitment. We would also like to thank Dr. Lorenzo Galluzzi for his intellectual contribution and constructive criticism. We want to particularly acknowledge the Biobank Nodo Hospital Virgen Macarena (Biobanco del Sistema Sanitario Público de Andalucía) integrated in the Spanish National biobanks Network (PT20/00069) supported by ISCIII and FEDER funds, for their collaboration in this work.

Conflict of interest

The authors declare that the research was conducted in the absence of any commercial or financial relationships that could be construed as a potential conflict of interest. The authors declared that they were an editorial board member of Frontiers, at the time of submission. This had no impact on the peer review process and the final decision.

Publisher's note

Supplementary material

The Supplementary Material for this article can be found online at: https://www.frontiersin.org/articles/10.3389/fimmu.2024.1293931/full#supplementary-material

References

1. Garcia-Dominguez DJ, Hontecillas-Prieto L, Palazon-Carrion N, Jimenez-Cortegana C, Sanchez-Margalet V, de la Cruz-Merino L. Tumor immune microenvironment in lymphoma: Focus on epigenetics. *Cancers (Basel)*. (2022) 14. doi: 10.3390/cancers14061469.

2. Jimenez-Cortegana C, Sanchez-Martinez PM, Palazon-Carrion N, Nogales-Fernandez E, Henao-Carrasco F, Martin Garcia-Sancho A, et al. Lower survival and increased circulating suppressor cells in patients with relapsed/refractory diffuse large B-cell lymphoma with deficit of vitamin D levels using R-GDP plus lenalidomide (R2-GDP): Results from the R2-GDP-GOTEL trial. *Cancers (Basel)*. (2021) 13. doi: 10.3390/cancers13184622.

3. Poletto S, Novo M, Paruzzo L, Frascione PMM, Vitolo U. Treatment strategies for patients with diffuse large B-cell lymphoma. *Cancer Treat Rev*. (2022) 110:102443. doi: 10.1016/j.ctrv.2022.102443.

4. Pierce S, Geanes ES, Bradley T. Targeting natural killer cells for improved immunity and control of the adaptive immune response. *Front Cell Infect Microbiol*. (2020) 10:231. doi: 10.3389/fcimb.2020.00231.

5. Glennie MJ, French RR, Cragg MS, Taylor RP. Mechanisms of killing by anti-CD20 monoclonal antibodies. *Mol Immunol*. (2007) 44:3823–37. doi: 10.1016/j.molimm.2007.06.151.

6. Boross P, Leusen JH. Mechanisms of action of CD20 antibodies. *Am J Cancer Res*. (2012) 2:676–90.

7. Plonquet A, Haioun C, Jais JP, Debard AL, Salles G, Bene MC, et al. Peripheral blood natural killer cell count is associated with clinical outcome in patients with aaIPI 2-3 diffuse large B-cell lymphoma. *Ann Oncol*. (2007) 18:1209–15. doi: 10.1093/annonc/mdm110.

8. Klanova M, Oestergaard MZ, Trneny M, Hiddemann W, Marcus R, Sehn LH, et al. Prognostic impact of natural killer cell count in follicular lymphoma and diffuse large B-cell lymphoma patients treated with immunochemotherapy. *Clin Cancer Res*. (2019) 25:4634–43. doi: 10.1158/1078-0432.CCR-18-3270.

9. Lucia B, Jennings C, Cauda R, Ortona L, Landay AL. Evidence of a selective depletion of a CD16+ CD56+ CD8+ natural killer cell subset during HIV infection. *Cytometry*. (1995) 22:10–5. doi: 10.1002/cyto.990220103.

10. Cooper MA, Fehniger TA, Caligiuri MA. The biology of human natural killer-cell subsets. *Trends Immunol*. (2001) 22:633–40. doi: 10.1016/S1471-4906(01)02060-9.

11. Berahovich RD, Lai NL, Wei Z, Lanier LL, Schall TJ. Evidence for NK cell subsets based on chemokine receptor expression. *J Immunol*. (2006) 177:7833–40. doi: 10.4049/jimmunol.177.11.7833.

12. Addison EG, North J, Bakhsh I, Marden C, Haq S, Al-Sarraj S, et al. Ligation of CD8alpha on human natural killer cells prevents activation-induced apoptosis and enhances cytolytic activity. *Immunology*. (2005) 116:354–61. doi: 10.1111/j.1365-2567.2005.02235.x.

13. Mckinney EF, Cuthbertson I, Harris KM, Smilek DE, Connor C, Manferrari G, et al. A CD8(+) NK cell transcriptomic signature associated with clinical outcome in relapsing remitting multiple sclerosis. *Nat Commun*. (2021) 12:635. doi: 10.1038/s41467-020-20594-2.

14. Srour EF, Leemhuis T, Jenski L, Redmond R, Jansen J. Cytolytic activity of human natural killer cell subpopulations isolated by four-color immunofluorescence flow cytometric cell sorting. *Cytometry*. (1990) 11:442–6. doi: 10.1002/cyto.990110316.

15. Fuchshuber PR, Lotzova E. Differential oncolytic effect of NK-enriched subsets in long-term interleukin-2 cultures. *Lymphokine Cytokine Res*. (1992) 11:271–6.

16. Kushima K, Fujita M, Shigeta A, Horiuchi H, Matsuda H, Furusawa S. Flow cytometric analysis of chicken NK activity and its use on the effect of restraint stress. *J Vet Med Sci*. (2003) 65:995–1000. doi: 10.1292/jvms.65.995.

17. Ahmad F, Hong HS, Jackel M, Jablonka A, Lu IN, Bhatnagar N, et al. High frequencies of polyfunctional CD8+ NK cells in chronic HIV-1 infection are associated with slower disease progression. *J Virol*. (2014) 88:12397–408. doi: 10.1128/JVI.01420-14.

18. Lowdell MW, Ray N, Craston R, Corbett T, Deane M, Prentice HG. The *in vitro* detection of anti-leukaemia-specific cytotoxicity after autologous bone marrow transplantation for acute leukaemia. *Bone Marrow Transplant*. (1997) 19:891–7. doi: 10.1038/sj.bmt.1700756.

19. Lowdell MW, Craston R, Samuel D, Wood ME, O'neill E, Saha V, et al. Evidence that continued remission in patients treated for acute leukaemia is dependent upon autologous natural killer cells. *Br J Haematol*. (2002) 117:821–7. doi: 10.1046/j.1365-2141.2002.03495.x.

20. Jimenez-Cortegana C, Palazon-Carrion N, Martin Garcia-Sancho A, Nogales-Fernandez E, Carnicero-Gonzalez F, Rios-Herranz E, et al. Circulating myeloid-derived suppressor cells and regulatory T cells as immunological biomarkers in refractory/relapsed diffuse large B-cell lymphoma: translational results from the R2-GDP-GOTEL trial. *J Immunother Cancer*. (2021) 9. doi: 10.1136/jitc-2020-002323.

21. Palazon-Carrion N, Martin Garcia-Sancho A, Nogales-Fernandez E, Jimenez-Cortegana C, Carnicero-Gonzalez F, Rios-Herranz E, et al. Lenalidomide plus R-GDP (R2-GDP) in relapsed/refractory diffuse large B-cell lymphoma: Final results of the R2-GDP-GOTEL trial and immune biomarker subanalysis. *Clin Cancer Res*. (2022) 28:3658–68. doi: 10.1158/1078-0432.CCR-22-0588.

22. Cheson BD, Pfistner B, Juweid ME, Gascoyne RD, Specht L, Horning SJ, et al. Revised response criteria for Malignant lymphoma. *J Clin Oncol*. (2007) 25:579–86. doi: 10.1200/JCO.2006.09.2403.

23. Crump M, Neelapu SS, Farooq U, Van Den Neste E, Kuruvilla J, Westin J, et al. Outcomes in refractory diffuse large B-cell lymphoma: results from the international SCHOLAR-1 study. *Blood*. (2017) 130:1800–8. doi: 10.1182/blood-2017-03-769620.

24. Lopez-Soto A, Gonzalez S, Smyth MJ, Galluzzi L. Control of metastasis by NK cells. *Cancer Cell*. (2017) 32:135–54. doi: 10.1016/j.ccell.2017.06.009.

25. Chiossone L, Dumas PY, Vienne M, Vivier E. Natural killer cells and other innate lymphoid cells in cancer. *Nat Rev Immunol*. (2018) 18:671–88. doi: 10.1038/s41577-018-0061-z.

26. Al Omar SY, Marshall E, Middleton D, Christmas SE. Increased killer immunoglobulin-like receptor expression and functional defects in natural killer cells in lung cancer. *Immunology*. (2011) 133:94–104. doi: 10.1111/j.1365-2567.2011.03415.x.

27. Tang YP, Xie MZ, Li KZ, Li JL, Cai ZM, Hu BL. Prognostic value of peripheral blood natural killer cells in colorectal cancer. *BMC Gastroenterol*. (2020) 20:31. doi: 10.1186/s12876-020-1177-8.

28. Waidhauser J, Schuh A, Trepel M, Schmalter AK, Rank A. Chemotherapy markedly reduces B cells but not T cells and NK cells in patients with cancer. *Cancer Immunol Immunother*. (2020) 69:147–57. doi: 10.1007/s00262-019-02449-y.

29. Laskowski TJ, Biederstadt A, Rezvani K. Natural killer cells in antitumour adoptive cell immunotherapy. *Nat Rev Cancer*. (2022) 22:557–75. doi: 10.1038/s41568-022-00491-0.

30. Gao XH, Tian L, Wu J, Ma XL, Zhang CY, Zhou Y, et al. Circulating CD14(+) HLA-DR(-/low) myeloid-derived suppressor cells predicted early recurrence of hepatocellular carcinoma after surgery. *Hepatol Res*. (2017) 47:1061–71. doi: 10.1111/hepr.12831.

31. Deng X, Li X, Guo X, Lu Y, Xie Y, Huang X, et al. Myeloid-derived suppressor cells promote tumor growth and sorafenib resistance by inducing FGF1 upregulation and fibrosis. *Neoplasia*. (2022) 28:100788. doi: 10.1016/j.neo.2022.100788.

32. Awan FT, Lapalombella R, Trotta R, Butchar JP, Yu B, Benson DM Jr., et al. CD19 targeting of chronic lymphocytic leukemia with a novel Fc-domain-engineered monoclonal antibody. *Blood*. (2010) 115:1204–13. doi: 10.1182/blood-2009-06-229039.

33. Gribben JG, Fowler N, Morschhauser F. Mechanisms of action of lenalidomide in B-cell non-hodgkin lymphoma. *J Clin Oncol*. (2015) 33:2803–11. doi: 10.1200/JCO.2014.59.5363.

34. Duell J, Maddocks KJ, Gonzalez-Barca E, Jurczak W, Liberati AM, De Vos S, et al. Long-term outcomes from the Phase II L-MIND study of tafasitamab (MOR208) plus lenalidomide in patients with relapsed or refractory diffuse large B-cell lymphoma. *Haematologica*. (2021) 106:2417–26. doi: 10.3324/haematol.2020.275958.

frontiers | Frontiers in Immunology

TYPE Case Report
PUBLISHED 12 March 2024
DOI 10.3389/fimmu.2024.1303310

OPEN ACCESS

EDITED BY
Robert Ohgami,
The University of Utah, United States

REVIEWED BY
Xianhuo Wang,
Tianjin Medical University Cancer Institute and Hospital, China
Anil Kumar,
City of Hope National Medical Center, United States

*CORRESPONDENCE
Liling Zhang
lily-1228@hotmail.com

†These authors have contributed equally to this work and share first authorship

RECEIVED 27 September 2023
ACCEPTED 21 February 2024
PUBLISHED 12 March 2024

CITATION
Zhao K, Li Q, Li P, Liu T, Liu X, Zhu F and Zhang L (2024) Single-cell transcriptome sequencing provides insight into multiple chemotherapy resistance in a patient with refractory DLBCL: a case report. *Front. Immunol.* 15:1303310. doi: 10.3389/fimmu.2024.1303310

Single-cell transcriptome sequencing provides insight into multiple chemotherapy resistance in a patient with refractory DLBCL: a case report

Kewei Zhao†, Qiuhui Li†, Pengye Li, Tao Liu, Xinxiu Liu, Fang Zhu and Liling Zhang*

Cancer Center, Union Hospital, Tongji Medical College, Huazhong University of Science and Technology, Wuhan, China

Relapsed and refractory diffuse large B-cell lymphoma (DLBCL) is associated with poor prognosis. As such, a comprehensive analysis of intratumoral components, intratumoral heterogeneity, and the immune microenvironment is essential to elucidate the mechanisms driving the progression of DLBCL and to develop new therapeutics. Here, we used single-cell transcriptome sequencing and conventional bulk next-generation sequencing (NGS) to understand the composite tumor landscape of a single patient who had experienced multiple tumor recurrences following several chemotherapy treatments. NGS revealed several key somatic mutations that are known to contribute to drug resistance. Based on gene expression profiles at the single-cell level, we identified four clusters of malignant B cells with distinct transcriptional signatures, showing high intra-tumoral heterogeneity. Among them, heterogeneity was reflected in activating several key pathways, human leukocyte antigen (HLA)-related molecules' expression, and key oncogenes, which may lead to multi-drug resistance. In addition, FOXP3+ regulatory CD4+ T cells and exhausted cytotoxic CD8+ T cells were identified, accounted for a significant proportion, and showed highly immunosuppressive properties. Finally, cell communication analysis indicated complex interactions between malignant B cells and T cells. In conclusion, this case report demonstrates the value of single-cell RNA sequencing for visualizing the tumor microenvironment and identifying potential therapeutic targets in a patient with treatment-refractory DLBCL. The combination of NGS and single-cell RNA sequencing may facilitate clinical decision-making and drug selection in challenging DLBCL cases.

KEYWORDS

diffuse large B-cell lymphoma, single-cell RNA sequencing, treatment resistance, tumor heterogeneity, tumor immune microenvironment

1 Introduction

Diffuse large B-cell lymphoma (DLBCL) is a highly heterogeneous malignant tumor with regard to clinical features, histological morphology, and genetic and molecular phenotype. Although standard first-line treatment with R-CHOP can cure DLBCL in 60% of patients, 40% of patients remain refractory to treatment or relapse after remission (1). The exact mechanisms driving disease relapse or refractoriness remain largely unknown, which can present a barrier to selecting appropriate treatment options.

Our understanding of the pathogenesis and progression of lymphoma has expanded considerably with knowledge of genetic alterations and dysregulation of intracellular pathways (2). By contrast, the role of the microenvironment in B-cell lymphoma has been underestimated. It is important to note that since B cells are an important part of the normal functioning immune system, the interactions between malignant cells and immune cells in the tumor microenvironment of B-cell lymphomas are more complex than in other solid tumors (3). The lymphoma microenvironment (LME) is a complicated interaction network of tumor, immune, and stromal cells with intra- and inter-tumor heterogeneity. Moreover, cytokines and chemokines secreted throughout the LME transmit various tumor-promoting and tumor-suppressing signals to regulate tumor growth and evolution, thereby affecting tumor progression and response to immunotherapy (3, 4). As a result, the LME is increasingly becoming a focus of attention in B-cell lymphoma pathophysiology and treatment resistance research.

Single-cell RNA sequencing enables comprehensive characterization of the cellular compositions and transcriptional features of malignant cells and infiltrating immune cells in many types of cancer (5). In order to explore the heterogeneity of DLBCL, decode the components of DLBCL tumor microenvironment and intratumor crosstalk of distinct cells, we conducted single-cell transcriptomic analysis of a patient who was resistant to multi-course chemotherapy, hoping to find some evidence related to tumor malignant progression and drug resistance.

2 Case presentation

A 71-year-old female patient presented with a painless and growing right supraclavicular mass in December 2020. The patient underwent ultrasound-guided puncture biopsy at Union Hospital, Tongji Medical College, Huazhong University of Science and Technology on February 1, 2021, and postoperative pathology showed the following: CD5-positive diffuse large B-cell lymphoma of germinal center B cell (GCB) origin with dual immune-expression of BCL2 and C-MYC. Immunohistochemical staining identified the following proteins in tumor cells: CD20 (+), CD3 (-), CD19 (+), CD22 (+), CD5 (+), CD10 (+), BCL6 (+), MUM1(+), BCL2 (+), C-MYC (60+), P53 (60%+), Ki67 (LI:90%) and EBER ISH (-). Fluorescence *in situ* hybridization (FISH) showed a negative C-MYC/IgH gene fusion test. Further PET/CT imaging was performed that showed the following: huge soft tissue masses in the right superior/inferior clavicle region, chest wall muscle space, right armpit, involving the right pectoralis major and pectoralis minor, multiple enlarged lymph nodes in the right neck, right armpit, left thoracic wall muscle space, left side of the erectus spinalis, mediastinum 2R region, right side of the sternum, and left medial psoas major, with partial fusion and abnormal increased metabolism. The spleen was enlarged and localized metabolism was increased. We also identified a soft tissue mass in the left iliac socket, involving the left iliopsoas muscle, piriformis muscle, and obturator internus muscle, with an abnormal increase in metabolism. These lesions were considered malignant lymphoma infiltration. There were no obvious abnormalities in bone marrow cytology and immunotyping. The patient was eventually diagnosed with CD5-positive DLBCL, GCB, stage IV, IPI score 4, with BCL2 and C-MYC dual expression.

Subsequently, the patient received four cycles of R-CHOP starting in February 2021, and a partial response (PR) was evaluated after two cycles of chemotherapy. After four cycles of chemotherapy, the patient developed a new mass in the right chest wall, and PET-CT indicated a progression of disease (PD). On June 23, 2021, the patient received combined rituximab, lenalidomide and zanubrutinib for 1 cycle. However, the mass in the patient's chest wall continued to increase in size. On August 4, 2021, the patient underwent a second ultrasound-guided puncture biopsy of a recurrent right chest wall mass. The specimens were sequenced by bulk next-generation sequencing and single-cell transcriptome sequencing. The patient was then enrolled in the ATG 010 clinical trial in August, 2021 (protocol No: Atg-010-DLBCL -001). Unfortunately, after 2 cycles of ATG-010 drug therapy, the patient still had PD in October 2021. The patient received palliative radiotherapy for the right chest wall tumor starting in November 2021. After radiotherapy with dose of 36Gy/18F, the mass of chest wall significantly reduced in size. However, the patient discontinued treatment due to severe bone marrow suppression caused by radiotherapy and previous chemotherapy and died in May 2022.

2.1 Next-generation sequencing revealed tumor-specific mutations

To better understand the mutational landscape of the patient's tumors, potential next-generation sequencing (NGS) was performed on biopsy tumor tissue and blood samples. The most important findings were: TP53 gene copy number deletion (copy number: 0.8) and missense mutation of p.D281G exon 8 (abundance: 51.3%). Other abnormalities included a nonsense mutation of CD83 gene p.W49* exon 2 (c.147G>A, abundance: 43%), CDKN2A and CDKN2B gene copy number deletion (copy number: 0.4), a shear mutation in intron 8 of the FAS gene (c.676 + 1G>A, abundance: 34.3%), missense mutation of p.C479G exon 13 in LYN gene (c.1435T>G, abundance: 30.0%), and missense mutation of p.P84L exon 2 in PRDM1 gene (c.251C>T, abundance: 50.2%).

2.2 Single-cell transcriptomic analysis

2.2.1 Identification of the five major cell types of DLBCL

After data quality control and filtering, a total of 9044 cells were analyzed. After dimensionality reduction and clustering, twelve major cell subpopulations were obtained using graph-based clustering (Figure 1). Five major cell types were identified using canonical marker genes: B cells (marker genes: CD19, MS4A1 and CD79A), T cells (marker genes: CD3D, CD3E, CD2), NK cells (marker genes: GNLY and NCAM1), myeloid cells (marker genes: LYZ and CD14), and fibroblasts (marker genes: COL1A1). Notably, B cells and T cells are the major cell subsets of DLBCL.

2.2.2 Identification of malignant B cells

To investigate the transcriptomic heterogeneity of malignant B cells in DLBCL tissues, we re-clustered the B cells and identified four cell subpopulations (Figure 2A). To further distinguish malignant B cells from non-malignant B cells, we took advantage of the fact that the malignant B cell population expresses only one type of immunoglobulin light chain, i.e. κ or λ light chains (6). The IGKC fraction (IGKC/IGKC + IGLC2) method was used to distinguish malignant B cells (7). Figure 2A shows the IGKC fraction of the four

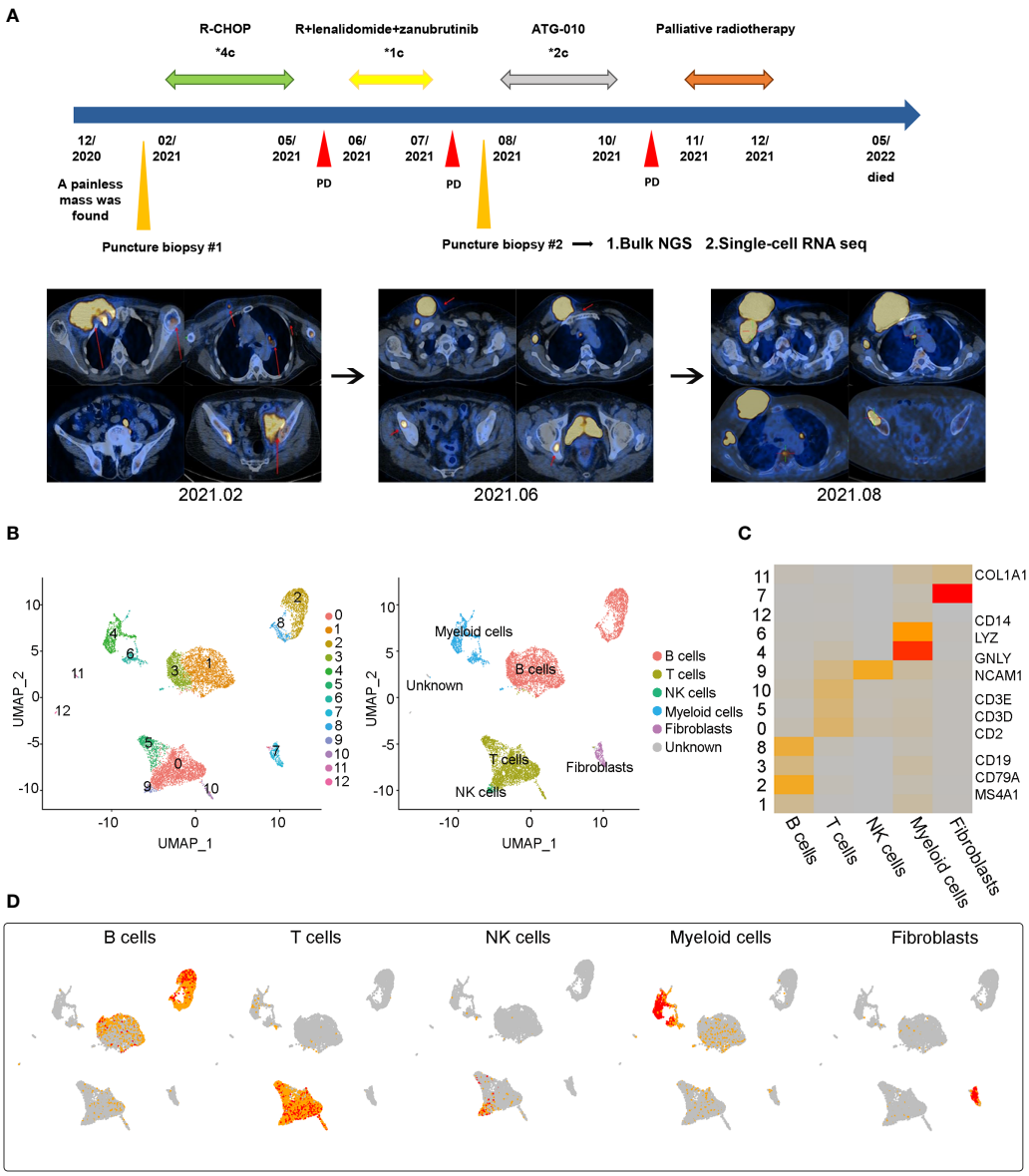

FIGURE 1
Case presentation and general overview of single cell transcriptome sequencing results in a refractory DLBCL sample **(A)** The treatment process of a 78-year-old woman and the representative CT images at the time of diagnosis (2021.02) and at two points of disease progression (2021.06 and 2021.08) **(B)** Uniform Manifold Approximation and Projection (UMAP) representation of twelve clusters and five identified cell types. **(C)** Heatmap of the relative expression level of marker genes across cells, sorted by cell type. Marker genes included CD19, CD79A and MS4A1 for B cells, CD2, CD3D and CD3E for T cells, GNLY and NCAM1 for NK cells, CD14 and LYZ for Myeloid cells, COL1A1 for fibroblasts. The expression was measured as the z-score normalized log2 (count+1). **(D)** Expression levels of typical marker genes across 9044 cells illustrated as UMAP plots.

10.3389/fimmu.2024.1303310

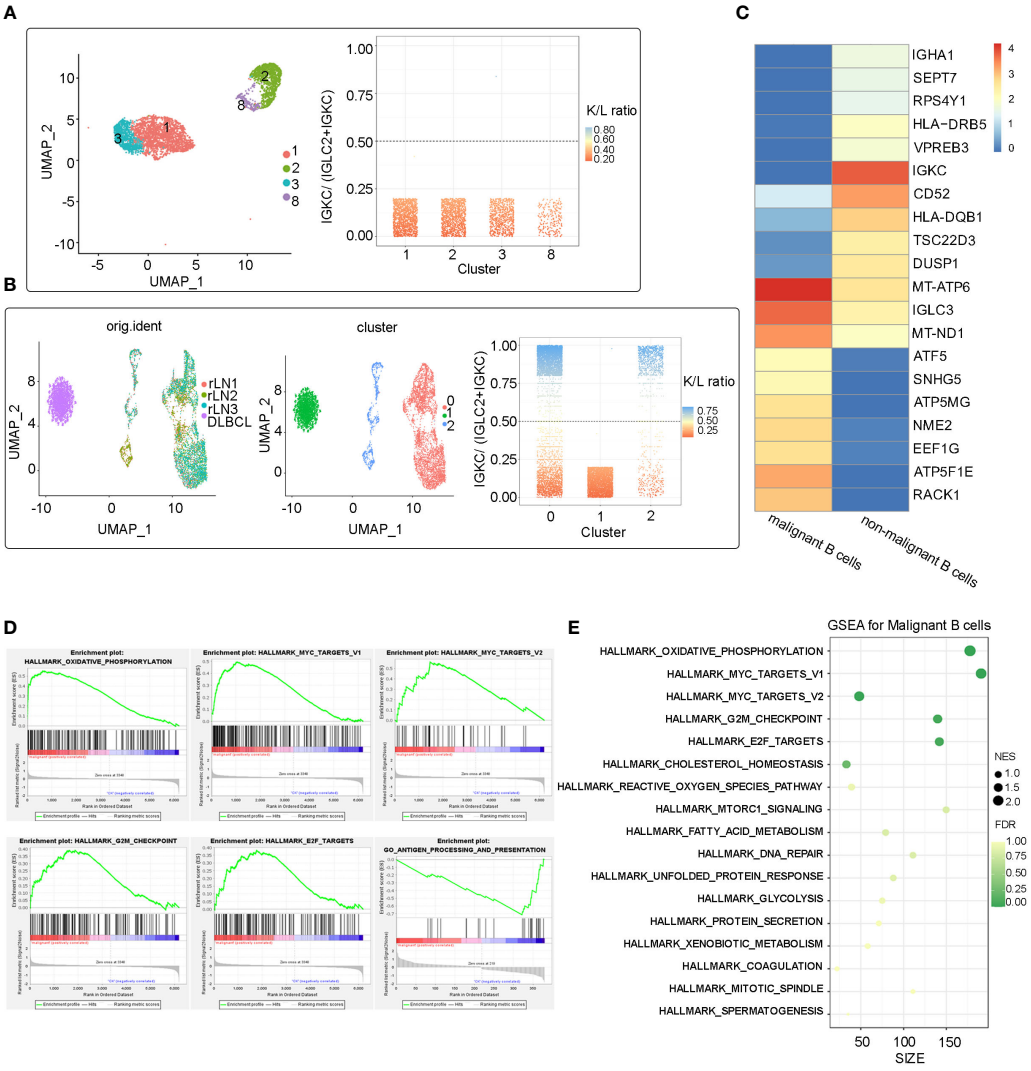

FIGURE 2
Malignant identification of B cells extracted from the refractory DLBCL patient's tissue and integration analysis of benign B cells from external data **(A)** UMAP plot of 4361 B cells from the refractory DLBCL tissue, showing the formation of the 4 main clusters. The IGKC fraction, IGKC ÷ (IGKC + IGLC2), was calculated for each B cell. If the IGKC fraction was >0.5, we classified a B cell as κ+, and if this ratio was below 0.5, we classified the B cell as λ+. The percentage of B cells expressing either κ or λ was calculated per ranscriptionally distinct B-cell cluster. The non-malignant healthy B-cell cluster contained approximately 50% κ- and 50% λ-expressing B cells, whereas the malignant clusters contained B cells homogeneously expressing the λ or κ light chain. All the four B cell clusers (cluster 1, 2, 3 and 8) identified in this refractory DLBCL sample expressed the λ light chain homogeneously and were therefore identified as malignant B cells. **(B)** After integrating the scRNA-Seq data from the study of Roider et al., three clusters were identified after re-clustering. Cluster 0,1 from external single-cell data was identified as benign B cell population, Cluster 1 from our refractory DLBCL sample was identified as malignant. **(C)** Heat map showing the top 10 differential expressed genes in the malignant B cell subpopulation and non-malignant B cell subpopulations (Wilcoxon test). **(D)** Several significant pathways had higher or lower activities in malignant B cell subpopulation than non-malignant B cell subpopulations by Gene Set Enrichment Analysis (GSEA). **(E)** Bubble map of significant pathways enriched in the malignant B cells subpopulation by GSEA.

B cell clusters 1, 2, 3, 8. It can be seen that the IGKC fraction of almost all B cells in these four clusters was lower than 0.25, indicating that they were B cells with uniform expression of λ+. Therefore, all four clusters of B cells were judged to be malignant B cells.

2.2.3 Comparison of malignant and Normal B cells by expression profiling

No benign B cells were found in the DLBCL sample. We next compared malignant B cells from this patient with benign non-malignant B cells from a study by Roider et al. (three tonsil and reactive lymph node samples as control samples, named rLN1, rLN2 and rLN3, respectively (7). Differentially expressed genes (DEG) and gene set enrichment analysis (GSEA) were analyzed. Reunion and integration analyses were also performed. The Uniform Manifold Approximation and Projection (UMAP) showed that all B cells of the four samples were clustered into three clusters (0, 1, 2), and one malignant cluster (cluster 1) identified by the IGKC scoring method was well distinguished from the other two non-malignant clusters (cluster 0, 2) (Figure 2B).

DEG analysis revealed molecular disparity among malignant and non-malignant B cells. We constructed a heat map showing that the top 10 genes expressed in malignant B cells were related to

ATP synthesis (ATP5F1E, ATP5MG, and ATP5MC2) and transcription regulation (ATF5, EEF1G, and ELOB), as well as LNCRNA (GAS5 and SNHG5) and ribosomal protein (RACK1) (Figure 2C). Notably, three of the ten genes that were significantly overexpressed were associated with ATP synthesis, which may be due to malignant B cells' adjustment in response to metabolic stress in the DLBCL microenvironment. GSEA revealed that genes upregulated in malignant B cells were enriched in oxidative phosphorylation pathways and cancer-related pathways (MYC targets V1, MYC targets V2, G2/M checkpoint, E2F targets). In addition, HLA-DQB1 and HLA-DRB5, which are both MHC class II molecules, were significantly downregulated in malignant B cells suggesting immune escape in DLBCL. Furthermore, GSEA analysis showed that antigen processing and presentation enrichment were significantly downregulated in malignant B cells compared with normal B cells (Figures 2D, E). Taken together, these results indicate high levels of oxidative phosphorylation, activation of pro-tumor pathways such as MYC and E2F, and decreased immunogenicity caused by low expression of MHC molecules, which may be a key factor in initiating or accelerating oncogenic signaling in malignant B-cell carcinoma.

2.2.4 Inter-transcriptomic heterogeneity of malignant B cells in DLBCL

Using scRNA-seq, we identified two large malignant B cell subpopulations (including cluster1_3 and cluster2_8), showing high heterogeneity. The significantly differentially expressed genes in the cluster1_3 and cluster2_8 subpopulations were identified (avg_log2FC>=0.5 & p_val_adj <= 0.01) and the Volcano Plot was mapped (Figure 3A). Further GSEA analysis showed that hallmarks of TNFA signaling via NFKB, IL2/STAT5 signaling, IL6/JAK/STAT3 signaling, inflammatory response signaling, and interferon-gamma signaling were highly enriched in cluster2_8 compared with cluster1_3 (Figure 3B). In addition, we compared the expression levels of different pathogenic signaling pathways in B-cell lymphoma in two subpopulations and the results showed that expression of BCR signaling, CD40 signaling, and NFKB signaling was generally higher in cluster2_8 vs. cluster1_3. In addition, cluster1_3 showed low expression of HLA I and II molecules, which may be beneficial for evasion of immune surveillance (Figure 3C).

Double-expression lymphoma (DEL) refers to DLBCL with immunohistochemical evidence of the co-expression of MYC and BCL2. In addition to cell-of-origin (COO), microenvironment transcription markers, and some genetic drive markers, MYC and BCL2 double expression have also been used to classify DLBCL and predict prognosis (8, 9). The patient in this case was identified as having dual expression of MYC and BCL2 proteins by immunohistochemistry. Therefore, we analyzed MYC and BCL2 gene expression in B cell clusters and found that the expression of both two genes was significantly higher in cluster2_8 than in cluster1_3 (Figure 3D). Therefore, in the subsequent analysis, we named cluster2_8 as MYC+BCL2+ B cells, which were identified as MYC/BCL2 double expression subpopulations at the single-cell level, and cluster 1_3 as MYC-BCL2- B cells. In addition, the expression of CD274 and CD47, two immunosuppressive immune checkpoints, were higher in cluster2_8 than in cluster1_3

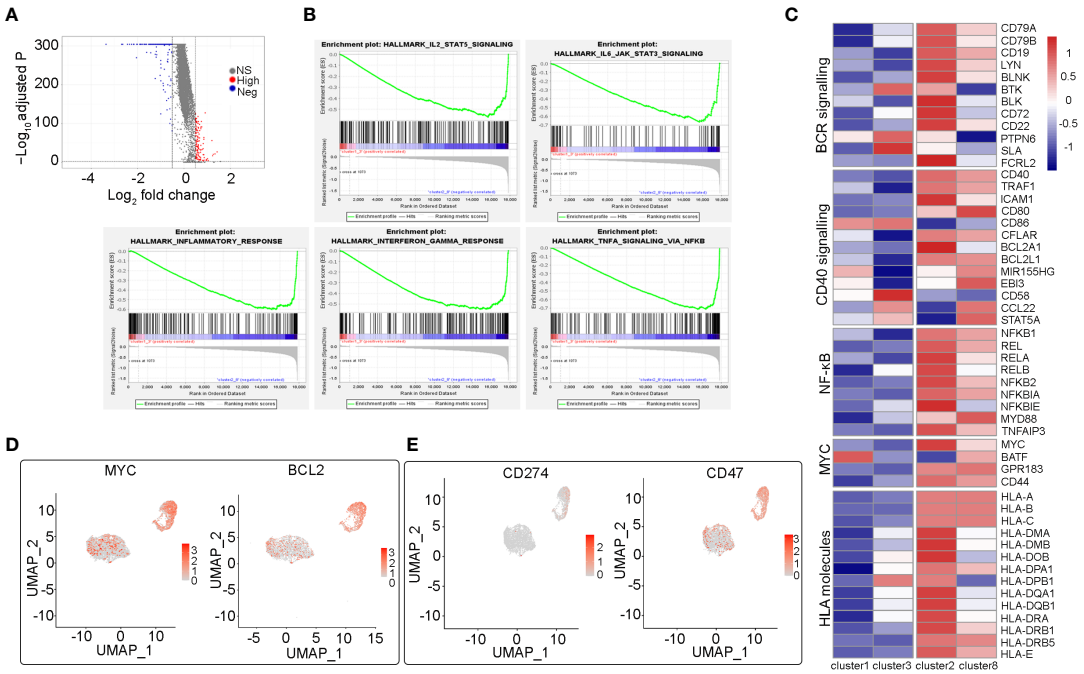

FIGURE 3
Heterogeneity analysis among two malignant B cell subpopulations (cluster2_8 vs cluster1_3) **(A)** The volcano map shows the differentially expressed genes between cluster2_8 and cluster1_3. **(B)** Several significant pathways with higher activities in cluster2_8 than cluster1_3 by GSEA. **(C)** Heatmap of the relative expression fold change (log2) of genes in essential pathogenic signaling pathways and HLA molecules in cluster2_8 and cluster1_3. **(D)** UMAP plots of selected genes (MYC, BCL2) expression level of different subsets of B cells. **(E)** UMAP plots of two immune checkpoint related genes (CD274, CD47) expression.

(Figure 3E). Overall, our results reveal a high degree of inter-tumor heterogeneity in DLBCL.

2.2.5 Identification of immunosuppressive T-cell subsets

Tumor-infiltrating immune cells, especially T lymphocytes in the LME, are highly heterogeneous and play a crucial role in tumor immune evasion and immunotherapeutic efficacy. To study the intrinsic transcriptome characteristics of infiltrating T cells in DLBCL, particularly those with immunosuppressive properties, we re-clustered T cells and identified 10 CD4+ or CD8+ T cell subsets (Figures 4A, B). Increasing evidence has shown that a large number of regulatory T cells (Tregs) exist in tumor tissues, which are the main regulators of autoimmune tolerance. They inhibit anti-tumor immune responses by inhibiting cytokine production and inhibiting the proliferation of CD8+ T cells, which may lead to ineffective anti-tumor responses and the proliferation of cancer cells (10, 11). FOXP3+ Tregs have been reported to be associated with adverse outcomes in DLBCL (12, 13). In accordance with established markers (CD4+, IL2RA+, FOXP3+), the C2 cluster was identified as CD4+ Tregs (Figures 4B, D), which makes up a large percentage of CD4+ T cells. In addition, based on increased expression of exhausted markers (LAG3, PDCD1, TIGIT, HAVCR2, CTLA4, and TOX), we identified two typical exhausted CD8+ T cell clusters (C3 and C6, Figures 4B, C). Tregs cells and CD8+ exhausted T cells were significantly enriched in this relapsed/refractory patient, highlighting the microenvironment's immunosuppressive nature. This finding suggests that this patient may benefit from immune checkpoint blockade therapies.

2.2.6 Cellular communication in diffuse large B-cell lymphoma

In order to explore the internal crosstalk between malignant B cells and T cells, a ligand–receptor analysis was conducted. We analyzed the interactions between both MYC+BCL2+ B cells and MYC-BCL2- B cells with T cells, and found that MYC+BCL2+ B cells maintain the most frequent interactions with T cells (Figure 4E). TNF-TNFR2 and TNF-ICOS interactions were more enriched between MYC+BCL2+ B cells and T cells, suggesting that MYC+BCL2+ B cells may contribute to the maintenance of the

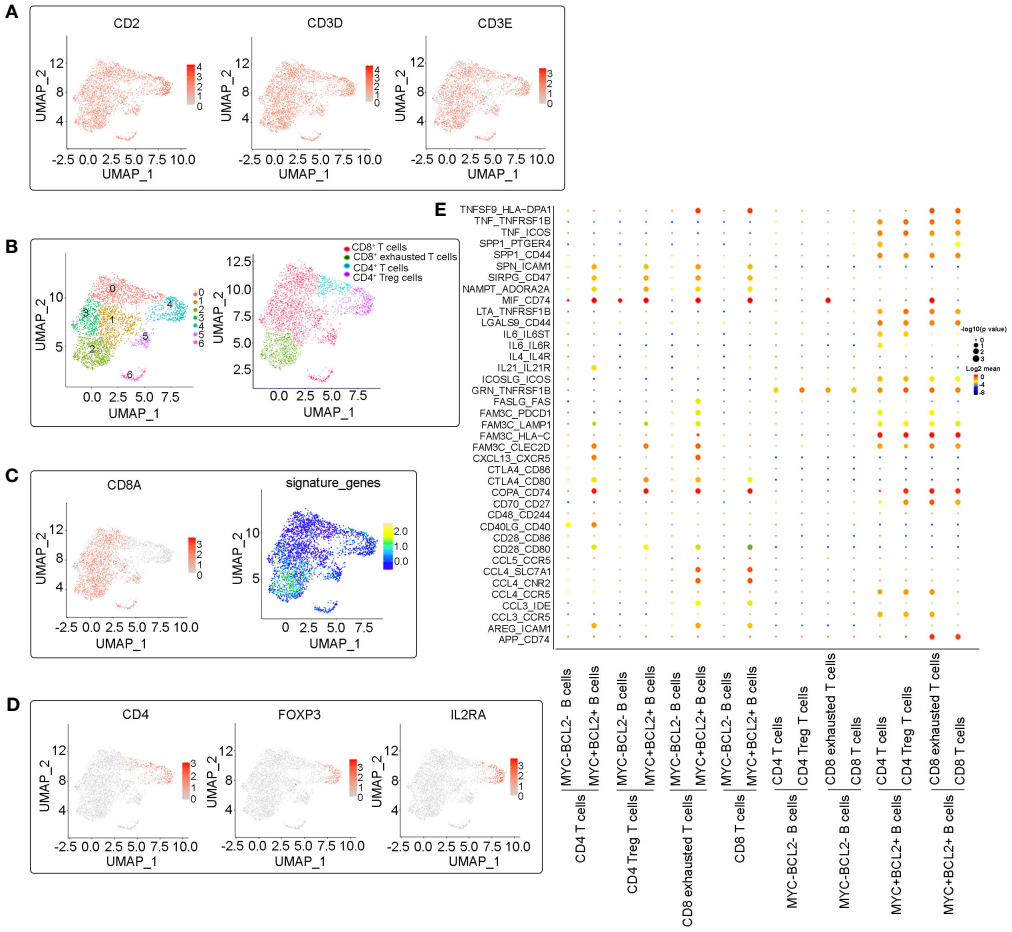

FIGURE 4
Subclustering analysis of T cells. **(A)** UMAP plots of expression of marker genes (CD2, CD3D and CD3E) in identified T cell clusters. **(B)** Identification and annotation of T cell subsets. Cells were colored according to their cluster or type. **(C)** UMAP plots plot showing the CD8 positive T cells clusters and exhausted-related signature genes (LAG3, PDCD1, TIGIT, HAVCR2, CTLA4, and TOX) expression in CD8 positive T cells clusters. **(D)** UMAP plots plot showing the expression of marker genes (CD4, IL2RA, FOXP3) in CD4 Treg cells. **(E)** Dot plot of predicted ligand-receptor interactions between different cell subsets in the microenvironments.

tumor-friendly immune microenvironment. This is because TNF-TNFR2 and TNF-ICOS signals have been shown to recruit immunosuppressant immune cells (14–16). Similarly, MYC +BCL2+ B cells may inhibit T-cell proliferation via interactions with SPP1-CD44 (17). In addition, MYC+BCL2+ malignant B cells may induce an immunosuppressive microenvironment via SIRPG_CD47 (18), INAMPT_A2RA2A (19), and CTLA-4_CD80 (20) interactions. This suggests that an immunosuppressive microenvironment may be more likely in DLBCL overexpression of MYC and BCL2 than in DCBCL with negative or low expression of MYC and BCL2.

3 Discussion

In this study, we combined conventional bulk sequencing and single-cell sequencing with a high-resolution perspective to analyze DLBCL cells from a patient resistant to multi-course therapy. The results revealed that the causes of drug resistance were not only somatic mutations identified by bulk sequencing, but also heterogeneity among malignant cells and an immunosuppressive microenvironment.

TP53 is an important tumor suppressor gene (21). However, mutation of the TP53 gene leads to abnormal production of the p53 protein, which results in disordered proliferation of tumor cells and the emergence of drug resistance (21). TP53 mutations have been identified as a poor prognostic factor in DLBCL, and such patients do not respond well to standard first-line therapies (22, 23). TP53 mutation occurs in 20–25% of patients with DLBCL and is one of the most commonly mutated genes in this patient population (24). In this case, the patient was identified by NGS sequencing as having copy number deletion and a missense mutation (exon 8) in the TP53 gene, which may be a significant cause of drug resistance.

In addition to conventional NGS sequencing, we carried out single-cell sequencing, which can offer a high-resolution perspective to investigate intra-tumor heterogeneity and the tumor microenvironment. We identified malignant cell subpopulations with distinct transcriptional characteristics. First, we found that oxidative phosphorylation is significantly enriched in malignant B cells compared with normal B cells, suggesting that oxidative phosphorylation may be an essential factor in carcinogenesis. This is consistent with a previous study on DLBCL, which showed that DLBCL metabolism is heavily dependent on oxidative phosphorylation (OXPHOS) (25). This metabolic change can be beneficial in providing the energy needs of rapidly growing, high-grade lymphoma cells, and OXPHOS inhibition therapy appears to be effective in these tumor subtypes (26). In addition, hallmark pathways in malignant B cells were mainly enriched in the MYC TARGETS and E2F TARGETS, suggesting that MYC and E2F play essential roles in promoting the proliferation of DLBCL tumor cells.

Tumor heterogeneity is an important characteristic in tumor occurrence and development, especially in DLBCL, and an important factor in multi-drug resistance. We identified four malignant B cell clusters with different transcriptional information using scRNA-seq, suggesting a high degree of inter-tumor heterogeneity. Since clusters 1 and 3 and clusters 2 and 8 have transcriptional similarities, they were analyzed together. The continuous abnormal activation of the B cell receptor (BCR) signaling pathway is believed to be closely related to patient survival and the malignant proliferation of tumors. The inhibition of essential kinases in the BCR signaling pathway has become the main focus of drug development for B-cell lymphoma (27). Abnormal activation of the NF-κB pathway can upregulate the expression of multiple anti-apoptotic genes, including Bcl-2, TRAFs, and IAPs, which contribute to the continuous malignant proliferation of cells and the occurrence of cancer. Abnormal activation of the NF-κB signaling pathway has been previously demonstrated in DLBCL (27). Activation of CD40 signaling can enhance the survival of tumor B cells; therefore, targeting CD40 with a monoclonal antibody could inhibit this process (28). Our single-cell transcriptome data showed that the corresponding molecule expression of BCR signaling, CD40 signaling, and NF-κB signaling in cluster2_8 was generally higher than cluster1_3, suggesting that these pathways were more active in cluster2_8. Monoclonal antibodies or specific medications that target these pathways have emerged as potential anti-cancer therapies, such as BTK inhibitors and CD40 monoclonal antibodies. However, due to intra-tumoral heterogeneity, these drugs may not kill all tumor cells, leading to drug resistance and potentially relapse.

Loss of MHC expression on cancer cells represents one of the tumor immune evasion mechanisms and is usually associated with poor prognosis (29). Here, we showed that the MYC+BCL2+ B cells expressed higher levels of MHC class I and II genes than MYC-BCL2- B cells, suggesting weak immunogenicity of MYC-BCL2- B cells and thus inducing immune escape. Although MYC+BCL2+ malignant B cells show higher MHC expression, which increases immune system recognition and makes them more likely to induce “hot tumors” compared to MYC-BCL2- malignant B cells, some subsets of MYC +BCL2+ malignant B cells can actually create an immunosuppressive microenvironment. In our analysis, GSEA analysis showed that several inflammations and immune-related signaling pathways including IL2_STAT5_signaling, IL6_JAK_STAT3_signaling, inflammatory_response, interferon_gamma_response, and TNFA_signaling_via_NFKB were specifically enriched in cluster 2_8. Inflammatory responses play a pivotal role during tumor development, invasion, and metastasis (30). Consistent with our results, it was reported that tumor cells and stromal cells in DLBCL can promote inflammation and immunosuppression through IL6_JAK_STAT3 and NF-kB signaling and induce immune system evasion (31). We found that MYC+BCL2+ B cells can cause an inflammatory microenvironment with immunosuppressive characteristics through some immune inflammatory signaling pathways. This is consistent with the conclusion of recent studies, which showed that lymphoma cells with obvious proliferative characteristics have the potential to induce a ‘depleted’ microenvironment (32–34). The patient in this case was not only confirmed as a double-expressed patient by immunohistochemistry, but at the cellular level, we also identified a malignant B subgroup of “MYC+ BCL2+”, indicating high proliferation of B cells in the patient’s tumor.

Cell–cell interaction analysis also revealed that MYC+BCL2+ B cells seem to have more communications with T cells and may contribute to the maintenance of a tumor-friendly immune

microenvironment through TNF-TNFR2, TNF-ICOS, SPP1-CD44, SIRPG_CD47, INAMPT_A2RA2A and CTLA-4_CD80 interaction (14–20). Exhausted CD8+ T cells and Tregs play an important role in the immunosuppressive microenvironment (10–13). Our analysis identified a high proportion of exhausted CD8+ T cells and FOXP3+ Tregs, which may indicate an immunosuppressive microenvironment induced by MYC+BCL2+ B cells interacting with T cells. This conclusion is consistent with two previous reports of immunosuppressive tumor microenvironments in DLBCL (35, 36). Immunotherapy, especially immune checkpoint inhibitors (ICIs), has made remarkable progress in the treatment of tumors. Depleted T cells express immunosuppressive receptors (such as LAG3, PDCD1, TIGIT, HAVCR2, CTLA4), and ICIs can block these signals, reverse depleted T cells, and restore the function of tumor-infiltrating T cells in the tumor microenvironment (37). Depending on the patient's deep sequencing results, an immune checkpoint inhibitor, such as anti-PD-1 antibodies, alone or in combination with chemotherapy (if the blood hemogram permits) can then be tried.

In conclusion, by combining NGS and single-cell transcriptome sequencing technology, this study provides insight into somatic mutations, transcriptional features in malignant B cells, and the immune microenvironment landscape in a patient with muti-drug resistant DLBCL. The results revealed that several critical somatic mutations, highly heterogeneous tumor cells, and immunosuppressive tumor microenvironment jointly contribute to multi-drug resistance. This in-depth biological exploration can provide therapeutic targets and immunotherapy biomarkers for relapsed and refractory DLBCL patients.

Data availability statement

The original contributions presented in the study are included in the article/supplementary materials. Further inquiries can be directed to the corresponding author.

Ethics statement

The studies involving humans were approved by Medical Ethics Committee of Tongji Medical College, Huazhong University of Science and Technology. The studies were conducted in accordance with the local legislation and institutional requirements. The participants provided their written informed consent to participate in this study. Written informed consent was obtained from the individual(s) for the publication of any potentially identifiable images or data included in this article.

Author contributions

KZ: Formal analysis, Methodology, Resources, Validation, Writing – original draft, Writing – review & editing. QL: Formal analysis, Methodology, Software, Validation, Writing – original draft, Writing – review & editing. PL: Methodology, Software, Validation, Writing – review & editing. TL: Supervision, Writing – review & editing. XL: Supervision, Writing – review & editing. FZ: Supervision, Writing – review & editing. LZ: Conceptualization, Project administration, Validation, Writing – review & editing.

Funding

The author(s) declare that no financial support was received for the research, authorship, and/or publication of this article.

Conflict of interest

The authors declare that the research was conducted in the absence of any commercial or financial relationships that could be construed as a potential conflict of interest.

Publisher's note

References

1. Li S, Young KH, Medeiros LJ. Diffuse large B-cell lymphoma. *Pathology*. (2018) 50:74–87. doi: 10.1016/j.pathol.2017.09.006

2. Shaffer AL 3rd, Young RM, Staudt LM. Pathogenesis of human B cell lymphomas. *Annu Rev Immunol*. (2012) 30:565–610. doi: 10.1146/annurev-immunol-020711-075027

3. Ansell SM, Vonderheide RH. Cellular composition of the tumor microenvironment. *Am Soc Clin Oncol Educ Book Am Soc Clin Oncol Annu Meeting*. (2013). doi: 10.1200/EdBook_AM.2013.33.e91

4. Coupland SE. The challenge of the microenvironment in B-cell lymphomas. *Histopathology*. (2011) 58:69–80. doi: 10.1111/his.2011.58.issue-1

5. Baslan T, Hicks J. Unravelling biology and shifting paradigms in cancer with single-cell sequencing. *Nat Rev Cancer*. (2017) 17:557–69. doi: 10.1038/nrc.2017.58

6. Kaleem Z, Zehnbauer BA, White G, Zutter MM. Lack of expression of surface immunoglobulin light chains in B-cell non-hodgkin lymphomas. *Am J Clin Pathol*. (2000) 113:399–405. doi: 10.1309/28ED-MM0T-DT3B-MT4P

7. Roider T, Seufert J, Uvarovskii A, Frauhammer F, Bordas M, Abedpour N, et al. Dissecting intratumour heterogeneity of nodal B-cell lymphomas at the transcriptional, genetic and drug-response levels. *Nat Cell Biol*. (2020) 22:896–906. doi: 10.1038/s41556-020-0532-x

8. Chapuy B, Stewart C, Dunford AJ, Kim J, Kamburov A, Redd RA, et al. Molecular subtypes of diffuse large B cell lymphoma are associated with distinct pathogenic mechanisms and outcomes. *Nat Med*. (2018) 24:679–90. doi: 10.1038/s41591-018-0016-8

9. Schmitz R, Wright GW, Huang DW, Johnson CA, Phelan JD, Wang JQ, et al. Genetics and pathogenesis of diffuse large B-cell lymphoma. *New Engl J Med*. (2018) 378:1396–407. doi: 10.1056/NEJMoa1801445

10. Fontenot JD, Rasmussen JP, Williams LM, Dooley JL, Farr AG, Rudensky AY. Regulatory T cell lineage specification by the forkhead transcription factor foxp3. *Immunity*. (2005) 22:329–41. doi: 10.1016/j.immuni.2005.01.016

11. Dadey RE, Workman CJ, Vignali DAA. Regulatory T cells in the tumor microenvironment. *Adv Exp Med Biol*. (2020) 1273:105–34. doi: 10.1007/978-3-030-49270-0_6

12. Chang C, Wu SY, Kang YW, Lin KP, Chen TY, Medeiros LJ, et al. High levels of regulatory T cells in blood are a poor prognostic factor in patients with diffuse large B-cell lymphoma. *Am J Clin Pathol*. (2015) 144:935–44. doi: 10.1309/AJCPUJGMVV6ZF4GG

13. Nakayama S, Yokote T, Akioka T, Hiraoka N, Nishiwaki U, Miyoshi T, et al. Infiltration of effector regulatory T cells predicts poor prognosis of diffuse large B-cell lymphoma, not otherwise specified. *Blood Adv*. (2017) 1:486–93. doi: 10.1182/bloodadvances.2016000885

14. Chen X, Plebanski M. Editorial: the role of tnf-tnfr2 signal in immunosuppressive cells and its therapeutic implications. *Front Immunol*. (2019) 10:2126. doi: 10.3389/fimmu.2019.02126

15. He T, Zhao Y, Zhao P, Zhao L, Zakaria J, Wang K. Signaling pathway(S) of tnfr2 required for the immunoregulatory effect of cd4(+)Foxp3(+) regulatory T cells. *Int Immunopharmacol*. (2022) 108:108823. doi: 10.1016/j.intimp.2022.108823

16. Grinberg-Bleyer Y, Baeyens A, You S, Elhage R, Fourcade G, Gregoire S, et al. Il-2 reverses established type 1 diabetes in nod mice by a local effect on pancreatic regulatory T cells. *J Exp Med*. (2010) 207:1871–8. doi: 10.1084/jem.20100209

17. Cheng M, Liang G, Yin Z, Lin X, Sun Q, Liu Y. Immunosuppressive role of spp1-cd44 in the tumor microenvironment of intrahepatic cholangiocarcinoma assessed by single-cell rna sequencing. *J Cancer Res Clin Oncol*. (2022) 2023(149):5497–5512. doi: 10.1007/s00432-022-04498-w

18. Xu C, Jin G, Wu H, Cui W, Wang YH, Manne RK, et al. Sirpγ-expressing cancer stem-like cells promote immune escape of lung cancer via hippo signaling. *J Clin Invest*. (2022) 132:e141797. doi: 10.1172/jci141797

19. Willingham SB, Hotson AN, Miller RA. Targeting the A2ar in cancer; early lessons from the clinic. *Curr Opin Pharmacol*. (2020) 53:126–33. doi: 10.1016/j.coph.2020.08.003

20. Sansom DM. Cd28, ctla-4 and their ligands: who does what and to whom? *Immunology*. (2000) 101:169–77. doi: 10.1046/j.1365-2567.2000.00121.x

21. Whibley C, Pharoah PD, Hollstein M. P53 polymorphisms: cancer implications. *Nat Rev Cancer*. (2009) 9:95–107. doi: 10.1038/nrc2584

22. Ichikawa A, Hotta T, Takagi N, Tsushita K, Kinoshita T, Nagai H, et al. Mutations of P53 gene and their relation to disease progression in B-cell lymphoma. *Blood*. (1992) 79:2701–7. doi: 10.1182/blood.V79.10.2701.2701

23. Ichikawa A, Kinoshita T, Watanabe T, Kato H, Nagai H, Tsushita K, et al. Mutations of the P53 gene as a prognostic factor in aggressive B-cell lymphoma. *New Engl J Med*. (1997) 337:529–34. doi: 10.1056/nejm199708213370804

24. Xu-Monette ZY, Medeiros LJ, Li Y, Orlowski RZ, Andreeff M, Bueso-Ramos CE, et al. Dysfunction of the tp53 tumor suppressor gene in lymphoid Malignancies. *Blood*. (2012) 119:3668–83. doi: 10.1182/blood-2011-11-366062

25. Caro P, Kishan AU, Norberg E, Stanley IA, Chapuy B, Ficarro SB, et al. Metabolic signatures uncover distinct targets in molecular subsets of diffuse large B cell lymphoma. *Cancer Cell*. (2012) 22:547–60. doi: 10.1016/j.ccr.2012.08.014

26. Ashton TM, McKenna WG, Kunz-Schughart LA, Higgins GS. Oxidative phosphorylation as an emerging target in cancer therapy. *Clin Cancer Res: Off J Am Assoc Cancer Res*. (2018) 24:2482–90. doi: 10.1158/1078-0432.Ccr-17-3070

27. Xu W, Berning P, Lenz G. Targeting B-cell receptor and pi3k signaling in diffuse large B-cell lymphoma. *Blood*. (2021) 138:1110–9. doi: 10.1182/blood.2020006784

28. Hömig-Hölzel C, Hojer C, Rastelli J, Casola S, Strobl LJ, Müller W, et al. Constitutive cd40 signaling in B cells selectively activates the noncanonical nf-kappab pathway and promotes lymphomagenesis. *J Exp Med*. (2008) 205:1317–29. doi: 10.1084/jem.20080238

29. Roemer MGM, Redd RA, Cader FZ, Pak CJ, Abdelrahman S, Ouyang J, et al. Major histocompatibility complex class ii and programmed death ligand 1 expression predict outcome after programmed death 1 blockade in classic hodgkin lymphoma. *J Clin Oncol: Off J Am Soc Clin Oncol*. (2018) 36:942–50. doi: 10.1200/jco.2017.77.3994

30. Diakos CI, Charles KA, McMillan DC, Clarke SJ. Cancer-related inflammation and treatment effectiveness. *Lancet Oncol*. (2014) 15:e493–503. doi: 10.1016/s1470-2045(14)70263-3

31. Lu L, Zhu F, Zhang M, Li Y, Drennan AC, Kimpara S, et al. Gene regulation and suppression of type I interferon signaling by stat3 in diffuse large B cell lymphoma. *Proc Natl Acad Sci United States America*. (2018) 115:E498–e505. doi: 10.1073/pnas.1715118115

32. Kotlov N, Bagaev A, Revuelta MV, Phillip JM, Cacciapuoti MT, Antysheva Z, et al. Clinical and biological subtypes of B-cell lymphoma revealed by microenvironmental signatures. *Cancer Discovery*. (2021) 11:1468–89. doi: 10.1158/2159-8290.Cd-20-0839

33. Xu-Monette ZY, Wei L, Fang X, Au Q, Nunns H, Nagy M, et al. Genetic subtyping and phenotypic characterization of the immune microenvironment and myc/bcl2 double expression reveal heterogeneity in diffuse large B-cell lymphoma. *Clin Cancer Res: Off J Am Assoc Cancer Res*. (2022) 28:972–83. doi: 10.1158/1078-0432.Ccr-21-2949

34. Kumar A, Taghi Khani A, Duault C, Aramburo S, Sanchez Ortiz A, Lee SJ, et al. Intrinsic suppression of type I interferon production underlies the therapeutic efficacy of il-15-producing natural killer cells in B-cell acute lymphoblastic leukemia. *J Immunother Cancer*. (2023) 11:e006649. doi: 10.1136/jitc-2022-006649

35. Georgiou K, Chen L, Berglund M, Ren W, de Miranda NF, Lisboa S, et al. Genetic basis of pd-L1 overexpression in diffuse large B-cell lymphomas. *Blood*. (2016) 127:3026–34. doi: 10.1182/blood-2015-12-686550

36. Zhang T, Liu H, Jiao L, Zhang Z, He J, Li L, et al. Genetic characteristics involving the pd-1/pd-L1/L2 and cd73/A2ar axes and the immunosuppressive microenvironment in dlbcl. *J Immunother Cancer*. (2022) 10:e004114. doi: 10.1136/jitc-2021-004114

37. Bagchi S, Yuan R, Engleman EG. Immune checkpoint inhibitors for the treatment of cancer: clinical impact and mechanisms of response and resistance. *Annu Rev Pathol*. (2021) 16:223–49. doi: 10.1146/annurev-pathol-042020-042741

frontiers | Frontiers in Oncology

TYPE Original Research
PUBLISHED 06 June 2024
DOI 10.3389/fonc.2024.1408238

OPEN ACCESS

EDITED BY
Shimin Hu,
University of Texas MD Anderson Cancer Center, United States

REVIEWED BY
Mohammad Vasef,
University of New Mexico, United States
Luis Alberto De Pádua Covas Lage,
University of São Paulo, Brazil

*CORRESPONDENCE
Joshua R. Menke
jmenke@stanford.edu
Dita A. Gratzinger
ditag@stanford.edu

RECEIVED 27 March 2024
ACCEPTED 15 May 2024
PUBLISHED 06 June 2024

CITATION
Menke JR, Aypar U, Bangs CD, Cook SL, Gupta S, Hasserjian RP, Kong CS, Lin O, Long SR, Ly A, Menke JAS, Natkunam Y, Ruiz-Cordero R, Spiteri E, Ye J, Zadeh SL and Gratzinger DA (2024) Performance of *MYC*, *BCL2*, and *BCL6* break-apart FISH in small biopsies with large B-cell lymphoma: a retrospective Cytopathology Hematopathology Interinstitutional Consortium study.
Front. Oncol. 14:1408238.
doi: 10.3389/fonc.2024.1408238

Performance of *MYC*, *BCL2*, and *BCL6* break-apart FISH in small biopsies with large B-cell lymphoma: a retrospective Cytopathology Hematopathology Interinstitutional Consortium study

Joshua R. Menke[1*], Umut Aypar[2], Charles D. Bangs[3], Stephen L. Cook[4], Srishti Gupta[1,5], Robert P. Hasserjian[6], Christina S. Kong[7], Oscar Lin[8], Steven R. Long[9], Amy Ly[10], Jacob A. S. Menke[11], Yasodha Natkunam[1], Roberto Ruiz-Cordero[8,12], Elizabeth Spiteri[3], Julia Ye[9], Sara L. Zadeh[13] and Dita A. Gratzinger[1*] on behalf of the Cytopathology Hematopathology Interinstitutional Consortium (CHIC)

[1]Division of Hematopathology, Department of Pathology, Stanford University, Stanford, CA, United States, [2]Division of Cytogenetics, Department of Pathology and Laboratory Medicine, Memorial Sloan Kettering Cancer Center, New York, NY, United States, [3]Division of Cytogenetics, Department of Pathology, Stanford University, Stanford, CA, United States, [4]Department of Laboratory Medicine, San Francisco Veterans Administration Health Care System, San Francisco, CA, United States, [5]Division of Hematopathology, Department of Laboratory Medicine, San Francisco, CA, United States, [6]Division of Hematopathology, Department of Pathology, Massachusetts General Hospital, Boston, MA, United States, [7]Division of Cytopathology, Department of Pathology, Stanford University, Stanford, CA, United States, [8]Division of Cytopathology, Department of Pathology and Laboratory Medicine, Memorial Sloan Kettering Cancer Center, New York, NY, United States, [9]Division of Cytopathology, Department of Pathology, University of California, San Francisco, San Francisco, CA, United States, [10]Division of Cytopathology, Department of Pathology, Massachusetts General Hospital, Boston, MA, United States, [11]Senior Backend Engineer, Big Nerd Ranch, Atlanta, GA, United States, [12]Divisons of Molecular Genetic Pathology, Cytopathology, and Hematopathology, Department of Pathology and Laboratory Medicine, University of Miami, Miami, FL, United States, [13]Division of Cytopathology, Department of Pathology, University of Virginia, Charlottesville, VA, United States

Introduction: Fluorescence *in situ* hybridization (FISH) is an essential ancillary study used to identify clinically aggressive subsets of large B-cell lymphomas that have *MYC, BCL2*, or *BCL6* rearrangements. Small-volume biopsies such as fine needle aspiration biopsy (FNAB) and core needle biopsy (CNB) are increasingly used to diagnose lymphoma and obtain material for ancillary studies such as FISH. However, the performance of FISH in small biopsies has not been thoroughly evaluated or compared to surgical biopsies.

Methods: We describe the results of *MYC, BCL2,* and *BCL6* FISH in a series of 222 biopsy specimens, including FNAB with cell blocks, CNBs, and surgical excisional

or incisional biopsies from 208 unique patients aggregated from 6 academic medical centers. A subset of patients had FNAB followed by a surgical biopsy (either CNB or excisional biopsy) obtained from the same or contiguous anatomic site as part of the same clinical workup; FISH results were compared for these paired specimens.

Results: FISH had a low hybridization failure rate of around 1% across all specimen types. FISH identified concurrent *MYC* and *BCL2* rearrangements in 20 of 197 (10%) specimens and concurrent *MYC* and *BCL6* rearrangements in 3 of 182 (1.6%) specimens. The paired FNAB and surgical biopsy specimens did not show any discrepancies for *MYC* or *BCL2* FISH; of the 17 patients with 34 paired cytology and surgical specimens, only 2 of the 49 FISH probes compared (4% of all comparisons) showed any discrepancy and both were at the *BCL6* locus. One discrepancy was due to necrosis of the CNB specimen causing a false negative *BCL6* FISH result when compared to the FNAB cell block that demonstrated a *BCL6* rearrangement.

Discussion: FISH showed a similar hybridization failure rate in all biopsy types. Ultimately, *MYC, BCL2*, or *BCL6* FISH showed 96% concordance when compared across paired cytology and surgical specimens, suggesting FNAB with cell block is equivalent to other biopsy alternatives for evaluation of DLBCL or HGBCL FISH testing.

KEYWORDS

diffuse large B-cell lymphoma, high-grade B-cell lymphoma, double-hit lymphoma, FISH, BCL2 rearrangement, MYC rearrangement

1 Introduction

An important subset of diffuse large B-cell lymphoma (DLBCL) and high-grade B-cell lymphoma (HGBCL) have *MYC* and *BCL2* rearrangements Large B-cell lymphoma or high-grade B-cell lymphoma with *MYC* and *BCL2* rearrangements are commonly referred to as "double-hit" lymphoma (DHL), which portends more aggressive clinical behavior and inferior progression-free survival compared to other cases of diffuse large B-cell lymphoma, germinal center B-cell subtype, or other high-grade B-cell lymphoma (1–5). Both the 5th Edition of the World Health Organization Classification of Haematolymphoid tumors (WHO5) (6) and the International Consensus Classification of Lymphoid Neoplasms (ICC) (7) now classify diffuse large B-cell lymphoma and high-grade B-cell lymphoma with concurrent *MYC* and *BCL6* "double-hit" lymphomas separately due to the unclear prognostic significance of this combination, with some studies not showing distinct biology for these cases (1, 2), but other studies demonstrating an association with a poor outcome (3, 8–11). Fluorescence *in situ* hybridization (FISH) is a frequently used technique to detect *MYC*, *BCL2*, and *BCL6* rearrangements. Because diffuse large B-cell lymphoma and other high-grade B-cell lymphoma can look identical morphologically to "double-hit" lymphoma, at a minimum *MYC* FISH must be obtained in every case (see Figure 1 for an example of a case that has similar morphology to diffuse large B-cell lymphoma, NOS on various slide stain preparations, but ended up having both *MYC* and *BCL2* rearrangements). In one survey of cytogenetics laboratories, the most common test strategy (67%) was upfront testing of *MYC*, *BCL2*, and *BCL6* FISH on every case while fewer labs (26%) performed *BCL2* and *BCL6* FISH testing only if *MYC* is rearranged (12). In the same survey study, 56% of laboratories performed *MYC* break-apart probe (BAP) in combination with *IGH/MYC* dual fusion probe while 43% of laboratories performed only *MYC* BAP. MYC and BCL2 IHC are known to be poor predictors of *MYC* rearrangements at the gene level and polymorphisms have even been shown to create false negative MYC IHC results (13). Data are less clear regarding *MYC* and *BCL6* rearrangements, but many institutions continue to test for *BCL6* rearrangements given some data indicating these cases may have an inferior outcome (3, 8–11).

Fine needle aspiration biopsy (FNAB) is increasingly used for triage of lymphadenopathy and diagnosis of lymphoma. Additionally, cell blocks (CB) and smear slides from FNAB can effectively be used for FISH in various neoplasms (14–17). However, only a few, small single institutional studies have described FISH

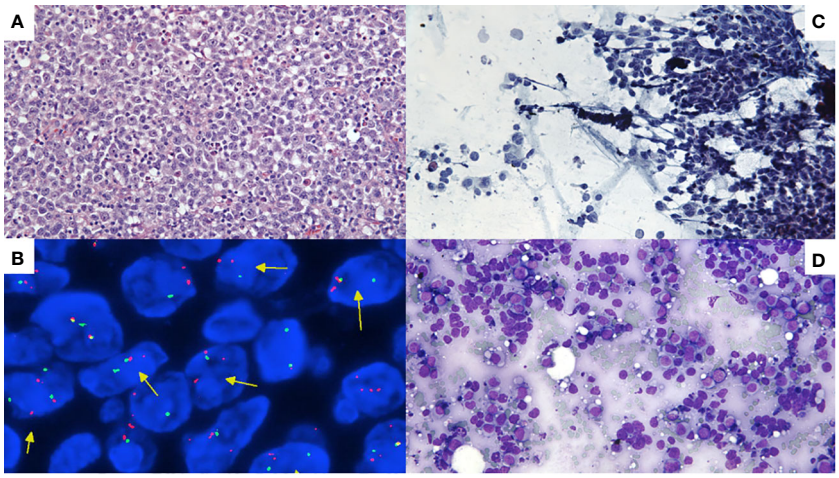

FIGURE 1
(A) H&E-stained section of lymph node cell block demonstrating effacement by high-grade B-cell lymphoma with *MYC* and *BCL2* rearrangements. **(B)** *MYC* interphase FISH showing separation of orange and green signals indicating a *MYC* rearrangement (see arrows). **(C)** Pap-stained smear slide showing aggregates of large atypical lymphoid cells. **(D)** May-Grünwald Giemsa (MGG)-stained smear slide of cytology smear slide similarly showing large cells. In general, Pap stains and MGG stains are complementary and helpful to obtain in all lymph node FNAB: Pap-stained slides demonstrate greater nuclear detail but make cells appear smaller and have poor cytoplasmic detail while May-Grünwald Giemsa stains show greater cytoplasmic detail and larger cell size but poor nuclear detail.

(such as *MYC*) in FNAB smears and cell block for lymphoma (18–21) and no comparisons to core biopsy or the gold standard excisional biopsy exist to our knowledge. We have two principal aims in this multi-institutional study of FISH performance in diffuse large B-cell lymphoma and high-grade B-cell lymphoma: 1) compare the success rate of *MYC, BCL2*, and *BCL6* FISH hybridization across FNAB with cell block, core biopsy, and excisional biopsy, 2) compare FNAB to either core biopsy or excisional biopsy for FISH from the same patient.

2 Materials and methods

Six academic medical centers participated in this study. The medical centers were assigned data access groups in REDCap (see section below on REDCap) and they consisted of Massachusetts General Hospital (MGH), Memorial Sloan Kettering Cancer Center (MSKCC), San Francisco Veterans Administration Health Care System (SFVAHCS), Stanford, University of California San Francisco (UCSF), and University of Virginia (UVA).

A retrospective search was conducted of the pathology informatics systems with keywords "FISH" AND "diffuse large B-cell lymphoma" OR "high-grade B-cell lymphoma" over the 10-year period from 1/1/2010 to 12/31/2019. A complementary search was performed of cytogenetics lab data for all *MYC* FISH studies performed on cytology samples to catch cases missed by the pathology data system and then identify paired surgical samples through the pathology archive. Only specimens that had *MYC* FISH performed were included (n=222); of these cases, 200 had *BCL2* FISH performed (90%) and 186 (84%) *BCL6* FISH performed. Exclusion criteria included bone marrow biopsy specimens (due to alternative fixation used in some of these specimens and decalcification that could cause false negatives), and body fluid specimens (due to the numerous pre-analytic variables such as fixative type that might influence FISH performance in cell blocks). The age of the patient was recorded for each biopsy, but for Tables 1, 2, the age of the patient was determined as the age at the first biopsy specimen. The WHO4R classification terminology "high-grade B-cell lymphoma with *MYC* and *BCL2* and/or *BCL6* rearrangements" was originally used for "double hit" or "triple hit" cases in this patient biopsy cohort with an endpoint in 2019 irrespective of whether the morphology was more in keeping with diffuse large B-cell lymphoma or high-grade B-cell lymphoma (22). In keeping with the WHO5 and ICC, we subsequently distinguished *MYC* and *BCL2* rearranged cases from *MYC* and *BCL6* rearranged cases. This manuscript uses the terms high-grade B-cell lymphoma-*MYC/BCL2* or high-grade B-cell lymphoma-*MYC/BCL6* to distinguish these two groups regardless of whether the morphology was originally interpreted as diffuse large B-cell lymphoma or high-grade B-cell lymphoma.

All data extracted from pathology reports was entered into REDCap (Research Electronic Data Capture), a secure, encrypted online database. Study data were collected and managed using REDCap electronic data capture tools hosted at Stanford (23, 24). REDCap (Research Electronic Data Capture) is a secure, web-based software platform designed to support data capture for research studies, providing 1) an intuitive interface for validated data capture; 2) audit trails for tracking data manipulation and export procedures; 3) automated export procedures for seamless data downloads to common statistical packages; and 4) procedures for data integration and interoperability with external sources.

At Stanford Cytogenetics Laboratory, FISH was performed on formalin-fixed, paraffin-embedded (FFPE) sections; the area of interest was circled on the corresponding H&E stained slide by the ordering pathologist. ZytoLight (ZytoVision Gmbh, Bremerhaven, Germany) break-apart probe sets were used for

10.3389/fonc.2024.1408238

TABLE 1 Clinical characteristics of all 208 patients included in study.

Number of patients	208
Age (mean (SD))	63.65 (16.55)
Gender = Male (%)	123 (59.1)
Gender = Female (%)	83 (40.3)
Data Access Group (%)	
MGH	25 (12.0)
MSKCC	13 (6.2)
SFVAHCS	13 (6.2)
Stanford	134 (64.4)
UCSF	21 (10.1)
UVA	2 (1.0)
History of B-cell non Hodgkin lymphoma? = Yes (%)	81 (39.3)
Prior large B cell lymphoma diagnosis (%)	23 (29.1)
DLBCL, NOS	22 (95.6)
Prior follicular lymphoma diagnosis (%)	52 (64.2)
Classic follicular lymphoma (grade 1–2)	42 (80.8)
Classic follicular lymphoma (grade 3A)	6 (11.5)
other or unknown	2 (3.8)
Primary cutaneous follicle center lymphoma	2 (3.8)
Prior diagnosis of low grade B cell lymphoma (%)	13 (16.5)
CLL/SLL	4 (30.8)
EMZL	2 (15.4)
LPL	2 (15.4)
Mantle cell lymphoma	1 (7.7)
NMZL	1 (7.7)
other or unknown	1 (7.7)
Primary cutaneous MZL	1 (7.7)
SMZL	1 (7.7)
High-grade B-cell lymphoma diagnosis (%)	4 (5.1)
Burkitt lymphoma	1 (25.0)
High grade B-cell lymphoma, with MYC and BCL2 rearrangements	1 (25.0)
High grade B-cell lymphoma, NOS	2 (50.0)
Prior solid organ or stem cell transplant (%)	16 (7.7)
Stem cell transplant	9 (56.2)
Solid organ transplant	7 (43.8)
Prior chemotherapy (%)	52 (26.0)
Reason for chemotherapy (%)	
carcinoma	4 (7.7)
carcinoma and lymphoma	1 (1.9)
lymphoma	46 (88.5)
other or unknown	1 (1.9)

The classification used for all diagnoses was the WHOR4, which is equivalent to WHO5 and ICC for these diagnoses. Abbreviations used: CLL/SLL (chronic lymphocytic leukemia/small lymphocytic lymphoma), EMZL (extranodal marginal zone lymphoma), LPL (lymphoplasmacytic lymphoma), NMZL (nodal marginal zone lymphoma), MZL (marginal zone lymphoma), SMZL (splenic marginal zone lymphoma), MGH (Massachusetts General Hospital), MSKCC (Memorial Sloan Kettering Cancer Center), SFVAHCS (San Francisco Veterans Administration Health Care System), UCSF (University of California San Francisco), UVA (University of Virginia).

MYC, *BCL2*, and *BCL6* FISH. The *MYC* probe set was used with orange probe 5' to *MYC* and green probe 3' to *MYC* on 8q24.21. *BCL2* (18q21) probe set included 3'*BCL2* in green and 5'*BCL2* in orange. The same probe configuration was used for *BCL6* (3q27): 3'*BCL6* is green, 5'*BCL6* is orange. All FISH results were scored in 100 interphase cells. A rearrangement was reported if 10% or more cells showed a split signal. The results of these FISH tests were compared to existing FISH results on a different specimen when available. Paired specimens were either obtained from the same anatomic site or from contiguous sites e.g. neck lymph node draining the thyroid or CNS lymphoma spreading to the eye.

At the MSKCC, FISH analyses for *MYC, BCL2*, and *BCL6* (Abbott Molecular, Des Plaines, IL) were performed following a standard protocol, as previously described (25). The area of interest was usually circled on the slide, and the cytogenetics lab staff reviewed the slide to confirm a tumor-rich area was tested in all cases. For each probe set, 100 interphase cells were analyzed. A rearrangement was reported if 10% or more cells showed a split signal.

At UCSF, FISH analysis was performed on formalin-fixed paraffin-embedded (FFPE) tissue sections. The area of interest was circled by the ordering pathologist. Abbott Vysis Dual Color Break Apart probe sets (Des Plaines, IL) were used and FISH was set up according to the probe manufacturer's instructions (https://www.molecular.abbott/int/en/vysis-fish-knowledge-center/fish-on-isolated-nuclei-from-paraffin). FISH signals were imaged and analyzed using MetaSystems software (Medford, MA). For each probe set, 50 interphase cells were analyzed. A *MYC, BCL2*, or *BCL6* rearrangement was reported if 6.0% or more of cells showed split signals.

At SFVAHCS, *MYC, BCL2*, and *BCL6* FISH were performed at Quest Diagnostics in San Juan Capistrano, CA. Because this was an external lab, the area to perform FISH was not specified or circled. FISH was performed using the probes specific for 3q27 (BCL6), 8q24.1 (MYC), 14q32.3 (IGH), and 18q21.1 (BCL2) [Abbott Molecular and SureFISH, Agilent DAKO]. The cutoff values for *BCL6* rearrangement, *MYC* rearrangement, and t(14;18) in the

10.3389/fonc.2024.1408238

TABLE 2 Pathologic characteristics and FISH results of all 222 specimens compared across different biopsy types (fine needle aspiration biopsy, core needle biopsy, and excisional biopsy) with p values.

	Fine needle aspiration biopsy	Core needle biopsy	Excisional biopsy	P value
Number	46	112	64	
Age (mean (SD))	64.47 (15.70)	65.00 (16.66)	60.38 (15.81)	0.178
Gender (%)				0.209
Female	19 (41.3)	42 (37.5)	31 (48.4)	
Male	27 (58.7)	70 (62.5)	33 (51.6)	
Data Access Group (%)				<0.001
MGH	2 (4.3)	19 (17.0)	6 (9.4)	
MSKCC	4 (8.7)	12 (10.7)	0 (0.0)	
SFVAHCS	6 (13.0)	6 (5.4)	1 (1.6)	
Stanford	20 (43.5)	66 (58.9)	54 (84.4)	
UCSF	14 (30.4)	7 (6.2)	3 (4.7)	
UVA	0 (0.0)	2 (1.8)	0 (0.0)	
Indication (%)				<0.001
Additional diagnostic tissue	1 (2.2)	15 (13.4)	27 (42.2)	
Additional tissue for ancillary studies	0 (0.0)	1 (0.9)	2 (3.1)	
Clinical trial	0 (0.0)	1 (0.9)	0 (0.0)	
Initial diagnosis	27 (58.7)	38 (33.9)	11 (17.2)	
Other/unknown	0 (0.0)	2 (1.8)	0 (0.0)	
R/o recurrence	10 (21.7)	19 (17.0)	7 (10.9)	
R/o transformation	7 (15.2)	36 (32.1)	15 (23.4)	
Staging	1 (2.2)	0 (0.0)	2 (3.1)	
Tissue site (%)				0.832
Bone	1 (2.2)	6 (5.4)	2 (3.1)	
Lymph node or related	29 (63.0)	60 (53.6)	41 (64.1)	
Mediastinum	1 (2.2)	6 (5.4)	2 (3.1)	
Organ	7 (15.2)	23 (20.5)	7 (10.9)	
Other or unknown	1 (2.2)	2 (1.8)	2 (3.1)	
Soft tissue	7 (15.2)	15 (13.4)	10 (15.6)	
Final WHO diagnosis (%)				0.206
Burkitt	1 (2.2)	3 (2.7)	1 (1.6)	
DLBCL	31 (67.4)	85 (75.9)	57 (89.1)	
HGBCL	4 (8.7)	3 (2.7)	2 (3.1)	
HGBCL-MYC/BCL2	7 (15.2)	10 (8.9)	2 (3.1)	
Other/unknown	3 (6.5)	8 (7.1)	0 (0.0)	
PMLBCL	0 (0.0)	2 (1.8)	1 (1.6)	
TCHRLBCL	0 (0.0)	1 (0.9)	1 (1.6)	
MYC FISH (%)				0.527

(Continued)

TABLE 2 Continued

	Fine needle aspiration biopsy	Core needle biopsy	Excisional biopsy	P value
negative	33 (71.7)	86 (76.8)	55 (85.9)	
not done	0 (0.0)	0 (0.0)	1 (1.6)	
positive	11 (23.9)	21 (18.8)	7 (10.9)	
unsuccessful	1 (2.2)	3 (2.7)	0 (0.0)	
variant 3' signal loss	1 (2.2)	1 (0.9)	1 (1.6)	
variant extra 5' signaling	0 (0.0)	1 (0.9)	0 (0.0)	
BCL2 FISH (%)				0.274
extra BCL2 signal on add(3)	0 (0.0)	0 (0.0)	1 (1.6)	
negative	28 (60.9)	60 (53.6)	41 (64.1)	
not done	6 (13.0)	14 (12.5)	2 (3.1)	
positive	12 (26.1)	36 (32.1)	20 (31.2)	
unsuccessful	0 (0.0)	2 (1.8)	0 (0.0)	
BCL6 FISH (%)				0.718
negative	31 (67.4)	70 (63.1)	40 (62.5)	
not done	7 (15.2)	20 (18.0)	9 (14.1)	
positive	8 (17.4)	18 (16.2)	13 (20.3)	
unsuccessful	0 (0.0)	2 (1.8)	0 (0.0)	
variant 5' signal loss	0 (0.0)	1 (0.9)	2 (3.2)	

CNB (core needle biopsy), DLBCL (diffuse large B-cell lymphoma), EB (excisional biopsy), FNAB (fine needle aspiration biopsy), HGBCL (high-grade B-cell lymphoma, NOS), HGBCL-MYC/BCL2 (high-grade B-cell lymphoma with MYC and BCL2 rearrangements), PMLBCL (primary mediastinal large B-cell lymphoma), TCHRLBCL (T-cell, histiocytic-rich large B-cell lymphoma), MGH (Massachusetts General Hospital), MSKCC (Memorial Sloan Kettering Cancer Center), SFVAHCS (San Francisco Veterans Administration Health Care System), UCSF (University of California San Francisco, UVA (University of Virginia).

paraffin-embedded tumor tissue are 11%, 15%, and 3%. For each probe set, 100 cells were analyzed.

At MGH, FISH was performed on 5-micron sections of FFPE tissue; an H&E section was reviewed to select regions for hybridization that contained a majority of tumor cells. Break-apart probes (MYC: Vysis LSI MYC Dual Color, Break Apart Rearrangement Probe; BCL2: Leica Kreatech BCL2 Proximal Green [18Q001B495] and BCL2 Distal Red [18Q002B550) probes]; BCL6: Leica Kreatech BCL6 Proximal Green [03Q008B495] and BCL6 Distal Red [03Q007B550] probes) were hybridized and used to calculate the number of cells out of 50 scored containing a rearrangement. A rearrangement was reported if more than 15% of cells showed split signals.

3 Results

A total of 222 specimens from 208 unique patients were identified with a large/high-grade B-cell lymphoma diagnosis and performance of either *MYC*, *BCL2*, or *BCL6* FISH. The clinical characteristics of all patients are described in Table 1. The pathologic characteristics of all specimens are compared across different specimen types and corresponding p values in Table 2. The final large B-cell lymphoma diagnosis was established after FISH resulted e.g. high-grade B-cell lymphoma with *MYC* and *BCL2* rearrangements or Burkitt lymphoma; the breakdown of different diagnoses can be seen under the header "Final WHO Diagnosis" in Table 2. A breakdown of the diagnoses in our cohort is shown in Figure 2.

The breakdown of biopsy specimens by data access group (assigned to academic medical centers as previously described), specimen type collected, and specimen type that had FISH performed is shown by a Sankey diagram in Figure 3. Despite the diversity and complexity of some specimen types, for instance, FNAB with cell block and core biopsy with varying degrees of imaging guidance, only three specimen types ultimately had FISH performed: cell block from FNAB, core biopsy, and surgical excisional or incisional biopsy. Most specimens with both a cell block from FNAB and core biopsy had FISH performed on the core biopsy with one specimen having FISH performed on the cell block. Most specimens undergoing FISH were lymph nodes (n=129), followed by non-nodal sites such as solid organs (n=37) or soft tissue (n=32), among others (see Table 2). Of the lymph nodes, most were cervical (n=37), retroperitoneal (n=21), inguinal (n=18), or axillary (n=15). All the indications for biopsy are shown in Table 2; the four most common indications were initial diagnosis (n=76), obtaining additional diagnostic tissue (n=43), evaluating for recurrence (n=36), and ruling out transformation (n=58).

FISH detected a *MYC* rearrangement in 39 of 217 specimens successfully tested (18%), no rearrangement in 174 specimens, 4

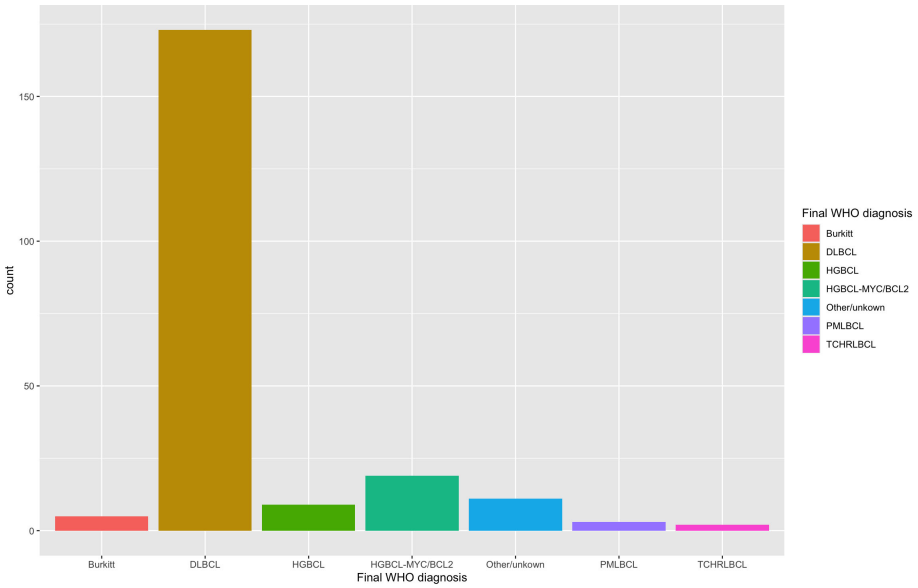

FIGURE 2
Diagnosis of all large B-cell lymphoma specimens with *MYC, BCL2*, and/or *BCL6* FISH performed. The diagnosis was retrieved retrospectively with FISH results already incorporated. Most cases were diffuse large B-cell lymphoma (DLBCL) (n=173). High-grade B-cell lymphoma with *MYC* and *BCL2* rearrangements (HGBCL-*MYC/BCL2*) (n=19) and high-grade B-cell lymphoma, NOS (HGBCL) (n=9) were smaller subsets. Burkitt lymphoma (n=5), primary mediastinal large B-cell lymphoma (PMLBCL; n=3) and T-cell, histiocyte-rich large B-cell lymphoma (TCHRLBCL; n=2) were rare in this cohort.

variant *MYC* FISH results (three with 3'signal loss and one with extra 5' signaling), and 4 unsuccessful hybridizations (Figure 4). One specimen was not evaluated for *MYC* FISH but was evaluated for *BCL2* and *BCL6* FISH; this specimen was included in this study because the patient had a prior biopsy in this cohort that was evaluated for a *MYC* rearrangement, and the additional biopsy was to obtain more tissue for ancillary testing. FISH detected *BCL2* rearrangements in 68 of 198 specimens successfully tested (34%), did not show a rearrangement in 129 specimens, 1 extra signal *BCL2* FISH result on an add(3), 2 unsuccessful hybridizations and 22 specimens without any *BCL2* FISH performed (Figure 5). *BCL2* rearrangements were detected in 20 of 37 *MYC* rearranged cases (54%), and these "double-hit" lymphomas are described in the next paragraph. FISH detected *BCL6* rearrangements in 39 of 183 specimens successfully tested (21%), did not show a

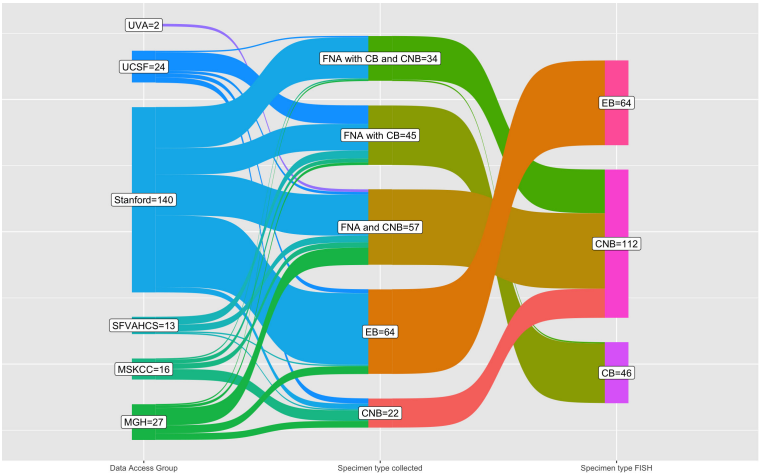

FIGURE 3
Sankey diagram of specimen type collected and specimen type undergoing FISH testing by institution (data access group). Of all the 222 specimens that underwent FISH testing in this cohort (right column), the majority are core biopsy, followed by excisional biopsy, and cell block. The core biopsy that have FISH performed include, of course, core biopsy only specimens but also FNAB with core biopsy and all FNA with cell block and core biopsy. One FNA with cell block and core biopsy had FISH performed on the cell block due to decalcification of the core biopsy (bone specimen). Abbreviations used: FNA (fine needle aspiration), CB (cell block from FNA), core biopsy (core needle biopsy), EB (excisional biopsy), MGH (Massachusetts General Hospital), MSKCC (Memorial Sloan Kettering Cancer Center), SFVAHCS (San Francisco Veterans Administration Health Care System), UCSF (University of California San Francisco), UVA (University of Virginia).

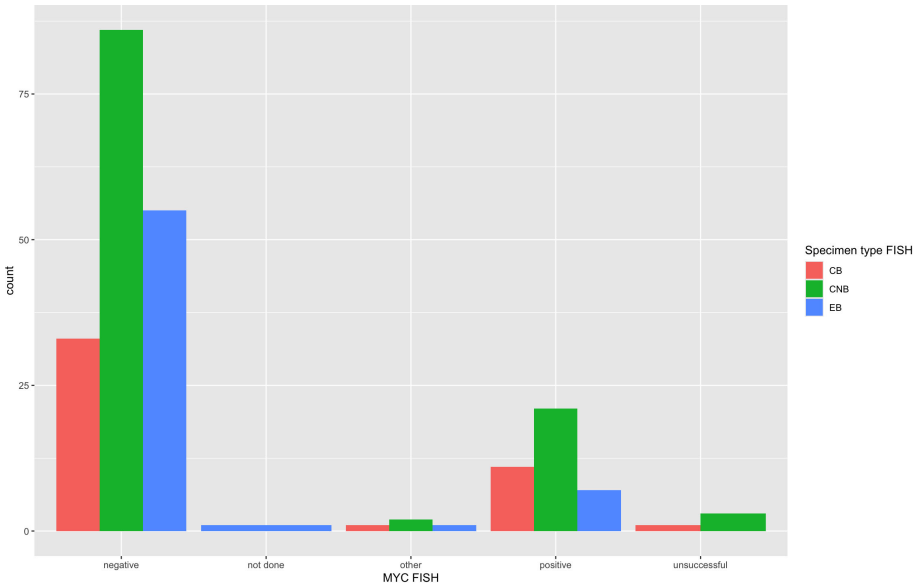

FIGURE 4
MYC FISH results across specimen types. *MYC* FISH results from all 222 specimens are arranged per specimen type that had FISH performed. *MYC* was rearranged in 18% of specimens and showed 4 "other" variant *MYC* FISH results, which included 3 specimens with 3' signal loss and 1 with extra 5' signaling. The unsuccessful or hybridization failure rate was overall low at 1.8% and similar across specimen types.

rearrangement in 141 specimens, 3 specimens with variant 5' *BCL6* signal loss patterns, 2 unsuccessful hybridizations, and 36 specimens without any *BCL6* FISH performed. The hybridization failure rate was low for *MYC* (4 of 221 or 1.8%), *BCL2* (2 of 200 or 1.0%), and *BCL6* (2 of 185 or 1.1%) probes. Of the 8 unsuccessful hybridizations, 5 (63%) showed tissue limitations such as crush artifact, fibrosis, necrosis, and paucicellularity. FISH results across different biopsy types are shown in Table 2.

Concurrent *MYC* and *BCL2* rearrangements were detected in 20 of the 197 specimens (10%) that had FISH successfully performed at both *MYC* and *BCL2* loci; for 19 of these 20 specimens, this result established the diagnosis as high-grade B-cell lymphoma with *MYC* and *BCL2* rearrangements (high-grade B-cell lymphoma-*MYC/BCL2*). One case was indeterminate due to the morphologic differential diagnosis of high-grade B-cell lymphoma-*MYC/BCL2* versus follicular lymphoma with *MYC* and *BCL2* rearrangements,

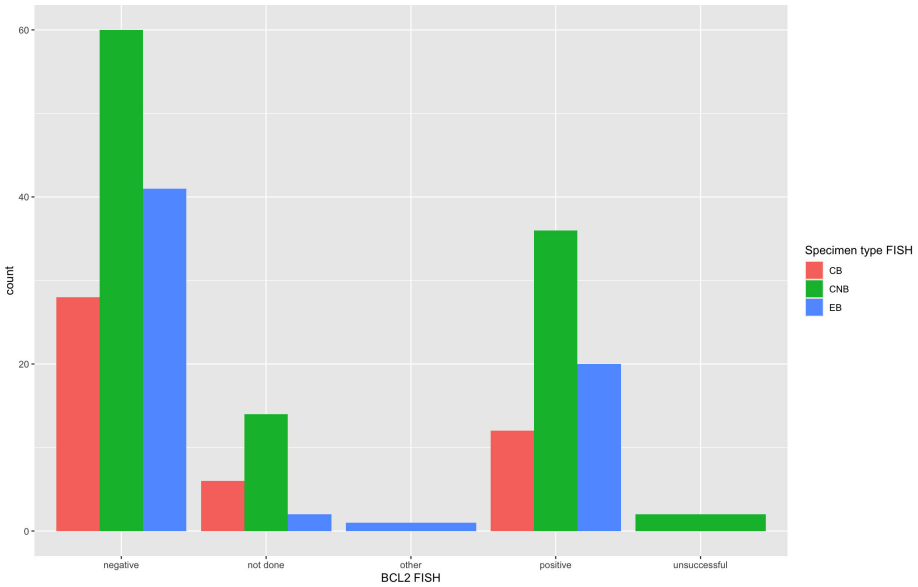

FIGURE 5
BCL2 FISH results across specimen types. *BCL2* FISH results from all 222 specimens are arranged per specimen type that had FISH performed. *BCL2* was rearranged in 34% of cases by FISH and showed 1 "other" variant result with 1 extra signal *BCL2* FISH result on an add(3). The unsuccessful or hybridization failure rate was low at 1.0% and similar across specimen types.

which is not regarded as equivalent to "double-hit" lymphoma according to WHO5/ICC. Of note, 4 additional cases (4 of 197 or 2%) had variant *MYC* FISH results, including 3 with 3' signal loss and 1 with extra 5' signaling. All four of these cases with variant *MYC* FISH results also had *BCL2* rearrangements, raising the possibility of high-grade B-cell lymphoma with *MYC* and *BCL2* rearrangements, without a definitive diagnosis. Of the "double-hit" lymphoma cases, 7 had FISH performed on FNA cell blocks, 10 had FISH on core biopsies, and 2 had FISH on the excisional biopsy. The clinical indications for these biopsy specimens were as follows: 7 for ruling out transformation, 7 for initial diagnosis, 4 for ruling out recurrence, and 1 for additional diagnostic tissue. Of note, one of the 19 "double-hit" lymphoma cases showed rearrangements with all three FISH probes *MYC*, *BCL2*, and *BCL6*, which falls in the same diagnostic category as cases with *MYC* and *BCL2* rearrangements only but has been called "triple-hit" lymphoma in the literature. Three specimens of 182 (1.6%) showed *MYC* and *BCL6* rearrangements, which according to the ICC, is diagnostic of the provisional entity high-grade B-cell lymphoma with *MYC* and *BCL6* rearrangements. The WHO5 classification does not recognize this provisional entity but addresses the need for additional data in this patient group.

Of the 222 specimens with FISH performed, 16 paired cytology and surgical specimens were identified from 8 different patients (each patient had exactly one set of paired specimens). An additional 9 patients with paired cytology and surgical biopsy specimens were identified at one institution (Stanford) that had FISH performed on only one set of the pair; completion FISH was performed at Stanford on a research basis on the specimen missing FISH to enlarge the paired specimen cohort. In total, 34 paired specimens were analyzed from 17 patients (Table 3). The 17 cytology cases included 13 FNAB with cell block and 4 FNAB with cell block and core biopsy (listed as core biopsy in Table 3, because FISH was performed on the core biopsy). The 17 surgical cases were 10 excisional biopsies, 6 core biopsies, and 1 small bowel resection. Of the 102 possible FISH tests (3 different FISH loci across 34 paired specimens), *MYC*, *BCL2*, or *BCL6* FISH was performed in 100 instances (98%). Patient 13 only had *BCL2* FISH performed in both specimens and thus *MYC* and *BCL6* FISH results were not comparable (Table 3). Out of the 49 comparisons drawn between these 98 paired FISH tests, 2 comparisons (4%) were discrepant: both showed a *BCL6* rearrangement in the FNA-cell block specimen but not in the paired excisional biopsy from patient 3 or core biopsy from patient 10 (see Table 3). No *MYC* or *BCL2* rearrangements were present in any of the discrepant samples. The date of specimens was closely matched for the discrepant pairs, including differences of 5 days and 10 days between the acquisition of the cytology specimen and the surgical specimen. Both patients had the same lymph node sampled by FNA and excisional biopsy or core biopsy. For patient 10, necrosis was noted in the core biopsy with the negative *BCL6* FISH.

4 Discussion

4.1 MYC, BCL2, and BCL6 FISH demonstrate highly successful hybridization rates across all specimen types with no statistically significant difference noted between FNAB, core biopsy, and surgical excisions. Tissue limitations may explain the rare failures

The FISH failure rate was low for all three FISH probes: 1.8% for *MYC* (4 of 220), 1.0% for *BCL2* (2 of 208), and 1.1% for *BCL6* (2 of 187). The hybridization rate is essentially the same across small-volume specimens such as FNAB cell block and core biopsy and larger-volume specimens such as an excisional biopsy with a statistically non-significant p-value across all three specimen types (see Table 2). Figures 4, 5 also demonstrate the breakdown of *MYC* and *BCL2* FISH results across various specimen types and graphically show that hybridization failure rates are low and similar across specimen types. The 8 FISH probe failures were from 6 specimens (one case had failure at all three FISH probes). These 6 specimens consisted of 5 core biopsies (all of which also had FNABs and one of which also had a cell block) and 1 cell block from FNAB. Five of the 6 specimens with failed FISH attempts were noted to have tissue limitations such as crush artifact, fibrosis, necrosis, and paucicellularity, any or all of which may partially explain why these cases had probe hybridization failure.

4.2 High-grade B-cell lymphoma with MYC and BCL2 rearrangements was identified across all specimen types

MYC FISH detected a rearrangement in 18% of specimens, which is similar to prior series (1, 8, 9, 26, 27). High-grade B-cell lymphoma with *MYC* and *BCL2* rearrangements comprised 9% of all large B-cell lymphoma specimens in our cohort, typical of the 8–10% rate reported in the literature (10, 28). Identification of this subset is critical due to the more aggressive clinical behavior that prompts more aggressive therapy. Figure 1 illustrates images from a case that was called diffuse large B-cell lymphoma at diagnosis but was later refined to HGBL-*MYC/BCL2* based on FISH results; the images demonstrate three preparations routinely made for FNAB samples of lymph nodes in many cytopathology practices—H&E-stained section of cell block, Pap-stained smear slide (alcohol fixed), and May-Grünwald Giemsa-stained slide (air dried). *MYC* break-apart FISH was performed on the cell block of this FNAB specimen and is depicted. Morphology and even immunohistochemistry are poor predictors of high-grade B-cell lymphoma-*MYC/BCL2*, and FISH or other comparable fusion detection assay such as targeted or whole genome next generation sequencing (12, 29, 30), RNA based sequencing (31), or integrated

TABLE 3 FISH results from 17 paired FNAB or core biopsy and surgical samples are displayed.

Patient	Biopsy 1					Biopsy 2				
	site	Biopsy type	*MYC*	*BCL2*	*BCL6*	site	Biopsy type	*MYC*	*BCL2*	*BCL6*
1	Left axillary	FNA-CB	1	0	0	Lymph nodes (Floor of mouth)	EB	1	0	0
2	Lymph node, left supraclavicular	FNA-CB	0	1	0	Left supraclavicular mass	EB	0	1	0
3	Lymph node, left neck	FNA-CB	0	0	1	Left neck node	EB	0	0	0
4	Lymph node, left neck level 2	FNA-CB	0	0	0	Neck level 2 lymph nodes	EB	0	0	0
5	Right cervical level 2 lymph node	FNA-CB	0	0	0	Lymph node, right neck	EB	0	0	0
6	Left neck lymph node	FNA-CB	0	0	0	Lymph node, left neck	EB	0	0	0
7	Left thyroid	FNA-CB	1	0	1	Left level 5 lymph nodes	EB	1	0	1
8	Lymph node, axillary	FNA-CB	1	0	0	Lymph node, cervical	EB	1	0	0
9	Vitreous	FNA-CB	0	0	0	Brain	EB	0	0	0
10	Lymph node, axillary	FNA-CB	0	0	1	Lymph node, axillary	CNB	0	0	0
11	Lymph node, inguinal	FNA-CB	0	0	0	Lymph node, inguinal	CNB	0	0	0
12	Bone	FNA-CB	1	1	0	Bone	CNB	1	1	0
13	Soft tissue, other or unknown	FNA-CB	0	1	0	Chest wall	CNB	ND	1	ND
14	Right lower quadrant abdomen	CNB	1	0	0	Small Bowel	Resection	1	0	0
15	Pelvis	CNB	0	0	0	Iliac lymph node biopsy	EB	0	0	0
16	Mesentery	CNB	0	1	0	Lymph node, left mesenteric	CNB	0	1	0
17	Left abdominal wall	CNB	0	0	0	Left abdominal mass	CNB	0	0	0

FISH results are reported qualitatively as 0 (negative), 1 (positive), or ND (not done). FISH results are colored green for concordance between small volume biopsy and surgical, red for discordance, and yellow for indeterminate because both specimens were not tested for the same probe. All cases are matched for anatomic site. Two discrepancies were noted between an FNA with cell block (FNA-CB) and surgical case (see BCL6 FISH result for patient 3 and 10); the discrepancy for patient 10 is likely attributable to necrosis noted on the core biopsy specimen causing a false negative FISH result.

FNAB-CB (fine needle aspiration biopsy with cell block), CNB (core needle biopsy), EB (excisional biopsy).

10.3389/fonc.2024.1408238

DNA/RNA sequencing (32) must be performed to identify this important subset of large B-cell lymphoma (28).

Rare variant signal patterns were found with both *MYC* and *BCL2* FISH probes, including signal loss and gain. Our cohort includes 3 patients with variant *3'MYC* loss and 1 patient with *5'MYC* poly-signaling; all the patients in our cohort with variant *MYC* signaling had concurrent *BCL2* rearrangements, raising the possibility of whether these were "double-hit" lymphoma. In general, a scarcity of literature and clinical outcomes about these rare cases exists (33). Copy number variations of *MYC* and *BCL2* have been previously shown to have different biology than structural rearrangements of both genes (13). Another study of variant *MYC* translocations in aggressive B-cell lymphomas found patients with *5'MYC* gain were more refractory to chemotherapy or had an early relapse with a median event-free survival of only 6 months compared to patients with *3'MYC* deletion who often responded to chemotherapy and had an event-free survival of 24 months (34). This study suggested based on survival data and the presence of *IGH/MYC* fusions or other *IGK, IGL* rearrangements in a subset that *5'MYC* gain likely represents an unbalanced *MYC* rearrangement whereas the *3'MYC* deletions were likely unrelated to *MYC* rearrangement. Based on this data, our cases with *3'MYC* signal loss should be excluded from the "double-hit" lymphoma category. This data also suggests our *5'MYC* gain case could be included in "double-hit" lymphoma, but given the overall lack of data and consensus in the literature at this point, the 5'*MYC* gain case was not included in the "double-hit" lymphoma category for our study.

High-grade B-cell lymphoma with *MYC* and *BCL6* rearrangements was much less common in our cohort with 3 cases out of 182 specimens rearranged at both loci (1.6%). As previously mentioned, the significance of these cases is currently controversial. Some studies have not shown distinct biology for these cases (1, 2), but other studies have found an association with a poor outcome (3, 8–11). An additional 3 specimens show variant *BCL6* rearrangements, all 5'BCL6 signal loss, but these specimens were *MYC* FISH negative. Additional studies are needed to further clarify the biology, clinical outcomes, and significance of these cases.

FISH may fail to identify a subset of diffuse large B-cell lymphoma and high-grade B-cell lymphoma that have inferior clinical outcomes. Gene expression profiling of germinal center B-cell diffuse large B-cell lymphoma can identify a double hit-like signature and inferior outcomes, but only half of these cases have structural rearrangements that can be detected by routine *MYC* and *BCL2* break-apart FISH (5). Whole genome sequencing of these cases revealed cryptic *MYC* and *BCL2* rearrangements, copy number gains and amplifications of *MYC* and *MIR17HG*, and focal deletions of the *PVT1* promoter (5). While other technologies in the future may more effectively detect biologically equivalent "double-hit" lymphoma, FISH currently remains the current clinical gold standard for detecting "double-hit" lymphoma.

4.3 Paired specimens demonstrate 96% concordance with *MYC, BCL2, and BCL6* FISH results across FNABs, core biopsies, and excisional biopsies

When matched for anatomic site and tissue limitations, paired cytology and surgical specimens in our study showed 96% concordance for FISH results (Table 3). Two FISH discrepancies were found and both showed the following pattern: *BCL6* rearrangement was detected in the FNAB while no *BCL6* rearrangement was detected in the paired surgical specimen. Necrosis was noted in the core biopsy from patient 10, and this core biopsy yielded a negative BCL6 result, suggesting that this may be a false negative result. Because no *MYC* rearrangements were present in any of the discrepant samples, the diagnosis would not have changed whether a *BCL6* rearrangement was or was not present.

Overall, this paired data suggests that FNAB cell block is a reasonable alternative to core biopsy or even excisional biopsy for diffuse large B-cell lymphoma and high-grade B-cell lymphoma FISH testing. No *MYC* or *BCL2* FISH discrepancies were found in any pair and, therefore, assessment for "double-hit" lymphoma would not have changed. The only discrepancies between paired samples were at the *BCL6* FISH locus; one of these discrepancies ultimately was attributed to a confounding variable described above.

A major limitation of this study is the heterogeneity of this retrospective and multi-institutional data set, which may limit applicability to some cytogenetic labs and pathology practice settings. Each institution used a different FISH lab with different probe sets and acquisition systems, different split signal thresholds for establishing the presence of a rearrangement, different numbers of interphase cells analyzed, and so on; these differences are reflected in the methods section. The biopsy specimens also have variable indications, which range from initial diagnosis to recurrence or transformation in the post-therapy setting. The data was collected from academic medical centers with highly specialized proceduralists and pathologists subspecializing in cytopathology and hematopathology, which may limit applicability to the community practice setting.

5 Conclusions

MYC, *BCL2*, and *BCL6* FISH have highly successful hybridization rates that are similar across different specimen types in this cohort, including FNAB, core biopsy, and excisional biopsy. High-grade B-cell lymphoma with *MYC* and *BCL2* rearrangements was detected in 9% of all large B-cell lymphoma specimens, including one case with rearrangements at all three loci *MYC, BCL2*, and *BCL6*; *MYC* and *BCL6* rearrangements were found in 1.6% of specimens. No significant difference was found across biopsy types. Paired cytology and surgical specimens

demonstrated 96% concordance at all three *MYC, BCL2*, and *BCL6* FISH loci. FNAB with cell block is an equally effective alternative to core biopsy and excisional biopsy for assessment of *MYC, BCL2, and BCL6* FISH, which is required for identification of the clinically aggressive subset of large B-cell lymphomas that carry both *MYC* and *BCL2* rearrangements.

Data availability statement

The raw data supporting the conclusions of this article will be made available by the authors, without undue reservation.

Ethics statement

The studies involving humans were approved by Stanford University IRB protocol 38992. The studies were conducted in accordance with the local legislation and institutional requirements. Written informed consent for participation was not required from the participants or the participants' legal guardians/next of kin in accordance with the national legislation and institutional requirements.

Author contributions

JM: Writing – review & editing, Writing – original draft, Visualization, Supervision, Software, Project administration, Methodology, Investigation, Formal analysis, Data curation, Conceptualization. UA: Writing – review & editing, Writing – original draft, Methodology, Data curation. CB: Writing – review & editing, Writing – original draft, Methodology, Data curation. SC: Data curation, Methodology, Writing – original draft, Writing – review & editing. SG: Data curation, Project administration, Writing – original draft, Writing – review & editing. RH: Conceptualization, Data curation, Supervision, Writing – original draft, Writing – review & editing. CK: Writing – review & editing, Writing – original draft, Supervision, Conceptualization. OL: Data curation, Supervision, Writing – original draft, Writing – review & editing, Conceptualization. SL: Conceptualization, Data curation, Supervision, Writing – original draft, Writing – review & editing. AL: Writing – review & editing, Writing – original draft, Supervision, Data curation, Conceptualization. JM: Formal analysis, Methodology, Software, Visualization, Writing – original draft, Writing – review & editing. YN: Supervision, Writing – original draft, Writing – review & editing. RR: Writing – original draft, Writing – review & editing. ES: Writing – review & editing, Writing – original draft, Methodology, Investigation. JY: Data curation, Writing – original draft, Writing – review & editing. SZ: Data curation, Writing – original draft, Writing – review & editing. DG: Writing – review & editing, Writing – original draft, Visualization, Validation, Supervision, Software, Resources, Project administration, Methodology, Investigation, Funding acquisition, Formal analysis, Data curation, Conceptualization.

Funding

The author(s) declare financial support was received for the research, authorship, and/or publication of this article. REDCap was funded by Stanford CTSA award number UL1 TR001085 from NIH/NCRR. Value-Based Award in Pathology from Stanford Healthcare supported the additional FISH testing and data entry at Stanford. The work at Memorial Sloan Kettering Cancer Center was funded by Grant/Award Number P30CA008748.

Acknowledgments

The R code for statistical analysis was built on several packages such as R-package ggsankey by David Sjoberg, ggplot2 by Hadley Wickham, table one by Kazuki Yoshida. These R packages were invaluable for statistical analysis of this data set.

Conflict of interest

The authors declare that the research was conducted in the absence of any commercial or financial relationships that could be construed as a potential conflict of interest.

Publisher's note

References

1. Cucco F, Barrans S, Sha C, Clipson A, Crouch S, Dobson R, et al. Distinct genetic changes reveal evolutionary history and heterogeneous molecular grade of DLBCL with MYC/BCL2 double-hit. *Leukemia*. (2020) 34:1329–41. doi: 10.1038/s41375–019-0691–6

2. Evrard SM, Péricart S, Grand D. Targeted next generation sequencing reveals high mutation frequency of CREBBP, BCL2 and KMT2D in high-grade B-cell lymphoma with MYC and BCL2 and/or BCL6 rearrangements. *Haematologica*. (2019) 104(4):e154–7. doi: 10.1016/j.morpho.2019.10.013

3. Ennishi D, Jiang A, Boyle M, Collinge B, Grande BM, Ben-Neriah S, et al. Double-hit gene expression signature defines a distinct subgroup of germinal center B-cell-like diffuse large B-cell lymphoma. *JCO*. (2019) 37:190–201. doi: 10.1200/JCO.18.01583

4. Sha C, Barrans S, Cucco F, Bentley MA, Care MA, Cummin T, et al. Molecular high-grade B-cell lymphoma: defining a poor-risk group that requires different approaches to therapy. *JCO*. (2019) 37:202–12. doi: 10.1200/JCO.18.01314

5. Hilton LK, Tang J, Ben-Neriah S, Alcaide M, Jiang A, Grande BM, et al. The double-hit signature identifies double-hit diffuse large B-cell lymphoma with genetic events cryptic to FISH. *Blood*. (2019) 134:1528–32. doi: 10.1182/blood.2019002600

6. Alaggio R, Amador C, Anagnostopoulos I, Attygalle AD, Araujo IBDO, Berti E, et al. The 5th edition of the world health organization classification of hematolymphoid tumors: lymphoid neoplasms. *Leukemia*. (2022) 36:1720–48. doi: 10.1038/s41375–022-01620–2

7. Campo E, Jaffe ES, Cook JR, Quintanilla-Martinez L, Swerdlow SH, Anderson KC, et al. The international consensus classification of mature lymphoid neoplasms: a report from the clinical advisory committee. *Blood*. (2022) 140:1229–53. doi: 10.1182/blood.2022015851

8. Li S, Desai P, Lin P, Yin CC, Tang G, Wang XJ, et al. *MYC / BCL 6* double-hit lymphoma (DHL): a tumor associated with an aggressive clinical course and poor prognosis. *Histopathology*. (2016) 68:1090–8. doi: 10.1111/his.12884

9. Ye Q, Xu-Monette ZY, Tzankov A, Deng L, Wang X, Manyam GC, et al. Prognostic impact of concurrent *MYC* and *BCL6* rearrangements and expression in *de novo* diffuse large B-cell lymphoma. *Oncotarget*. (2016) 7:2401–16. doi: 10.18632/oncotarget.6262

10. Rosenwald A, Bens S, Advani R, Barrans S, Copie-Bergman C, Elsensohn MH, et al. Prognostic significance of *MYC* rearrangement and translocation partner in diffuse large B-cell lymphoma: A study by the lunenburg lymphoma biomarker consortium. *JCO*. (2019) 37:3359–68. doi: 10.1200/JCO.19.00743

11. Pillai RK, Sathanoori M, Van Oss SB, Swerdlow SH. Double-hit B-cell lymphomas with BCL6 and MYC translocations are aggressive, frequently extranodal lymphomas distinct from BCL2 double-hit B-cell lymphomas. *Am J Surg Pathol*. (2013) 37:323–32. doi: 10.1097/PAS.0b013e31826cebad

12. Gagnon MF, Penheiter AR, Harris F, Sadeghian D, Johnson SH, Karagouga G, et al. Unraveling the genomic underpinnings of unbalanced MYC break-apart FISH results using whole genome sequencing analysis. *Blood Cancer J*. (2023) 13:190. doi: 10.1038/s41408–023-00967–8

13. Collinge B, Ben-Neriah S, Chong L, Boyle M, Jiang A, Miyata-Takata T, et al. The impact of MYC and BCL2 structural variants in tumors of DLBCL morphology and mechanisms of false-negative MYC IHC. *Blood*. (2021) 137(16):2196–208. doi: 10.1182/blood.2020007193

14. Aisner DL, Sams SB. The role of cytology specimens in molecular testing of solid tumors: Techniques, limitations, and opportunities. *Diagn Cytopathol*. (2012) 40:511–24. doi: 10.1002/dc.22820

15. Aisner DL, Rumery MD, Merrick DT, Kondo KL, Nijmeh H, Linderman DJ, et al. Do more with less: tips and techniques for maximizing small biopsy and cytology specimens for molecular and ancillary testing: the university of colorado experience. *Arch Pathol Lab Med*. (2016) 140:1206–20. doi: 10.5858/arpa.2016-0156-RA

16. Jain D, Mathur SR, Iyer VK. Cell blocks in cytopathology: a review of preparative methods, utility in diagnosis and role in ancillary studies. *Cytopathology*. (2014) 25:356–71. doi: 10.1111/cyt.12174

17. Darras N, Mooney KL, Long SR. Diagnostic utility of fluorescence in *situ* hybridization testing on cytology cell blocks for the definitive classification of salivary gland neoplasms. *J Am Soc Cytopathol*. (2019) 8:157–64. doi: 10.1016/j.jasc.2019.01.006

18. Mayall F. Fine needle aspiration cytology in the diagnosis of uncommon types of lymphoma. *J Clin Pathol*. (2003) 56:821–5. doi: 10.1136/jcp.56.11.821

19. Monaco SE, Teot LA, Felgar RE, Surti U, Cai G. Fluorescence in *situ* hybridization studies on direct smears: An approach to enhance the fine-needle aspiration biopsy diagnosis of B-cell non-Hodgkin lymphomas. *Cancer Cytopathol*. (2009) 117:338–48. doi: 10.1002/cncy.20040

20. Zhang S, Abreo F, Lowery-Nordberg M, Veillon DM, Cotelingam JD. The role of fluorescence in *situ* hybridization and polymerase chain reaction in the diagnosis and classification of lymphoproliferative disorders on fine-needle aspiration. *Cancer Cytopathol*. (2010) 118:105–12. doi: 10.1002/cncy.20070

21. Karabachev AD, Brundage WJ, Sajisevi MB, Ciolino AL. Feasibility of fine needle aspiration for diagnosis of b-cell lymphoma of the thyroid: a case series and review of the literature. *Diagn Pathol*. (2023) 18:69. doi: 10.1186/s13000–023-01346–4

22. Swerdlow SH, Campo E, Pileri SA, Harris NL, Stein H, Siebert R, et al. The 2016 revision of the World Health Organization classification of lymphoid neoplasms. *Blood*. (2016) 127:2375–90. doi: 10.1182/blood-2016–01-643569

23. Harris PA, Taylor R, Thielke R, Payne J, Gonzalez N, Conde JG. Research electronic data capture (REDCap)—A metadata-driven methodology and workflow process for providing translational research informatics support. *J Biomed Informatics*. (2009) 42:377–81. doi: 10.1016/j.jbi.2008.08.010

24. Harris PA, Taylor R, Minor BL, Elliott V, Fernandez M, O'Neal L, et al. The REDCap consortium: Building an international community of software platform partners. *J Biomed Informatics*. (2019) 95:103208. doi: 10.1016/j.jbi.2019.103208

25. Yang SR, Aypar U, Rosen EY, Mata DA, Benayed R, Mullaney K, et al. A performance comparison of commonly used assays to detect RET fusions. *Clin Cancer Res*. (2021) 27:1316–28. doi: 10.1158/1078–0432.CCR-20–3208

26. Ennishi D, Mottok A, Ben-Neriah S, Shulha HP, Farinha P, Chan FC, et al. Genetic profiling of MYC and BCL2 in diffuse large B-cell lymphoma determines cell-of-origin–specific clinical impact. *Blood*. (2017) 129:2760–70. doi: 10.1182/blood-2016–11-747022

27. Künstner A, Witte HM, Riedl J, Bernard V, Stölting S, Merz H, et al. Mutational landscape of high-grade B-cell lymphoma with *MYC*-, *BCL2* and/or *BCL6* rearrangements characterized by whole-exome sequencing. *haematol*. (2021) 107:1850–63. doi: 10.3324/haematol.2021.279631

28. Scott DW, King RL, Staiger AM, Ben-Neriah S, Jiang A, Horn H, et al. High-grade B-cell lymphoma with *MYC* and *BCL2* and/or *BCL6* rearrangements with diffuse large B-cell lymphoma morphology. *Blood*. (2018) 131:2060–4. doi: 10.1182/blood-2017–12-820605

29. Chong LC, Ben-Neriah S, Slack GW, Freeman C, Ennishi D, Mottok A, et al. High-resolution architecture and partner genes of MYC rearrangements in lymphoma with DLBCL morphology. *Blood Adv*. (2018) 2:2755–65. doi: 10.1182/bloodadvances.2018023572

30. Chapuy B, Stewart C, Dunford AJ, Kim J, Kamburov A, Redd RA, et al. Molecular subtypes of diffuse large B cell lymphoma are associated with distinct pathogenic mechanisms and outcomes. *Nat Med*. (2018) 24:679–90. doi: 10.1038/s41591–018-0016–8

31. Wang X, Johnson V, Johnson L, Cook JR. RNA-Based next generation sequencing complements but does not replace fluorescence in situ hybridization studies for the classification of aggressive B-Cell lymphomas. *Cancer Genet*. (2021) 252–253:43–7. doi: 10.1016/j.cancergen.2020.12.004

32. Cassidy DP, Chapman JR, Lopez R, White K, Fan YS, Casas C, et al. Comparison between integrated genomic DNA/ RNA profiling and fluorescence *in situ* hybridization in the detection of MYC, BCL-2, and BCL-6 gene rearrangements in large B-cell lymphomas. *Am J Clin Pathol*. (2020) 153(3):353–9. doi: 10.1093/ajcp/aqz172

33. Gagnon MF. MYC break-apart FISH probe set reveals frequent unbalanced patterns of uncertain significance when evaluating aggressive B-cell lymphoma. *Blood Cancer J*. (2021) 11(11):184. doi: 10.1038/s41408-021-00578-1

34. Tang G, Li S, Toruner GA, Jain P, Tang Z, Hu S, et al. Clinical impact of 5 MYC or 3 MYC gain/loss detected by FISH in patients with aggressive B-cell lymphomas. *Cancer Genet*. (2023) 272-273:1–8. doi: 10.1016/j.cancergen.2022.12.001

Frontiers in Oncology

Advances knowledge of carcinogenesis and tumor progression for better treatment and management

The third most-cited oncology journal, which highlights research in carcinogenesis and tumor progression, bridging the gap between basic research and applications to imrpove diagnosis, therapeutics and management strategies.

Discover the latest Research Topics

See more →

Frontiers

Avenue du Tribunal-Fédéral 34
1005 Lausanne, Switzerland
frontiersin.org

Contact us

+41 (0)21 510 17 00
frontiersin.org/about/contact